DEVELOPMENT OF TWO-PHASE REINFORCED ALUMINA NANOCOMPOSITE FOR CUTTING TOOLS APPLICATIONS

BY

KHWAJA MOHAMMAD

A Dissertation Presented to the

DEANSHIP OF GRADUATE STUDIES

KING FAHD UNIVERSITY OF PETROLEUM & MINERALS

DHAHRAN, SAUDI ARABIA

In Partial Fulfillment of the

Requirements for the Degree of

DOCTOR OF PHILOSOPHY

In

MECHANICAL ENGINEERING

January 2017

KING FAHD UNIVERSITY OF PETROLEUM & MINERALS

DHAHRAN- 31261, SAUDI ARABIA

DEANSHIP OF GRADUATE STUDIES

This thesis, written by **KHWAJA MOHAMMAD** under the direction his thesis advisor and approved by his thesis committee, has been presented and accepted by the Dean of Graduate Studies, in partial fulfillment of the requirements for the degree of **DOCTOR OF PHILOSOPHY IN MECHANICAL ENGINEERING**

Dr. Saheb Nouari
(Advisor)

Dr. Zuhair Mattoug Gasem
Department Chairman

Dr. Nasser Al-Aqeeli
(Member)

Dr. Salam A. Zummo
Dean of Graduate Studies

Dr. Tahar Laoui
(Member)

8/3/17
Date

Dr. Abul Fazal M. Arif
(Member)

Dr. Ahsan ul haq Quraishi
(Member)

January 2017

DEDICATTION

I dedicate my research at KFUPM to

My Parents, family and all well-wishers

ACKNOWLEDGEMENTS

First and foremost I must thank my LORD, Allah Subhana wa Taghala for all His blessing throughout, allowing for in-time and quality completion of this research.

I offer my highest gratitude to my thesis advisor, Dr. Nouari Saheb, who supervised and played a vital role in contributing technical, ethical, social and financial support though out my thesis. His patience and knowledge positively tailored the room to work in. Beside all my shortcomings, I attribute the level of my PhD degree to his untiring attitude, encouragement and efforts and without him this thesis, too, would not have been completed or written. His humble and extreme kindness can never be forgotten.

Professor Nasser Aqeeli! A role model, an idol leader, a promising teacher and supervisor. I really had the honor to have been working under his propitious guidance during my Research at KFUPM. He has remarkably stimulated and supplemented my growth as a student, a researcher and a scientist.

I must also thank Prof. Tahar Laoui, Prof. Arif Abul Fazal, and Dr. Ahsan-ul haq for all their contribution through this research work and engaging themselves in floating their all-time guidance, dedicated attention, expertise and knowledge which forwarded value to this research.

Dr. Abbas Saeed Hakeem is highly acknowledged for his all—time technical support and assistance, unflinching encouragement and support, always ready to help and discuss and for all the most what he attributes.

I wish to acknowledge the help from Dr. Zain Yamani, who have always welcomed me to use any of the required equipment, with-out any time scale, especially SPS and FESEM and

further for extending his full support which contributed to the completion of this research work.

Special thanks to Mr. Lateef hashmi, Mr. Sadaqat Ali and all other supporting staff and my colleagues and well-wishers for all their assistance, care, provision and support.

I am obligated to King Fahd University of petroleum and minerals, and in particularly to mechanical engineering department for giving me an opportunity and prospects to step-up in my educational carrier. I enjoyed the entire supportive research oriented environment, from best lecture room, best available laboratory equipment's, on-campus accommodation, and family-like care. I am very sure with-out all this, it would have been difficult to achieve targets of this research.

Further, the financial support, which I received from KFUPM during my stay, is an extra edge. Besides KFUPM, I would also like to Thank KACST for extending funds towards completion of this work through project AR-34-3.

TABLE OF CONTENTS

LIST OF FIGURES

LIST OF TABLES

ABSTRACT

Full Name : [Khwaja Mohammad]

Thesis Title : [DEVELOPMENT OF TWO-PHASE REINFORCED ALUMINA NANOCOMPOSITE FOR CUTTING TOOLS APPLICATIONS

Major Field : [Mechanical Engineering]
Date of Degree : [January 2017]

The high stiffness and hardness of ceramic materials made them attractive for various applications. However, their low toughness limit their use in many structural applications such as cutting tools. Reinforcing ceramics by two nanoscale phases, having different morphologies, is a new methodology that has been adopted to develop hybrid nanostructure with improved mechanical properties. However, achieving a uniform distribution/dispersion of the nanosize reinforcements in the matrix and retaining nanostructure during consolidation process are major challenges in synthesizing these highly claimed materials.

In this research work, an approach for the synthesis of homogenous Al_2O_3-SiC-CNTs hybrid nanocomposite powders via molecular level mixing was developed. In addition, Al_2O_3-SiC-CNTs nanocomposite powders was also synthesized using ball-milling technique. Synthesized powders were consolidated using spark plasma sintering technique. The influence of synthesis and sintering parameters, and reinforcements' content on the microstructure, densification, hardness, fracture toughness, and bending strength of the composites was investigated.

The prepared materials were characterized, wherever needed using FE-SEM, TEM, X-ray mapping, XRD, FT-IR, and TGA. The nanocomposite powders synthesised via molecular level mixing or ball milling as well as sintered samples showed uniform distribution of SiC and CNTs.

The final microstructure of sintered samples comprised intergranular CNTs, along with inter- and intergranular SiC nanoparticles, which restricted grain growth. Fully dense monolithic alumina and almost fully dense hybrid nanocomposites were obtained (relative density higher than 98%). The mode of fracture changed from intergranular mode for the monolithic alumina to almost complete transgranular mode for the Al_2O_3-SiC-CNTs nanocomposites, which along with other toughening mechanisms improved the fracture toughness.

The Al_2O_3-5SiC-1CNTs composite, synthesised using molecular level mixing and sintered at 1600°C for 10 min, possessed both high hardness and toughness values of 23.32GPa and 7.10 $MPam^{1/2}$, respectively. This constitutes an increase in hardness and toughness of 25.6 and 96%, respectively, compared to alumina.

As for the composites prepared using ball milling and sintered at 1500°C for 10 min, Al_2O_3-10SiC-2CNT possessed a high fracture toughness value of 6.98 $MPam^{1/2}$, representing an increase of 94% compared to alumina. Al_2O_3-10SiC-1CNT possessed a high hardness value of 20.81GPa, representing an increase of 12 % compared to alumina.

ملخص الرسالة

الاسم الكامل: خواجة محمد

عنوان الرسالة: تطوير مواد مركبة متناهية الصغر من الألومينا المدعومة بطورين لتطبيقات مواد القطع

التخصص: مهندس ميكانيكى

تاريخ الدرجة العلمية: يناير 2017

تعتبر صلابة وصلادة المواد الخزفية أهم المحفزات لاستعمالها في مختلف المجالات. لكن ضعف مقاومتها للكسر حد من استعماها في كثير من التطبيقات مثل مواد القطع. لحسن الحظ أصبح ممكنا تحسين خواصها الميكانيكية عن طريق إضافة طورين داعمين متناهيي الصغر وأشكال مختلفة. لكن يبقى الحصول على خليط متجانس من المساحيق المدعومة بأطوار ذات أبعاد من رتبة النانو والقدرة على منع نمو الحبيبات صعب التحقيق. في هذا البحث تم لأول مرة تطوير مقاربة جديدة لتحظير مواد مركبة هجينة نانو خزفية من أكسيد الألومنيوم المدعوم بالسلكون كاربيد المتناهي الصغر وأنابيب الكاربون المتناهية الصغر عبر الخلط على مستوى الجزيئات. بالإضافة إلى ذلك تم استعمال طريقة الطحن الميكانيكي لتحظير نفس مساحيق المواد المركبة المتجانسة الهجينة. ثم تم تلبيد المساحيق المنتجة باستخدام طريقة شرارة البلازما. تمت دراسة تأثير ظروف وشروط التحضير وكدلك نسبة الأطوار المضافة على البنية المجهرية، الكثافة، الصلابة، معامل الممانعة للكسر، واجهاد الثني للعينات المحظرة. أستعمل المجهر الإلكتروني ذو مجال الانبعاث، المجهر الإلكتروني النافذ، التخطيط عن طريق الأشعة السينية، حيود الأشعة السينية، تحويل فوريه الطيفي للأشعة تحت الحمراء، المسح الحراري التفاضلي، التحليل الحراري الوزني، جهاز قياس صلابة، وجهاز الاختبار الموحد، لتوصيف المواد المطورة. المساحيق الهجينة المركبة والمتناهية الصغر المحظرة عن طريق الطحن الميكانيكي أو الخلط على مستوى الجزيآت وكذلك العينات الملبدة عن طريق شرارة البلازما أظهرت توزيع منتظم للسلكون كاربيد المتناهي الصغر وأنابيب الكاربون المتناهية الصغر في أكسيد الألومنيوم. البنية المجهرية للعينات النهائية احتوت على طور السلكون كاربيد داخل حبيبات أكسيد الألومنيوم وكذلك أنابيب الكاربون والسلكون كاربيد موزعان بين الحدود الحبيبية لأكسيد الألومنيوم. وجد أن آلية الكسر تغيرت من كسر عبر الحدود الحبيبية بالنسبة لأكسيد الألومنيوم أحادي الطور إلى كسر عبر الحبيبات بالنسبة الى المواد المركبة الهجينة مع ظهور آليات أخرى أدى الى الزيادة في معامل الممانعة للكسر .تم الحصول على أكسيد الألومنيوم أحادي الطور تام الكثافة ومركبات هجينة متناهية الصغر عالية الكثافة (كثافة نسبية

أعلى من 98%). بالنسبة للمركب الهجين المحظر عبر الخلط على مستوى الجزيئات والمدعوم بنسبة 5 % سلكون كاربيد و1 % أنابيب الكاربون والملبد لمدة عشر دقائق عند درجة حرارة 1600 درجة مئوية وجد أنه يملك معامل ممانعة للكسر عالي مقداره 7.10 ($MPa.m^{1/2}$) أي بزيادة مقدارها 96 % وصلابة عالية مقدارها 23.32 (MPa) أي بزيادة مقدارها 25.6 % بالمقارنة مع أكسيد الألومنيوم الأحادي الطور. بالنسبة للمواد المركبة الهجينة المحظرة عن طريق الطحن الميكانيكي والملبدة لمدة عشر دقائق عند درجة حرارة 1500 درجة مئوية المركب المدعوم بنسبة 10 % سلكون كاربيد و2 % أنابيب الكاربون اظهر معامل ممانعة للكسر مقداره 6.98 ($MPa.m^{1/2}$) أي بزيادة مقدارها 94 % بالمقارنة مع أكسيد الألومنيوم لأحادي الطور. أما المركب المدعوم بنسبة 10 % سلكون كاربيد و1 % أنابيب الكاربون أظهر صلابة مقدارها 20.81 (MPa) أي بزيادة مقدارها 12 بالمقارنة مع أكسيد الألومنيوم الأحادي الطور

CHAPTER 1

INTRODUCTION 1

Cutting tools are one of the most important components in the machining process, as their performance determines the efficiency of operation. Therefore the selection of tool material is very important. During its operation, the tool experiences high stresses and temperatures, in addition to undergoing abrasion. Therefore tool material needs to have high levels of hardness, toughness, and wear resistance. Materials which are considered to be suitable for cutting tools are high-speed steel and cast alloys, cemented carbides, and ceramics. However, most of the steel alloys and even carbides lose their hardness at high temperatures during machining, which damages both the tool material and its efficiency of operation. Ceramics, on the other hand, which can maintain chemical stability and hardness at high temperatures, are a suitable tool material for efficient, high performance machining processes.

Ceramic materials such as alumina, silicon carbide, aluminum nitride, silicon nitride, zirconia, etc. are known for their high hardness, high temperature tolerance, chemical stability and low density. However, their intrinsic property of low toughness limits their use in many industrial applications such as space vehicles, the tooling industry, electrical insulators, refractory materials, wear-resistant components and several other load-bearing structural and bio- applications [1][2].

Therefore enhancing fracture toughness is an essential consideration during the micro structural design of materials for these kind of applications [3]. The addition of second phase reinforcement in the ceramic matrix, by developing a ceramic composite, can induce a significant increase in fracture toughness [4]. The shape and size of reinforcement, in addition to its chemical affinity or interfacial bonding with the matrix, control the expected mechanical properties of the developed composite [5] and, usually owing to increased surface and contact area, fine particles [6], whiskers [7], platelets [8], and reinforced nanocomposites are developed to target high toughness in the material.

Previous studies reported that the incorporation of fine SiC particles [9][10][11] in alumina, exhibited an increase in strength which was attributed to the grain boundary strengthening effect. Similar studies, however, reported little, if any, increase in toughness of the material [12][13][14].

Due to their high mechanical properties, low density and high aspect ratio, CNTs have also received wide attention and have been widely used for reinforcement [12]–[16] in alumina. Numerous efforts were made to boost the mechanical properties, particularly fracture toughness, of alumina using carbon nanotubes as reinforcement [21][18][22]. However, unsatisfactory consequences were reported for these composites due to the agglomeration of MWCNTs in alumina [18] [23][24][25].

This is because, in addition to the matrix and the type, size and content of reinforcement, the extent of reinforcement dispersion in the ceramic matrix is equally important and plays a vital role in controlling the final properties of the nanocomposite. Therefore, attaining a uniform distribution of MWCNTs remained a challenge in developing nanocomposites with the expected enhanced properties [26]. The dispersion of reinforcement in the ceramic

matrix was achieved using conventional, sol-gel and colloidal processing. In conventional powder processing, shear forces are applied through ball milling to break and to de-agglomerate reinforcement in the matrix. Colloidal processing modifies the surfaces of the reinforcement to increase the stability of suspension. Sol–gel processing entraps reinforcement particles and/ or fibers, within the gel network and then allows reinforcement to grow on the surface of the ceramic matrix.

Although different techniques were used to minimize the agglomeration of fine reinforcement and fibers in the ceramic matrix, the results were still not as promising as expected [18][24]. While in some cases increased fracture toughness has been achieved, it has come at the cost of hardness, density and strength [27][28][29][30][21]. This inferior strength is due to the thermal mismatch between CNT (coefficient of thermal expansion CTE= ~Zero) and alumina (coefficient of thermal expansion CTE =~$8X10^{-6/}$K) [31]. However, adding reinforcement such as SiC (CTE~=$4X10^{-6}$ /K) [32] was reported to increase interfacial bonding due to the reduced difference in the thermal expansion coefficient between alumina and SiC. Furthermore, SiC restricts grain growth through the pinning effect and increases the hardness of the material [33][34].

Therefore, a new class of ceramic nanocomposite (hybrid microstructure) with MWCNT and SiC reinforced alumina has been used [35][36] to provide mutually enhanced toughening and strengthening properties, respectively, in the developed hybrid nanocomposite. Strengthening of the grain boundaries and partial toughening of the matrix is attributed to nanosized SiC particles, while a number of toughening mechanisms are activated due to the addition of MWCNTs.

Few papers have been published on designing hybrid microstructure Al_2O_3-SiC-CNT [29], Al_2O_3-SiC-CNF [31], Al_2O_3-SiC-GPL [8], Al_2O_3-CNTs-GPL [37], and Al_2O_3-SiCw-CNT [38], aiming to increase the toughness of the material.

Ahmed and Pan [29] investigated the influence of 0,5,7, and 10 vol.% MWCNTs in Al_2O_3-1SiC. Sonication and ball milling were used to prepare the respective compositions which were further consolidated using spark plasma sintering. The authors reported the high fracture toughness of 7Mpam$^{1/2}$ but a low hardness value for 16Gpa. Umino and his colleagues [31] prepared Al_2O_3-20CNF (carbon nanofibers) with 0vol% and 10vol% SiC by using the electrostatic adsorption technique and reported that the addition of SiC increased the interfacial shear strength of the material. Liu and co-workers[8] investigated the effect of 1, 3, and 5vol% of SiC in alumina-0.38vol% GPL (graphene platelets) synthesized through ball milling and spark plasma sintering and found that a 3vol% addition of SiC resulted in the optimum combination of properties showing a densification of 98.85%, hardness of 24Gpa and fracture toughness of 5.0MPam$^{1/2}$. Yazdani et al. [37] obtained dense Al_2O_3–GNT composites (>98%) by SPS for 10 mins at 1650 °C and 40 MPa. A high fracture toughness value of 5.5 MPa m$^{1/2}$ was obtained. Lee and Yoon [38] investigated the mechanical properties of alumina containing 0, 0.1, 0.5 and 1wt% MWCNTs, with and without 25wt% SiC whiskers (SiCw), and reported that sintering was significantly retarded by the presence of SiCw. The authors further attributed lower than expected mechanical properties to the inhomogeneous distribution of CNTs in the alumina matrix.

Lower than expected mechanical properties in the hybrid microstructure [29] [31] [8], [37] [38] designed with two different reinforcement morphologies have been attributed to either

the agglomeration of nano-reinforcement or weak matrix-reinforcement interface bonding, for obtaining these unsatisfying results. However, the development of these exceptional nanocomposites is vital in certain load-bearing applications, which require enhancement in the hardness, together with the fracture toughness, of the material.

Therefore, in this research work, ball milling and molecular level mixing processes, were used as a synthesis technique to boost the degree of homogeneous distribution and to intensify the bonding strength at the alumina-reinforcement interface. Synthesized powder was consolidated using spark plasma sintering aiming to obtain a finer dense microstructure with mutually enhanced toughening and strengthening properties.

CHAPTER 2

LITERATURE REVIEW 2

2.1 Ceramic Matrix Nanocomposites

During last few decades, there is a significant increase in demand for using ceramic in various engineering components such as in gas turbine, automobile, spacecraft, cutting tool materials, etc. due to their excellent high-temperature resistance, significant corrosion and wear resistance. However, their inherent brittleness, low toughness, strength and poor resistance to creep, fatigue and thermal shock have limited their use in such applications. Luckily, microstructural engineering of ceramic material can solve these deficiencies. One of the prominent methods is to developed ceramic matrix composite material by adding reinforcing agents in the ceramic matrix to profit from the combined effect of each material. Nano-composites are characterized by the ultra-fine microstructure, where dimensions of physical features like grains, particle or fiber diameters are less than 100nm. Increased surface area and the number of exposed atoms in nanostructure significantly increases the activity of such material and correspondingly changes its properties. Therefore, nano-dimensional features of added or incorporated secondary phases in the ceramic matrix, controls the properties of the resultant material.

Incorporation of secondary phase in ceramic matrix introduces a large number of in-homogeneities at the reinforcement-matrix interface, which is then effective obstructions for crack propagation in the material. For instance, incorporation of fibers, whiskers or

elongated grains can bridge the crack face while fine spherical particles can deflect the crack propagation and thus increases the toughness of the material.

Combined characteristic features of ceramic matrix and reinforcing agent in CMCs (ceramic matrix nanocomposite) with specifically tailored properties have made them a potential material to meet challenging and demanding needs of the structural and high-temperature applications, particularly in load bearing application.

Expected enhanced properties in CMCs can be attributed to the (nano-dimensional) starting powder or pre-cursors which should be in high purity and fully dispersed reinforcement. These unique characteristics increased solid state diffusion during sintering due to their increased surface to volume ratio, which leads to the formation of high-performance ceramic matrix nanocomposites.

Nanocomposite can be synthesized from nanopowder either through the solid phase (evaporation-condensation, mechanical alloying, laser ablation and or self-propagating high-temperature synthesis), the liquid phase (sol-gel and spray drying of solutions) or gas phase (chemical vapor deposition, laser, and plasma synthesis).

Ceramic nano-composite can exhibit microstructural features, where both inter and intra-granular sites in a ceramic matrix are occupied by single rounded nanoparticles such as SiC **Figure *2.1***(a), or elongated reinforcement such as CNTs **Figure *2.1***(b) or both round and elongated reinforcement with different morphologies **Figure *2.1***(c).

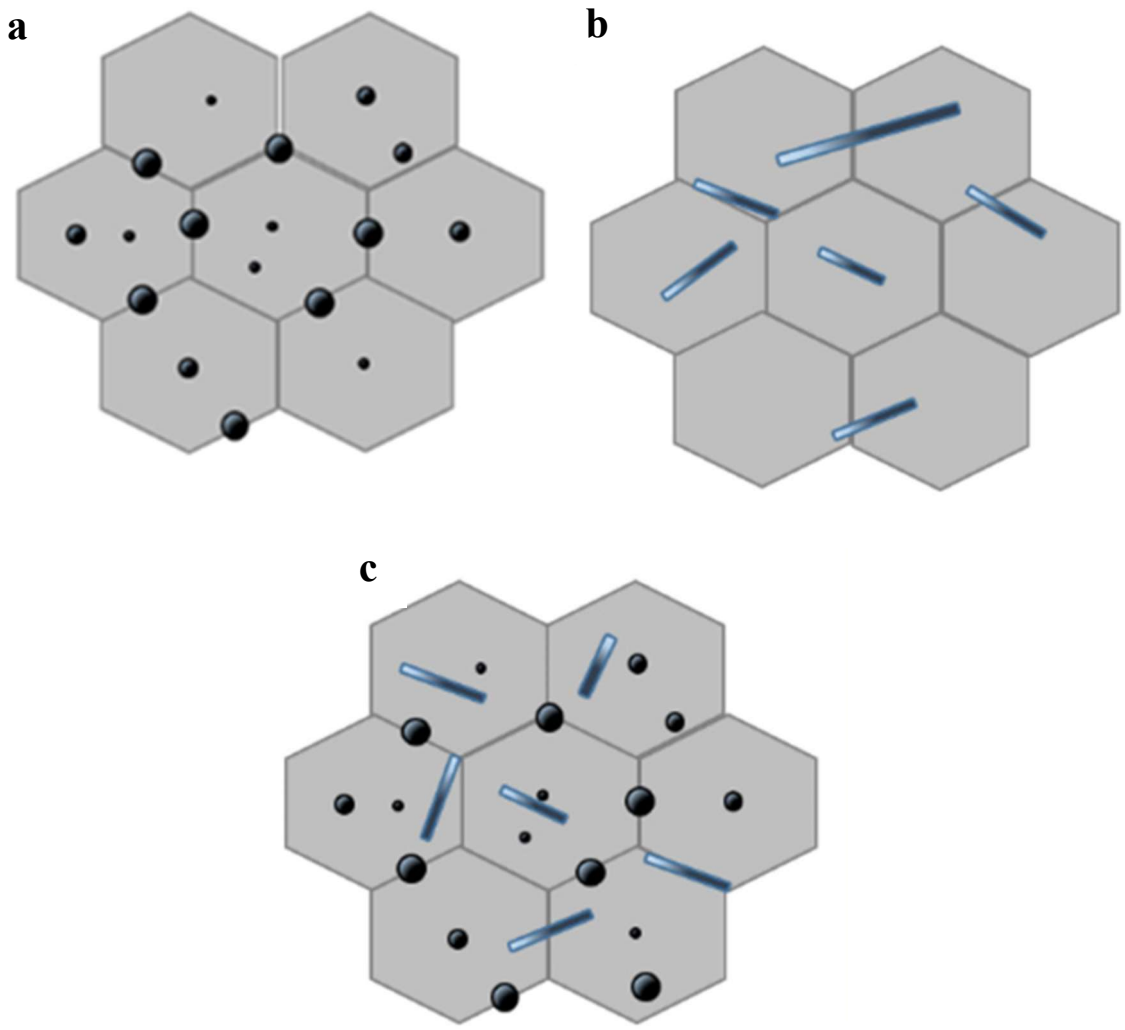

Figure 2.1 *Scheme of common (nano)composite structures for ceramic materials, with rounded nanoparticles occupying both inter- and intra-granular positions (a), with elongated nano-reinforcements inside ceramic matrix and (c), hybrid nanocomposite, containing both rounded and elongated nano-reinforcements, embedded in ceramic matrix*[4]

2.2 Nanocomposite Powder Synthesis

2.2.1 Ball Milling

Ball milling is a promising powder processing technique used for milling and or mixing of the powder mixture. In addition to being simple, versatile, and economical, it results in the homogeneous distribution of reinforcements with-in matrix[19]. It allows mixing and or milling of powder mixture through energy provided during the collision between powder particles and hard balls[39]. Ball milling is generally divided into low energy and high energy ball mill, based on the level of energy being induced into powder mixture during the milling process. Low energy horizontal mill is usually used for grinding or mixing, however, high energy mills such as planetary, attrition, vibratory are usually employed for change in chemical composition of the mixture

Surface and interface contamination is a major concern while preparing nanocomposite powder mixture through ball milling. Milling media and or trace impurities of gasses during milling can be a source of these contaminations. Beside contamination, milling process lacks control over particle morphology, the range of particle size, agglomeration and residual strains. Further, there are high chances of damaging, particular reinforcement such as CNTs thus reducing their high aspect ratio, during milling, which further reduces their inherent mechanical properties.

Beside these deficiencies and limitations, ball milling is still dominant mixing techniques due to its lower cost of installation, power and grinding medium. Further, it is suitable for both continuous and batch operations and can handle almost all materials of different harnesses.

Inam *et al* [40]compared the use of different solvents in dispersing CNTs and carbon black during sonication. Author dispersed multi-wall CNTs in dimethylformamide (DMF) using high power sonication for 2 hours. Further alumina was hand mixed with it for 2 min. The author found DMF as more active than ethanol in dispersing and homogenizing composite powder.

The wet slurry was initially ball-milled for 8 hours and then dried overnight at 75ºC. The dried mixed composite powder was passed through.200mesh size to break down soft agglomerate Author compared CNTs with carbon black and it was found that CNTs were well dispersed in the composite, although agglomeration was found instead when carbon black was used. It was further found that CNTs accumulates around grain as shown in **Figure 2.2** TEM image, illustrating CNTs around grains in the nanocomposite.

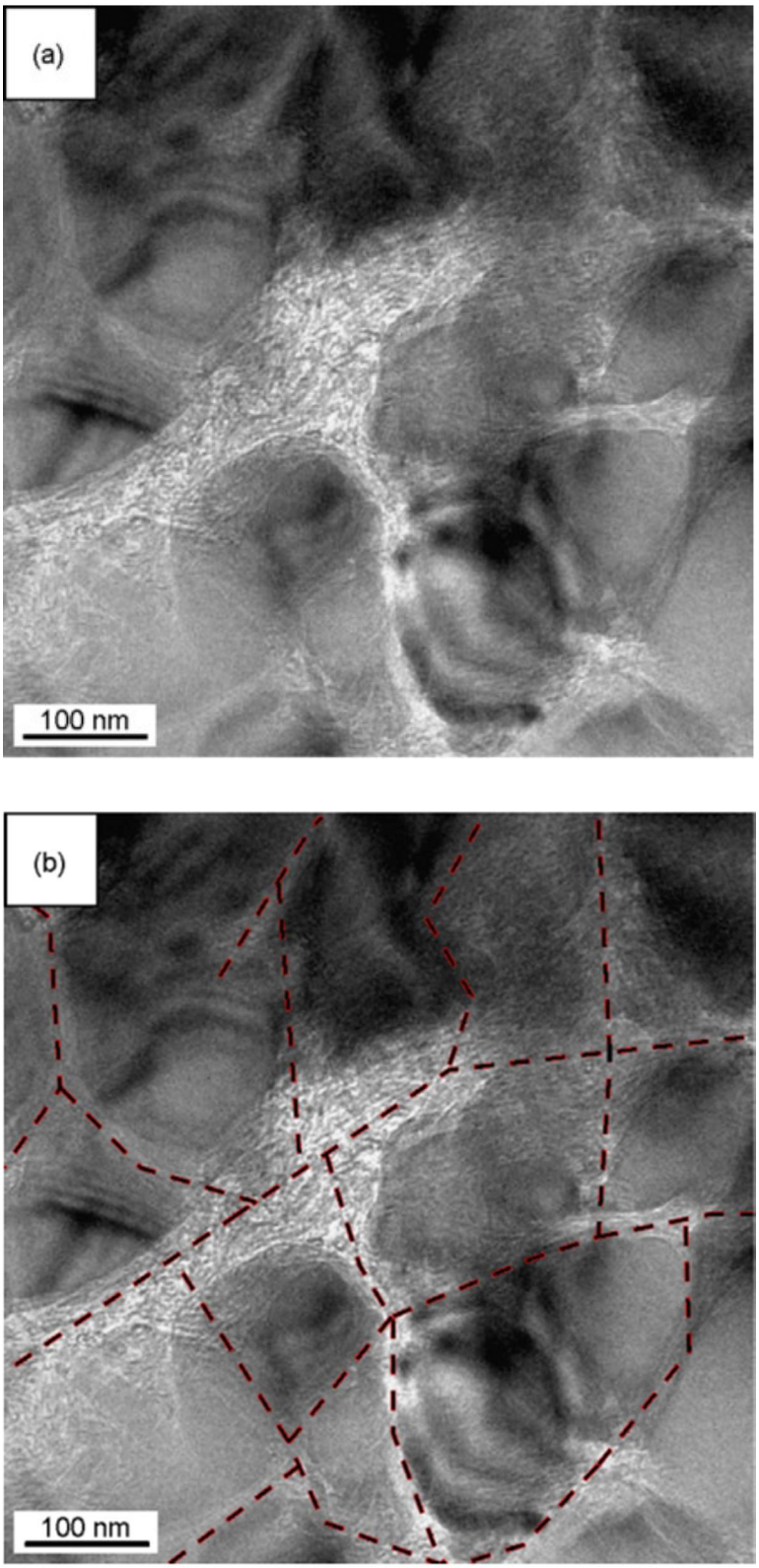

Figure 2.2 *TEM image showing (a) CNTs around the grains (b) highlighted CNTs network over the grain boundaries* [40]

Zhan *et al* [41]used ethanol to disperse SWCNT during sonication process and further alumina, separately dispersed in ethanol, was added to it slowly. He further sieved it through 200 mesh and ball milled the wet mixture using zirconia balls for 24 hours. Author claimed homogeneous distribution of CNTs within alumina matrix, as shown in **Figure 2.3**

Ahmed *et al*[29]discussed the effect, of altering MWCNTs contents in Al_2O_3-1SiC nanocomposite. Author used (0, 5, 7, and 10) (vol%) of MWNT with Al_2O_3-1SiC. Each composition was first ultrasonication of powder in ethanol and further used ball milling for 24hours in order to reach homogeneous distribution of reinforcement in the alumina matrix. After drying, powder mixtures were ready for consolidation. It was claimed the MWCNTS to reside over the grain boundaries, while SiC was found both on the grain boundary and with-in grains, as shown schematically in **Figure 2.4** and in actual FESEM micrographs **Figure 2.5**

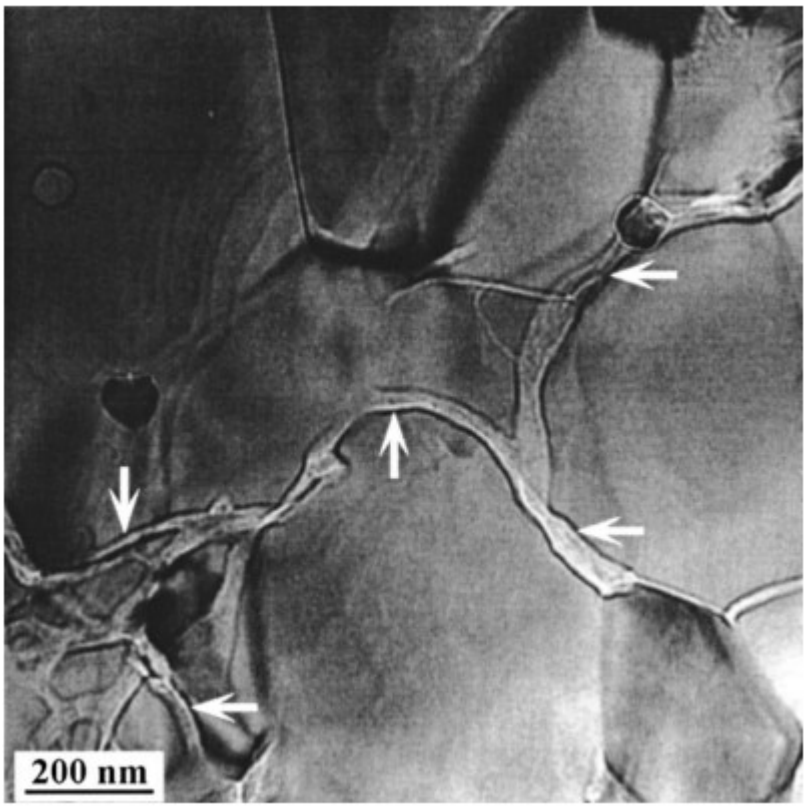

Figure 2.3 *TEM image of Al_2O_3-CNT nanocomposite, showing network of CNTs in matrix, as indicated by white arrows, at grain boundary* [41]

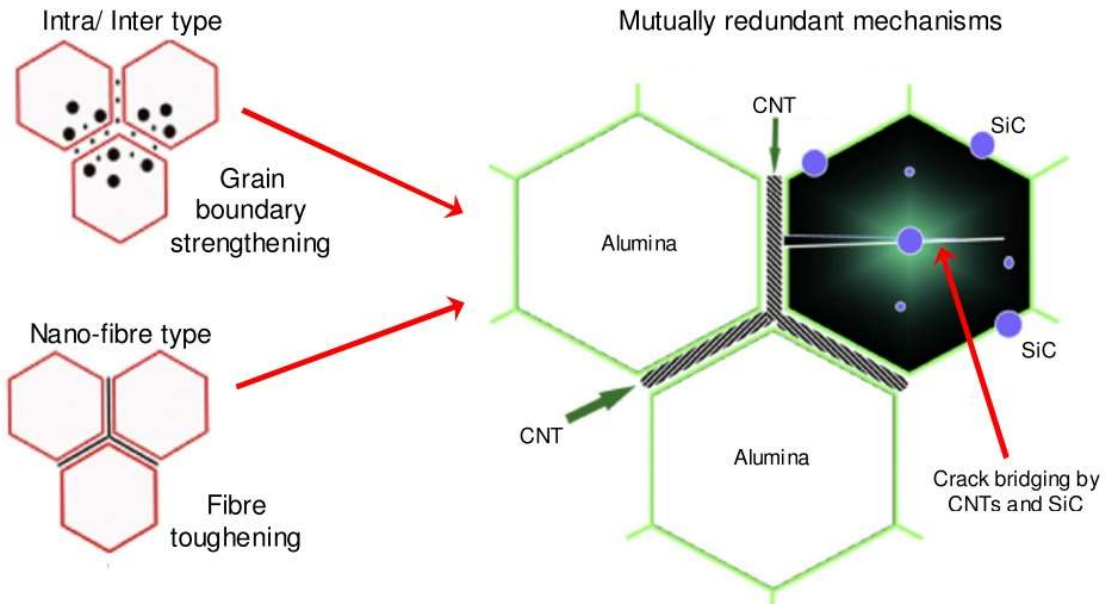

Figure 2.4 *Schematic of hybrid microstructure design of alumina reinforced by MWNTs and SiC nanoparticles* [29].

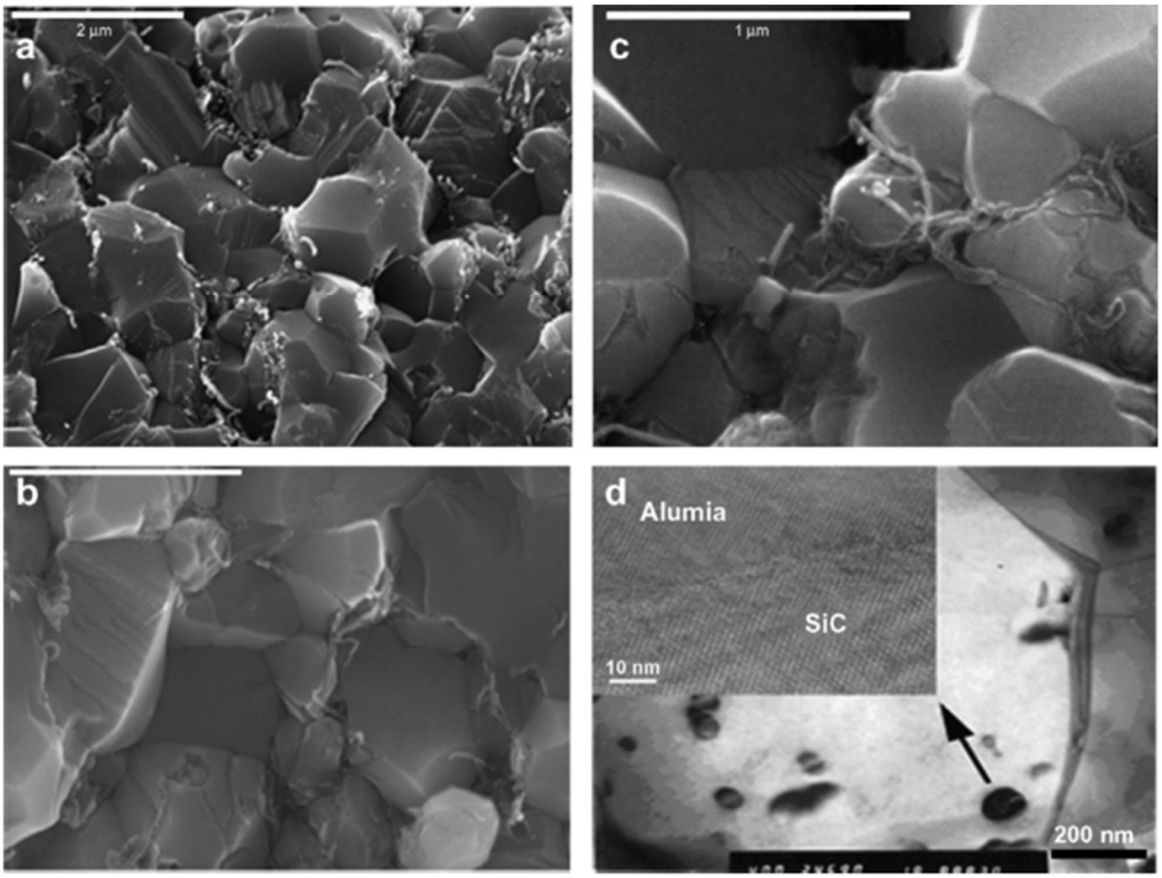

Figure 2.5 *(a) MWNTs (5 vol.%) are uniformly distributed in hybrid alumina composite. (b, c) Networks of MWNT around the alumina grains in 7 and 10 vol.% of MWNT with 1 vol.% of SiC reinforced alumina composites. (d) HRTEM picture shows typical microstructure of SiC* [29]

Further (a) showing uniform distribution in Al_2O_3-5CNTs-1SiC, (b & c) showing CNTs network in Al_2O_3-7CNTs-1SiC and Al_2O_3-10CNTs-1SiC, (d) showing TEM image of Al_2O_3-SiC interface[29].

Govindraajan *et al*[1] compared the effect of adding SiC and CNTs separately to ZrB_2 ceramic as a matrix. The author used WC vials and balls as media for dry milling. A very high 500rpm was used, although for a shorter time of only 8mins. It was found that dry milling with-out any sonication ended up in the distribution of CNTs network rather than uniform consistent individual CNTs.

J.Arsecularatne *et al*[19]used ethanol as a solvent in ultrasonically dispersing CNTs, further mixed it to a separately dispersed alumina. The mixed slurry was ball milled, meshed through 200 and further dried at 100ºC, which were then broken down using mortar and pestle. The author found a uniform distribution within alumina matrix with a saturation of 10%MWCNTs, where then aggregation of CNTs clusters was found to degrade mechanical properties of the nanocomposite.

Csaba*et al*[42] used simple manual mixing of powder mixtures and then added ethanol to it before planetary ball milling for 3hours. Surfactants (polyethylene glycol PEG was added after sonication process. The mixed powder samples were dried and green pressed before final consolidation. Effective uniform distribution of CNTs in the matrix was positively defended by the author.

Kovalc ˇı´kova *et al*[43] investigated the influence of MWCNT, prepared by CVD method. These CNTs were mixed with alpha alumina and other additives in planetary ball milling under ethanol as a dispersant. Further surfactants like PEG were also added under sonication. However, the non-homogeneous distribution of CNTs in the matrices was found as a prime source of getting non-consistency in the distribution of CNTs in the matrix.

Baron et al[44] suggested using 0.4% darvan to be used as a dispersant, in addition to DMF or ethanol. Alumina nanopowder was hand mixed, further dispersed in 0.4Darwan as a solvent, for a few minutes. Further, wet-mixture was milled for 8hours and then dried at 75ºC. The dried agglomerated mixture was passed through 250 mesh Homogeneous dispersed mixed powder was found as a result, which further was consolidated.

Chunxi *et al*[45] synthesized composite powder mixture through milling of acid-treated CNTs in the alumina matrix. 0.5g of CNTs with treated with 60ml acids H_2SO_4: HNO_3

(3:1) to increase its hydrophobicity. The flow chart shown in **Figure 2.6** was then followed to reach homogeneous dispersion of CNTs in the composite.

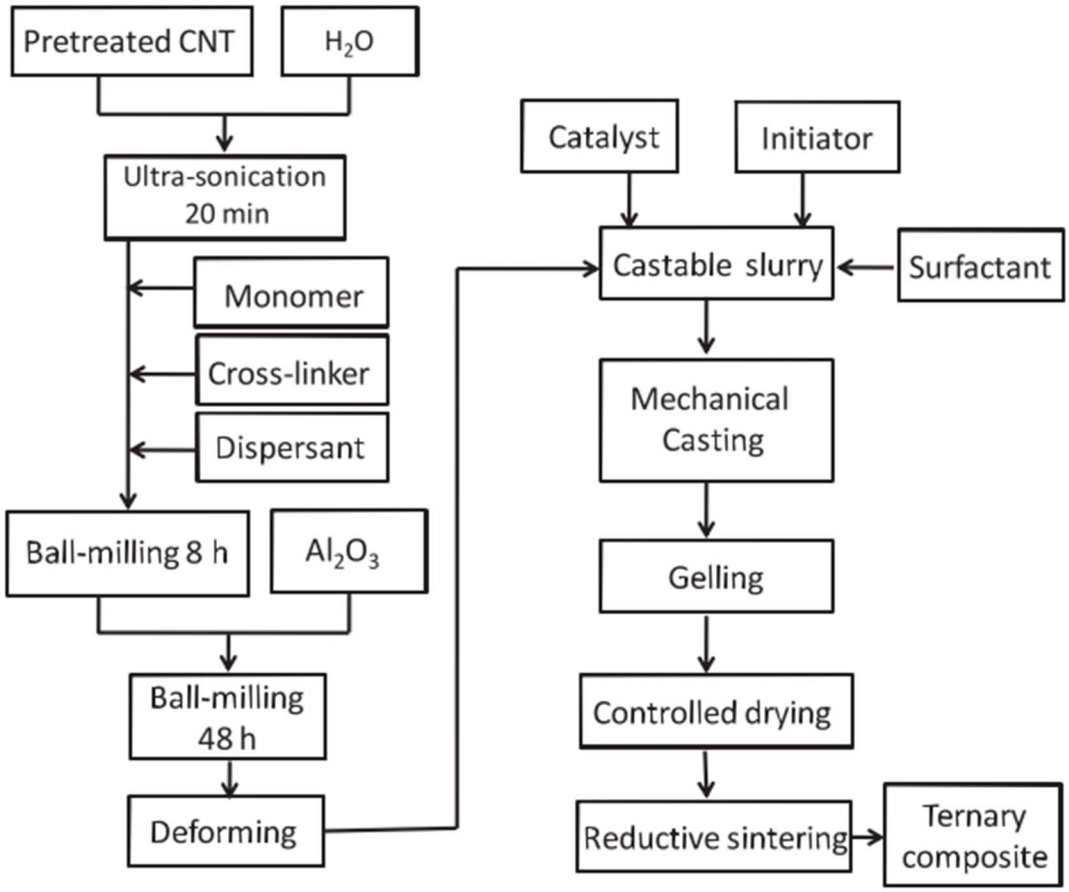

Figure 2.6 *Flowchart for processing of alumina-CNT nanocomposite* [45].

2.2.2 Sol-Gel Processing

The sol-gel process is an alternative route for homogeneously dispersing CNTs in inorganic matrices such as alumina. This wet chemical processing technique is superior to other solid state mixing processes, as it ensures excellent mixing of the multi-component system at an atomic level, high purity and low-temperature densification [47].Usually, precursors of ceramic matrices are used as starting materials, which are transformed to ceramic solution through hydrolysis followed by peptization of metal hydroxide. Further desired solid

phases, such as CNTs, can be added to it while sonication in water or any other solvent. At high temperature, a gel is produced due to precipitation within the solution [48]. The gel produced is further dried during calcination to achieve the homogeneous distribution of added nanoparticles into the matrix. The powder mixture resulted from this process is ready for consolidation through different sintering procedures.

Key advantages offered by sol-gel processes are using relatively low temperature during processing, synthesis of fine spherical powder particles, and further, it can produce compositions which are not possible by solid state fusion [49]. However, the cost of processing is usually high, which is main disadvantage of sol-gel processing. Further removing or vaporizing organics at later stages during processing, are harmful to health.

Peigney et al[50] synthesized Al_2O_3 based CNT-Fe nanocomposites using oxalates precursors of each component. Author decomposed the mixed solution of such oxalates at 200ºC and further got mixed powder composition after calcination at 1100ºC. XRD revealed monophase when Fe content was below the threshold value, however, multi-phases were observed otherwise. Later oxides were reduced to Fe+3 ions, which were found to be very active with the nanotube, and hence homogeneously distributed hybrid nanopowder mixture.

Chunxi hai et al[46] prepared homogeneous Al_2O_3-CNT nanocomposites by first dispersing 1 gram of pre-acid-treated CNTs in distilled water, and further milling it with alumina powder for 8hours. The slurry was meshed and further stirred with the aid of a vacuum pump to remove any traped air bubbles. Dried powder composite mixture showed homogeneous dispersion of CNT in the alumina matrix.

Homogeneous alumina-CNT nanocomposite powder was successfully prepared by chan Mo et al[51] using Aluminum tri-sec-butoxide (Al(OBus)3) as alumina precursor. An alumina sol was prepared using hydrolysis and peptization of (ALOOH). The author added separately dispersed MWCNTs in ethanol, which was added to alumina solution, and resulted in gel formation. Further, this gel was dried at 350ºC and after calcination at 1200ºC for 1hr, homogeneous dispersed alumina-CNT nanocomposite powder mixture was collected.

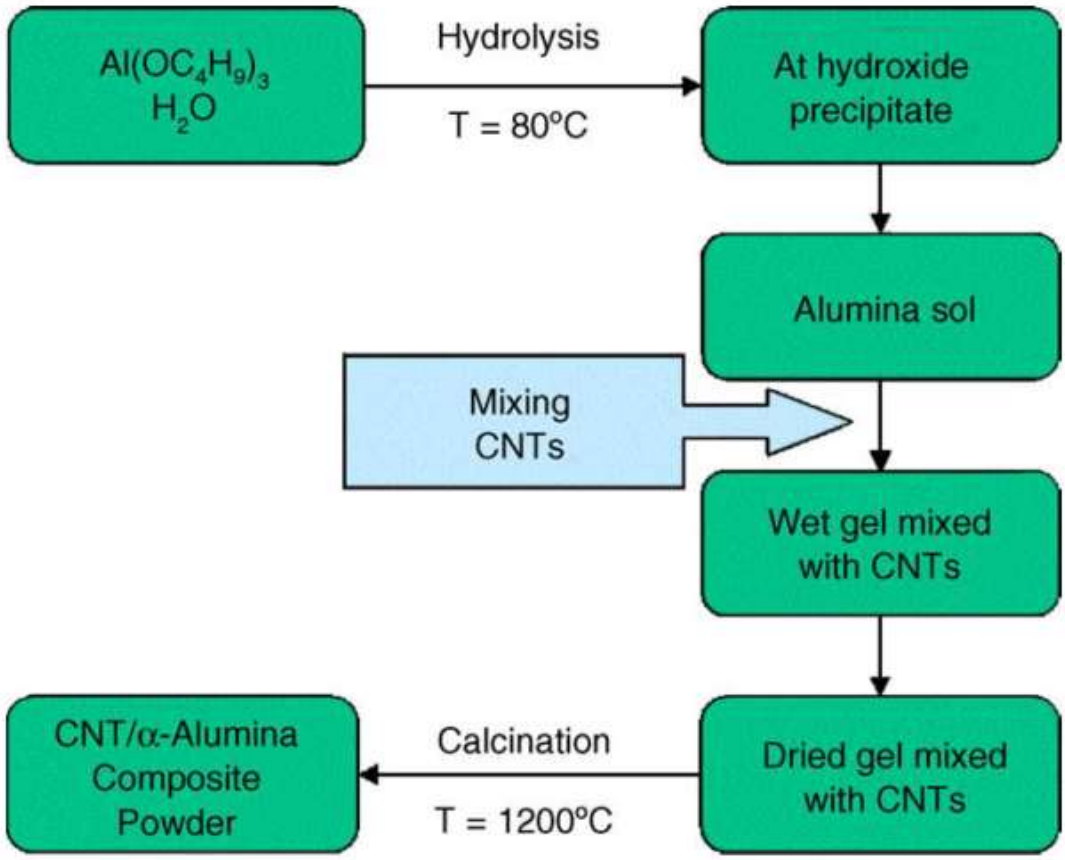

Figure 2.7 *Schematic chart for preparation of homogeneous Alumina-CNTs nanocomposite powder* [46].

2.2.3 Colloidal Processing

Uniform distribution of reinforcement in the ceramic matrix is obtained using the colloidal technique by controlling surface chemistry of suspended particles and CNTs in the solvent. Ceramic particles are coated on the CNTs surface. This helps to prevents agglomeration and favors homogeneous distribution of CNTs in the ceramic matrix. Impurity and surface charges of commercial fabricated CNTs are increased through acid treatment or functionalization, which adsorbs negatively, charged organic group and or oxygen containing groups. Hydrophilic nature of these treated CNTs enhances their stability in alumina based high PH aqueous solutions [15].

J. sun et al[24] prepared carbon nanotube (CNT)/alumina composites using colloidal processing. Pristine CNTs were first treated using NH3 to change their surface properties and were then put into a solution containing a dispersant (polyethyleneimine). A very dilute suspension of α – alumina was separately prepared using de-ionized water. NaOH was used to adjust PH of this dilute alumina solution, which was further drop-wise added to already prepared CNT suspension. The coated CNTs were collected and subsequently added to concentrated alumina suspension. Collected powder composition was collected and dried for further consolidation. It was found that only 0.1wt% surface modified CNTs in alumina enhanced fracture toughness of material from 3.7 to 4.9 $Mpam^{1/2}$.

Portman *et al* [48] prepared Al_2O_3-MWCNTs through colloidal processing. Water based CNT and Al_2O_3 suspensions were prepared separately at PH of 4. Both solutions were mixed after controlling zeta potential of each, confirming complete distribution of each. Liquid nitrogen was used to freeze homogeneity in suspensions, which later was freeze-dried. Complete homogeneous distribution was confirmed through FESEM analysis.

Kumari *et al* [49]used CVD method to prepare direct growth of CNTs over alumina nanoparticles. These CNT-alumina particles were further mixed in ethanol through sonication to further enhance the distribution of the surface attached alumina with the rest of alumina particles. Co(NO3)2-6H2Owas used as catalyst precursor in the reaction.

2.2.4 Molecular Level Mixing

The use of promising methods such as molecular-level mixing process [50] enabled researchers to uniformly disperse carbon nanotubes or graphene in metal [50][51][52] and ceramic [23][53] matrices. This process involves chemical bonding between functionalized CNTs and metallic ions [54]. CNTs are functionalized to generate COOH− functional groups on the surface of the tubes. The metallic ions are obtained through the dissociation of a metallic salt in an organic solvent. Heating of the dried mixture in normal atmosphere leads to the formation of an amorphous Al_2O_3 matrix, embedded with CNTs and SiC nanoparticles, which crystallizes during subsequent sintering.

The thermodynamic equations governing its formation were expressed by Lee and co-workers [53] according to [55][56] as follows:

$$Al^{3+} + 3(OH)^{-} \rightarrow Al(OH)_3 \, , \Delta H = 61.3 kJ/mol$$

$$Al(OH)_3 \rightarrow (1/2)\ Al_2O_3 + (32)H20, \Delta H = 101.89 kJ/mol \text{ at } 273K.$$

This newly developed mixing technique is an extension to the existing CNT/metal nanocomposite which involves matrix material in a solution instead of conventional powder form [50]. Metallic salts are used and dissociated into required positive metal ions. In

addition, certain organic groups negatively charged such as OH- and or COOH-, are being attached to CNTs through functionalization process as shown in Figure 2.8.

The ionic bonding between functionalized CNTs and positively charged metal ions associated mixing at molecular level which in addition to restricting agglomeration of CNTs, also enhances the interfacial bonding strength, as comparative to solid state mixing. Thus molecular level mixing addresses and solves both main hurdles, in reaching expected mechanical properties to CNT-ceramic nanocomposite. The process of molecular mixing involves mixing of metallic ions e.g Al^{+3} to surface treated CNTs. Negative groups such as COOH on the surface of CNTs, as shown in Figure 2.9, help to reduce vander walls attractive forces between CNTs thus restricts formation of clusters. Further metallic ions are added to surface treated CNTs through sonication process, which chemically attach these positive metallic ions to the negatively charged CNTs through columbic forces. This enhances interfacial bonding between alumina as matrix and added second phase CNTs [23]

The process of functionalization involves treating CNTs with different acids such as HF, HNO_3 andH_2SO_4, which further are oxidized at 190ºC for 4 h to remove catalysis particles and to generate functional groups on the surfaces of the nanotubes. Functionalization of CNTs is discussed in [57].

Al_2O_3 based nanocomposites can be synthesized through molecular level mixing which involves complete dispersion of acid-treated CNTs, in solvents such as distilled water, ethanol or DMF Dimethylformamide, through sonication process. Further Al-salts such as $Al(NO_3)_3.H_2O$ is dissociated into Al^{+3} when added into the same solvent suspension of CNTs. Al^{+3} appeals to CNTs through ionic bonding with improved interfacial strength.

Later mixed solution is dried, calcined to get desired homogeneous dispersion of CNTs in Alumina matrix.

Different other Al-salt, as shown in Table 2.1 can also be used. The two slurries were mixed and sonicated for another 15 hours.

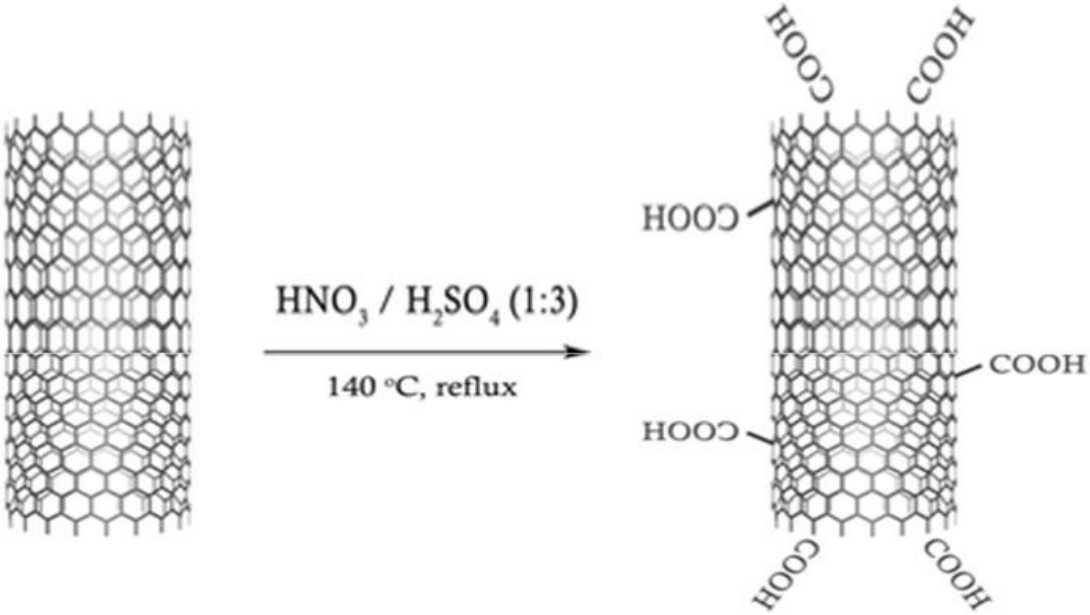

Figure 2.8 *schematics for chemical functionalization of carbon nanotube*[47]

Table 2.1 *Few Al-Salts, which can be used as Alumina pre-cursers.*

Name	Salt chemical formula	Formula weight	Concentration	g/l
Aluminum nitrate	$Al(NO_3)_3 \cdot 9H_2O$	375.13	0.1	37.5
Aluminum chloride	$AlCl_3 \cdot 6H_2O$	241.43	0.05 M	12.1
Aluminum sulfate	$Al_2(SO_4)_3 \cdot 18H_2O$	666.42	0.1	66.6

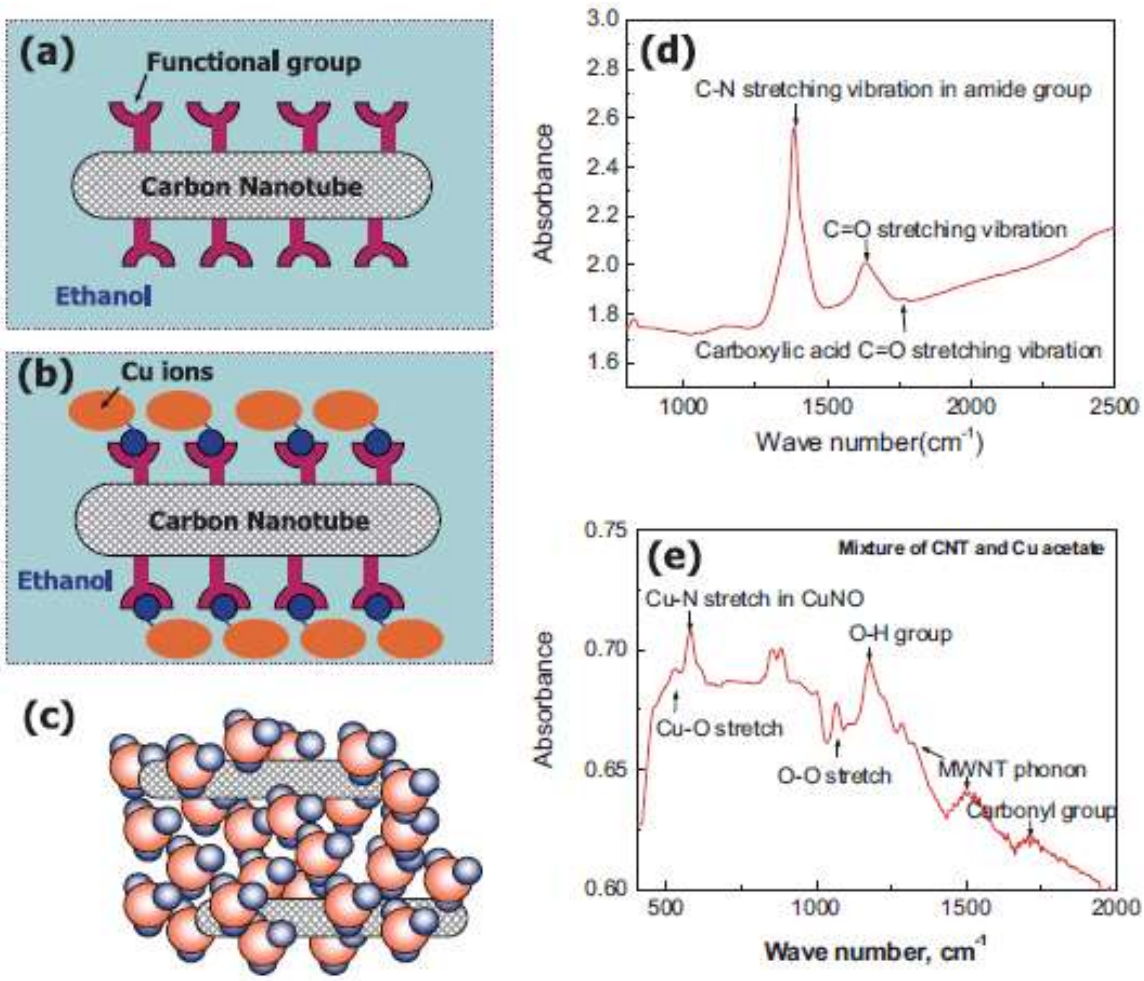

Figure 2.9 *Schematic diagrams showing different steps of molecular-level mixing process of Cu-CNT nanocomposte* [48]

2.3 Nanocomposite Powder Consolidation

2.3.1 Spark Plasma Sintering

Consolidation methods are processing of transforming loose powder into solid compact shapes using thermal energy. The process includes joining crystalline or amorphous powder particles together without being melting them. Although a small amount of liquid may form

between powder particles in certain cases, at high temperatures, as a result of the presence of any low-melting component in the powder mixture which is then called as liquid phase sintering. However actual bonding or fusion between distinct powder particles is the result of atomic diffusion which occurs at sintering temperatures which are well below the melting point of the materials.

Some of the advantages of consolidation are achieving complex compacted shapes with improved mechanical properties. Further, the powder materials can retain their inherited properties, as the sintering can be done under controlled environments. In addition purity of the material is also retained due to few processing steps involved during consolidation methods.

During the conventional sintering process, larger grains will consume smaller, thus further growing their sizes (grain growth), through Ostwald ripening processes. However increasing grain sizes reduces mechanical properties of the final consolidated product, therefore there is a growing demand for processing and consolidating nanopowders, in addition reserving their nanostructure during sintering process is another challenge.

Spark plasma sintering is a newly growing evolved sintering technique, which overcomes these obstacles and hurdles in holding back nanostructure of the final compact shape. Very high heating rates, lower sintering temperatures, and small dwell timings during spark plasma sintering makes it dominant over usual conventional sintering techniques. This helps in restricting grain growth to occur, thus retaining initial nanostructure and hence resulting in improved mechanical properties of the final consolidated product.

Spark plasma sintering, in addition to high applied pressure, generates high pulsed (plasma) discharge DC between powder particles, thus enabling efficient flow of heat and hence

diffusion between powder particles[59], [60]. These combinations of SPS parameters are effective in obtaining fully dense nanocrystalline composites.

Advantages of spark plasma sintering includes

- Generation of plasma between powder particles preserves integrity of initial structure without any grain growth.
- Combination of highly applied pressure and spontaneous powder particle heating drastically reduces sintering temperature and holding time.
- Intact plasma between particles increases surface activity and thus increases both diffusion rate and relative densities.

2.3.2 Microwave Sintering

Microwave sintering is another advanced non-conventional process, which uses microwave energy to transform powder composition to solid compacts. Microwave sintering is different from usual conventional heating processes, which conducts resistance heating to the inside of the powder to be compacted. However, in Microwave heating, volumetric electromagnetic heating is transformed into thermal energy, which is more uniform, instantaneous and rapid [61]. This energy is absorbed by materials having a high dielectric loss which increases its temperature. However certain materials have a low dielectric loss at lower temperatures, thus cannot increase its temperature, as microwave energy will be passing through Susceptor, as shown in Figure 2.10 are fine nano-SiC powders, which have a very high dielectric loss even at a lower temperature, are usually used in sintering such materials. The materials having a low dielectric loss at lower temperatures are placed within susceptors, which will be heated and which further will heat sample materials through

convection. This combined effect of microwave and microwave –coupled external heating source (microwave hybrid heating) is useful in heating sample material from both inside and outside [62].

Beside dielectric loss of the material, the ionic and electrical conductivity of the material and magnetic coupling are some of the important factors in contributing to the microwave heating. Some of the vital advantages of Microwave sintering listed in [63] are

- Drastic reduction of required energy, as directly heating sample materials preserves energy in heating furnace or reactor walls simultaneously.
- High heating rates reduces required sintering time.
- Direct volumetric heating reduces thermal gradients in sample materials.
- It results in more relative densification and more uniform grain size distribution.

Fine micro structural development, average fine grains, and uniform densification increases mechanical properties of the compact sample.

Selective heating is another significant characteristic of microwave sintering.

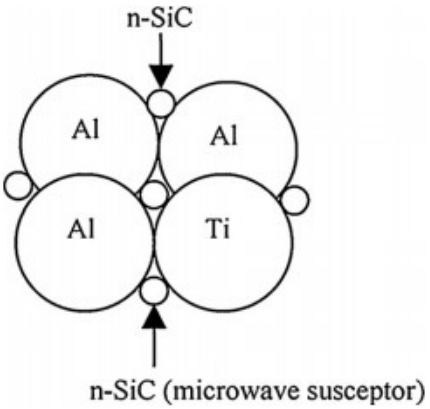

Figure 2.10 *Schematic of susceptors, being used for microwave sintering of materials having high dielectric loss at lower temperatures* [49]

2.3.3 Hot Pressing

As the name implies, hot iso-static pressing (HIP) is a combination of heating and high hydrostatic pressure, which are applied to powder particles, thus transforming them to solid compact shapes. During HIP process, powder mixture of different components are placed with a steel can, which is subjected to high temperature in addition to high applied hydrostatic pressure and very high vacuum to eliminate any internal micro shrinkages, resulting in complete homogeneous solid compact.

Some of the advantages of HIP are

- ❖ Combination of high pressure and heating provides uniform dense structures with improved mechanical properties.
- ❖ HIP produces near-net required shapes, thus reduces the machining operation on the final compact, which may degrade structure and hence properties.

2.4 Strengthening Mechanisms

Load transfer

The difference between young's modulus of matrix and reinforcement in composites gives rise to different stresses experienced by each when they are deformed at the same strain. Higher stresses are subjected to CNTs, having high modulus than Al_2O_3, and thus carry more load than the matrix. However, this load transfer from matrix to reinforcement requires a strong and intact interface between them. It is usually recommended to select reinforcement which satisfies a ratio of two or more between young modulus of reinforcement to that of the matrix. However, this is not the case for ceramic composite, where toughening rather than strength is the main concern.

Pre-stressing of matrix

The matrix experience low external applied stresses when it is pre-stressed with opposing compression stresses, which are generated due to its low thermal expansion coefficient than as compared to that of reinforcement. Internal compression stresses superimpose the external tensile stresses and thus reduces it.

Strengthening through toughening

Strength of the composite is directly related to its fracture toughness through the mathematical relationship, $\sigma_f = \beta(\frac{K1c}{C_2^1})$, where K1c is fracture toughness and c is the critical crack length, while β is a constant. The relationship shows a direct relationship between the toughness of a material to its strength, therefore increasing the toughness of the material through mechanism shown in the following section will automatically increase

the strength of the material. However, this requires keeping critical crack length below a certain limit, which otherwise will decrease the strength of the material. The critical crack or flaw size in a ceramic matrix is reduced by the fine dispersion of nano ceramic particles, resulting in an increase in strength for a nanocomposite. The introduction of nano ceramic particles, even at small volume fraction loading, into a ceramic matrix causes the development of residual stresses around the particles. These residual stresses significantly enhance strengthening of the matrix.

2.5 Toughening Mechanisms

Ceramic matrix composite consists of one or more reinforcement, being incorporated in a ceramic matrix. Different material (matrix and reinforcement) have different thermal expansion coefficient, which gives rise to residual stresses during cooling from sintering temperature, as each cools at a different rate. If the thermal coefficient of expansion of reinforcing agent (fiber or particulate) is greater than that of the matrix, a gap (vicinity) is formed at the matrix-reinforcement interface, as the matrix will cool slowly than reinforcement. This gives rise to radial tension in the matrix. While radial compression generated in case if thermal expansion coefficient is smaller than that of the matrix. These residual stresses can also be generated at matrix-reinforcement interface through the volumetric changes due to phase transformation, if any, during heating or cooling of the composite material. Several toughening mechanisms, as discussed below, can be activated and controlled by controlling magnitude and type of residual stresses. One or more toughening mechanism can be activated at a time in a ceramic composite material. The effectiveness of toughening mechanism depends on several factors such as

- Size, shape and morphology of the reinforcement.
- Interfacial bonding between matrix and reinforcement.
- Residual stresses due to either thermal expansion co-efficient difference and or phase transformation difference between matrix and reinforcement.

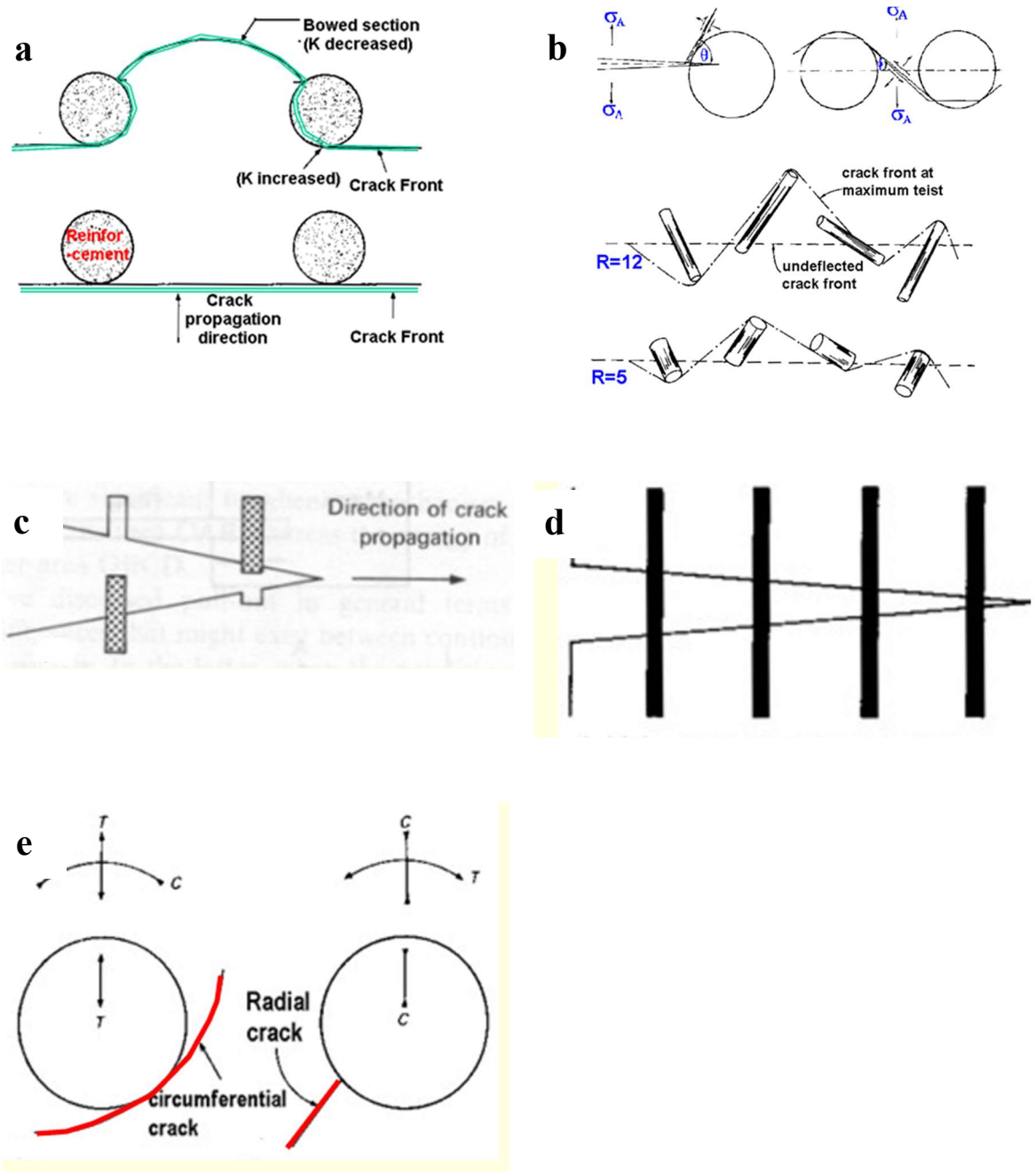

Figure 2.11 Different toughening mechanism in ceramic matrix composite, reinforced with round particles and or CNTs (a) crack approaching and then bowing around a round particle, (b) crack deflection around a particle and or elongated reinforcement with different aspect ratio 'R, (c) de-bonding and CNT pull out, (d) crack bridging and (e) micro-crack toughening mechanism.[50]

Crack bowing

Crack bowing mechanism is activated, when the energy of a primary propagating crack is consumed by bowing around the fibers or particles, rather than passing beyond it. Stress intensity factor decreases along the bowed section in the matrix, while it increases at the reinforcement. Crack is being bowed, as far as the stress intensity factor at the reinforcement is lower than that of the reinforcement itself. Bowing around the particle or elongated reinforcement consumes energy, which increases the toughness of the composite material. Crack bowing toughening increases with increasing volume fraction of the reinforcement, aspect ratio and properties of the reinforcement itself. Strong reinforcement and good interface, which can act as a strong barrier, is required in such toughening mechanism.

Crack deflection and branching

Primary crack extension direction may get deflected, if it interacts with any obstacle, such as fiber, or particle or even micro-cracks. Deflected crack will now travel longer and respectively the stress intensity is lowered at the crack tip. In the case of fiber reinforcement, a crack may be deflected along the fiber-matrix interface, which facilitates fiber-pull out, which is another toughing mechanism. Crack may also get a deflection or branched into more than one direction if it interacts with any microcracks present in the process zone.

Residual stress may also deflect a propagating crack. For example, the radial tension on a particle, having high thermal expansion coefficient than the matrix, will force the crack to travel around it [65]. Further compression stresses at a distance from the particle will contribute to enhancing toughness of the material. Second phase reinforcement with rod-like shape and high aspect ratio is most effective in enhancing crack deflection pull-put mechanism. Deflection toughening increases with increasing volume fraction and or aspect

ratio of the elongated reinforcement. High aspect ratio of the reinforcement increases the twist and deflection of a propagating crack.

De-bonding and Fiber pull-put mechanism

A shear stress is established in a particle and or CNT reinforced ceramic matrix composite and leads to a tensile stress along the CNT-matrix interface, as the applied load is transferred to the reinforcement. This tensile stress, if sufficient will pull the CNT from the matrix, which requires work and hence toughening mechanism is achieved in the system. However, the system requires a strong interface to give reasonably high work of pull out and to minimize strength in the material system. Interfacial bonding between matrix and fiber depends on chemical binding and or mechanical friction between the two surfaces. It is also possible to alter the interfacial characteristics through surface modification of the fiber reinforcing agent to enhance fiber toughening mechanism.

Crack bridging

If the propagating crack passes beyond reinforcing fiber, such that fiber remains intact and bridge the crack surface, which in-turn will make further propagation difficult and thus toughens the material. It is vital for the fiber to be prevented from damage, either through debonding of fiber from the matrix or high strengthen fibers. Toughening through crack bridging requires high strength, diameters and volume fraction of fibers.

Micro-cracking

The toughness of any material can be enhanced by the presence of micro-cracks, due to crack blunting, branching and or deflection. However micro-crack toughening mechanism is effective on limited density and size of the crack. Thermal miss-match between the matrix

and the second phase generates residual stresses. These stresses, if sufficiently large enough, will generate radial and or circumferential microcracks in the matrix. Usually, stresses and hence stress intensity factor is high at any macro-crack tip, if present. This forms micro-cracks in the vicinity of the macro-crack tip, thereby forming process zone around the macrocrack tip. Since the energy of the primary crack is consumed in generating new micro-crack surfaces in the process zone, thus reducing stresses and hence stress intensity factor at the primary crack tip. This increases the toughness of the material. Stress field around the macrocrack tip can also be lowered, if energy is consumed due to either volumetric deformation caused by phase transformation and or micro-ductility in the process zone. Further primary crack may get deflected or branched due to the presence of microcracks, which provides addition toughening mechanism..

.

2.6 Alumina Based nanocomposites

There is fast growing interest in new applications for high-performance ceramic based materials [66] and has an excessive potential to substitute high-temperature metals with superior performance due to its chemical stability and relatively high hardness and wear resistant [67]. Alumina, owing to its low-cost and ease availability [68] is dominant and most commonly preferred ceramic material in structural [69] and bioceramics [70].

However, its intrinsic property of low toughness [71] limits their relevance in many industrial applications such as tool industry [2] and several other load bearing structural and bio-applications [72].

The addition of second phase reinforcement in the alumina matrix, developing ceramic composite can induce a significant increase in fracture toughness [4]. Shape and size of reinforcement in addition to its chemical affinity or interfacial bonding with the matrix, controls the mechanical properties of the developed composite[5] and usually owing to increased surface and contact area, fine particles[6], whiskers[7], platelets[8] reinforced nanocomposites are developed to target high toughness in the material.

Second phase incorporation into alumina matrix, particularly with different morphologies such as SiC nanoparticles[51], carbon nanotubes [52], leading to the production of alumina matrix composites [53] has been the recent focus of scientific research.

2.6.1 Al_2O_3- SiC nanocomposites

Alumina ceramics are widely used in certain high-performance IC in electronic applications and tooling industry, which generates a large amount of heat during operations but low thermal conductivity of alumina substrate impedes heat dissipation from these materials thus lowering their performance efficiencies and life. SiC, having higher thermal conductivity, is therefore added to alumina substrate to drain generated heat at higher rates thus improving their performance and reliability.

Addition of SiC nano-particles (3,4), platelets(5) and whiskers(6), as second phase reinforcement, to alumina matrix improves its mechanical properties in addition to its thermal conductivity.

Table 2.2 *Synthesis parameters and consequent findings in Al_2O_3-SiC nanocomposite from literature*

Composite	**Synthesis method**	**Consolidation method**	**Remarks**	**Ref**
Al_2O_3-SiC	Ball milling	Hot pressed	Composite containing 20 vol.% of coarse-grained SiC resulted in maximum flexural strength (655 ± 90 MPa) . However insufficient improvement in hardness and fracture toughness were reported.	[10]
Al_2O_3-0.2SiCNW	Ball milling	Hot pressing	Grain size of alumina reduced by 20%, which increased hardness by 10%, while reducing fracture toughness by 15%. Further thermal conductivity increased by 45%, by addition of only 0.2%SiC.	[12]
Al_2O_3-SiC	Ball milling	Hot pressing	5 vol% SiC resulted in almost 50% increases in strength of the nano composite. Hardness at the cost of toughness was increased. Relative densification slightly reduced by addition SiC.	[30]
Al_2O_3-SiC	Milling + freeze granulation of dispersed constituents	Pressure-less sintering in Ar atmosphere.	Highly homogenous distribution than as comparative to conventional Al_2O_3-SiC processing route. SiC was found to restrict grain growth. Nano particles of SiC were synthesized during in-situ sintering	[6]
Al_2O_3-SiC	Sonication	Pressure less sintering + hot pressing	Water based solvents were not suitable for complete dispersion. 0.5-5Vol% of ultrafine SiC hinders densification however restricts grain growth. Hot pressing was effective in getting almost full densification.	[54]
Al_2O_3-(1-20wt%)SiC	Ball milling	Hot pressing	Fracture toughness was reported to increases with increasing SiC and recorded maximum value of 7.6MPam$^{1/2}$ for 5wt%SiC. However it decreased with further increase in SiC content.	[55]

Al_2O_3–(0-30wt%)SiC	Ball milling	Hot pressing	Hardness increased with the addition of hard secondary phase SiC, which inhibited grain growth. Fracture toughness increased till 10wt% addition, and decreased for any further addition.	[56]
Al_2O_3-SiC			Hardness of Al_2O_3–SiC nanocomposites increased linearly with SiC content.	[57]
Al_2O_3-SiC	Ball milled	Pressure-less sintering	Increasing vol% of SiC up to 5, hardness and fracture toughness were improved, whereas by increasing more than 5 vol% of SiC, hardness increased but fracture toughness decreased. SiC nanoparticles inhibited the grain growth of Al_2O_3 and reduced the matrix grain size accordingly.	[58]
Al_2O_3-SiC		Spark plasma sintering	Lower additions of the reinforcing components showed full densification, however higher content addition reduced attained density. 20.7GPa and 4.7MPa.$m^{1/2}$ were documented as maximum hardness and fracture toughness.	[59]

M. Parchovianský et al[10] synthesized Al_2O_3–SiC using ball milling and then consolidated it using hot pressing. It was reported that composite containing 20 vol.% of coarse-grained SiC resulted in maximum flexural strength (655 ± 90 MPa). However, insufficient improvement in hardness and fracture toughness were reported.

N. Jiraborvornpongsa et al[12] used 0.2wt% SiCnw as reinforcement in alumina and prepared the composite mixture using ball milling. The mixed powder was further sintered using hot pressing. It was found that grain size of alumina was reduced by 20%, which increased the hardness of the composite by 10% while reducing fracture toughness by 15%. Further thermal conductivity, however, was increased by 45% for the same composite.

M. Sternitzke et al[30] prepared Al_2O_3-SiC using ball milling and further consolidated the composite using hot pressing. The author reported that addition of 5 vol% SiC resulted in almost 50% increases in strength of the nanocomposite. Hardness was also found to increase, although, at the cost of fracture toughness. Relative densification was also reported to reduce in the composite.

S. Gustafsson et al[6] synthesized Al_2O_3-SiC using wet milling. The author claimed to improve dispersion of SiC using freeze granulation of dispersed wet slurry and reported highly homogenous distribution than as comparative to conventional Al_2O_3-SiC processing route. The homogeneously dispersed composite powder was consolidated using pressureless sintering in an argon atmosphere. It was reported that SiC was found to increase the hardness of the composite, which was accredited to restricting grain growth.

B. Mar [76] documented that. 0.5-5Vol% of ultrafine SiC hinders the densification behavior, however, restricts grain growth, which further increases mechanical properties of the nanocomposite.

Dong et al. [77] prepared Al_2O_3-SiC composites with 1-20 wt.% SiC by hot pressing at 1908 K and 25 MPa pressure for 1 hr. The authors found that the fracture toughness increased with the addition of SiC up to 5 wt.% to reach a value of 7.6 $MPam^{1/2}$ and decreased with further increases in SiC content.

Ko et al. [78] demonstrated that the fracture toughness of Al_2O_3-SiC composites with 5-30 wt.% SiC hot pressed for 2 h at 1823-1973 K at a pressure of 25 MPa remained constant up to 10 wt.% of SiC. The hardness of the composite was found to enhance due to secondary phase SiC, which inhibited grain growth.

Nakahira [79] reported hardness of Al_2O_3–SiC nanocomposites increased with increasing SiC content.

S. Ghadami and R. Baharvandi [80] investigated the influence of SiC content in the Al_2O_3-SiC composite. The author reported that hardness and fracture toughness were improved with increasing SiC up to 5vol%, whereas increasing more than 5 vol% of SiC, hardness was found to increase but fracture toughness decreased. The increase in hardness was attributed to SiC nanoparticles, which inhibited the grain growth of Al_2O_3 and reduced the matrix grain size accordingly.

J. Oluwagbenga and Rokebrand [81] investigated densification and respective mechanical properties as a function of SiC content. It was reported that lower additions of the reinforcing components showed full densification, however, higher content addition reduced attained density. Maximum hardness and fracture toughness values of 20.7GPa and 4.7$MPa.m^{1/2}$ respectively were documented for the composite.

2.6.2 Al_2O_3-CNTs nanocomposites

Due to high mechanical properties, low density and high aspect ratio, CNTs have received wide attention and thus are widely used as reinforcement in alumina, intending to increases toughness of material. CNTs were added in alumina matrix through ball milling [41][82][83], sol-gel[24][27] [47][48] [84] and or through molecular level mixing method[23] [85].

Carbon nanotubes have high electrical conductivity than carbon black [41] and therefore electrical conductivity of Al_2O_3-CNT was found to increase by 4 times, when carbon black was replaced by fibrous CNTs, due to increased density of CNTs at the grain boundaries. Additionally, CNTs were also found to have self-lubricating property at the grain boundary [82]. It was reported that full densification can be ascertained at lower temperatures by addition of CNTs. Further strong CNTs network around alumina grains restricts their abnormal growth. Low wear loss in Al_2O_3-CNT composite is also reported earlier [83]. Strong CNT network is attributed to its intrinsic behavior of making agglomeration and thus hinders homogeneous distribution of CNTs in a matrix. Dispersion of CNTS is further complex in composites having higher CNT content, which if not distributed well in the matrix, will degrade mechanical properties of the composite. The Al_2O_3-CNT composite powder was prepared using colloidal process instead of ball milling, in-order to reduce the risk of reducing CNT length during milling operation [84]. The author reported a mixture of gum arabic and SDS sodium dodecyl sulphate, to be very effective dispersant. Acid treated CNTs instead of pristine are also reported to increases dispersion and homogeneity in the microstructure. G. Yamamoto *et al* [20] reported increased dispersion and homogeneous microstructure with the addition of less than 1Vol% acid-treated CNTs

instead of pristine. 27% and 25% increase in bending strength (689.6±29.1MPa) and fracture toughness (5.90±0.27 MPam1/2) respectively was reported for the composite containing acid-treated CNTs.

Sun *et al* [18] reported the homogeneous distribution of CNTs in alumina matrix and documented subsequent 32% increases in fracture toughness and 10% in Bending strength. Author, however, reported that longer dwell time at sintering temperature sharply decreased mechanical properties due to grain growth.

However higher content of CNT in alumina matrix is found to increases risk of agglomeration and reduce complete dispersion [27]. The author reported a remarkable increase in fracture toughness although at the cost of hardness, density and flexural strength. It was also documented that mechanical properties of 2% were better that 5%CNTs. Higher CNT content increases the possibility of cluster formation and the rigid network of CNTs [48] around alumina grains, which effectively reduces density (92-93%) although high thermal conductivity was reported due to high aspect ratio. However higher content of CNTs was found to reduce toughness. The same findings were reported earlier [19], where vickers hardness of Al_2O_3-CNT composite decreases after 10%MWCNTs. However higher CNT content of 12vol%CNTs in alumina reported 4%decreases in bending strength, although showed 80% increase in fracture toughness (5.55±0.26) $MPam^{1/2}$ [21]. CNTs were also replaced by CNF and almost same findings were reported in [86], where 13% increase in fracture toughness was documented at the maximum addition of 2.5vol% of CNF, however mechanical properties were degraded with the further addition of CNFs. Fan et al[22] reported that addition of only 1% SWCNTs increased fracture toughness by 103%

reaching values of 6.40±0.3 $MPam^{1/2}$. Crack bridging and deflection were noticed as the prime toughening mechanism.

Pal *et al* [85] reported that maximum amount of CNT, that can be homogeneously distributed was increased from 3% to 10% when molecular level mixing method was adopted instead of conventional mixing. The author further reported that high-temperature sintering resulted in higher densification and consequently high hardness values. Maximum hardness of 11.50Gpa, (12.21%increases) was achieved with 7.5vol% CNTs.

***Table** 2.3 Synthesis parameters and consequent findings in Al_2O_3-CNT nanocomposite from literature*

Composite	**Synthesis Method**	**Consolidation Method**	**Remarks**	**Ref**
Al_2O_3- CNTs	Ball milling	Spark plasma sintering	Electrical conductivity increased by 4 times, when carbon black was replaced by fibrous CNTs, due to increased density of CNTs at the grain boundaries.	[40]
Al_2O_3- CNTs	Ball milling	Spark plasma sintering	Addition of CNTs reduced the sintering temperature required for full densification due to self-lubrication properties. Further strong CNTs network around grain restricts their abnormal growth.	[60]
Al_2O_3- CNTs	Ball milling	Hot pressing	Introduction of CNTs in alumina ceramics reduces the wear loss of the composite.	[61]
Al_2O_3-MWCNTs	Colloidal Process	Spark plasma sintering	Highest electrical conductivity reported for 1%CNTs is almost 90 (S/m) while fracture toughness achieved was 4.8Mpam$^{1/2}$. Mixture of gum arabic and SDS sodium dodecyl sulphate was found to be very effective dispersant.	[62]
Al_2O_3-CNT	Stress distribution and intensity at Al_2O_3-CNT interface is studied using COX model.		Stress distribution over the interfacial area has been studies using cohesive law, which narrates a maximum tensile stress of 0.68Gpa at strain of 0.68%. Further maximum stress affordable by the wander waals interaction, after which interfacial slip starts to occur, was also found.	[63]
Al_2O_3-MWCNT	Colloidal	Hot pressing	Fracture toughness remarkably increased although at the cost of hardness, density and flexural strength. Mechanical properties of 2% were better that 5%CNTs. An interfacial intermediate phase Al_2O_3 was noticed at Grain boundary b/w CNT and alumina.	[27]
Al_2O_3-MWCNTs	Colloidal	Hot Pressing	Stabilization of the constituents was accomplished by controlling zeta potential through electro static repulsion. Lower density (92-93%) was attributed to rigid	[64]

			network of CNTs. However high thermal conductivity due to high aspect ratio was found.	
Al_2O_3-7MWCNT	Direct CVD method for mixed powder preparation	Spark plasma	Thermal diffusivity value of 13.98mm^2/s at 25^oC (60% increases, to that of pure alumina) and thermal conductivity of 90.4W/mk at 100^oC (228% increase to that of alumina) was observed with 7%CNTs.	[65]
Al_2O_3-CNT	Molecular level mixing	Spark plasma	Uniform dispersion of CNTs in matrix, contributed to higher toughness, crack deflection and CNT-pullout as prime mechanism.	[66]
Al_2O_3-MWCNTs	Acid treated CNTs + Al_2O_3-precursor	Spark plasma	Addition of less than 1Vol% acid treated CNTs resulted in 27% and 25% increase in bending strength (689.6±29.1MPa) and fracture toughness (5.90±0.27 $MPam^{1/2}$) of the composite. Further addition of CNTs reduced toughness.	[20]
Al_2O_3-MWCNT	Ultra sonication + Ball milling	Hot pressing	Vickers hardness decreased after addition of 10%MWCNTs, electrical conductivity remains almost unchanged below 8% and a slight increase as it reached 10%.	[19]
Al_2O_3-CNF	Ball milling + Ultrasonic agitation	Hot pressing	An improvement in fracture toughness of 13% was noticed at maximum addition of 2.5vol% of CNF, where after mechanical properties were degraded.	[67]
Al_2O_3-MWCNT	Heterocoagulation process	Spark plasma	Only 1% SWCNTs increased fracture toughness by 103% reaching values of 6.40±0.3 $MPam^{1/2}$, flexural strength by 20%. Crack bridging was noticed as prime toughening mechanism.	[22]
Al_2O_3-CNT	Ball milling+ Sonication.	Hot pressed	Increased it fracture toughness (5.55±0.26) by 80% at the cost of 4%decreases in bending strength was noticed, as a result of 12vol%CNT addition.	[21]

Al_2O_3-MWCNT	Molecular level mixing process	In-situ spark plasma sintering	Enhanced Hardness & toughness	[23]
Al_2O_3-MWCNT	Sol-gel + molecular level mixing.	Hot pressing	Max. amount of CNTs homogeneously distributed was 3%, however the amount was increased to 10%, when molecular level mixing method was adopted instead of sol-gel. High temperature sintering resulted in higher hardness values. Maximum hardness of 11.50Gpa, (12.21%increases) was achieved with 7.5vol% CNTs	[68]
Al_2O_3-CNT	Colloidal process	Hot pressing	Homogeneous distribution, 32%fracture toughness while 10%Bending strength was improved. Longer dwell time at sintering temperature, however sharply decreased mechanical properties.	[18]
Al_2O_3-CNT	Sol-gel process	Spark plasma sintering	Beside increasing hardness by 7%, crack bridging effect increased with increasing CNTs to enhance fracture toughness by 10%.	[46]
Al_2O_3-MWCNT	Colloidal processing	Spark plasma	0.1%CNTs addition resulted in increase of fracture toughness from 3.7 to 4.9Mpam$^{1/2}$	[24]
Al_2O_3-CNT	Ultrasonic probe sonication	Hot pressing in argon atmosphere	24%increase in fracture toughness was noticed.	[25]
Al_2O_3-CNT	Dispersing CNTs through sonication and further.	Hot pressing in Ar atmosphere	10vol% CNT resulted in 24%increase in fracture toughness (4.2Mpam).Hardness of the composite decreased by increasing Vol% of CNT, further it also decreased when CNT was replaced by graphite. y-phase alumina powder was transformed to α-phase by heating in a box furnace in air at 1300°C for a few minutes.	[69]

2.6.3 Al_2O_3-SiC-CNTs hybrid nanocomposites

The addition of reinforcement, at micro and nanoscopic scale to produce ceramic composites and nanocomposites, is an adequate method of increasing toughness [19]. However previous studies reported that incorporation of fine SiC particles [9][10][11] in alumina, illustrated an increase in strength which was attributed to grain boundary strengthening effect. Similar studies, however, reported small, if any increase in toughness of the material [12][13][14]

It is reported that CNT reinforced alumina composite have remarkably increased fracture toughness although at the cost of hardness, density and strength [27][28][29].

This paved research towards two-phase reinforced nanocomposite, which enhanced both hardness and toughness of the nanocomposites

Jian Liu *et al* [8] studied the effect of graphene platelets and SiC addition to Al_2O_3 matrix using sonication assisted ball milling technique. He found an increase of approximately 50% in the fracture toughness in addition to 36% increase in hardness and 40% in flexural strength. Increase hardness was attributed to homogeneous dispersion and presence of SiC as a secondary phase in the nanocomposite. Fei et al[90] prepared Al_2O_3-TiC-TiN through ball milling and further hot-pressed under vacuum at 1500^oC recorded flexural strength of 841 MPa, Vickers hardness of 21 GPa and fracture toughness of 6.53 MPam1/2.Xiao et al[91] developed self-lubricating tool material by mixing multi-components through ball milling and further hot pressing resulted in an increase in hardness, flexural and fracture toughness of 19%, 25%, and 6% respectively. In addition to dry powder mixing, Zhou *et al* [92] synthesized hybrid nanocomposite by adding pre-treated surface modified CNTs and

SiC, while stirring semi-molten magnesium alloys. It was found that difference in thermal coefficient of expansion between the matrix and re-enforcement was the major cause of higher strength properties. Further, SiC was found as dominant in refining microstructure, thus increases its hardness.

Although there is an extensive literature available on alumina reinforced with two nanoscale phases, however, it was very unfortunate that the obtained mechanical and or physical properties of these nanocomposites are lower than expected or even in some cases are lower than monolithic ceramics [54], [93], [94]. Comprehensive literature review documented agglomeration of nanopowder and weak bonding at matrix-reinforcement interface surface, as two prime reasons, for obtaining these unsatisfying results.

Despite the fact that high surface area to volume ratio of particles in nanocomposites has obvious and clear positive effects on their mechanical properties, but have been repeatedly reported to cause agglomeration during processing [26]. Most researchers have recorded this lower degree of dispersion as the basic hindrance in retrieving as-predicted enhanced mechanical and physical properties. Another deemed challenge to target predicted properties is to enhance interface bonding between reinforcement and matrix [94]–[96].

Interfacial bonding of matrix-reinforcement and their agglomeration is further complex if more than one reinforcement with different morphologies are added to the basic ceramic matrix. However, the development of this exceptional nanocomposite is vital in certain load bearing applications, which requires enhancement in hardness as well as fracture toughness of the material.

Table 2.4 *Synthesis parameters and consequent findings in Al_2O_3-hybrid nanocomposite from literature*

Composite	**Synthesis Method**	**Consolidation Method**	**Remarks**	**Ref**
Al_2O_3-SiC-Graphene	Ball Milling	Spark plasma	3vol% addition of SiC resulted in best properties showing relative density of 98.85%, hardness of 24GPa and fracture toughness of 5.0Mpam$^{1/2}$.	[8]
Al_2O_3–TiC–TiN	Ball milling	Hot Pressing	Both the flexural strength and the fracture toughness first increased and then decreased with increasing sintering parameters. Material developed for cutting tools was found to have toughness of 6.53 MPam$^{1/2}$ and vickers hardness of 20.70 GPa.	[70]
Al_2O_3/(W,Ti)C/CaF_2	Ball milling	Hot pressing in vacuume	Developed material was found to enhance flexural strength, toughness and hardness 25%, 6, and 19%, respectively.	[71]
Al_2O_3-SiCw-CNTs	Ball milling	Hot Pressing	Presence of SiC retarded the sintering of Al_2O_3 significantly. Lower than expected mechanical properties were attributed to non-homogeneous distribution of CNTs in matrix, although composite resulted to increased toughness by 60%.	[38]
Al_2O_3-Mg-CNTs	Ball milling	Microwave	Fractured surfaces were attributed to brittle fracture due to agglomeration or clustering of re-enforcement in the matrix. Although yield strength (89MPa) and UTS (140MPa) was found to increase.	[72]

Alumina-SiC-CNF	electrostatic adsorption technique	Spark plasma	SiC was found to increase interfacial shear strength	[31]
Al_2O_3-Ce-ZrO_2	Lamination process	Tap casting and	Residual stresses due to mis-match in expansion of the laminated composites, increase the indentation strength. Compressive stresses in outer layer were attributed to higher toughness in the composite.	[73]
Al_2O_3-SiC-CNTs	Sonication + Ball milling	Spark plasma sintering	SiC fine particles increased strength by pinning effect. Highest fracture toughness value of 7MPam$^{1/2}$ was achieved with 7%MWCNTs, although relative density was found to be 97.2% while hardness was found to be 16GPa.	[29]
Al_2O_3-FeO-CNTs	Chemical Vapor deposition		Powder characterization through SEM, TEM and XRD confirmed dispersion and crystallinity of alumina. Weight loss in TGA and DTA was associated to oxidation of CNTs, further FTIR confirmed the presence of functional group to MWCNTs.	[74]

2.7 Problem Statement and Objective

Reinforcing ceramics by two nanoscale phases, having different morphologies and/or attributes, so-called hybrid microstructure design is an efficient method to develop nanocomposites with tailored nanostructures and improved mechanical properties. However, there are challenges in developing high-performance and cost-effective ceramic hybrid nanocomposites for commercial applications. Uniform distribution/dispersion of the nanoscale reinforcements in the matrix is a major problem in synthesizing homogeneous nanocomposite powders. Inhibiting grain growth during sintering is another challenge to develop materials with preserved nanostructure features. Furthermore, the properties of ceramic nanocomposites strongly depend on the reinforcements' content as well as the synthesis and consolidation process parameters. Analysis of the literature showed that reinforcing alumina with two nano-phases led to the noticeable increase, marginal improvement, or even degradation in mechanical properties. The marginal improvement or degradation of the properties were attributed to the agglomeration of the reinforcements, growth of the matrix grain size, and inhibition of densification.

The main objective of this research work is to develop Al_2O_3-SiC-CNTs that have improved mechanical properties for cutting tool applications. The specific objectives are to:

1- Synthesise homogenous Al_2O_3-SiC-CNTs nanocomposite powders that have a uniform distribution of reinforcements using ball milling or molecular level mixing methods.

2- Consolidate the synthesised nanocomposite powders to high density using spark plasma sintering method.

3- Investigate the influence of reinforcements' content, synthesis and sintering parameters on the microstructure and mechanical properties of the developed materials.

4- Design alumina nanocomposites that have improved hardness and fracture toughness suitable for cutting tool applications.

CHAPTER 3

MATERIALS AND EXPERIMENTAL PROCEDURES 3

3.1 Raw Materials

α-Al_2O_3 (with an average particle size of 200 nm and 99.85% purity) supplied by ChemPUR Germany was used as matrix, while synthesizing composite powder using ball milling process. Aluminum nitrate nonahydrate ($Al(NO_3)_3 \cdot 9H_2O$), a precursor, supplied by ChemPUR Germany was used as a source of alumina matrix while synthesizing composite powder using molecular level mixing.

SiC_β (45-55 nm), 97.5% purity, supplied by Nanostructured and Amorphous Materials and locally synthesized functionalized CNTs, as explained elsewhere [36], were used as reinforcement in the hybrid nanocomposite synthesized using both milling and molecular level mixing process.

3.2 Powder Synthesis and Consolidation

3.2.1 Ball Milling

The experimental procedure adopted for synthesizing Al_2O_3–SiC-CNT nanocomposite powder using ball milling process is shown in ***Figure* 3.1**

The Required amount of Al_2O_3 and SiC were first added to distilled water and magnetically stirred for 15 minutes, the slurry was then sonicated for 2 hours using high energy probe

sonication. The sonicated slurry was transferred into cylindrical alumina vials (250 ml in volume) together with alumina balls (10 mm in diameter). A planetary ball mill (Fritsch Pulverisette equipment P5, Germany) was used to mill the mixture. Al_2O_3-5SiC was, primarily, milled at 300rpm for 2, 4, and 6 hours and characterized to analyze the distribution of SiC in Al_2O_3 matrix. Distribution of increased SiC content in Al_2O_3-10SiC was also analyzed with similar milling conditions. Different batches of Al_2O_3-5SiC and Al_2O_3-10SiC were finally synthesized at 300rpm for 4hours, as the optimum time for uniform distribution of SiC in alumina. MWCNTs (1 and 2 wt.%) were further added to each of the already milled slurries and further sonicated for 2 hours using high energy probe sonication. The mixture was finally dried in an oven at 120ºC for 15 hours. Al_2O_3-5SiC, Al_2O_3-10SiC, Al_2O_3-5SiC-1CNT, Al_2O_3-5SiC-2CNT, Al_2O_3-10SiC-1CNT, and Al_2O_3-10SiC-2CNT nanocomposite powders compositions with a uniform distribution of reinforcement were prepared under these conditions.

However, it was intended to explore the possibility of getting the same uniform distribution of reinforcement in the synthesized composite powder at lower milling speed (100rpm/2hours).

Selected hybrid compositions containing high SiC content (Al_2O_3-10SiC-1CNT and Al_2O_3-10SiC-2CNT) were additionally prepared, while keeping all other steps of preparation same, except that required amount of Al_2O_3 and SiC were milled at 100rpm for 02hours, instead of 300rpm for 04 hours.

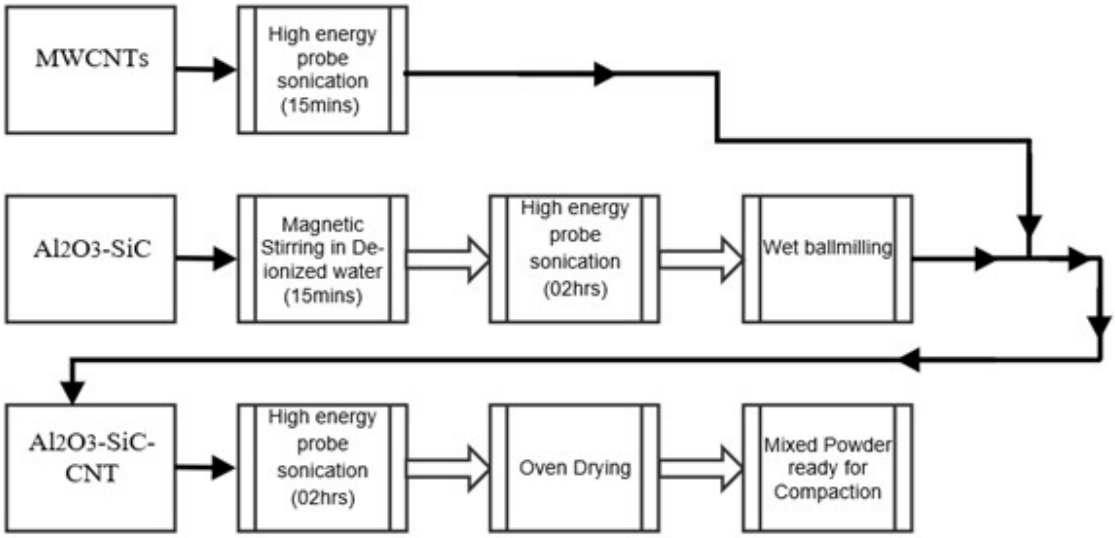

Figure 3.1 *Flow chart showing steps during Ball-milling-sonication process*

3.2.2 Molecular Level Mixing

Al_2O_3–5SiC-1CNTs nanocomposite powder was synthesized using molecular-level mixing (MLM) process. Flow chart showing synthesis procedure is shown in **Figure 3.2**

Carbon nanotubes (CNTs) produced using chemical vapor deposition (CVD) were functionalized to decorate its surface with negatively charged organic groups such as OH^- and/or $COOH^-$. Concentrated nitric acid was used as a solvent, during functionalization, to fully disperse CNTs first and further refluxed for 48 h at 120°C. 500 ml of deionized water was then added to the cooled mixture and then vacuum-filtered using a filter paper (3 μm porosity). These washing steps were repeated until the pH became same as deionized water pH. The mixture was finally dried under vacuum in an oven at 100 °C.

On the one hand, 17.3 g of aluminum nitrate nonahydrate was stirred in 100 ml of de-ionized water for 15 min to form Al^{+3} positive metallic ions. On the other hand, 50 mg of functionalized CNTs and 250 mg of SiC nanoparticles were suspended in 50 ml de-ionized water and magnetically stirred for 15 min. The two slurries were mixed and further sonicated using high energy probe sonication for 24 hours.

Mixing at the molecular level was accomplished through bonding between the positively charged Al^{+3} metallic ions and negatively charged COOH attached to the CNTs. The obtained mixture was then dried, while keeping it stirred, on a magnetic hot plate at 170 °C. The dried mixture was heat-treated at 400 °C for 4 h to remove unwanted gasses and oxidize aluminum attached to the surface of the functionalized CNTs.

The dried Al_2O_3-5SiC-1CNT composite powder was collected and analyzed for the formation of α-alumina phase from its precursor (Aluminum nitrate nonahydrate) and for distribution of CNT in the produced alumina matrix.

Al_2O_3–5SiC-1CNTs nanocomposite powder, was also synthesized by reducing the final sonication time from 24hours to 02hours at later stages to see the influence of sonication time. All other steps in synthesis, as discussed above, were kept un-changed.

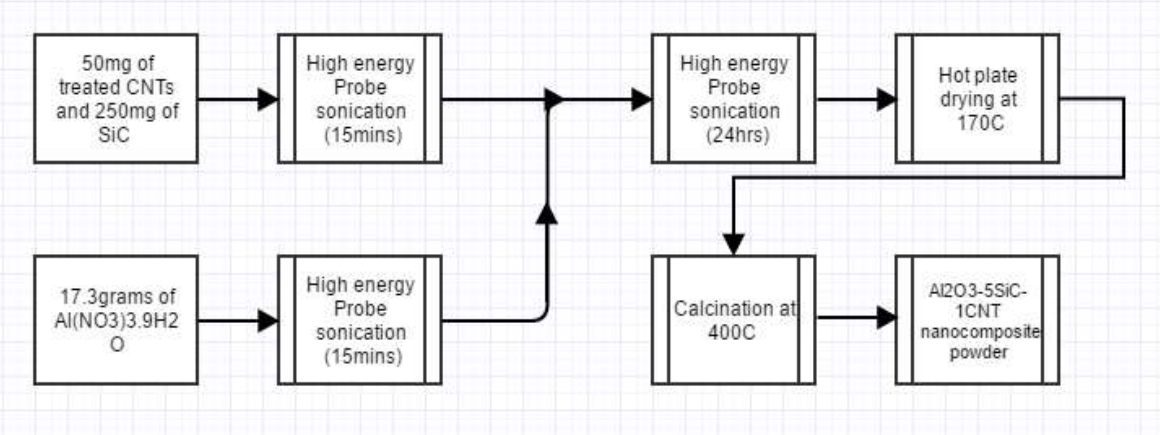

Figure 3.2 *Flow chart showing molecular level mixing process, which was used to synthesize Al_2O_3–5SiC-1CNT.*

3.2.3 Spark Plasma Sintering

Ball milled synthesized compositions, which were milled at 300rpm for 4hours (Al_2O_3-5SiC, Al_2O_3-10SiC, Al_2O_3-5SiC-1CNT, Al_2O_3-5SiC-2CNT, Al_2O_3-10SiC-1CNT, and Al_2O_3-10SiC-2CNT), as well as reference alumina nanopowder, were consolidated at 1500°C for 10min under applied pressure of 50MPa, using spark plasma sintering (SPS) machine (model HP D 5). The heating rate was kept at 100ºC/min. A pyrometer was used to measure the temperature. Friction was minimized using a sheet made of graphite placed between the die walls and the powder. In addition, the sheet facilitated the ejection of the consolidated specimens.

Al_2O_3-10SiC-1CNT and Al_2O_3-10SiC-2CNT, which were additionally prepared using milling at 100 rpm for 02hours were consolidated for 3, 5 and 10mins, at each sintering temperature of 1400°C, 1450°C, and 1500°C. Applied pressure of 50MPa and rate of heating (100ºC/min) were kept unchanged during the sintering process. All synthesized compositions attained dense structures when sintered at 1500ºC for 10mins under applied pressure of 50 MPa.

The same sintering conditions were chosen for Al_2O_3-5SiC-1CNT synthesized using molecular level mixing process, to keep consistency and easy to compare results. However, it's low attained density articulated that it was not well sintered under these sintering parameters. Therefore sintering temperature was raised to 1550ºC and 1600ºC, while keeping the same heating rate of 100ºC/min, dwell time of 10mins and applied pressure of 50MPa.

3.3 Characterization Methods

3.3.1 Transmission Electron Microscope (TEM)

A Philips transmission electron microscope (model CM200 200 kV) equipped with Oxford Instruments 80 mm^2 SDD EDX system running Aztec software was used to characterize the as-received raw powders, synthesized powders, and sintered bulk samples. Samples were prepared by core drilling a 3 mm disk, mechanical thinning to 100 μm, dimpled to 5 μm at the center of the disk and then ion polished using a gatan precision ion polishing system (PIPS) at between 5 and 3 kV at angles from 5 to 3 degrees until a hole appeared.

3.3.2 Field Emission Electron Microscope (FE-SEM)

A Tescan Lyra-3 Field Emission Scanning Electron Microscope (FE-SEM) with Energy Dispersive X-ray Spectroscopy (EDS) was used for characterization of the powders and analysis of the sintered samples. The distribution of the reinforcements in the powders and bulk samples was characterized by x-ray mapping using a constant number of 20 frames.

3.3.3 X-Ray Diffraction (XRD)

An x-ray diffractometer model D8 made by Bruker, USA, with a characteristic wavelength of 0.15405 nm, was used for recording XRD patterns of the synthesized powders and consolidated specimens. The diffraction angle (2θ) was varied between 20 and 90^{o} at a step increment of 0.02^{o} with a count time of 1 sec.

3.3.4 Fourier Transform Infrared spectroscopy (FT-IR)

The functionalized CNTs were analyzed using FTIR to confirm the presence of the COOH group on the surface of CNTs. In addition, the formation of Al-O-C bond in the synthesized nanopowder, an indication of mixing at molecular level, was also confirmed using FTIR. The analysis were carried within the range 400 to 4000 cm^{-1} using a NICOLET FT-IR machine model 6700. Samples were prepared by adding KBr to samples using hydraulic press.

3.3.5 Thermal Analysis (TGA)

A Netzsch thermal analyzer model STA 449F3-Jupiter was used for thermal characterization of the composite powder synthesized using molecular level mixing. Thermogravimetric Analysis (TGA) and differential scanning calorimetry (DSC) experiments were carried out under argon gas using a heating rate of 5 °C/min.

3.3.6 Density measurement

The density of the sintered samples was measured using Metler Toledo balance density determination KIT model AG285 and quantified according to Archimedes principle. The

relative density of the composite was calculated as the ratio of the measured to the theoretical value. The theoretical density of the composite was calculated by the rule of mixture [1], [20], [75], [76]using theoretical densities of 3.97, 3.21, and 2 g/cm3, for alumina [75] , SiC [51], and CNTs [77], respectively.

3.3.7 Hardness

Universal hardness testing machine (Zwick-Roell, ZHU250, Germany), having a vickers indenter, was used to measure the vickers hardness (HV10) of sintered samples.

The vickers indenter which is made of diamond is, in the form of a square-base pyramid having an angle of 136° between faces. The indenter was applied under a predetermined constant load of 10kg for 15 s. The diagonals of the square indentation are measured using the microscope and a *mean value* is calculated.

The vickers hardness number (VHN) is then calculated according to the formula:

$$VHN = 2P\sin(\frac{\theta}{2})/d^2 = \frac{1.854P}{d^2}$$

where P is the applied load in kilogram (kg), θ is the indenter face angle of 136°, and d is mean diagonal length in *mm*. The constant 1.854 incorporates value of $sin(\theta/2)$ and other conversion factors to give VHN a unit of kg/mm^2. The data reported were the average of 10 values

3.3.8 Fracture Toughness

Fracture toughness of the developed material was evaluated, from the crack length and indent length observed under an optical microscope, according to Antis' equation given below

$$K_{1c} = 0.016\sqrt{\frac{E}{H}}\frac{P}{C^{\frac{3}{2}}}$$

where E is the elastic modulus (GPa), H is the Vickers hardness in GPa, P is the applied load (N), and C is the diagonal crack length. Young's modulus values of 380, 475, and 1000 GPa for Al_2O_3 [75] , SiC [1] , and CNTs[1], respectively, were used to calculate the elastic modulus of the composite using the rule of mixture[75][1] [78].

3.3.9 Bending

Al_2O_3-10SiC-1CNT and Al_2O_3-10SiC-2CNT samples (prepared using ball milling at 100rpm for 2hours) and monolithic alumina were investigated for bending strength using 3-point bend test. A computer controlled Instron 3367 testing machine with capacity of 50KN was used to analyze rectangular samples with dimensions of 1.5mm X 02mm X 25mm (width X thickness X length) with a span length of 20mm and cross head speed of 0.05mm/min. 03 bars of each sample were tested to ensure consistency in results.

For a rectangular cross section, the bending strength σ_{fs} is equal to

$$\sigma_{fs} = \frac{3F_f L}{2bd^2},$$

where, F_f is the load at fracture in newton (N), L is the span length (distance between support points), b is the width and d is the depth, in mm, of the rectangular sample.

CHAPTER 4

RESULTS AND DISCUSSION 4

4.1 Ball Milled Composites

4.1.1 Powder synthesis

An FE-SEM micrograph of the as-received Al_2O_3 nanopowder is shown in ***Figure*** **4.1**(a). Morphology of the as-received alumina powder ranges from spherical to irregular, as shown in the same ***Figure***. A higher magnification micrograph taken using TEM is presented in ***Figure*** **4.1**(b) which reveals an average particle size of 200nm. The corresponding selected area diffraction pattern from a particle is presented in ***Figure*** **4.1**(c), where spots in the pattern indicate the presence of a few crystallites. A high-resolution micrograph of one single crystallite is shown in ***Figure*** **4.1**(d), which shows that the crystallite size is in the range of 20-30nm, which corresponds to 38nm as measured from Scherer's equation using the XRD pattern of as received alumina powder, as shown in ***Figure*** **4.2**. Sharp peaks at particular angles corresponding to the joint committee on powder diffraction standards data for α-alumina, reconfirms the crystalline phase of Al_2O_3 powder. This confirms that the material used in this study was α-alumina.

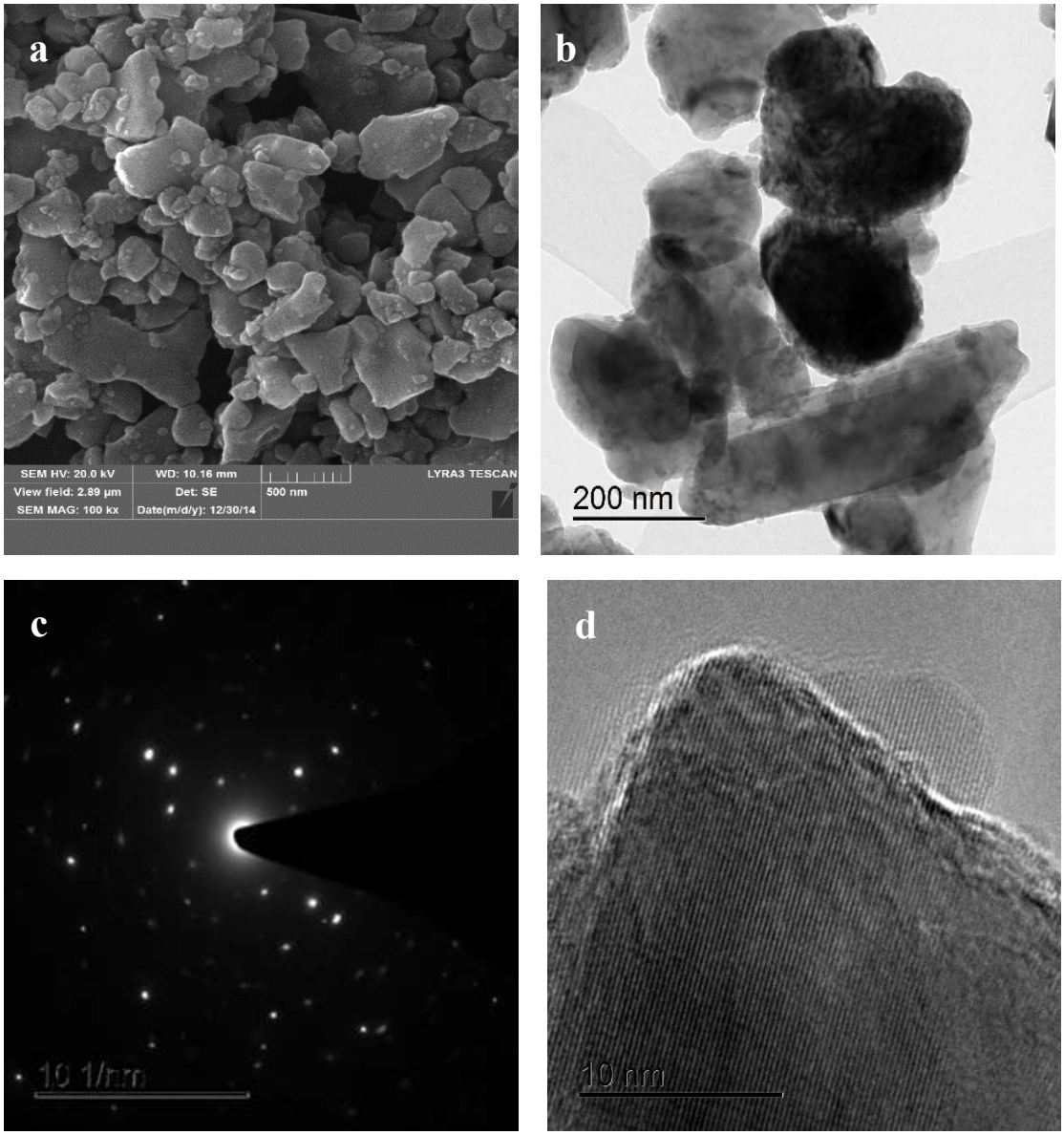

Figure 4.1 *showing FESEM (a) and TEM (b) of as received Al_2O_3. Selected area diffraction pattern (c) and size of lattice fringe (d) from a particle is shown.*

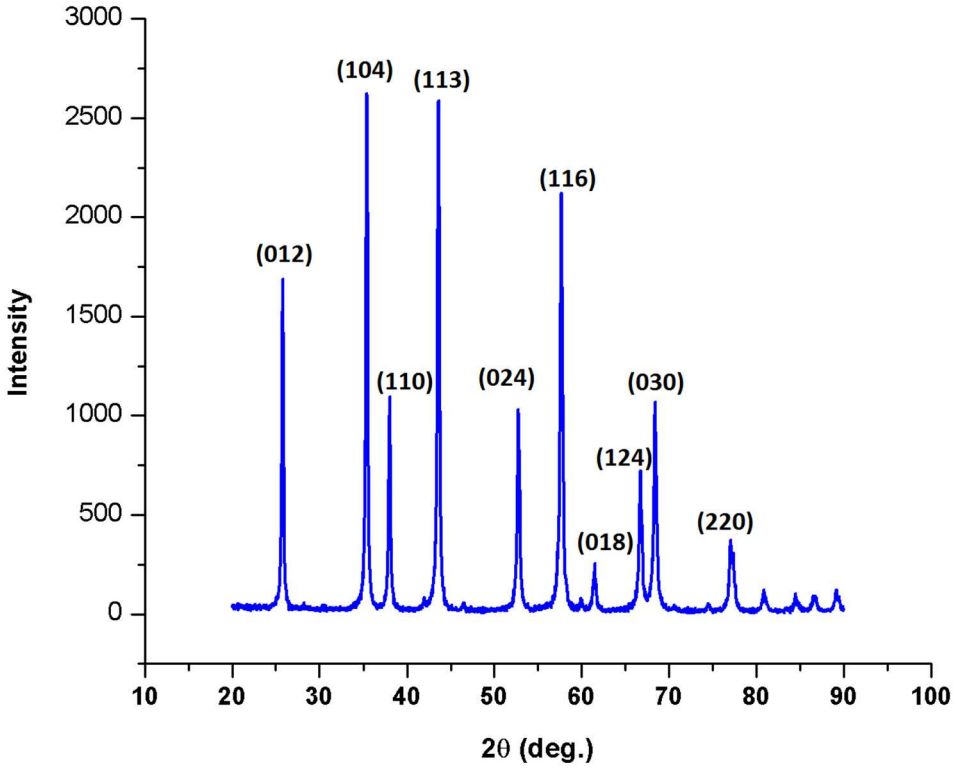

Figure 4.2 *Showing XRD of as received Al_2O_3 powder. Peaks corresponding to particular 2θ angle of JCPD, reveals single phase α-alumina.*

An FE-SEM micrograph of the as-received SiC nanopowder is shown in ***Figure*** **4.3** (a). The powder shows very fine spherical shaped particles. A bright field TEM image is presented in ***Figure*** **4.3** (b) which clearly presents dispersed nanoparticles with an average particle size of 50nm, while the corresponding diffraction of the selected area is presented in ***Figure*** **4.3** (c), which confirms its polycrystalline nature. A high-resolution micrograph of a particle shown in ***Figure*** **4.3** (d) reveals that it is made of few crystallites. The size of each crystallite is within the range of 10nm. Particular sharp characteristic peaks shown in the XRD pattern, as shown in ***Figure*** **4.4**, further confirm its crystalline nature.

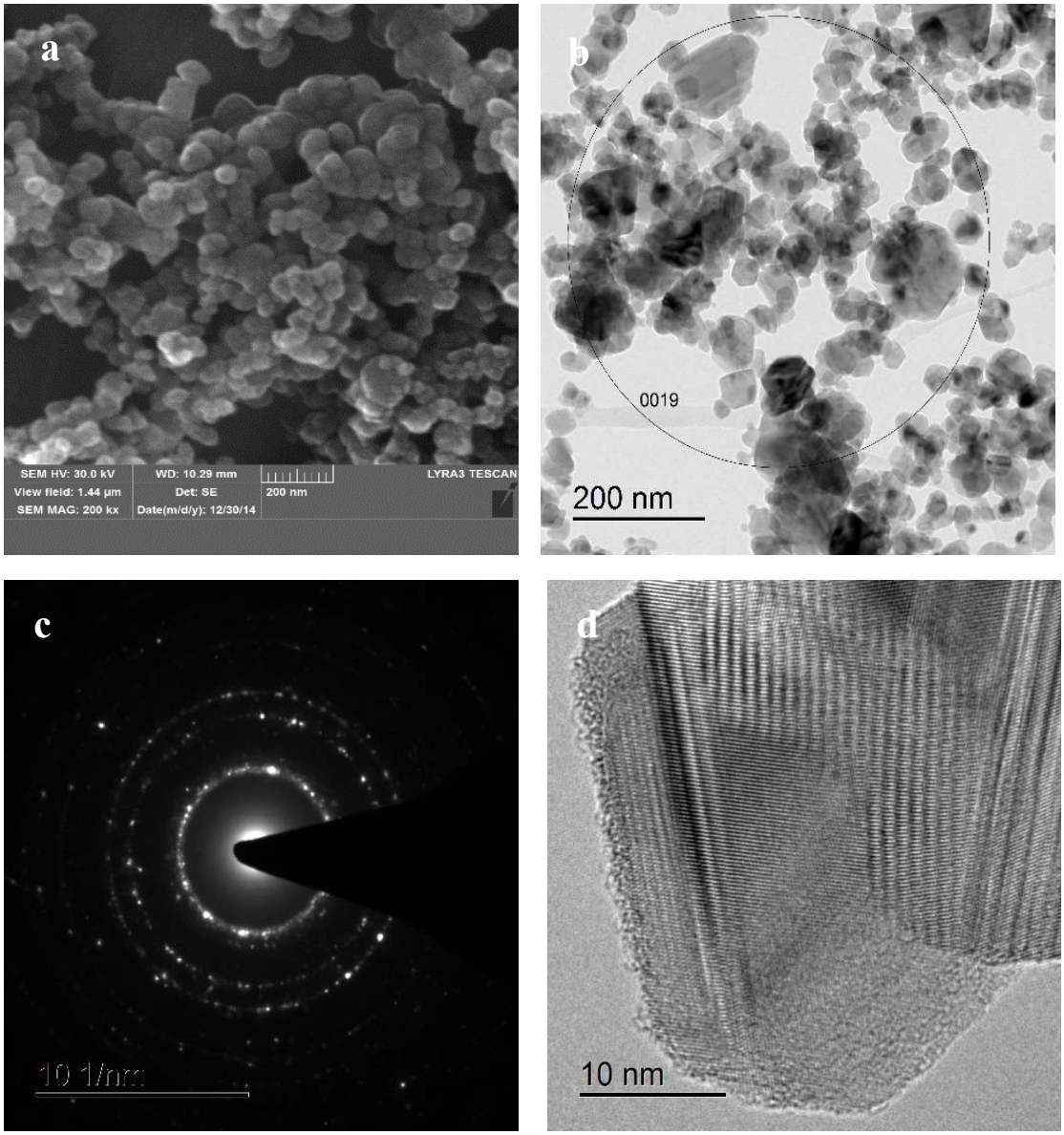

Figure 4.3 *showing FESEM (a) and bright field TEM (b) of as received SiC powder. Selected area diffraction pattern (c) and high resolution TEM of a SiC particle (d) showing that the particle is made of few crystallites.*

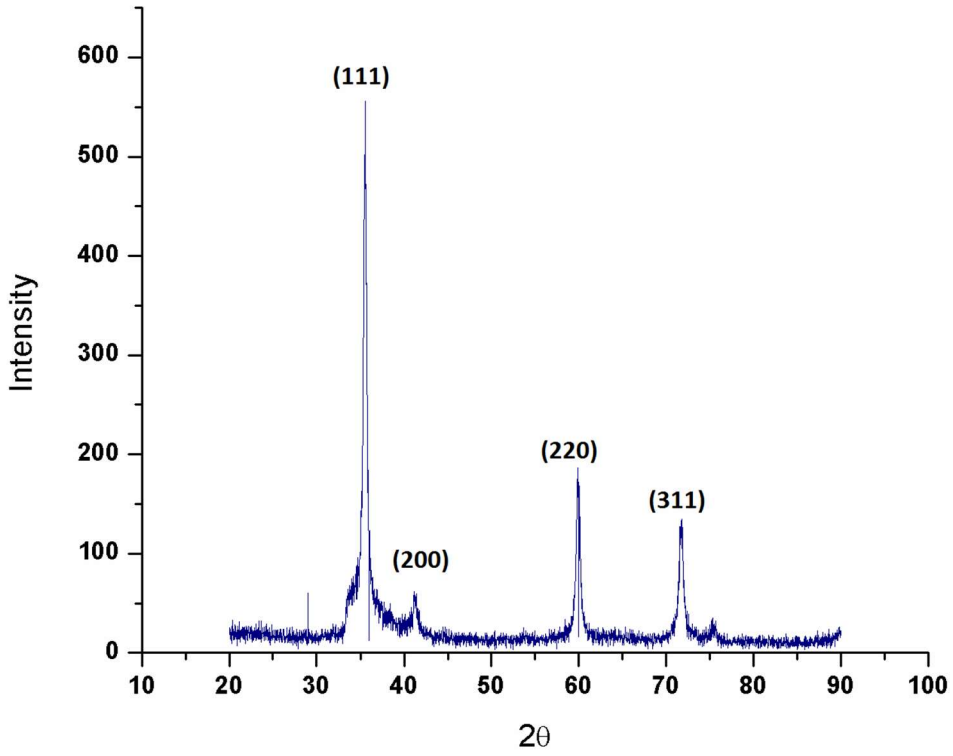

Figure 4.4 *is showing XRD of as received SiC powder. Peaks corresponding to particular 2θ angle of JCPD, reveals single phase β-SiC.*

Acid treated carbon nanotubes (CNTs) functionalized with an OH^- and or $COOH^-$ negatively charged organic group, were used during this study. Electrostatic repulsive forces between these functionalized CNTs restrict the formation of the CNT agglomeration, although it cannot be avoided completely [15][79]. A higher magnification micrograph taken using a TEM is presented in ***Figure 4.5*** (a,b) which clearly shows entanglement between the CNTs, even after functionalization. A high-resolution micrograph of one single acid treated carbon nanotube is shown in ***Figure 4.5*** (c,d), which reveals an inner die=5nm and an outer=15-20nm, in addition to almost 15 carbon layers around the tube.

A typical XRD pattern for functionalized MWCNT is shown in ***Figure* 4.6** (a). The strongest diffraction peak at the angle (2θ) of 25.5° can be indexed as the C(002) indicating hexagonal graphite structure [80]. The other characteristic diffraction peaks of graphite at 2θ of about 43°, 53°, and 77° are associated with C(100), C(004) and C(110) diffractions of graphite, respectively.

FTIR, Fourier Transform Infrared, is a unique testing methodology which can represent the consistency of the distribution or homogeneity of the analyzing sample. The absorption peaks in the pattern correspond to different frequencies of the atomic bonding in the sample structure, while the size or intensity of the peak corresponds to the amount of the components. Acid treated CNTs were first analyzed through FTIR to confirm the COOH bond, being attached to their surface, as shown in ***Figure* 4.6** (b). Particular absorption peaks confirmed the presence of the carboxylic group being attached to initially acid-treated CNTs.

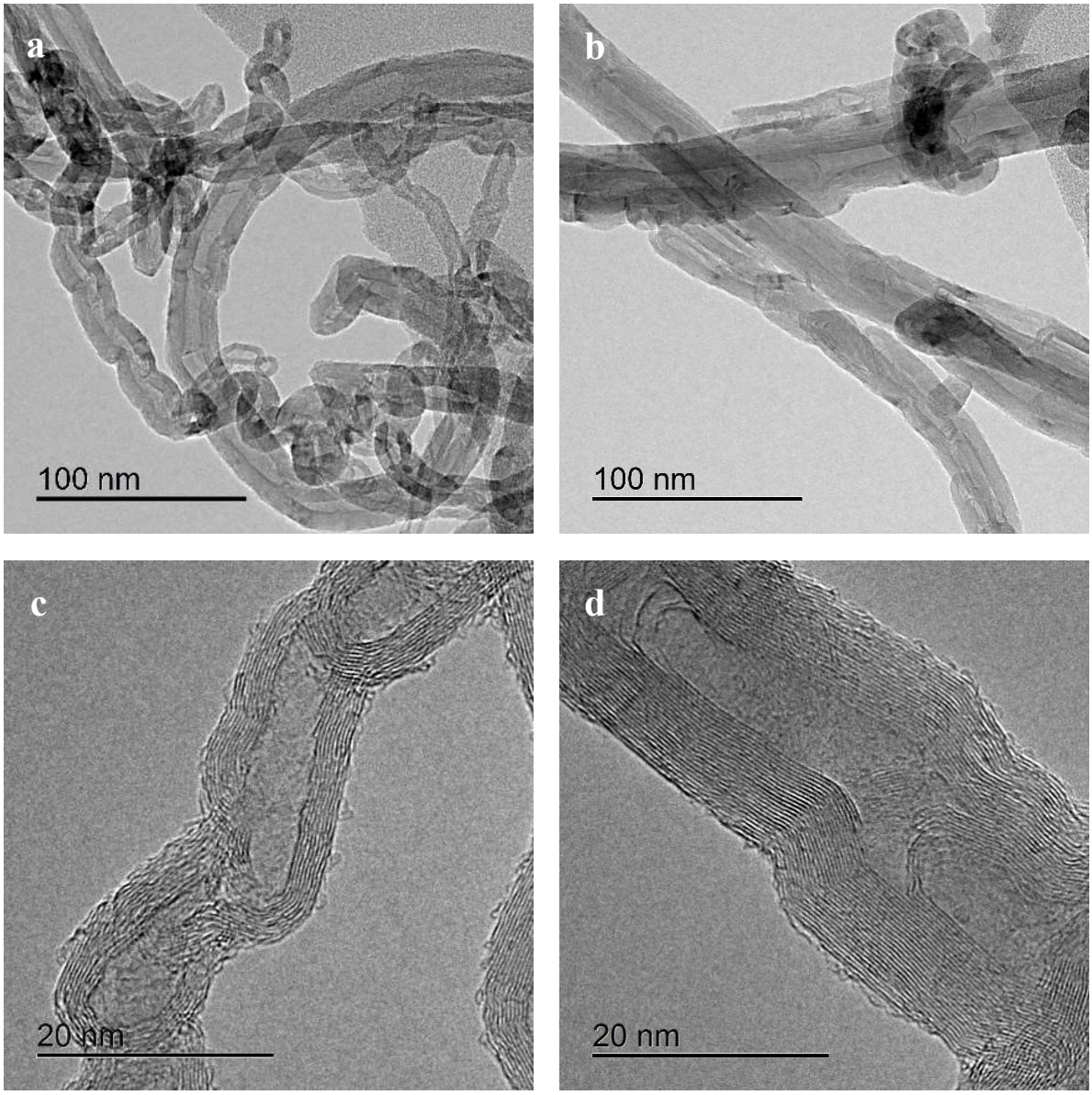

Figure 4.5 *TEM micrograph of functionalized CNTs, showing their intrinsic entangled nature (a, b) and high-resolution TEM micrograph (c, d), clearly indicating inner tube and number of outer carbon layers*

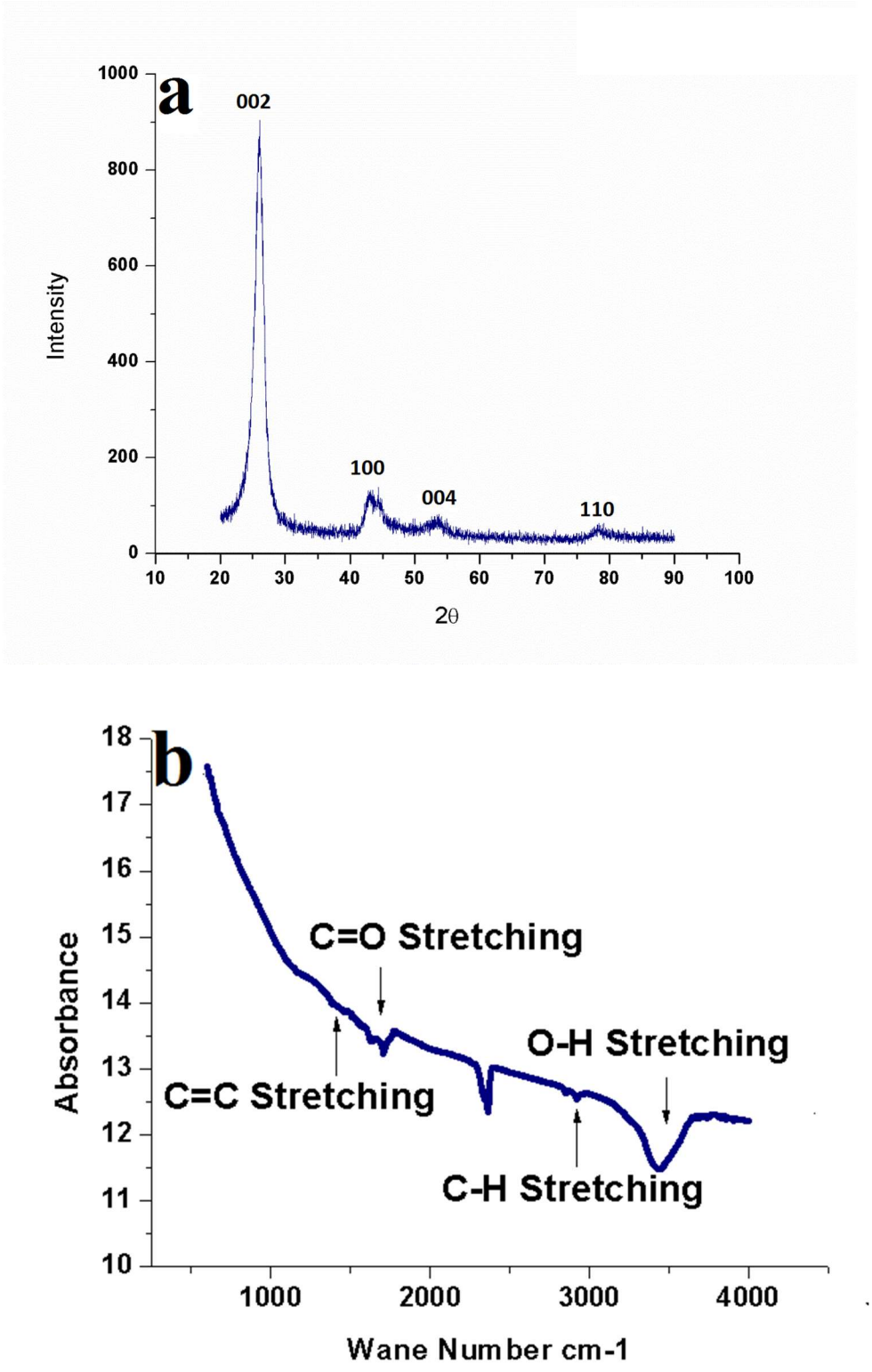

Figure 4.6 *X-Ray diffraction (a) and FTIR (b) of functionalized CNTs used during this study*

It was intended to synthesize all of the different compositions with the same milling parameters, to maintain consistency and to make it easy to compare results during this research work. Initially, the milling time was investigated by synthesizing Al_2O_3-5SiC and Al_2O_3-10SiC using ball milling at 300rpm (each for 2, 4 and 6 hours). These compositions were also synthesized at a lower milling speed (100rpm for 2 hours), in the later stages, to compare the distribution of the reinforcement and micro structural development.

Al_2O_3-5SiC was, primarily, milled at 300rpm for 2, 4, and 6 hours and characterized using FE-SEM and x-ray mapping, of C, to analyze the distribution of SiC within the Al_2O_3 matrix. FESEM micrographs (a, b, c) and x-ray mapping of C (d, e, f) showing the distribution of SiC in Al_2O_3-5SiC, milled for 2 hours, 4 hours and 6 hours respectively, are shown in ***Figure* 4.7**. Analysis of x-ray mapping showed that a milling time of 2 hours was enough to obtain a uniform distribution of SiC particles in the powder, however, a milling time of 4 hours gave a comparatively better distribution and improved the dispersion of the SiC particles. A further increase in milling time to 6 hours, however, did not show any meaningful improvement in the dispersion. Therefore, it was concluded that the optimum time to have a homogenous powder with a uniform distribution of SiC particles is 4 hours. As a result, all powder compositions prepared during this study through ball milling were milled for 4 hours at 300rpm.

FESEM micrographs (a, b), a high-resolution TEM (c) and a selected area diffraction pattern (e) of Al_2O_3-5SiC milled at 300 rpm for 4 hours are presented in ***Figure* 4.8**.

The appearance of small spots in the form of rings ***Figure* 4.8**(d) is an indication of poly-nano-crystalline material, as compared to the bright spots **Figure 4.1**(c) of as-received alumina crystalline material. It confirms that the crystallite size of alumina was reduced

during the 4-hour milling of alumina with hard silicon carbide particles. The results also corresponded to the crystallite size measured using the Scherrer equation by analyzing XRD patterns as shown in ***Figure* 4.14**.

XR-mapping of Si, Al, and O_2 in Al_2O_3-5SiC, milled for 4 hours, as shown in ***Figure* 4.9**, which undoubtedly claims the uniform dispersion of SiCin alumina matrix. XRD anaysis of the same powder, as shown in **Figure** 4.10, doesn't show any extra peak other than the characteristic peaks, which confirms the absence of any alloy formation during the milling operation.

Similar milling investigations were carried out on Al_2O_3-10SiC to confirm distribution of the increased SiC in the alumina matrix as shown in **Figure 4.11** which reveals that both 2 and 4 hours of milling were enough to achieve uniform distribution, and that 6 hours of milling didn't show any meaningful improvement. However, to ensure consistency when comparing results (between Al_2O_3-5SiC and Al_2O_3-10SiC) in the later stages, 4 hours of milling was suggested even in the case of Al_2O_3-10SiC, as was suggested for Al_2O_3-5SiC.

Uniform distribution of increased reinforcement content (10% SiC) is further illustrated through FESEM micrographs, as shown in **Figure 4.12**. The absence of any peak other than characteristic peaks in the XRD pattern of Al_2O_3-10SiC milled for 4 hours, as shown in **Figure 4.13**, confirms the absence of any other alloy formation during milling. Looking at the above uniform distribution of SiC in alumina with both lower and higher contents (5 and 10% respectively), it was decided to synthesize all further composition, during this study at 300rpm for 2 hours.

It was found through XRD analysis of synthesized Al_2O_3-5SiC and Al_2O_3-10SiC, that the crystallite size of reference material alumina was reduced from 38nm to 33 and 29nm respectively, as shown in ***Figure* 4.14**, after milling at 300rpm for 4 hours.

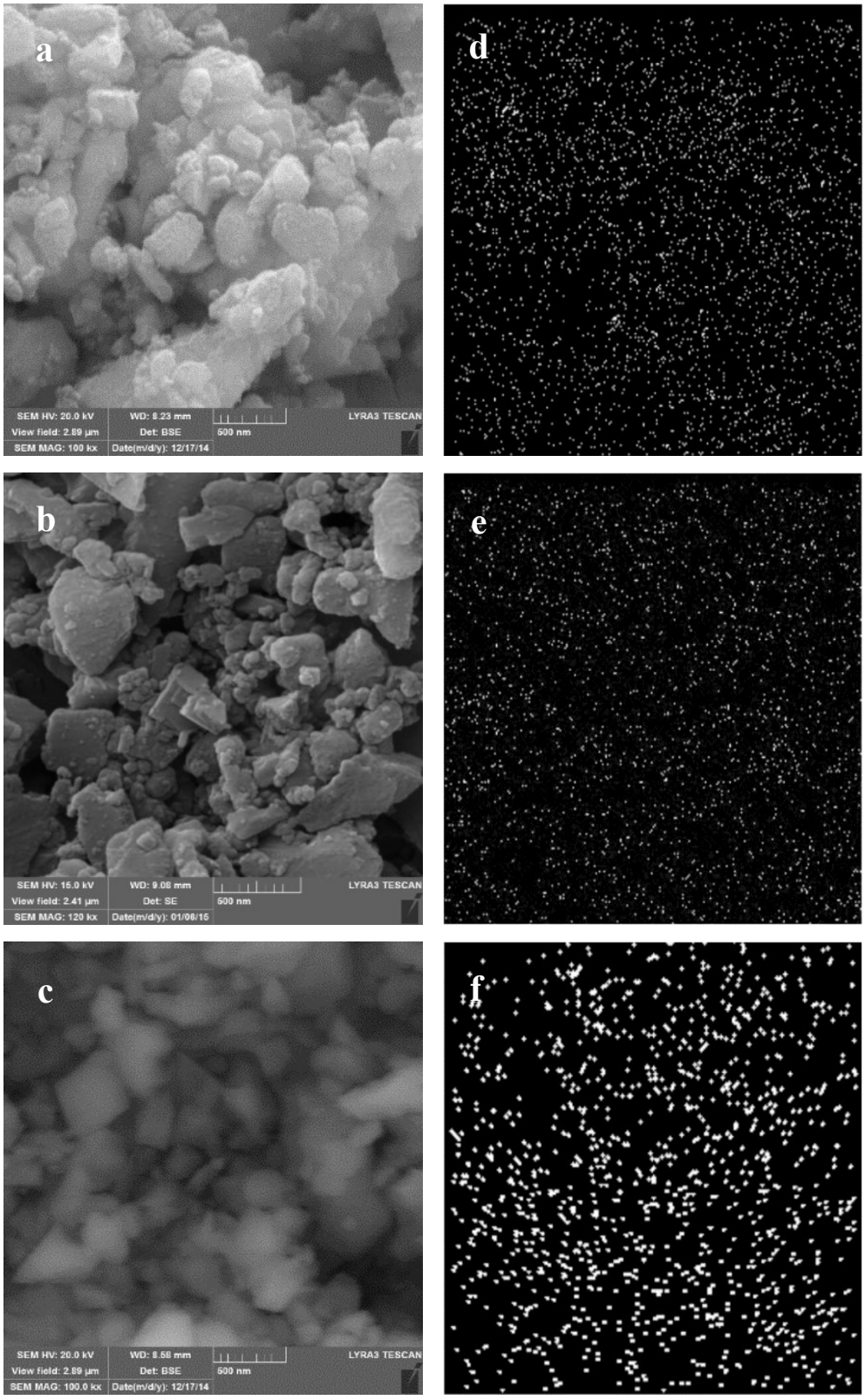

Figure 4.7 FESEM of Al_2O_3-5SiC (a, b, c) and XR-mapping of Si (d, e, f) in alumina matrix with respect to 2, 4, and 6hours milling @ 300rpm respectively

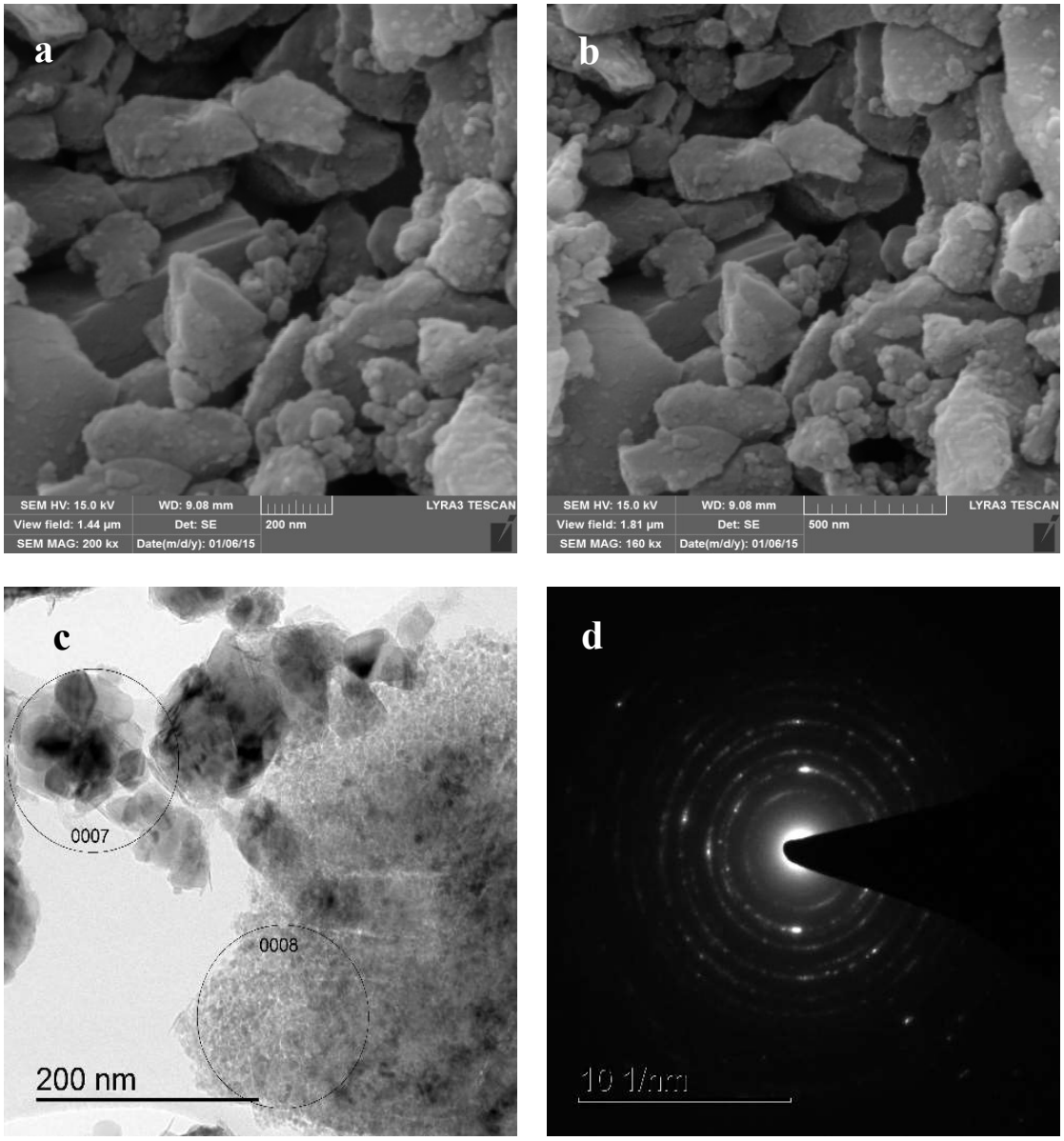

Figure 4.8 *FE-SEM micrographs (a,b), bright field image (c) and corresponding selected area diffraction pattern (d) of Al_2O_3-5SiC powder ball milled for 4h.*

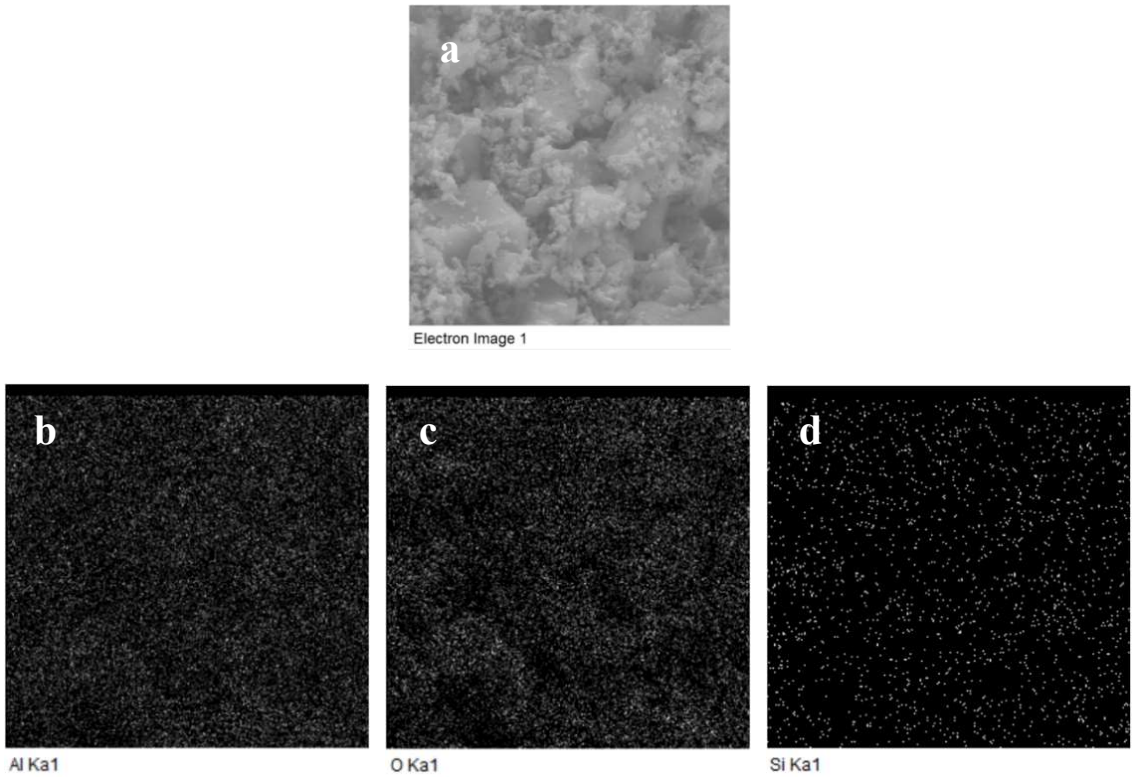

Figure 4.9 *FESEM micrograph (a) and X-ray mapping of Al(b), O(c), and Si(d) in Al_2O_3-5SiC powder ball- milled for 4hours, showing distribution of SiC in alumina marix.*

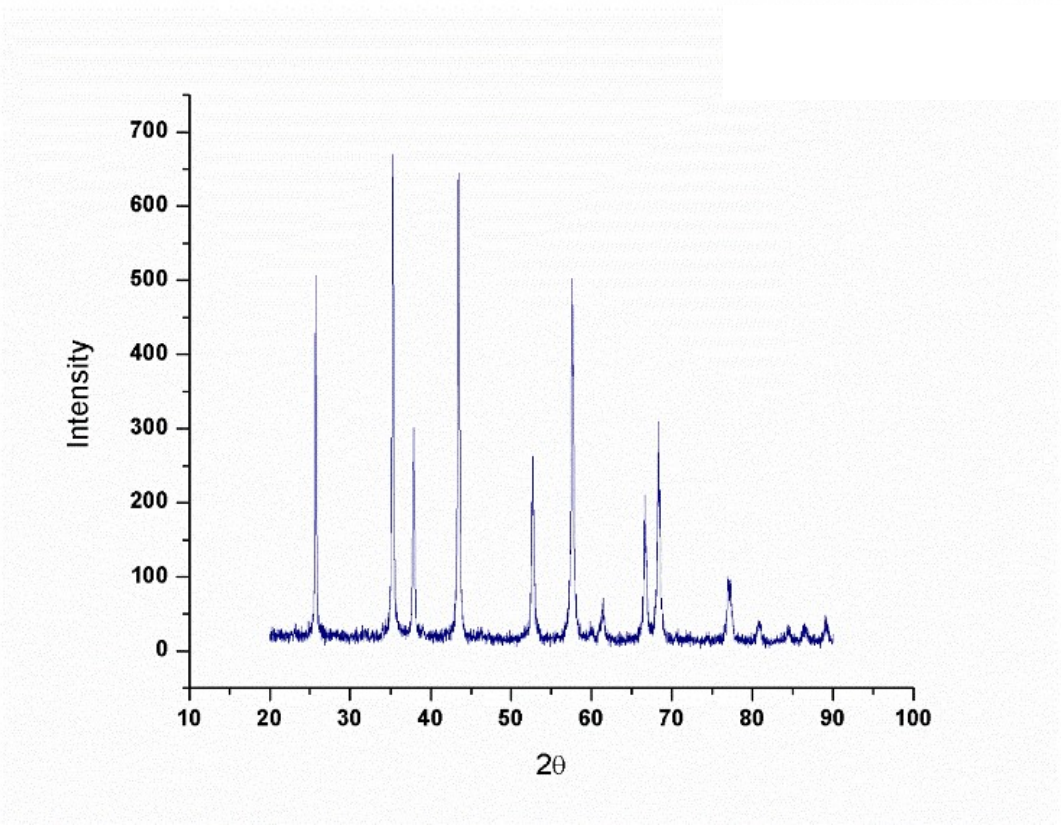

Figure 4.10 *XRD of Al_2O_3-5SiC milled for 4 hours*

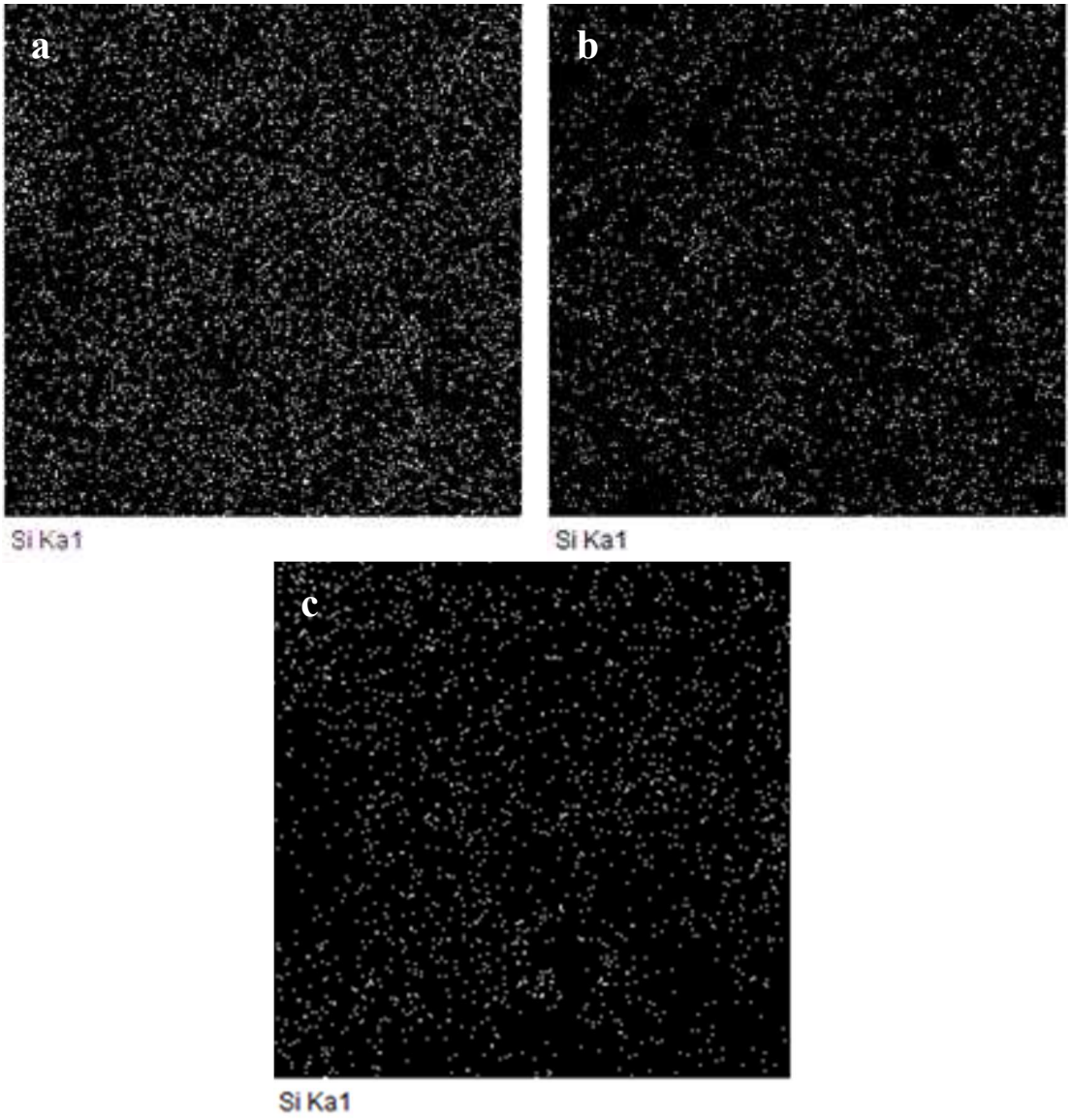

Figure 4.11 *X ray mapping of Si, in Al_2O_3-10SiC milled for (a) 02hours, (b) 04hours and (c) 06hours*

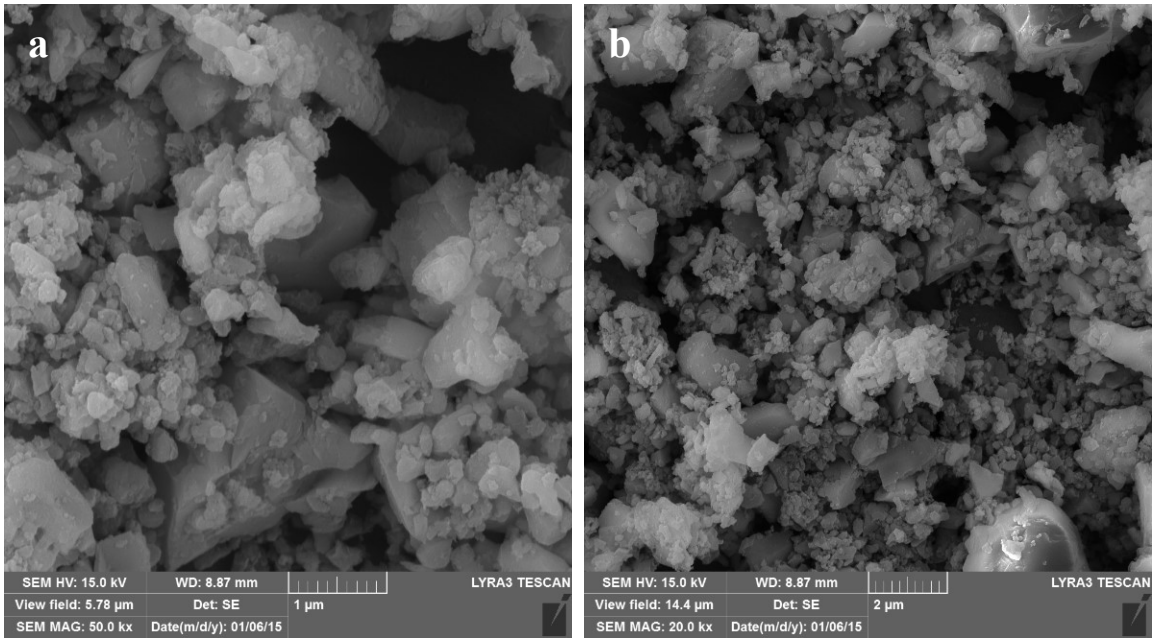

Figure 4.12 *FESEM showing distribution of SiC in Al_2O_3-10SiC milled for 04 hours at magnification of 50kx (a), and 20kx(b).*

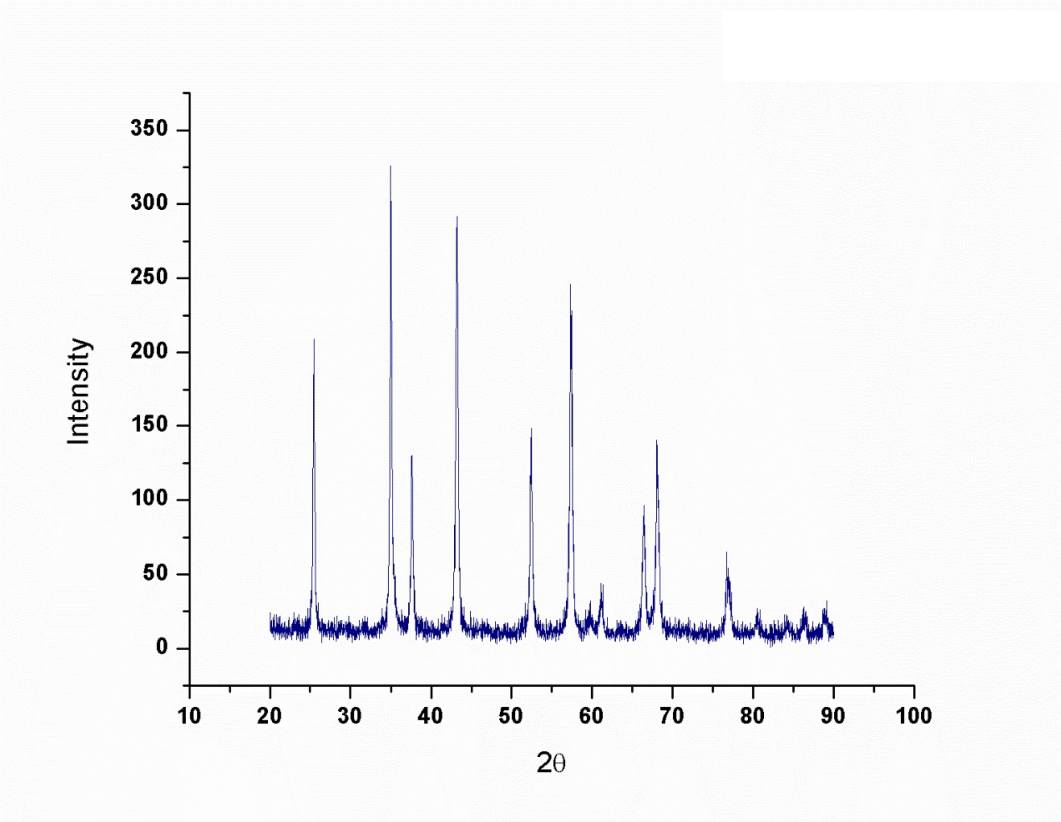

Figure 4.13 *XRD of Al_2O_3-10SiC milled for 4hours*

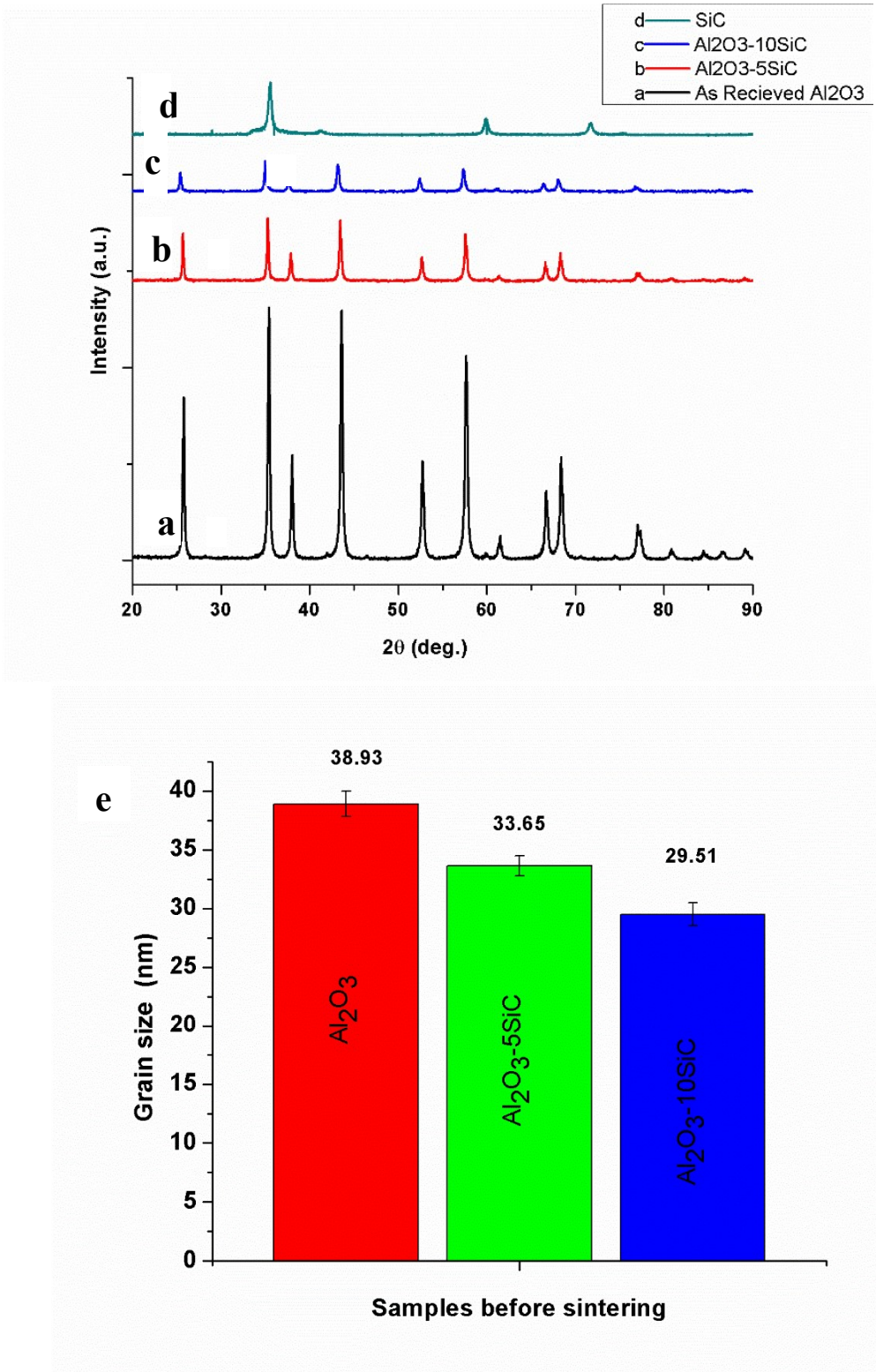

Figure 4.14 *XRD spectra of (a) as-received Al_2O_3, (c) Al_2O_3-5SiC, (c) Al_2O_3-10SiC Ball milled for 4h, and (d) as-received SiC. Reduction in crystallite size of alumina, as a result of milling is shown in (e).*

MWCNT content (1 and 2 %) were added through high energy probe sonication in the already synthesized Al_2O_3-5SiC and Al_2O_3-10SiC to obtain a hybrid nanocomposite powder composition. Al_2O_3-5SiC-1CNT, Al_2O_3-5SiC-2CNT, Al_2O_3-10SiC-1CNT and Al_2O_3-10SiC-2CNT hybrid powder compositions were prepared through the steps shown in ***Figure* 3.1** and were characterized using FESEM, X-ray mapping, and TEM to observe the distribution of both SiC and CNT in the alumina matrix. SiC plays a vital role in strengthening the grain boundaries and toughening the matrix, while the MWCNTs significantly increase the toughness value by introducing a number of the toughening mechanisms.

Besides the influential properties of CNTs, extensive literature has been written regarding their tendency to form agglomerates due to van der wall forces between them [63][20][81][65][82], and thus they are a major cause of nonhomogeneous distribution when used as reinforcement. However, using treated CNTs and mixing it to compositions through probe sonication and the particular processing parameters as shown in ***Figure* 3.1** to develop a hybrid nanocomposite powder, clearly indicates the homogeneous distribution of both SiC and CNTs as shown in **Figure 4.15** (a,b) and (c,d) respectively.

A typical x-ray mapping of Al, O, Si, and C in Al_2O_3-10SiC-2CNT is presented in ***Figure* 4.16**. It indicates uniform dispersion of SiC and CNTs in the sample.

TEM images of selected particles from Al_2O_3–5SiC-1CNTs powder, ball milled at 300rpm for 4 hours, is shown in ***Figure* 4.17**(a) and (b). It is clear that CNTs, as indicated by black arrows, are not agglomerated. This is mainly due to the use of functionalized CNTs, which minimized agglomeration [48][82]. The EDS analysis of particles marked 1 and 3, as

presented in ***Figure*** **4.17**(c) and (d), respectively, revealed that the particles are Al_2O_3 and SiC, respectively.

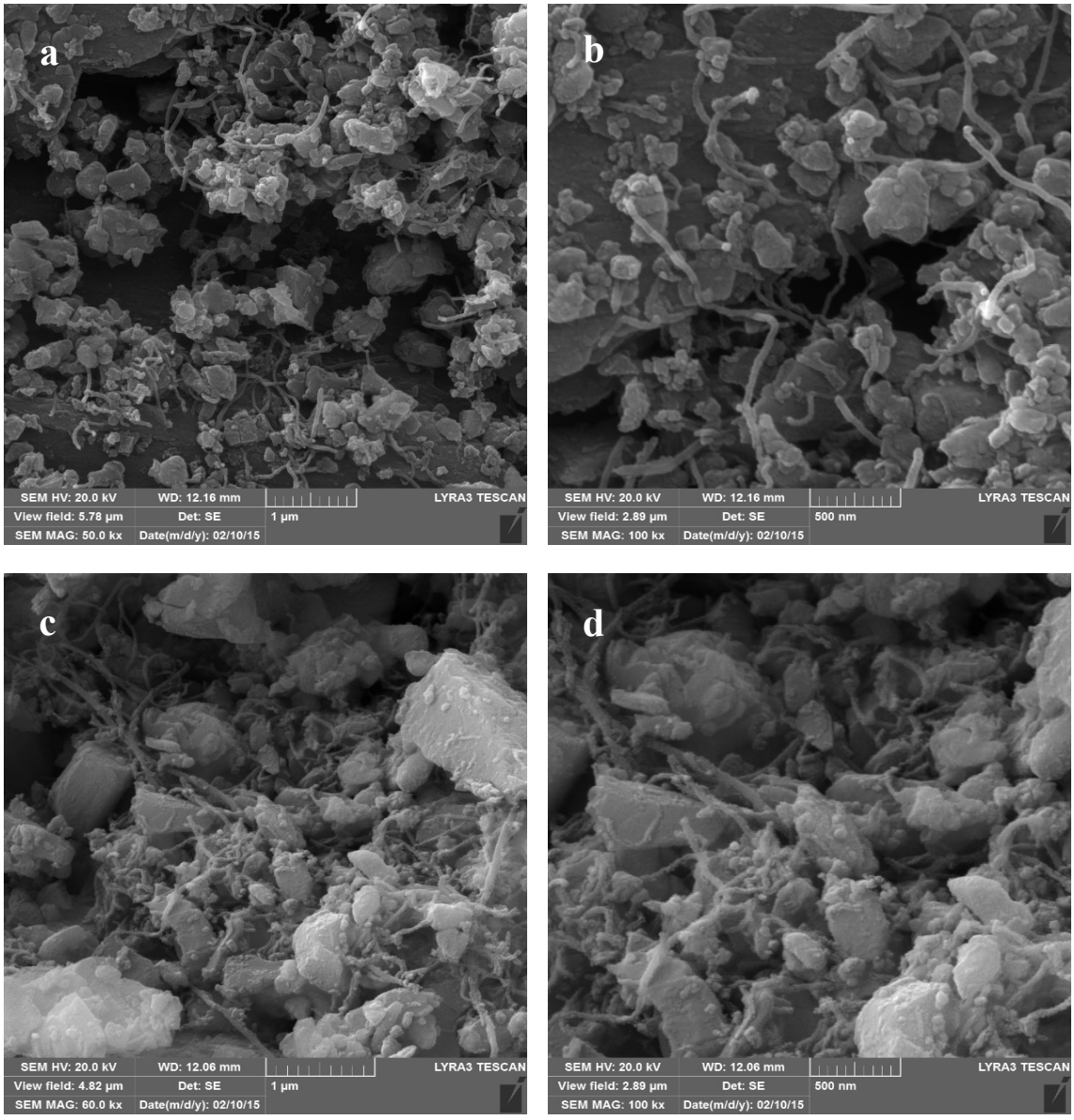

Figure 4.15 *FESEM of Al_2O_3-10SiC-1CNT (a,b) and Al_2O_3-10SiC-2CNT(c,d).*

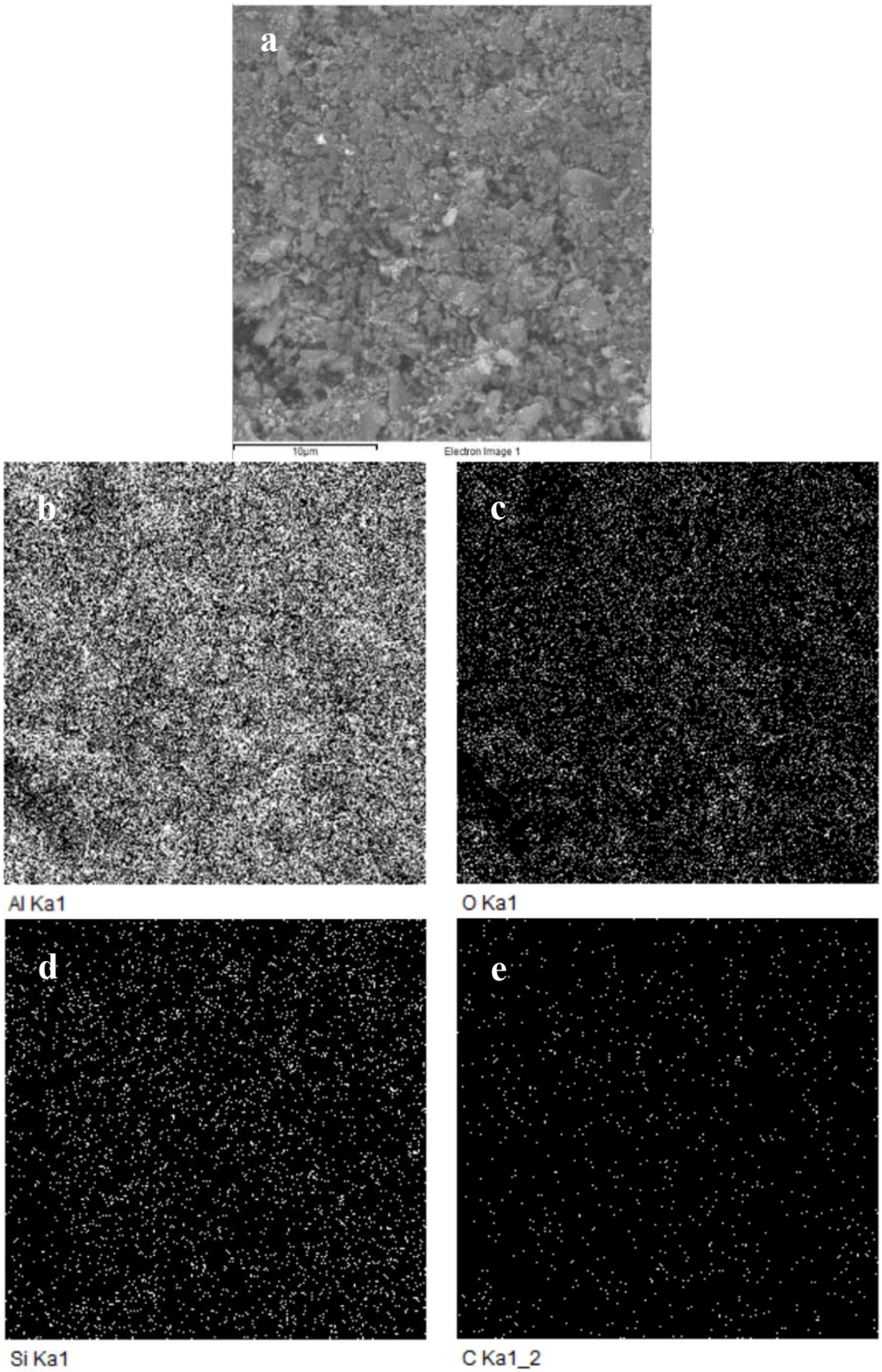

Figure 4.16 *FESEM (a) and X-ray mapping of Al(b), O(c), Si(d), and C(e) in Al_2O_3-10SiC-2CNT powder sonicated and milled for 4 hours.*

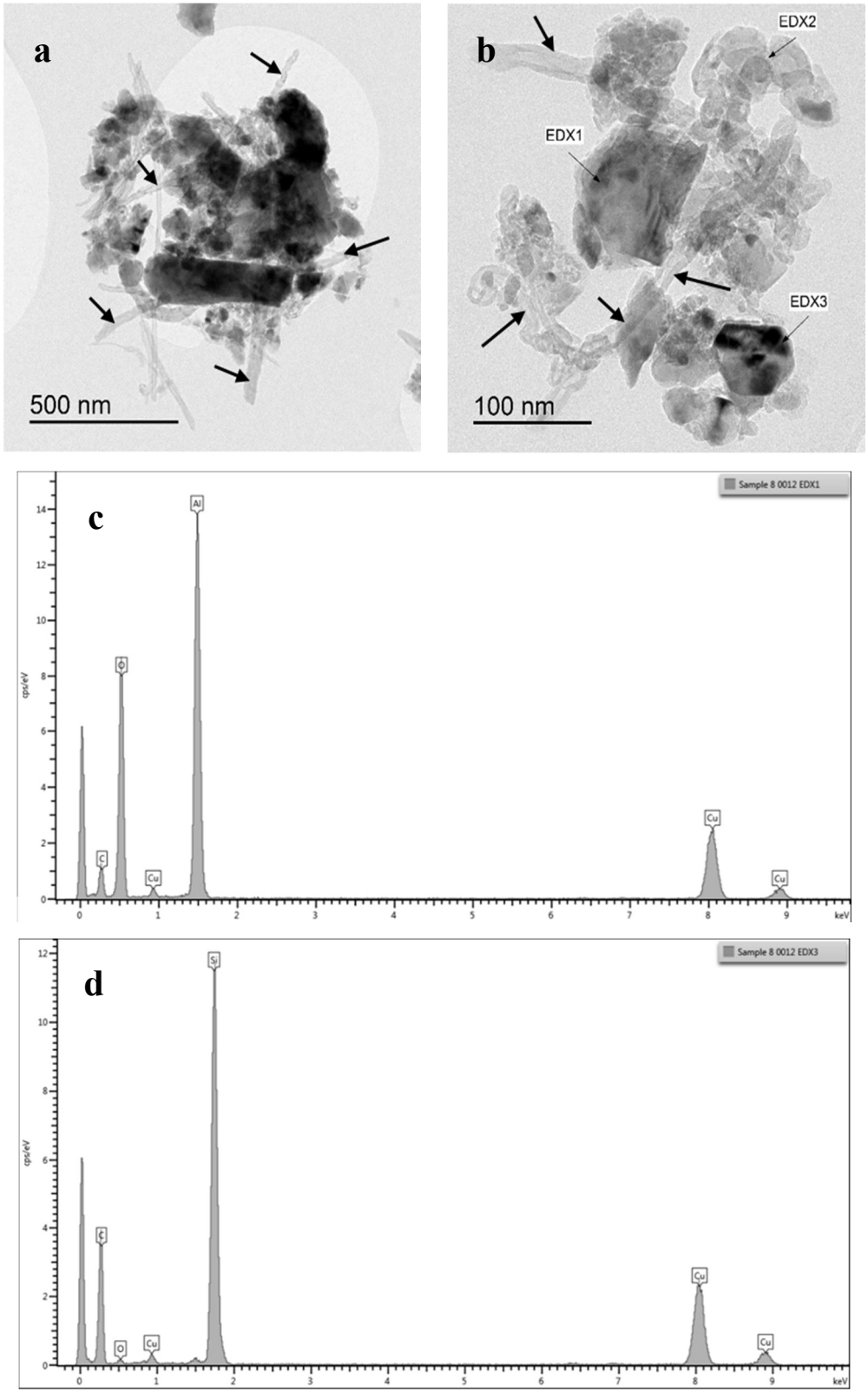

Figure 4.17 *HRTEM (a, b) and EDS (c, d) of Al_2O_3-5SiC-1CNT, showing homogeneous distribution of CNTs and SiC, as being depicted by the presence of each separate CNTs and SiC particles, even at high resolution micrographs.*

Micro-structural analysis revealed the uniform distribution of both SiC and MWCNTS in the developed hybrid nanocomposite, as explained above. Al_2O_3-SiC were first milled at 300rpm/4hours and CNTs were then added using high energy probe sonication. However, it was intended to explore the possibility of getting the same uniform distribution with enhanced mechanical properties at lower milling speeds and in a shorter time (100rpm/2hours) to reduce the risk of impurity during the milling of alumina with hard SiC.

The influence of milling conditions on reinforcement distribution is shown in ***Figure* 4.18.** The distribution of silicon and carbon in Al_2O_3-10SiC-1CNT was prepared using 100rpm/2hours ***Figure* 4.18** (b,c) and 300rpm/4hours ***Figure* 4.18** (e,f) respectively. It can be clearly seen that distribution is more homogeneously achieved in powder synthesized at 300rpm/4hours milling. This is due to the obvious formation of a comparatively high particle surface area and a reduction in crystallite size by ~23% as measured using the Scherrer equation from an XRD pattern of Al_2O_3-10SiC-1CNT powder. Powder synthesized using 100rpm/2hours showed only ~5% reduction in the crystallite size of alumina in the composite powder.

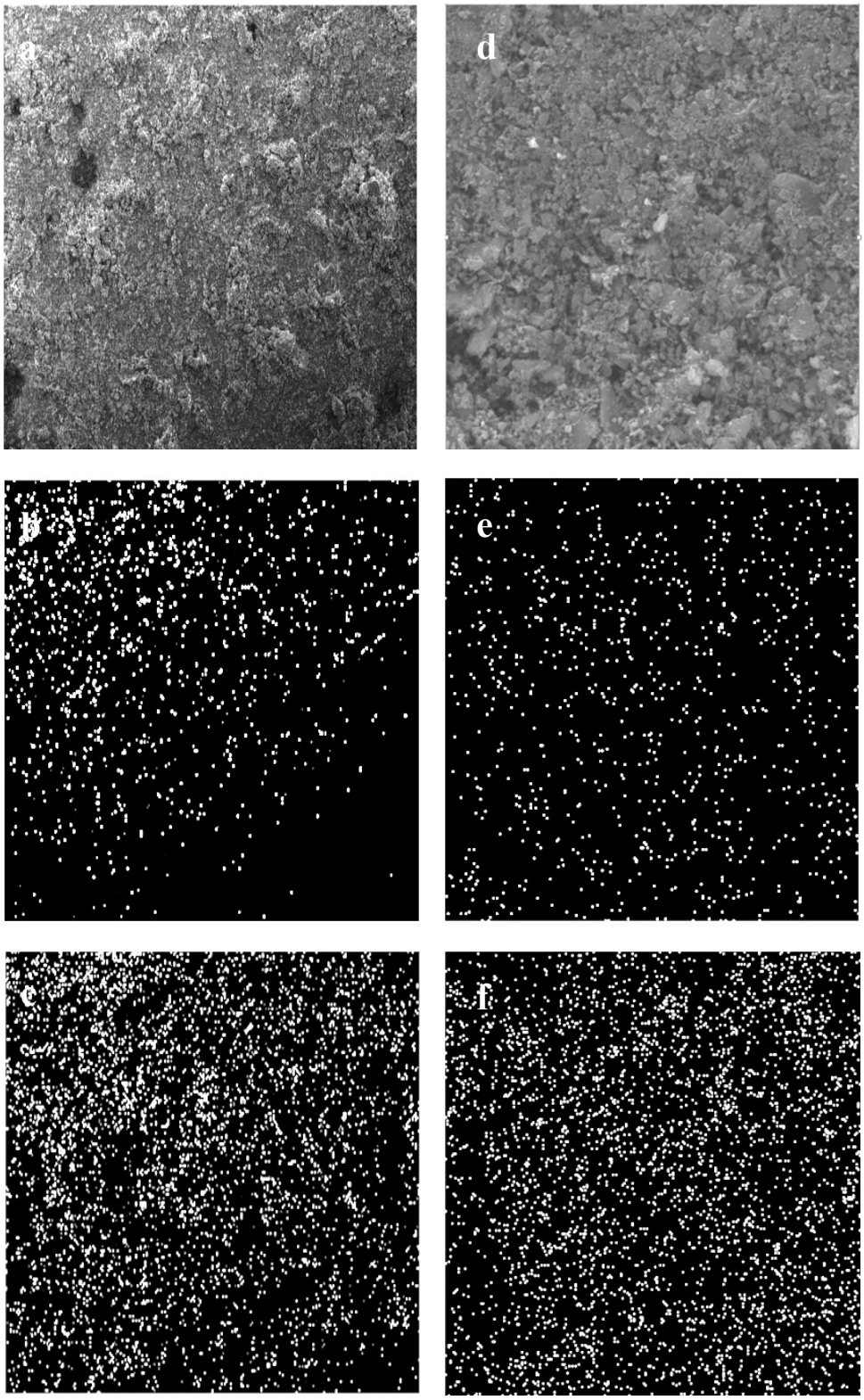

Figure 4.18 *FESEM micrographs of Al_2O_3-10SiC-1CNT showing distribution of silicon and carbon prepared using 100rpm/2hours (a,b,c) and 300rpm/4hours (d,e,f).*

4.1.2 Densification

All synthesized compositions along with α-alumina powder, as a reference material, attained dense structures when consolidated using spark plasma sintering at 1500ºC for a dwell time of 10min under a constant applied pressure of 50MPa.

Alumina is known to have poor sinterability [36]. However, high relative density values, as achieved in this work, show that almost fully dense monolithic alumina could be obtained using spark plasma sintering. Spark discharge generated between gaps and contact points of particle surfaces, during spark plasma sintering, increases the local temperature at these points. This either evaporates or melts the surface of the particles and leads to the formation of necks, which significantly increases the diffusion rate and results in higher density. Further rearrangement of the particles, during the spark plasma sintering process, is enhanced by the externally applied pressure, which also leads to increasing the driving force for densification. Higher densification rates during SPS lead to the development of a fine microstructure.

Monolithic alumina was found to have a relative density of 99.3%, which increased to 99.76% and 99.36% with the addition of small reinforcement contents (Al_2O_3-5SiC and Al_2O_3-5SiC-1CNT). Composites having comparatively higher reinforcement contents (Al_2O_3-5SiC-2CNT, Al_2O_3-10SiC, Al_2O_3-10Si-1CNT and Al_2O_3-10SiC-2CNT) showed a minimal reduction in density, although >98%, with respect to reference monolithic alumina. It is widely accepted that the addition of reinforcement reduces the densification and makes obtaining fully dense nanocomposites difficult. This is because the presence of the hard reinforcement hinders mass transportation and reduces the ability of the powder to plastically deform [36]. However, high relative density values, as achieved in this work,

show that almost fully dense monolithic alumina and hybrid composites could be obtained using spark plasma sintering. This can be attributed to higher local heating at particle surfaces due to spark discharge, the re-arrangement of particles, the breakdown of agglomerates which is due to higher applied pressure, and a fine microstructure which is due to the higher diffusion rate in spark plasma sintering.

This small reduction in relative densification, particularly for higher reinforcement contents, adversely effects the elimination of pores and hinders the diffusion mechanism thereby reducing the rate of diffusion and relative densification of the nanocomposite. However, beside the stated hindrance in the diffusion mechanism, attaining almost full densification in all samples (>98%), are higher than those reported for Al_2O_3–SiC-CNT composites (>95.1%) [29] and Al_2O_3–CNT-SiC composites (>96.4%) [83] obtained by SPS at 1550 °C and 50 MPa. However, the values are comparable with the Al_2O_3-graphene-CNT samples (>98%) prepared by SPS at 1650 °C for 10 mins and 40 MPa [37] and Al_2O_3–Graphene platelets-CNT composites (> 97.35%) obtained by SPS at 1500 °C for 3 mins and 50 MPa [8]. Higher relative density values were also reported for Al_2O_3-SiCw-CNT composites (>99%) obtained by hot-pressing at 1750 °C for 1 hour at 30 MPa [38] and Al_2O_3-Gaphene platelets-CNT composites (98%) obtained by hot-press sintering at 1650 °C for 1 hour and an external pressure of 40 MPa [84].

The phenomenon of getting lower densification, due to the addition of secondary phases, was also noticed by B.Mar *et al* [54] and Lima and Wook *et al* [85] while studying the effect of SiC and CNTs on the microstructure of alumina. In addition, Tatami *et al* [86] and Jiang *et al* [87] also observed the same findings while preparing silicon nitride and titanium nitride nanocomposites with CNTs, as reinforcement. Boccaccini *et al* [88] and Ning *et al*

[89] investigated the influence of adding CNTs to glass ceramic and found a reduction in densification due to the re-crystallization new rigid phase, which nucleated at points of CNTs presence.

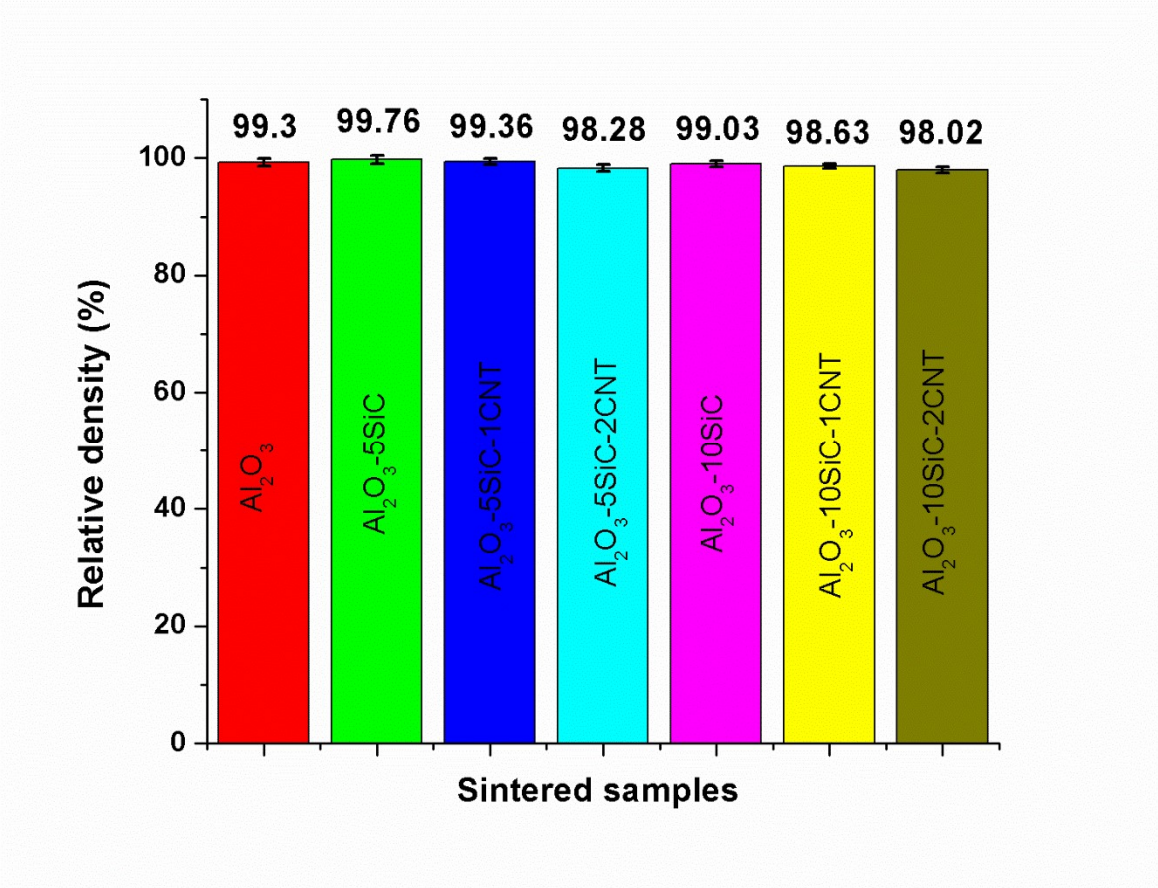

Figure 4.19 *Relative density of composites, synthesized through sonication and BM, sintered at 1500ºC for 10 minutes*

During spark plasma sintering of the Al_2O_3-SiC-CNT nanocomposite, densification behavior was closely observed by recording data on the punch displacement against processing temperature (1100-1500ºC) as shown in ***Figure* 4.20** (a). Three different rates of densification were observed, as marked (Stage-1, Stage-2 Stage-3). A minor amount of SPS ram displacement during initial heating (until 1150ºC) stage-1, can correspond to initial particle re-arrangement during sintering. Stage-2, presenting a steeper slope and a major

portion of ram displacement in the range 1150-1375ºC, was observed playing a dominant role in increasing the relative densification of the nanocomposite and infers higher shrinkage rates in the sample. The final stage-3 during densification still shows a certain ram displacement, although with a decreasing slope as compared to stage-2, which corresponds to the elimination of pores. The effect of CNT content in sample composition, on relative densification, as recorded by the ram displacement, is elaborated in ***Figure* 4.20** (b). The decreasing slope and reduced amount of ram displacement indicate that the higher CNTs content in Al_2O_3-10SiC-2CNT hinders densification during the sintering process. This agrees with the relative densification data, after the sintering process, as shown in ***Figure* 4.19** and ***Figure* 4.21.**

a

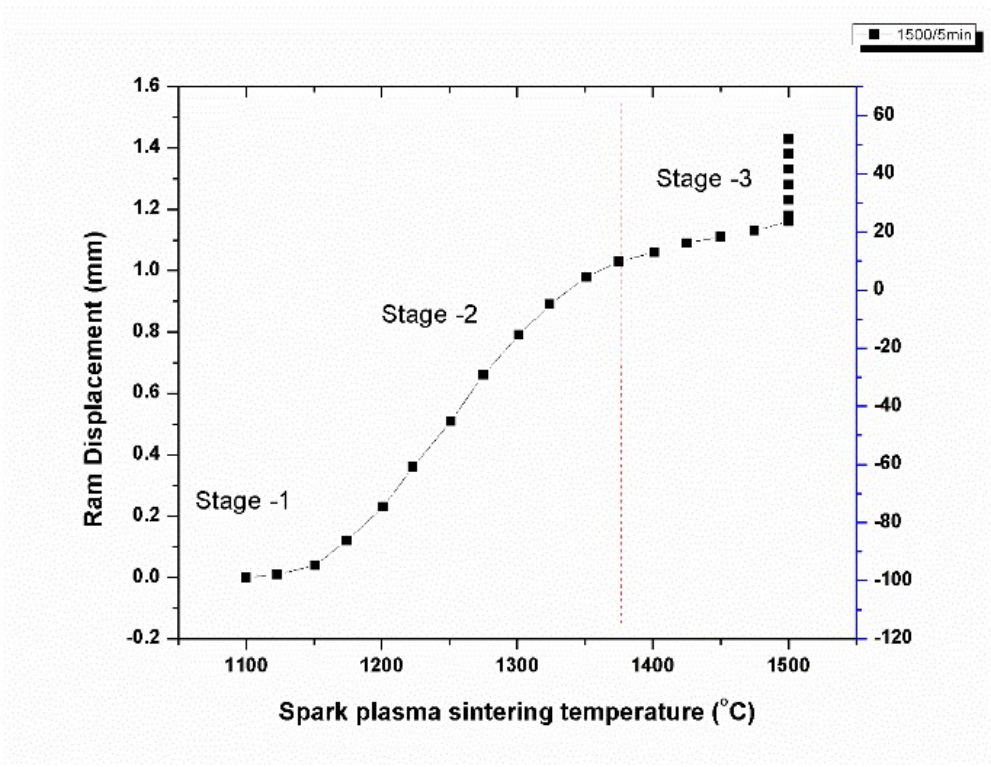

b

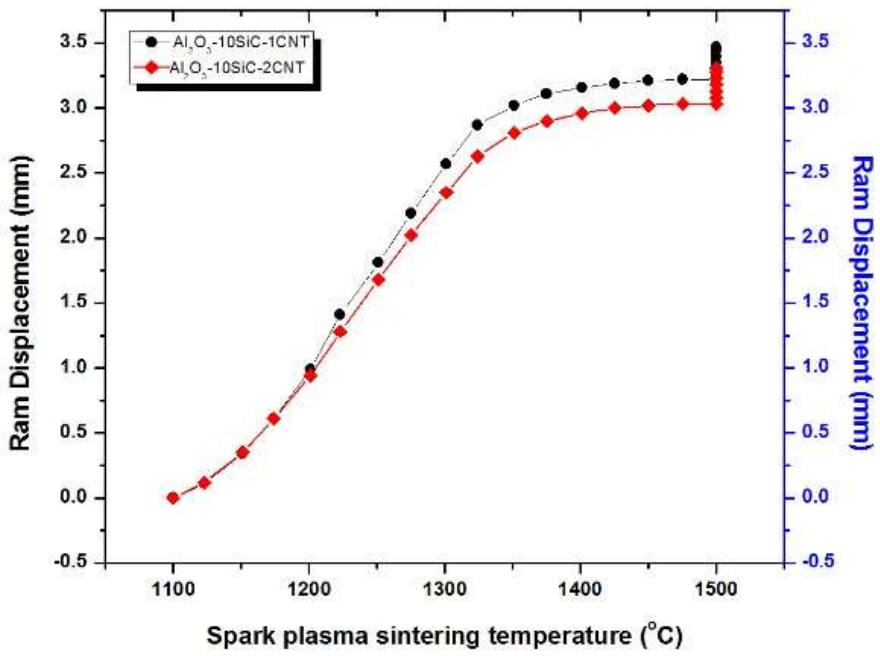

Figure 4.20*(a) indicates three different stages corresponding to different densification rates, which represents relative ram displacement during spark plasma sintering of Al_2O_3-SiC-CNT samples as a function of temperatures and (b) elaborates densification behavior as a function of CNT content.*

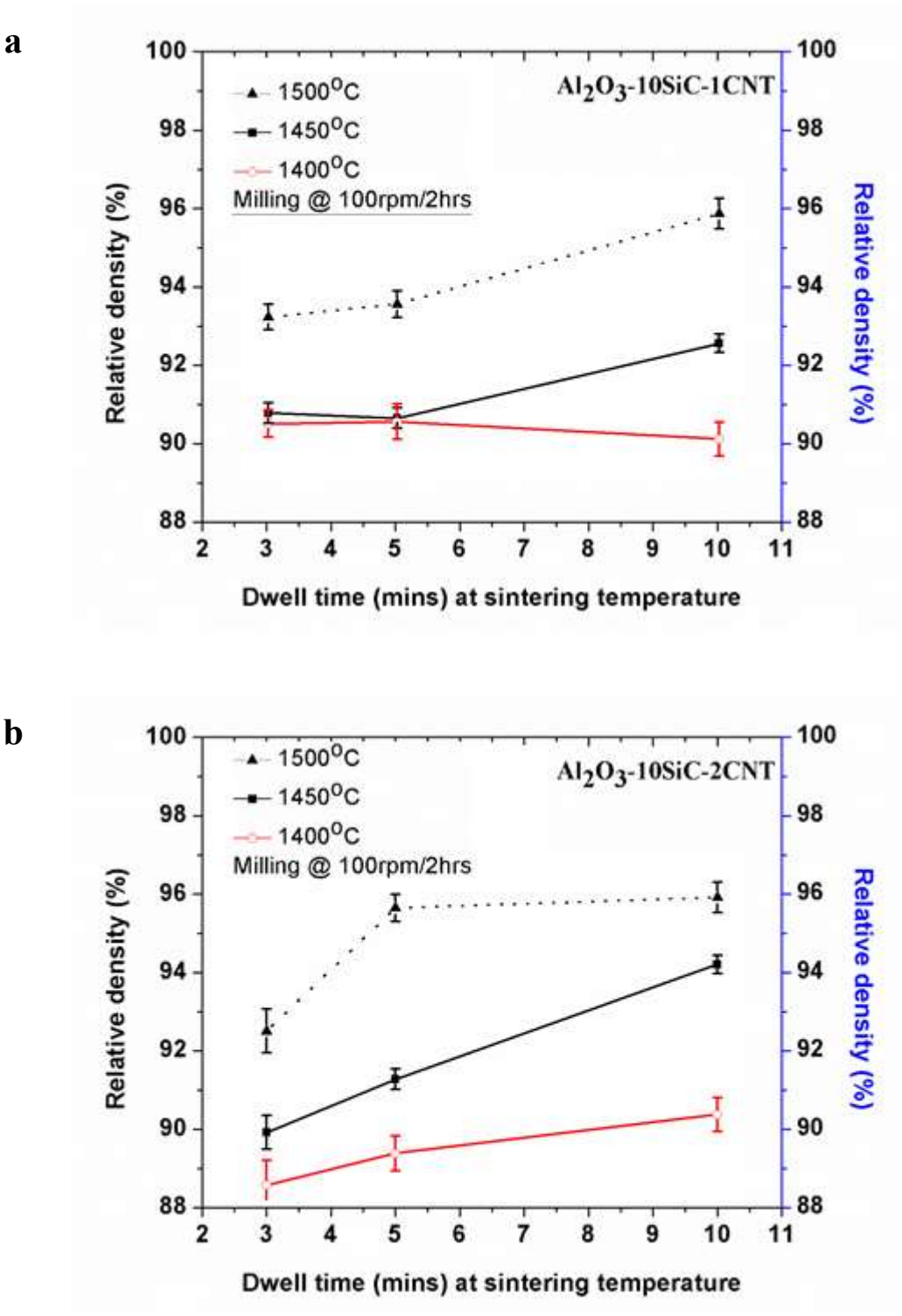

Figure 4.21 *Showing effect of sintering parameters on the relative densification of (a) Al_2O_3-10SiC-1CNT and (b) Al_2O_3-10SiC-2CNT, milled at 100rpm/2hours*

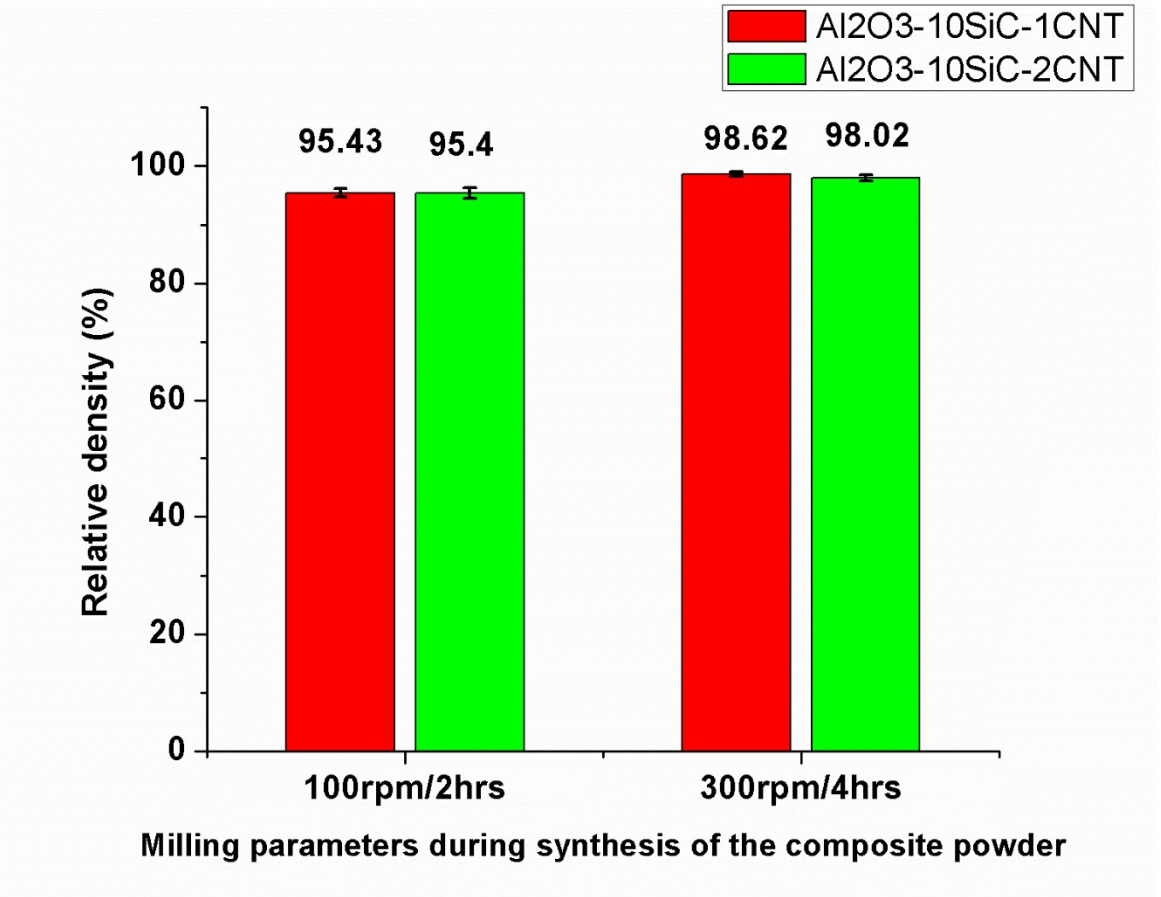

Figure 4.22 *Showing effect of milling conditions on the relative densification of the developed nanocomposite, when sintered at 1500oC/10min under 50MPa.*

Beside the presence of two reinforcements, with different morphology, in the alumina matrix, almost full densification was attained in these nanocomposites, as discussed above. Nevertheless, it was proposed to discover the opportunity for getting the same densification of these hybrid nanocomposites by using lower processing parameters than those reported above. Lower milling (100rpm for 2hours) and sintering parameters (1400ºC, 1450ºC and 1500ºC) for 3, 5 and 10mins, were chosen to reduce the risk of impurities during mass production and grain growth, if any, during the sintering process. Al_2O_3-10SiC-1CNT and

Al_2O_3-10SiC-2CNT prepared using ball milling at 100rpm for 2 hours, were chosen for this part of the study.

***Figure* 4.21** (a,b) represents the effect of CNT content on the relative densification of composite powder synthesized with lower milling parameters, as a function of sintering parameters (sintering temperature and holding time). All samples have shown a general increase in relative densification with an increase in sintering temperature and holding time. This is due to the high input of thermal activation energy which promotes joule heating of the powder interface with a higher intensity in order to reach full densification [90]. All samples, prepared using 100rpm/2hours, obtained lower densification at all three different soaking times, when sintered at 1400^{o}C and 1450^{o}C. However, a sudden increase in densification implies on-set temperature for rapid densification when sintered at 1500^{o}C for 10mins and obtained a maximum value of 95.4%. However, almost full densification (98.6%) was reported, when the same composition was milled instead at 300rpm/4hours, and sintered at the same sintering temperature as shown in **Figure 4.22**. This is because of the probable high surface area created and a 23% reduced crystallite size after milling at 300rpm/4hours. Powders which were milled at 100rpm/02hours have shown only a 5% reduction in crystallite size.

Powders have retained the tendency of lower densification with an increase in CNT content. Al_2O_3-10SiC-2CNT exhibited a comparatively lower compact-ability than Al_2O_3-10SiC-1CNT, thus reducing the relative density to 98.6% and 98.02% respectively, which agrees with the ram displacement data shown in **Figure 4.20**(b). Earlier literature reported that higher CNT content acts as stagnation and a source of grain growth retardation at grain boundary [91][92][87][42][27] and decreases the possibility to remove micro-porosity in

the entangled CNTs at the grain boundary [93], thus reducing the relative densification of the nanocomposite.

4.1.3 Microstructure

Homogeneous distribution of SiC and CNT in alumina was confirmed through x-ray mapping in the synthesized powder. After consolidation, these samples were again analyzed to observe the consistency in uniformity and the distribution of reinforcement in the alumina matrix. X-ray mapping of Al, O, Si, and C in Al_2O_3-10SiC-2CNT sintered sample having high reinforcement content is shown in ***Figure* 4.23**. It was found through analysis that uniformity and a homogeneous distribution of both SiC and CNT in the alumina matrix was retained even after consolidation.

Spark plasma sintered composite samples, along with the reference monolithic alumina, were fractured to explore the distribution of reinforcement and the mode of fracture in each sample. Typical FE-SEM micrographs for fractured surfaces of reference monolithic Al_2O_3 are shown in ***Figure* 4.24**. The x-ray diffraction pattern of the consolidated monolithic alumina was analyzed to measure crystallite size which was limited to below 100nm, while grain size was found to be in the range of 2-3μm, as can be seen from the fractured surfaces. The initial crystallite size of alumina powder was 38.93nm, however, it was increased to 93.39 nm during the sintering process, which is normal and is a normal phenomenon. Fractured surfaces were found to have completely intergranular crack propagation, which was also documented earlier [94][95].

Figure 4.25 presents high magnification FESEM micrographs of fractured surfaces of Al_2O_3-SiC and Al_2O_3-SiC-CNT nanocomposites. Enhanced distribution of SiC and CNT

was found in the samples. The absence of any cluster formation, even due to fine SiC, clearly indicates the uniform distribution of SiC in the consolidated samples. The same ***Figure*** shows almost all SiC nanoparticles predominantly located within grains contrary to comparatively large SiC and CNTs (having a larger aspect ratio) on the GB. The presence of SiC on the GB restricts grain growth thus promoting a uniform and finer microstructure as comparative to monolithic alumina.

The effect of SiC content and CNT content refining alumina grains and changing fracture mode is illustrated in ***Figure*** **4.26** and ***Figure*** **4.27** respectively. The extent of agglomerated nanoparticles, although at an unnoticeable level, at grain boundaries with an increasing amount of secondary phases was noticed. Morphology of the fractured surfaces illustrates a transfer of the almost intergranular fracture mode to a mixture of the inter and transgranular fracture mode, with the fraction of mixed fracture mode increasing with an increase in the amount of added secondary phases (SiC) and CNTs to the alumina matrix.

The absence of any extra than characteristic peaks, as shown in ***Figure*** **4.28**, in all sintered samples assures the non-existence or formation of any other phase or alloy formation during sintering of these nanocomposites.

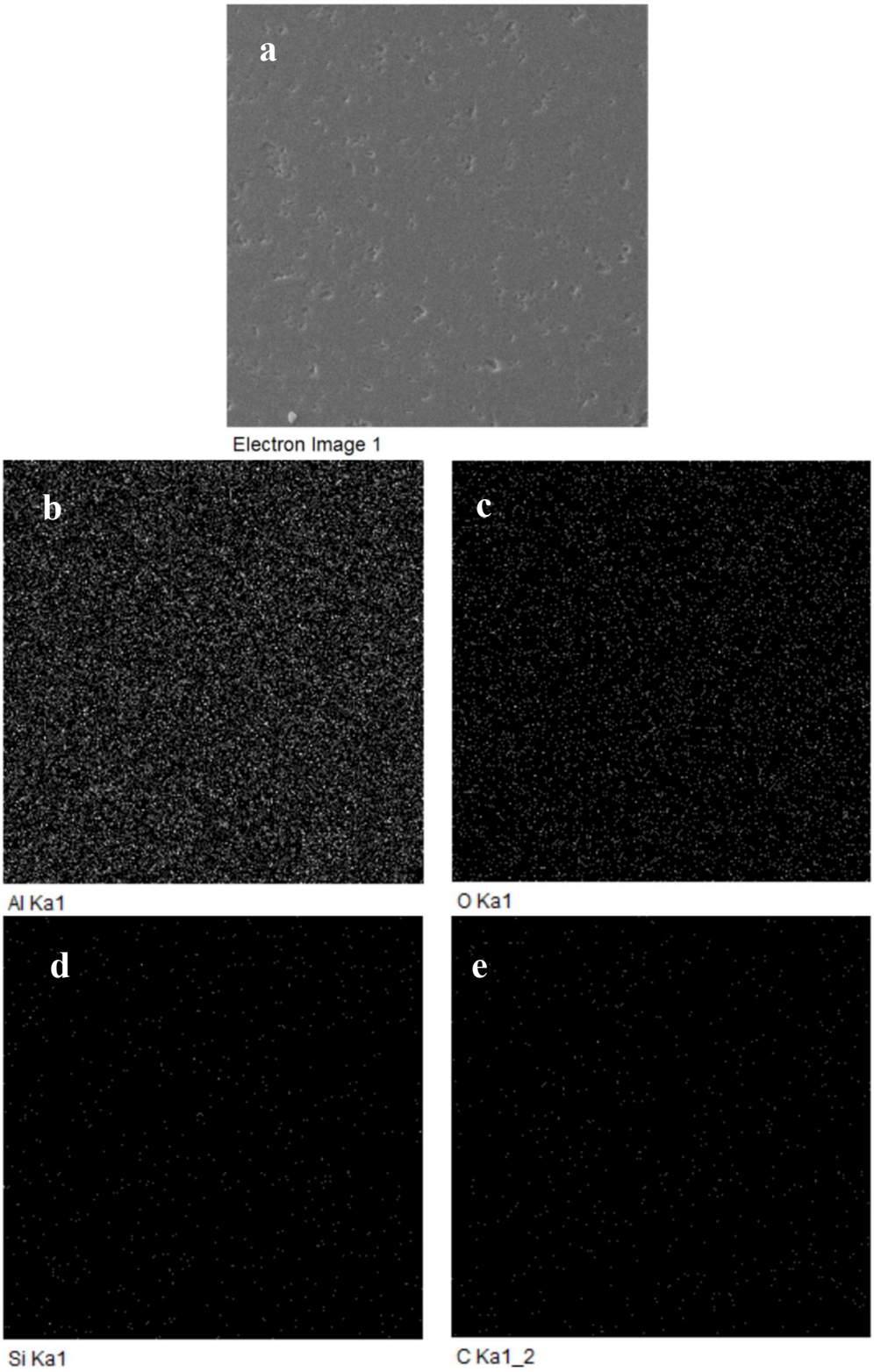

Figure 4.23 *FESEM (a) and X-ray mapping of Al_2O_3-10SiC-2CNT, showing complete and uniform distribution, of Al (b), O(c), Si(d), and C(e).*

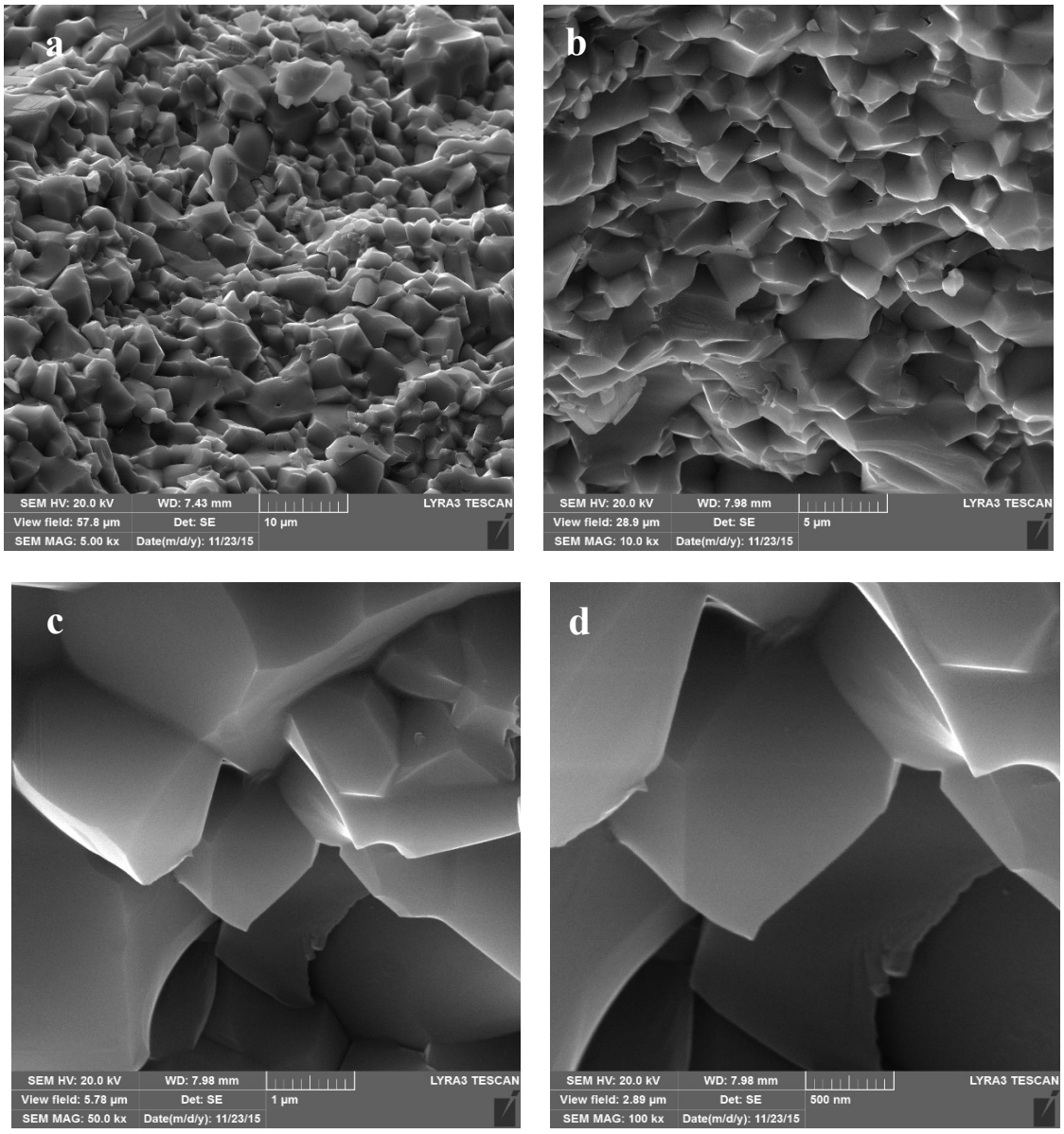

Figure 4.24 *FE-SEM micrographs at different magnification of 5kx(a), 10kx(b), 50kx(c) and 100kx (d) showing intergranular crack propagation in a fractured surface of* Al_2O_3.

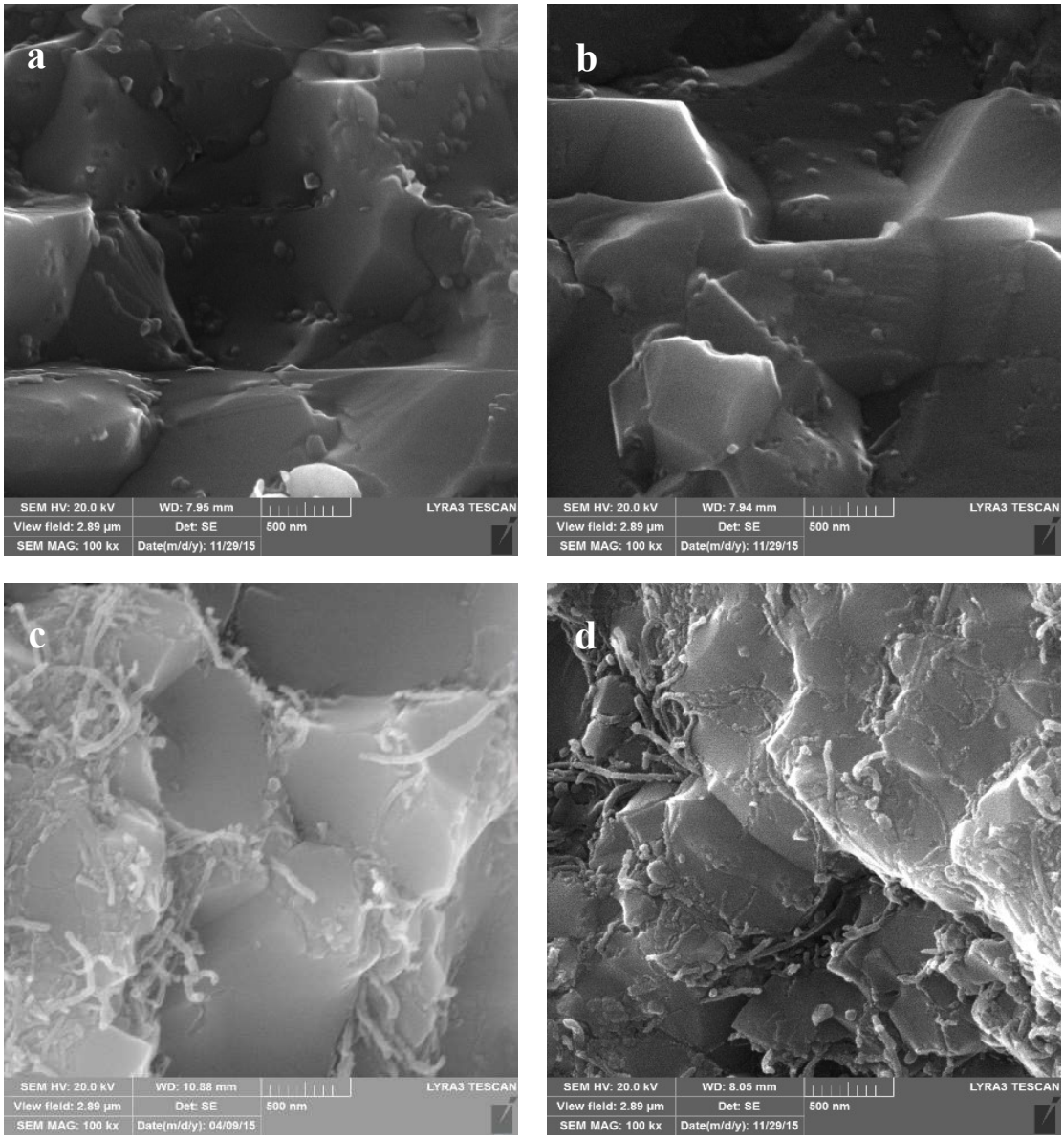

Figure 4.25 *FESEM micrographs showing fractured surfaces of (a) Al_2O_3-5SiC, (b) Al_2O_3-10SiC, (c) Al_2O_3-5SiC-2CNT, (d) Al_2O_3-10SiC-2CNT.*

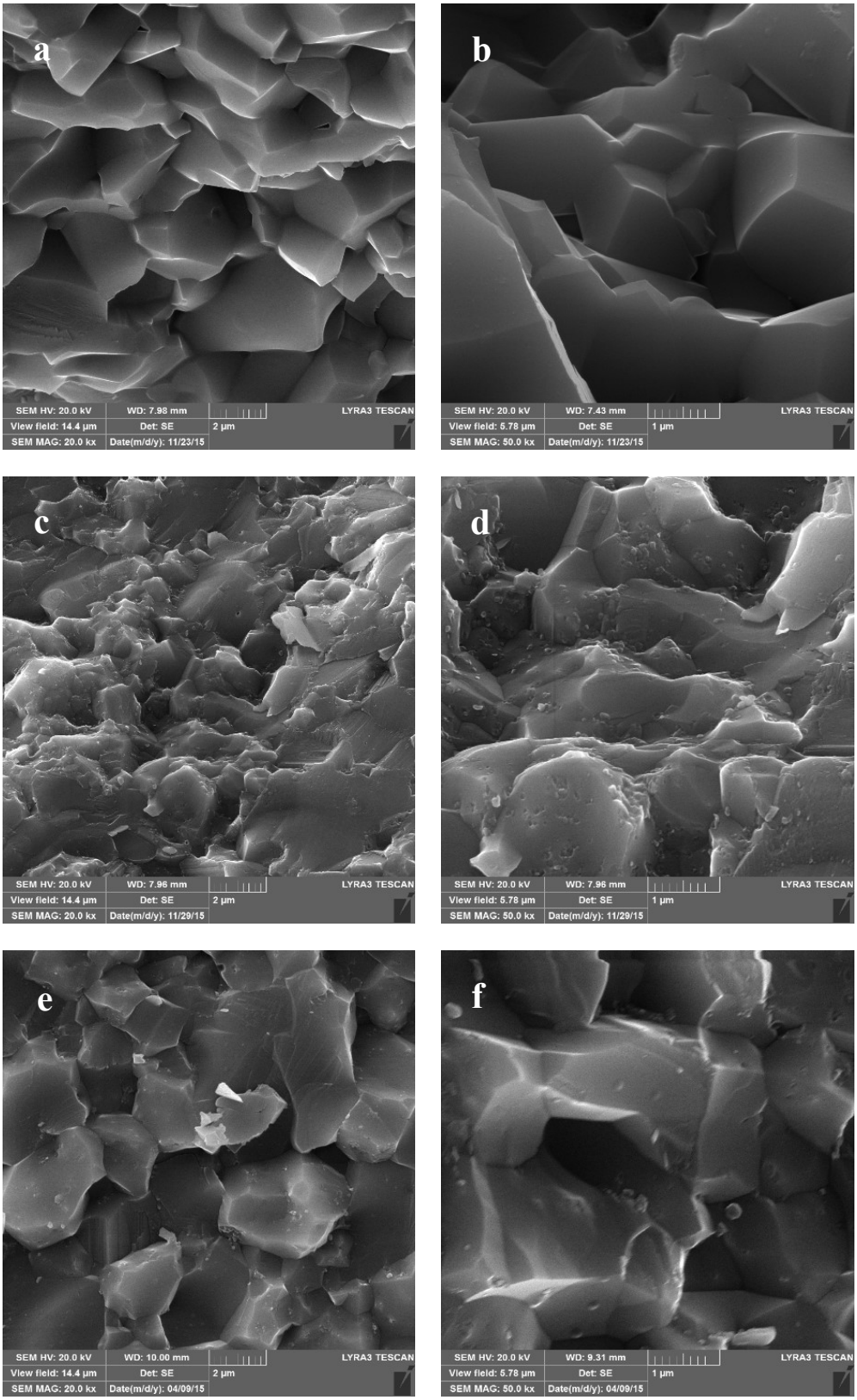

Figure 4.26 Effect of SiC in fracture surfaces of Al_2O_3 (a, b), Al_2O_3-5SiC (c, d) and Al_2O_3-10SiC (e, f)

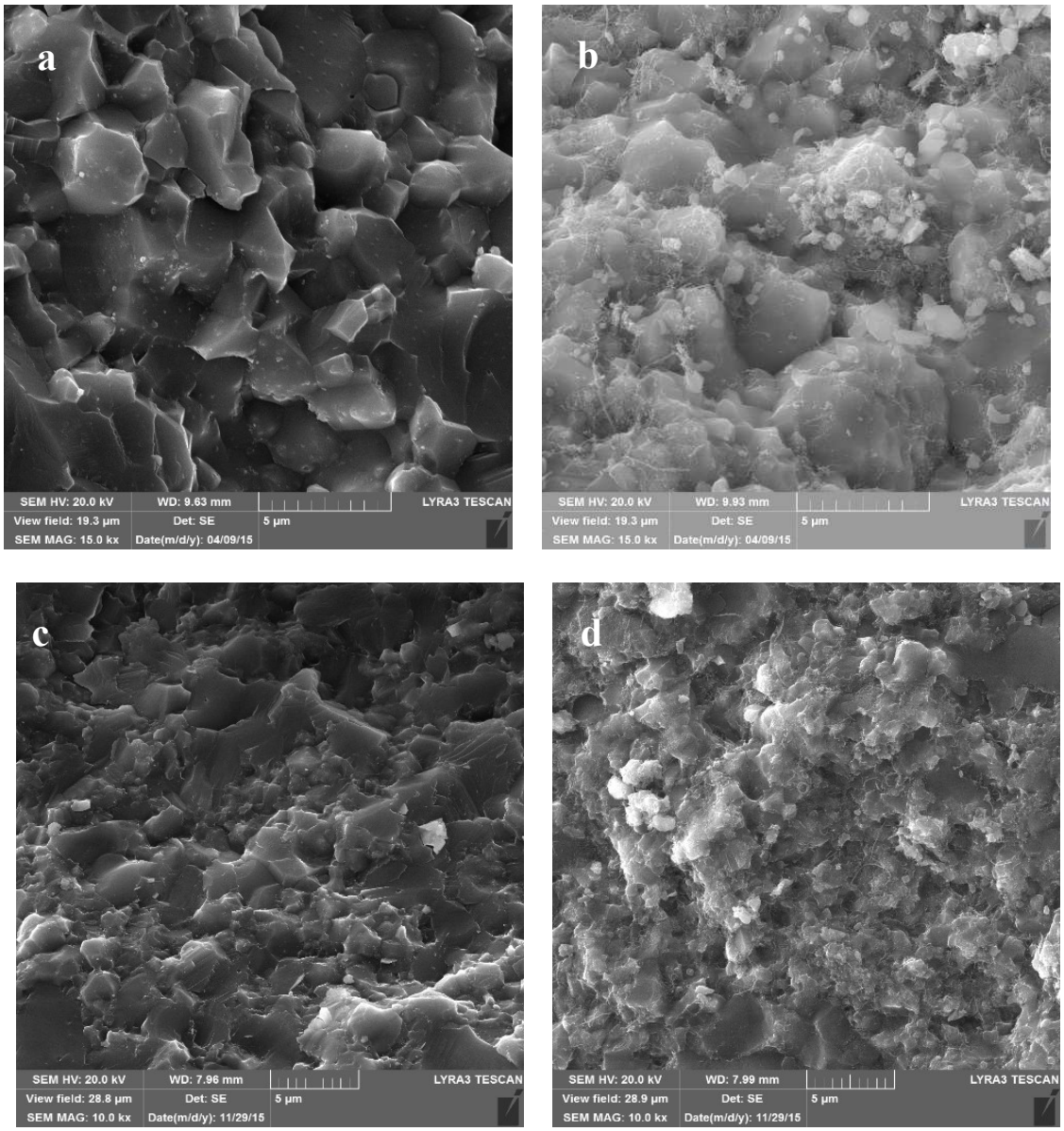

Figure 4.27 *Effect of CNTs in developing microstructure for fractured surfaces of (a)Al_2O_3-5SiC, (b) Al_2O_3-5SiC-2CNT, (c) Al_2O_3-10SiC, and (d) Al_2O_3-10SiC-2CNT*

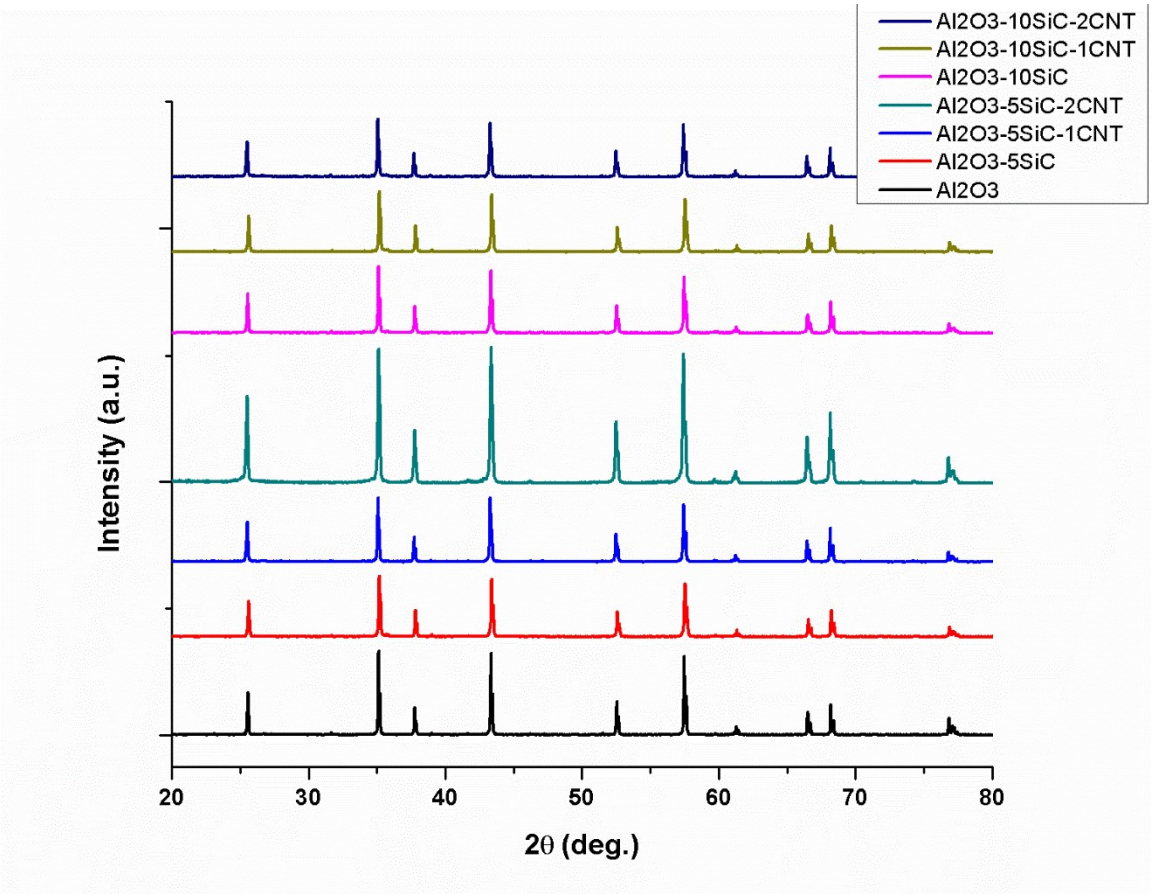

Figure 4.28 *XRD of sintered monolithic alumina, Al_2O_3-5SiC and Al_2O_3-10SiC and the corresponding hybrid nanocomposite*

4.1.4 Mechanical Properties

Hardness

The hardness values of all samples, prepared using 300rpm/4hours milling and sintered at 1500°C for 10mins under an applied pressure of 50MPa, are presented in ***Figure* 4.29**. Monolithic Al_2O_3 ceramic material recorded an Hv_{10} hardness of 18.56Gpa. However, the addition of 5% and 10% SiC to Al_2O_3 increased its hardness to 21.78Gpa and 20.89, respectively. This corresponds to an increase of 18% and 13% respectively compared with monolithic alumina. This increase in hardness is attributed to the presence of a hard

secondary phase (SiC), which results in a finer microstructure due to a pinning effect at the grain boundary. An increase in hardness, due to the addition of SiC, can also be explained by a reduced volume of micro-plastic deformations in finer alumina grains. The slightly reduced hardness of Al_2O_3-10SiC compared to Al_2O_3-5SiC corresponds to a relatively reduced density due to increased reinforcement content at the grain boundary which hinders densification, as discussed above. The hardness of this composite, however, remained higher than the hardness of the monolithic Al_2O_3. This is in agreement with the results obtained by Dong et al. [55] and Ko et al. [56]. Nakahira and Niihara [57] reported that the hardness of Al_2O_3–SiC nanocomposites followed a linear rule of mixtures as a function of the SiC content. This behavior was confirmed by Parchoviansky and co-workers [10] and Csehova el al. [96]. However, in this study, the change in hardness is in agreement with the trend observed by other researchers who found that the hardness of Al_2O_3-SiC nanocomposites increased with an increase of SiC content up to 5 wt.% [55], 7.5 vol% [58], and 10 vol% [59], then decreased with a further increase in the SiC content. The improvement in the hardness of Al_2O_3-SiC composites could be attributed to the presence of the SiC hard phase and the small grain size of the alumina matrix. The refinement of the microstructure in the presence of SiC particles, as observed from the fractured surfaces presented above, increases the hardness because grain boundaries restrict dislocation movement [97].

The addition of 1% CNTs to Al_2O_3-5SiC decreased its hardness from 21.78 to 19.77Gpa. A further increase of CNTs content to 2% decreased its hardness to 19.11. As for Al_2O_3-10SiC, the addition of 1% CNTs didn't show any significant change in hardness, although a further increase of CNTs content to 2% decreased it from to 20.81to 17.50Gpa, which

corresponds to respective densification. However, the hybrid nanocomposites exhibited improved hardness with respect to Al_2O_3, with the exception of the Al_2O_3-10SiC-2CNTs nanocomposite.

Al_2O_3-10SiC-1CNT exhibited a maximum hardness of 21GPa (13% increase relative to monolithic alumina). The hardness of any material is designated by its grain size [34]. CNTs are equally distributed at the grain boundary, while SiC are both at the grain boundary and within grains, as shown in ***Figure* 4.25** and reported earlier [29].

The presence of SiC retarded crystallite size by 18%, while both SiC and CNT at the grain boundary impeded it by 31%, as analyzed by their respective XRD patterns. The enhanced hardness of Al_2O_3-10SiC-1CNT are analogous to grain size reduction as explained by the Hall Petch law. This law estimates the micro-hardness of nanocomposites [98][99] and indicates the influence of crystallite size and thus the number of grain boundaries that impedes dislocation slips, in addition to obstructing dislocation pile-up and thereby affecting the hardness of the material

$Hv=H_0 + k \cdot d^{-½}$, where H0 is the intrinsic material resistance to dislocation motion, K is the material strengthening coefficient and d is the average particle size[34].

Lower hardness in Al_2O_3-10SiC-2CNT corresponds to the respective densification attained, as shown in ***Figure* 4.19** and can be attributed to the higher reinforcement content at the grain boundary, which reduces atomic diffusion coefficient at the grain boundary [60] and reduces cohesion between the grains [100], thus damaging the grain refinement phenomenon and hence densification and hardness. Reduced hardness values at a higher content of reinforcement was also documented earlier[29][30][27][21].

Al_2O_3-10SiC-1CNT exhibited maximum hardness, as discussed above, however the intension was to explore the possibility of either getting the same or even better hardness values of hybrid nanocomposite using lower milling and sintering parameters than reported above. Lower milling (100rpm for 2hours) and sintering parameters (1400°C, 1450°C and 1500°C) for 3, 5 and 10mins, were chosen to reduce the risk (if any) of impurities during mass production and grain growth during the sintering process. Al_2O_3-10SiC-1CNT and Al_2O_3-10SiC-2CNT were chosen for this part of the study.

Influence of CNT content on the vickers hardness of Al_2O_3-10SiC-1CNT and Al_2O_3-10SiC-2CNT, as a function of sintering temperature and holding time, is presented in ***Figure* 4.30**. These compositions were prepared using milling at 100rpm/2hours. Both compositions revealed an over-all tendency of increasing hardness with increasing sintering parameters, although samples containing 1% CNT resulted in comparatively higher values for each set of sintering parameters. The increasing trend of hardness corresponds to the respective relative densification data, shown in ***Figure* 4.21**.

The influence of milling conditions on the vickers hardness of powder composition is presented in **Figure 4.31**. The maximum hardness value of ~21GPa (a 13% increase relative to monolithic alumina) is obtained by a sample containing lower (1wt %) CNT content and by being milled for longer and under high-speed conditions (300rpm/4hours). These samples were consolidated at 1500°C for a holding of 10mins.

The hardness and densification of higher CNT content in Al_2O_3-10SiC-2CNT was adversely affected due to the decrease in the atomic diffusion coefficient by the presence of CNTs at the grain boundary [60] and due to a reduction in the cohesion between the grains

[100] thus damaging the grain refinement phenomenon and hence densification and hardness. The same behaviour was documented earlier [29][30][27][21].

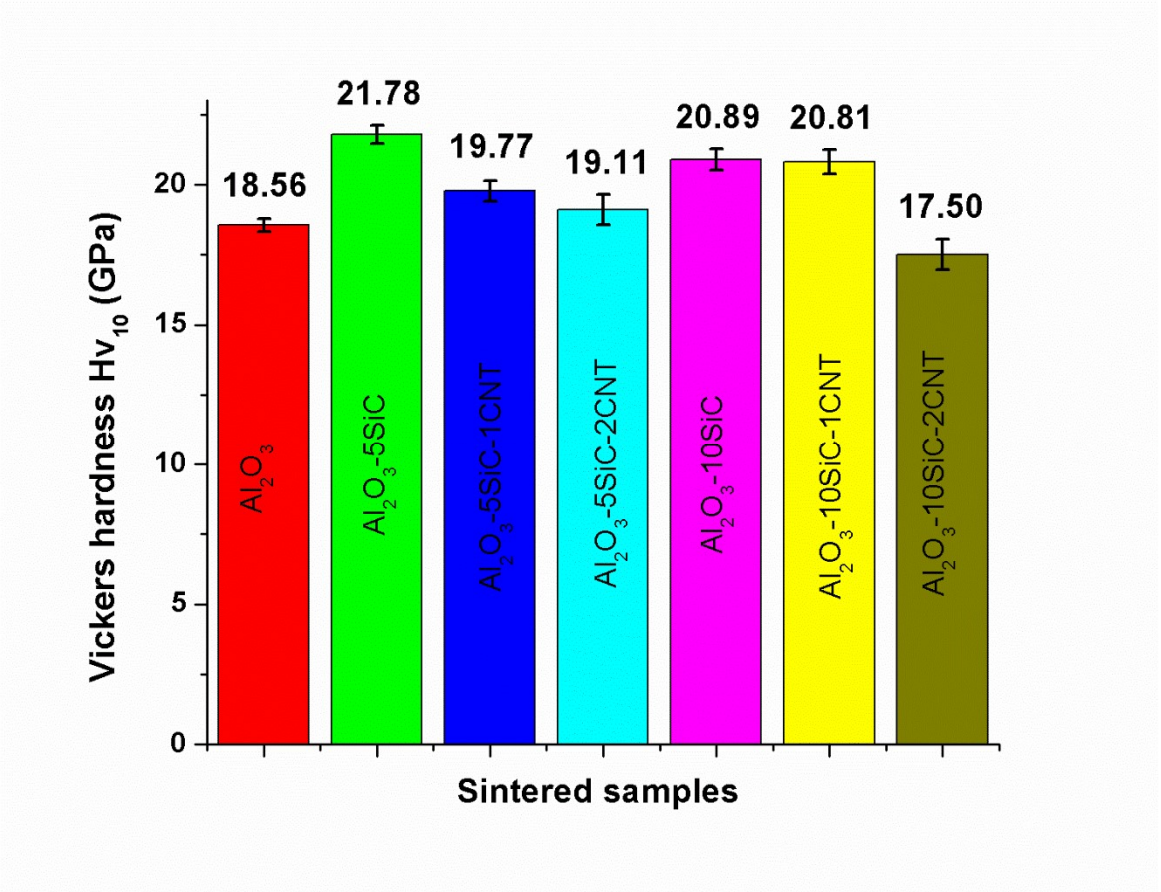

Figure 4.29 *Hardness of composites, synthesized through sonication and ball milling, sintered at 1500℃ for 10 minutes.*

a

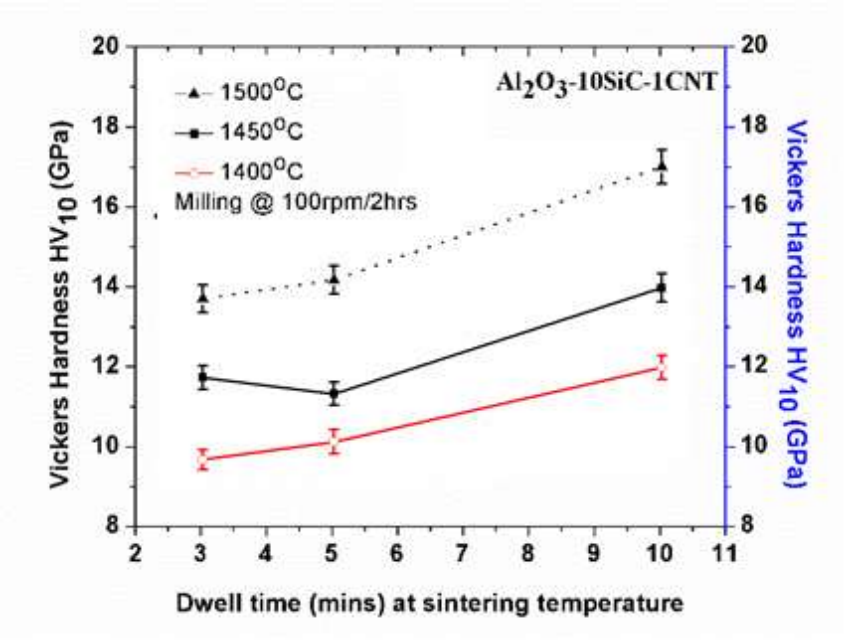

b

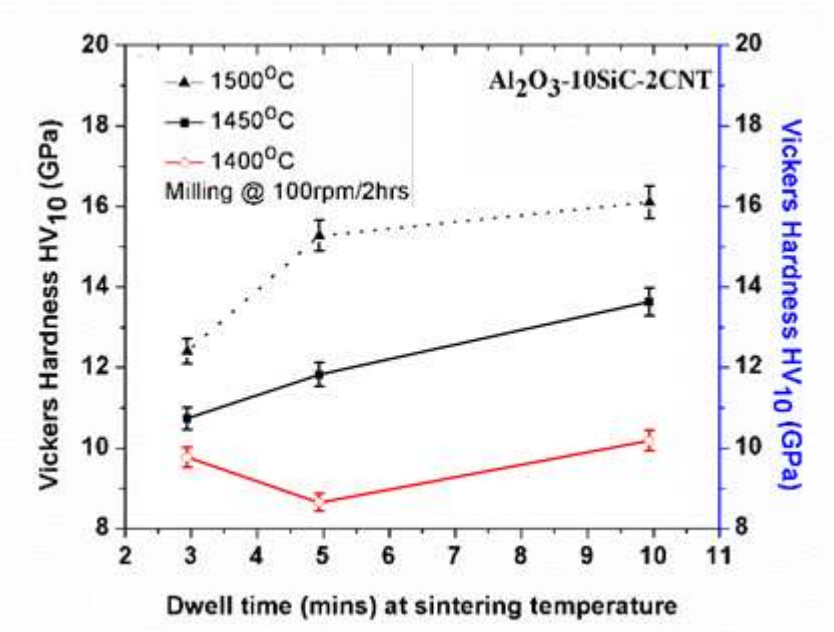

Figure 4.30 *Showing effect of sintering parameters on the vickers hardness of (a) Al_2O_3-10SiC-1CNT and (b)Al_2O_3-10SiC-2CNT, milled at 100rpm/2hours.*

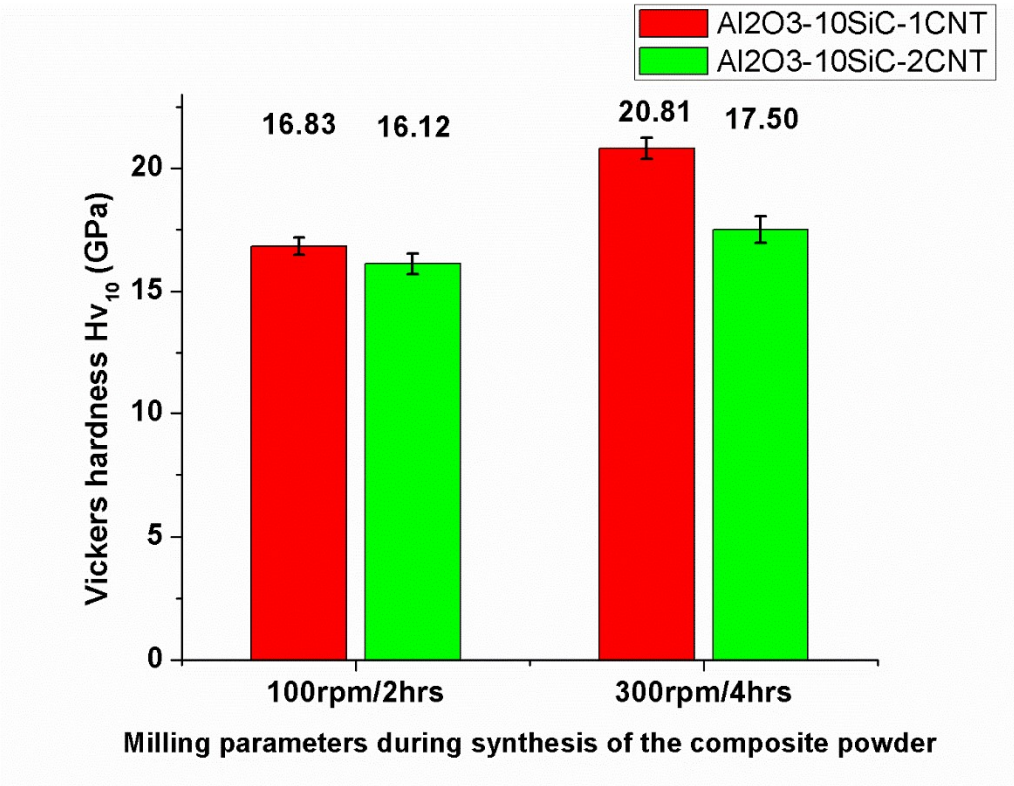

Figure 4.31 *Showing effect of milling conditions on the vickers hardness of hybrid nanocomposite, when sintered at 1500oC/10min under 50MPa*

Fracture toughness

The fracture toughness values of all of the samples, sintered at 1500°C for 10mins under an applied pressure of 50MPa, are presented in ***Figure*** **4.32**.

Monolithic alumina was found to have a toughness value of 3.61Mpa.$m^{1/2}$. The addition of 5SiC reduced its value to 2.65Mpa.$m^{1/2}$ while a further addition of 10% SiC didn't show any influential increase in the toughness value compared to alumina.

The reduction in toughness values of Al_2O_3-SiC is attributed to its fine microstructure, and resulted from the pinning effect of SiC. Crack propagating in the fine grain structure leads to almost straight crack propagation in the alumina-SiC composite. Frequent crack

deflection and the large tilt angle of the propagating crack in the alumina structure (comparatively large grained when compared with the Al_2O_3-SiC structure), consume more energy, leading to shorter crack length and higher fracture toughness in monolithic alumina. The fracture toughness value of Al_2O_3-10SiC is almost the same as the value for the fracture toughness of monolithic alumina. This is in agreement with the report by Ko et al. [56] that demonstrated that the fracture toughness of Al_2O_3-SiC composites with 5–30 wt.% SiC hot pressed for 2 h at 1823–1973 K at a pressure of 25 MPa remained constant up to 10 wt.% of SiC. However, Dong et al. [55] prepared Al_2O_3–SiC composites with 1–20 wt.% SiC by hot pressing at 1908 K and 25 MPa pressure for 1 h. The authors found that the fracture toughness increased with the addition of SiC up to 5 wt.% to reach a value of 7.6 MPa $m^{1/2}$ and decreased with further increases in SiC content.

The addition of 1% and 2% CNTs to Al_2O_3-10SiC increased the fracture toughness values to 4.58 and 6.98 $MPam^{1/2}$ respectively. The Al_2O_3-10SiC-1CNTs and Al_2O_3-10SiC-2CNTs hybrid nanocomposites exhibited improved fracture toughness by 26.86% and 93.95%, respectively, with respect to Al_2O_3. The Al_2O_3-10SiC-2CNTs composite showed a complete transgranular fracture mode as shown in ***Figure* 4.27**. In addition to the change in the fracture mode crack deflection and crack bridging, as shown in **Figure 4.34**., This contributes to the improvement in the fracture toughness.

The maximum fracture toughness value of 6.98 $MPa.m^{1/2}$ obtained in this investigation for Al_2O_3–SiC-CNTs is comparable with the value of approximately 7 $MPam^{1/2}$ reported for Al_2O_3-SiC-CNT [29] and is higher than the value of approximately 6 $MPam^{1/2}$ reported for Al_2O_3–CNT-SiC [101]. It is worth reiterating here that the composites investigated in references ([29] [101]) had low relative densities of 96.4% and 95.1%, respectively, and the

fracture toughness of these materials would have been affected by porosity. In addition, the obtained maximum fracture toughness value of 6.98 $MPam^{1/2}$ is higher than the maximum values of 4.5 $MPam^{1/2}$ [38], 5.03 $MPam^{1/2}$ [8], 5.5 $MPam^{1/2}$ [37], and 5.7 $MPam^{1/2}$ [84] reported for Al_2O_3-SiCw-CNT [38], Al_2O_3-Graphene platelets-CNT [8], Al_2O_3-graphene-CNTs [37], and Al_2O_3–Graphene platelets-CNT [84], respectively.

The fracture toughness value attained (6.9 $Mpam^{1/2}$) in samples having higher CNT content (2%) was higher than the results documented earlier in Al_2O_3-CNT[102][20], Al_2O_3-CNF[31], Al_2O_3-SiC-CNT[29] and in Al_2O_3-SiC-Graphene[8], K.Ahmed and Wei Pan [102] incorporated 1.1, 6.4 and 10.4 vol.% MWCNTS in alumina and consolidated it using the spark plasma sintering process. The maximum toughness reported was 5.5$Mpam^{1/2}$ for Al_2O_3-6.4vol% CNTs. G.Yamamoto *et al* [20] reported that the addition of 0.9 vol.% acid-treated MWCNT to alumina resulted in a fracture toughness of (5.90±0.27 $MPam^{1/2}$). K. Umino *et al*[31] fabricated alumina matrix composites reinforced by 0, 5, 10, and 20 vol.% carbon nanofibers (CNFs) using spark plasma sintering (SPS) and reported 2.79 $Mpam^{1/2}$ due to the open porosity in samples. K.Ahmad *et al* [29] fabricated a hybrid nanocomposite with different MWNT contents (0, 5, 7, and 10 vol%) and 1 vol.% SiC using spark plasma sintering and a reported 6.8 $Mpam^{1/2}$ for Al_2O_3-1SiC-7CNT. J. Liu *et al*[8] prepared alumina ceramic composites with 0.38 vol.% graphene platelets (GPLs) and 1, 3, and 5 vol.% SiC silicon carbide (SiC) nanoparticles using spark plasma sintering. The authors reported toughness value of 5.03 $Mpam^{1/2}$ for Al_2O_3-3SiC-0.38vol% graphene platelets (GPL).

The increase in the acquired fracture toughness can be due to a combination of certain causes. First, CNTs were added to Al_2O_3-10SiC through high energy probe sonication

rather than the usual ball-milling, which minimized damage, and/ or by shortening the CNT length which can reduce the toughness of the material [103][104]. Secondly, the change from inter to transgranular fractural mode due to the presence of CNTs, and the subsequent increasing toughness of the material, has been reported earlier [105].

The morphology of the fractured surface of monolithic alumina clearly indicates sharp and clear corners, which denotes the inter granular fracture mode, as shown in ***Figure*** **4.24**. However, blurry [27] and shear bands like [1] the fractural morphology in SiC and CNT reinforced alumina nanocomposite respectively, as shown in **Figure 4.25**, reveal the transgranular fracture mode. Further, crack bridging, load transfer partially trans granular fracture mode, and crack deflection, are the active toughening mechanisms in the developed Al_2O_3-SiC-CNT nanocomposites as shown in ***Figure*** **8** (a, b, c, and d) respectively.

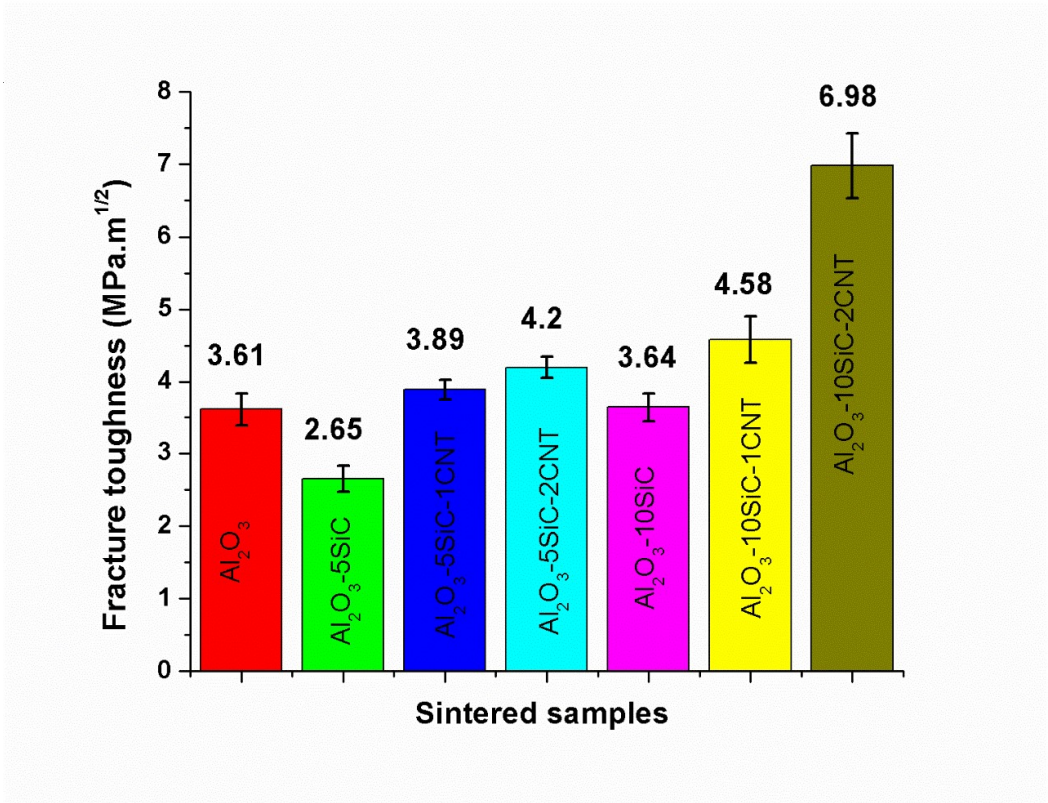

Figure ***4.32*** *fracture toughness of composites synthesized using sonication and ball milling, sintered at 1500℃ for 10 minutes.*

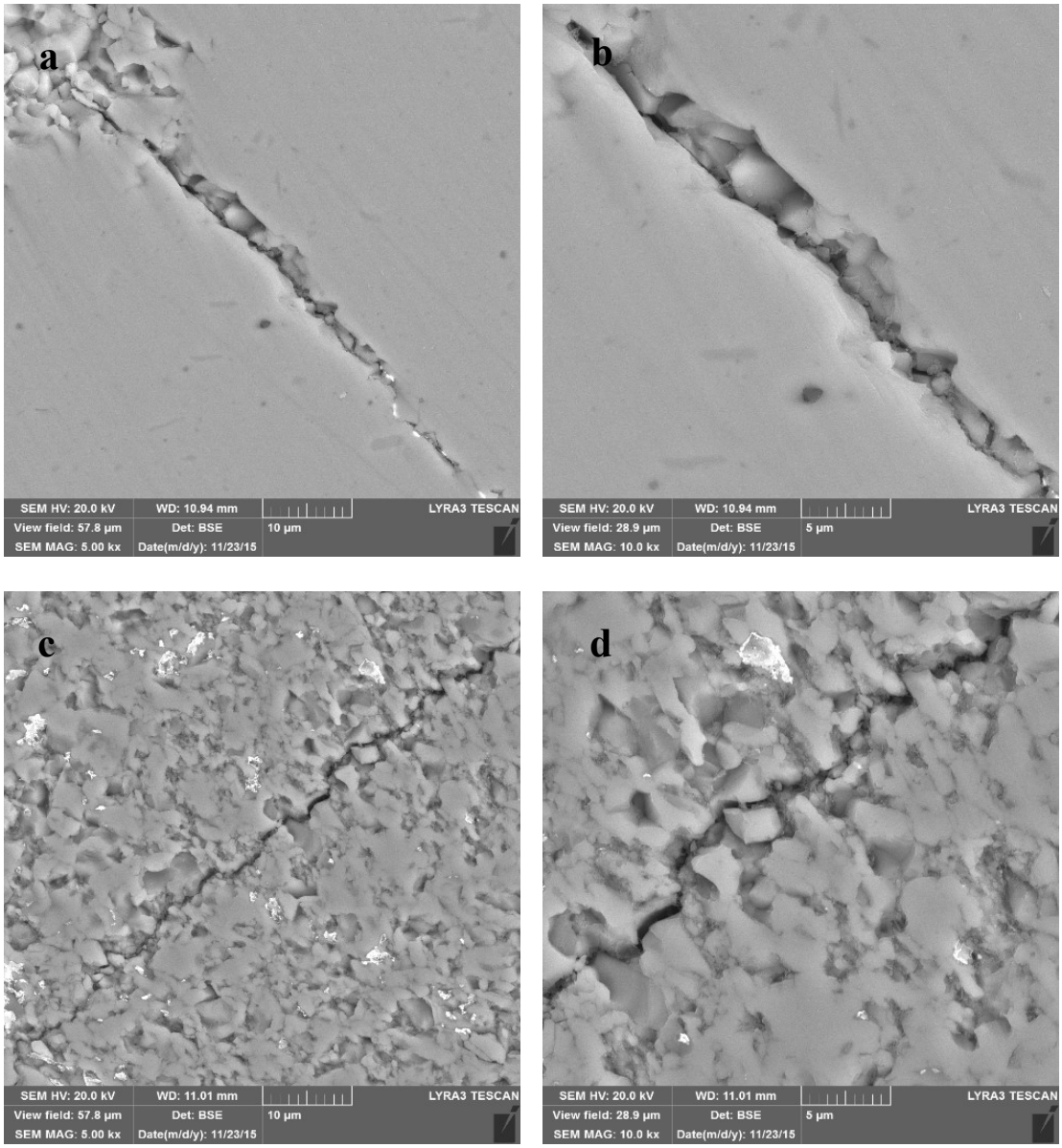

Figure 4.33 *Almost straight crack propagation in fine microstructure of Al_2O_3-10SiC (a, b) while deflected crack in Al_2O_3-5SiC-2CNT hybrid nanocomposite (c, d).*

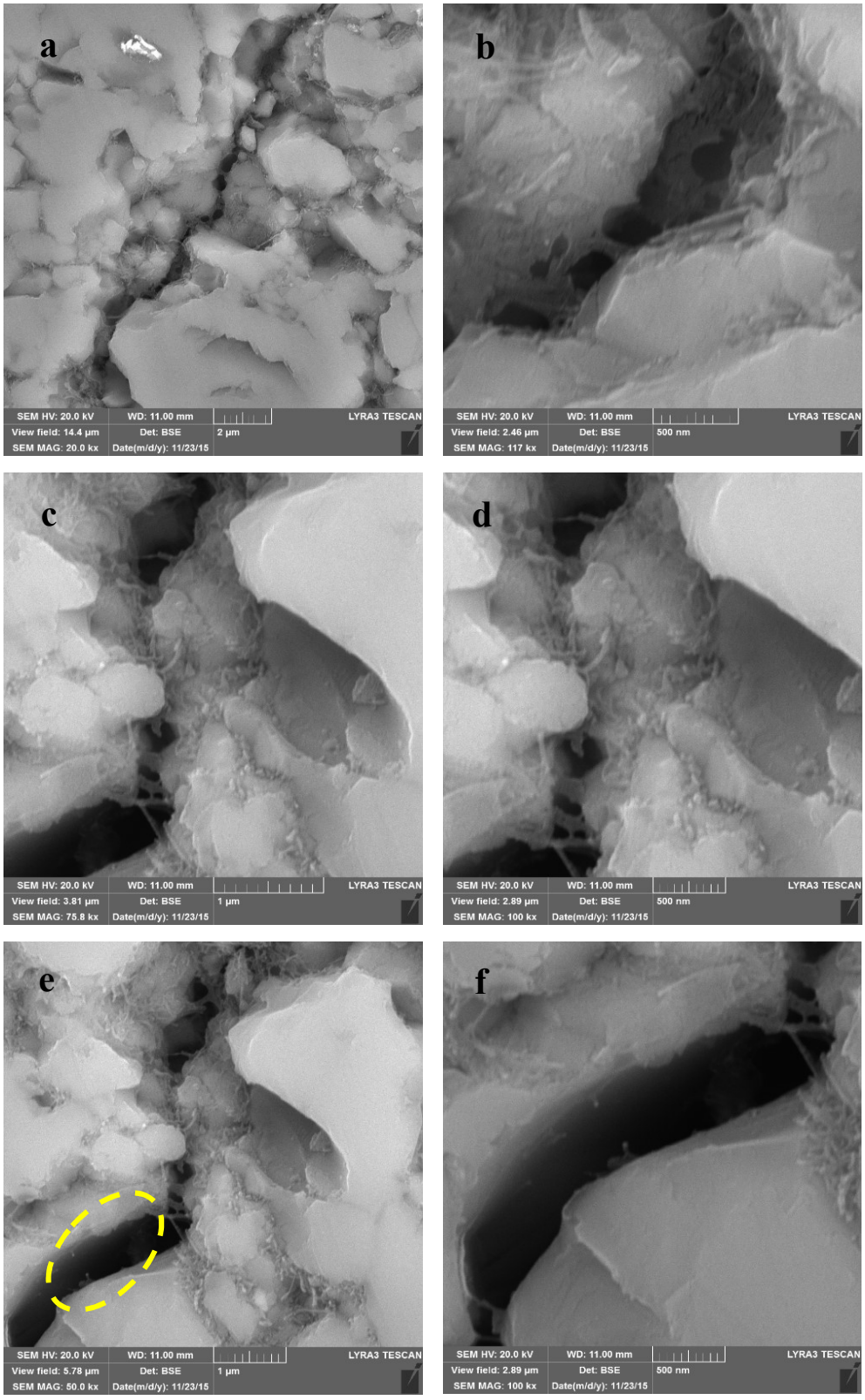

Figure 4.34 *crack bridging (a-d) and load transfer (e-f) mechanism is elaborated in developed hybrid nanocomposite*

Bending strength

Al_2O_3-10SiC-1CNT and Al_2O_3-10SiC-2CNT, prepared using milling at 100rpm for 2hours, along with monolithic alumina, were investigated for bending strength and the corresponding values are shown in **Figure 4.35**.

Monolithic alumina was found to have a flexural strength of 396MPa. Hybrid nanocomposite containing lower CNT content Al_2O_3-10SiC-1CNT showed a slightly reduced value of 373MPa as compared with Al_2O_3. However, Al_2O_3-10SiC-2CNT, containing higher CNT content, attained a value of 403MPa (a 2% marginal increase over monolithic alumina). A reduced or marginal increase in the bending strength of hybrid nanocomposite is mainly attributed to its low (95%) relative density as compared to full dense (~99%) monolithic alumina. Stress concentration around pores in a low dense material reduces fracture energy and results in low strength values [8]. However, comparatively higher CNT content in Al_2O_3-10SiC-2CNT, which increases capability in the load transfer mechanism [20], increases the flexural strength value of the nanocomposite. This increase is higher than monolithic alumina or hybrid nanocomposite containing comparatively lower (1%) CNT content.

The increase in bending strength value due to the load transfer mechanism is documented in Al_2O_3-CNT [102][20]. However, the addition of SiC to Al_2O_3-CNT, or using higher CNT content in hybrid nanocomposites, have shown a reduction in strength value [29] [31] [8] [37] due to the increasing probability of getting low dense material or an agglomeration of CNTs. Low density is due to the inhibition of the diffusion mechanism in the hybrid nanocomposite, which is due to the presence of both SiC and CNTs at the grain boundaries.

Using graphene platelets instead of CNTs or hot pressed particular hybrid materials have, however, shown higher values for the bending strength [70] [71].

K. Ahmed and Wei Pan [102] synthesized nanocomposites by incorporating 0.0, 1.1, 6.4 and 10.4 vol.% of multiwall carbon nanotubes (MWCNTs) in Al_2O_3 and consolidated it using spark plasma sintering. The authors reported 425MPa for Al_2O_3-1.1CNT as compared to low values of 350MPa for pure Alumina. Higher CNT content, however, has shown a reduced strength due to agglomeration of the CNTs. G. Yamamoto *et al* [20] also reported high values of 685MPa for Al_2O_3-0.5 CNT compared to 500MPa for monolithic alumina. This increase in strength was attributed to CNT bridging and the load transfer mechanism activated in Al_2O_3-CNT nanocomposites.

K. Ahmad and W. Pan [29] investigated Al_2O_3-1SiC with 5, 7 and 10 CNT and reported 450MPa for hybrid nanocomposite Al_2O_3-1SiC-10CNT against a high value of 550MPa for Al_2O_3-1SiC. The authors attributed the low strength values to inhibition of the diffusion mechanism in hybrid nanocomposite, which was due to the presence of both SiC and CNTs on the grain boundaries. K. Umino *et al* [31] reported very low values of 144MPa in an Al_2O_3-20vol.%CNF-10vol.SiC nanocomposite. J.Liu *et al* [8] prepared Al_2O_3-0.38GPL with (1,3,5%SiC) using sonication assisted ball milling techniques. A reduction in bending strength values from 572 to 535MPa, when SiC content was increased from 1%SiC to 5%SiC, was reported. The authors claimed the presence of porosity in the corresponding samples, which causes lower fracture energy due to stress concentration around the pores. B. Yazdani *et al* [37] reported a bending strength value of 350 MPa for Al_2O_3, which increased to a value of 450 MPa for (Al_2O_3-0.5wt.GNT-0.5wt.%CNT). However, further increasing the CNT content to 1 %, reduced it to a value of 325 MPa.

Fei *et al* [70] fabricated Al_2O_3–TiC–TiN tool material using a hot pressing technique and reported 901.9MPa for 6 vol% TiN. The authors attributed the high strength values to the high density and high hardness values which were attained. Xiao *et al* [71] developed a self-lubricating tool material by mixing multi-components through ball milling, and further hot pressing resulted in an increase of 25% in flexural strength.

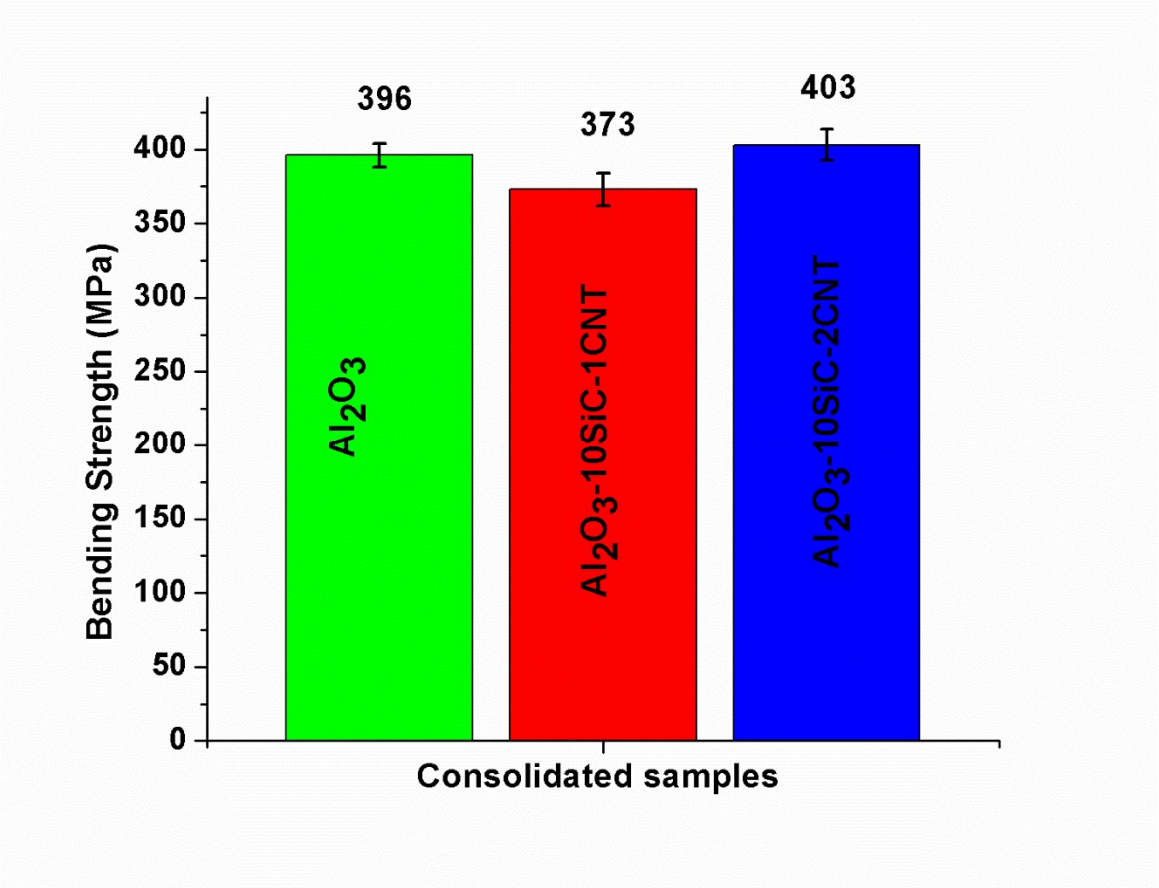

Figure 4.35 *Bending Strength Values for monolithic Al_2O_3 and hybrid nanocomposite synthesized using milling at 100rpm for 02hours and sintered at same 1500°C/10mins*

4.2 Molecular Level Mixed Composites

4.2.1 Powder Synthesis

***Figure* 4.36** (a) and (b) show FT-IR of functionalized CNTs and synthesized composite powder, respectively. Selected enlarged parts of ***Figure* 4.36** (a) and (b) are displayed in **Figure 4.36** (c) and (d), respectively. ***Figure* 4.36**(a) reveals the presence of carboxylic groups on the functionalized CNTs, which contributes to improved dispersion and prevents agglomeration. The presence of a new peak, just above 600 cm^{-1}, after calcination at 400°C, of the synthesized composite powder, as can be clearly seen in ***Figure* 4.36** (d), is due to bonding between CNT and alumina [23]. This bonding was initially established between the positively charged Al ions and negatively charged $COOH^-$ attached to the surface of the MWCNTs. Heat treatment of the dried mixture, synthesized through molecular mixing at 400°C for 4 hours led to the oxidation of aluminum and the formation of Al_2O_3. The precursors used and the process followed were selected in such a way that alumina will be formed [106][23]. The formation of alumina using molecular level mixing was reported in Al_2O_3-CNTs [23] and reduced graphene oxide/alumina [106] nanocomposites.

However, alumina, which was detected in FTIR, was found to be amorphous when synthesized composite powder was analyzed by XRD. The XRD spectrum of the synthesized and calcined (at 400°C) composite powder, presented in ***Figure* 4.37** (b), did not show the appearance of any alumina peaks, and reveals the presence of only SiC peaks (111), (200), (220), and (311). These observed peaks matched exactly with those revealed from pure SiC nanopowder as shown in ***Figure* 4.37** (a).

This indicated that alumina remained amorphous during the calcination treatment. Sintering at 1500°C for 10 mins led to the transformation from amorphous to crystalline alumina; and (104), (113), (116) peaks, with high intensity, characteristic of α- Al_2O_3 phase, can be clearly seen in the XRD spectrum of the sintered composite presented in ***Figure* 4.37** (c). In addition, the (111) (220), and (311) SiC peaks, with low intensity, can also be observed in ***Figure* 4.37** (c). The low intensity of SiC peaks is due to the low volume fraction of this phase.

Phase transformation from the amorphous to the crystalline phase was also investigated using TGA and DSC on the synthesized Al_2O_3-5SiC-1CNT nanocomposite powder, as shown in ***Figure* 4.38**, which were performed under argon at a heating rate of 5ºC/min.

Weight loss during initial heating is attributed to the loss of moisture [27] or initial degradation of the CNT-attached acidic group $COOH^-$ which completely decomposes at 783°C [107]. This decomposition released oxygen and caused oxidation of the CNT, which led to a small weight gain at higher temperatures. Crystallization of amorphous alumina started at around 1000°C and ended at around 1500°C as is evident from the peak on the DSC curve. This supports the fact that transformation of amorphous alumina to crystalline alumina occurs at a range of temperatures [23] [108][109]. In addition, TGA and DSC results complement those obtained from XRD, which showed that sintering at 1500°C for 10 mins led to the formation of α- alumina.

The microstructure of the synthesized composite powder was analyzed using TEM. ***Figure* 4.39** (a) shows a typical low-magnification TEM image of the powder which exhibits a particle size distribution with an average size around 1 μm. A micrograph taken at higher magnification, ***Figure* 4.39** (b), shows the presence of both fine SiC (represented by white

arrows) and CNTs (implanted in Al_2O_3 particles shown by black arrows). The absence of agglomerated CNTs or fine SiC indicated a uniform and homogeneous distribution of reinforcement in the synthesized nanocomposite powder. A TEM image of one single particle and the selected area electron diffraction (SAED) pattern are shown in ***Figure* 4.39** (c) and (d), respectively. Continuous rings with a few spots are an indication of the amorphous phase being superimposed on the polycrystalline material. The diffraction pattern elaborates on the amorphous phase of Al_2O_3, which was formed during the synthesis of the nanocomposite powder. This is in agreement with the XRD results shown in ***Figure* 4.37** (b).

Beside TEM, distribution of the reinforcements in the composite powder was also analyzed using x-ray mapping. A low-magnification FE-SEM micrograph and corresponding x-ray mapping of the different elements are presented in ***Figure* 4.40**. This indicates a uniform distribution of CNTs and SiC in the composite powder. This shows that the molecular-level mixing process is not only suitable for synthesizing homogeneous metal [48][110][111] and ceramic [106][23] matrix nanocomposites, as reported by other researchers, but also hybrid ceramic nanocomposites as demonstrated in this work.

FE-SEM micrographs, with different magnifications, of Al_2O_3-5SiC-1CNT powder prepared through molecular level mixing using a sonication time of 24 hours, are shown in ***Figure* 4.41** (a,b,c). It can be clearly seen that CNTs were embedded in the formed Al_2O_3 phase.

The micrographs clearly show that CNTs are not agglomerated and are homogeneously distributed in the Al_2O_3 phase. Moreover, it can be clearly seen that CNTs are implanted

uniformly within the alumina particle. This equal distribution of CNTs provides both classical and novel toughening mechanisms in the composite [28].

Each separate CNT embedded within the alumina matrix reduces the risk of agglomerate formation and fulfills claims of homogeneity and distribution at the molecular level.

Al_2O_3-5SiC-1CNT composite powder was also synthesized by reducing the sonication time from 24 hours to 2 hours during powder synthesis to investigate the corresponding effect on the distribution of reinforcement in the synthesized powder composition.

The low magnification FESEM micrograph **Figure 4.42** (a,b) reveals the morphology of synthesized powder with an irregular shape and an average particle size of 1μm, which is almost the same as that obtained using a sonication time of 24 hours. However, an improved, uniform distribution of CNTs in alumina was clearly observed when a particle shown in the same **Figure** was enlarged as shown in **Figure 4.42** (c). A single CNT being planted in an alumina matrix is shown in **Figure 4.42** (d). This improvement in the uniform distribution of CNTs in alumina plays a vital role in the toughening mechanism, such as crack bridging, deflection, and branching, which consumes energy from a propagating crack and hence increases the toughness of the composite. These micrographs clearly reveal each single CNT being separately implanted and equally distributed within the alumina matrix, at a lower sonication time of 2 hours. A higher sonication time increased the possibility of shortening the CNT length [112], thus reducing the aspect ratio, and increases the number of CNTs per unit volume, while correspondingly reducing the level of CNTs dispersion [113] in the matrix. However, an improved distribution of CNTs was attained during this work at a lower sonication time.

The distribution of reinforcement (SiC and CNT) in powder synthesized using a lower sonication of 2 hours was further analyzed using x-ray mapping, as shown in **Figure 4.43**. FESEM micrograph (a) and x-ray mapping of Al(b), O(c), Si(d) and C(e) in Al_2O_3-5SiC-1CNT show enhanced uniform distribution of reinforcement in alumina matrix. Analysis of x-ray mapping showed that a sonication time of 2 hours was enough to obtain a uniform distribution without any agglomeration or cluster formation in fine SiC and/ or CNTs.

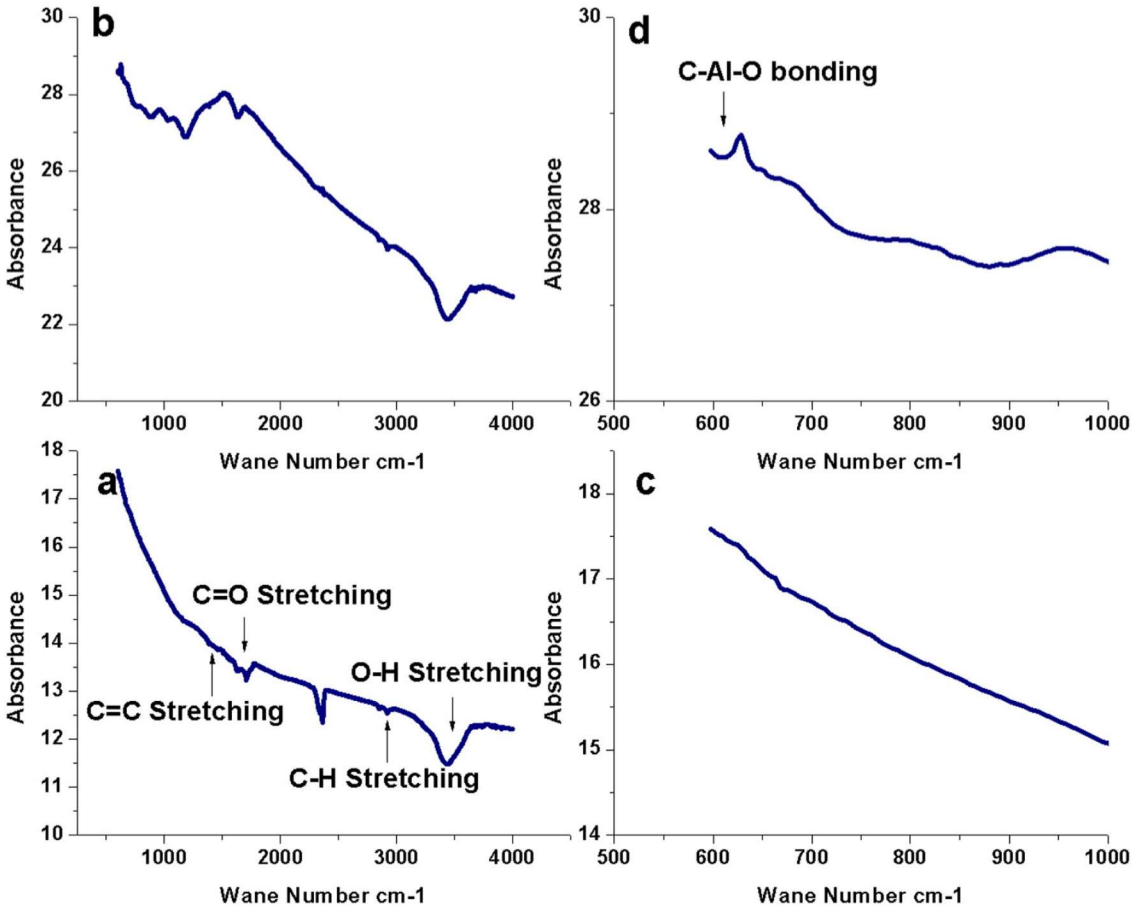

Figure 4.36 *FTIR spectrum of (a) functionalized CNTs, (b) after calcination of the composite powder prepared though MLM , (c) and (d) selected enlarged ranges in (a) and (b), respectively.*

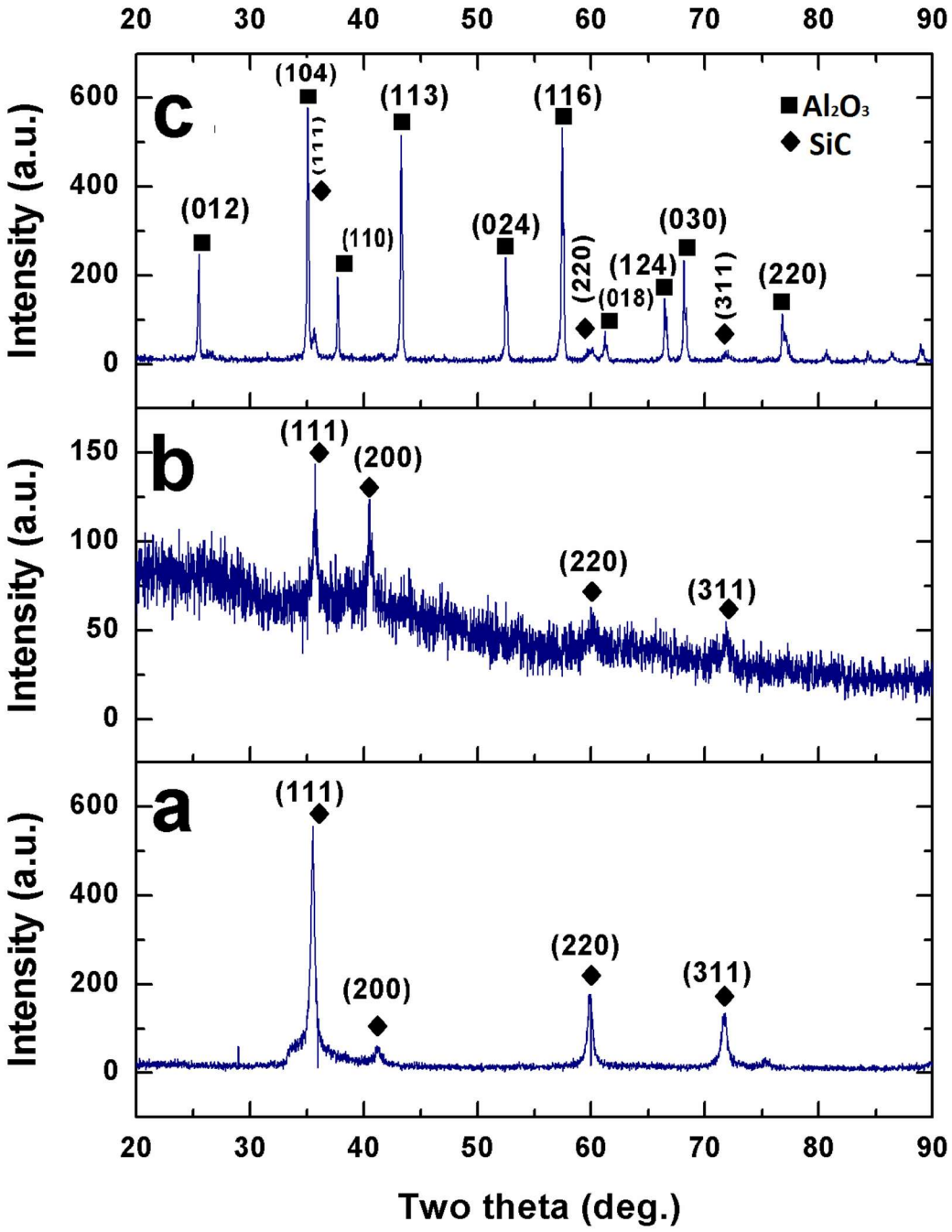

Figure 4.37 *XRD spectrum of (a) as-received SiC, Al_2O_3–5SiC-1CNTs powder synthesized using molecular level mixing after calcination at 400°C (b), and after consolidation at 1500°C for 10mins (c).*

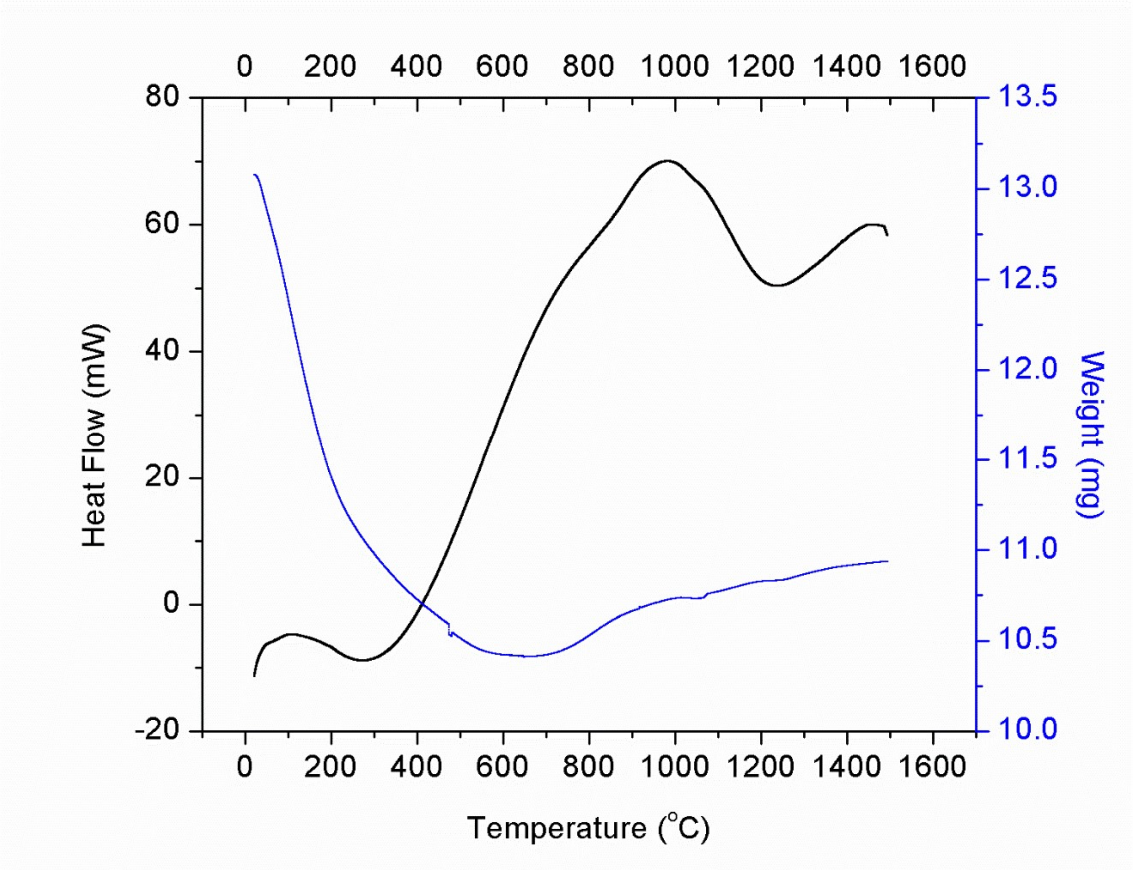

Figure 4.38 *TGA and DSC curves recorded between room temperature and 1500°C using a heating rate of 5°C/min.*

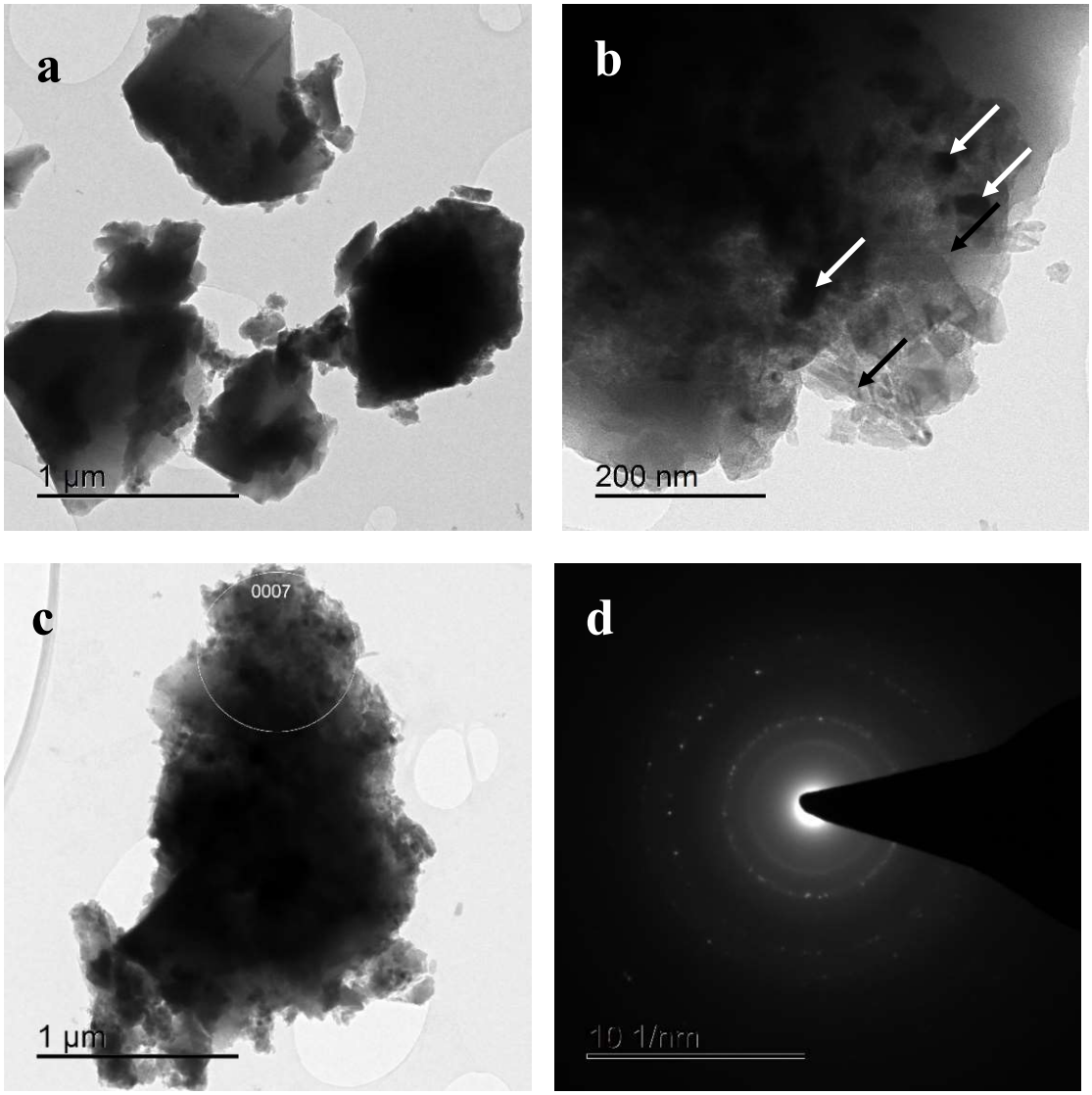

Figure 4.39 *(a) Low- and (b) high-magnification TEM images of composite powder, (c) TEM image of a particle and (d) selected area electron diffraction (SAED) pattern.*

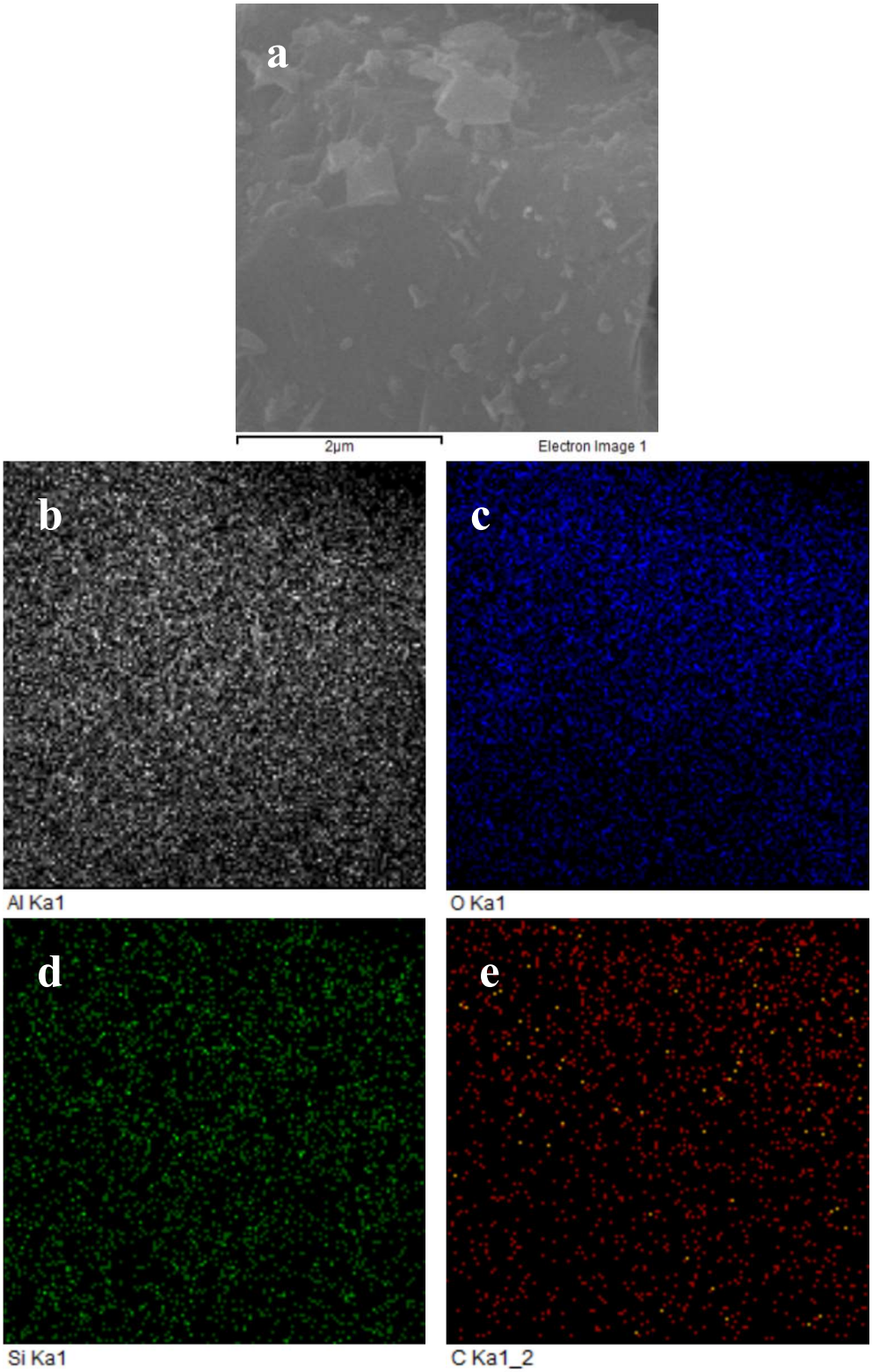

Figure 4.40 *(a) Low-magnification FE-SEM micrograph of molecular level mixed Al_2O_3-5SiC-1CNT and elemental x-ray mapping of (b) Al, (c) oxygen, (d) silicon, and (e) carbon.*

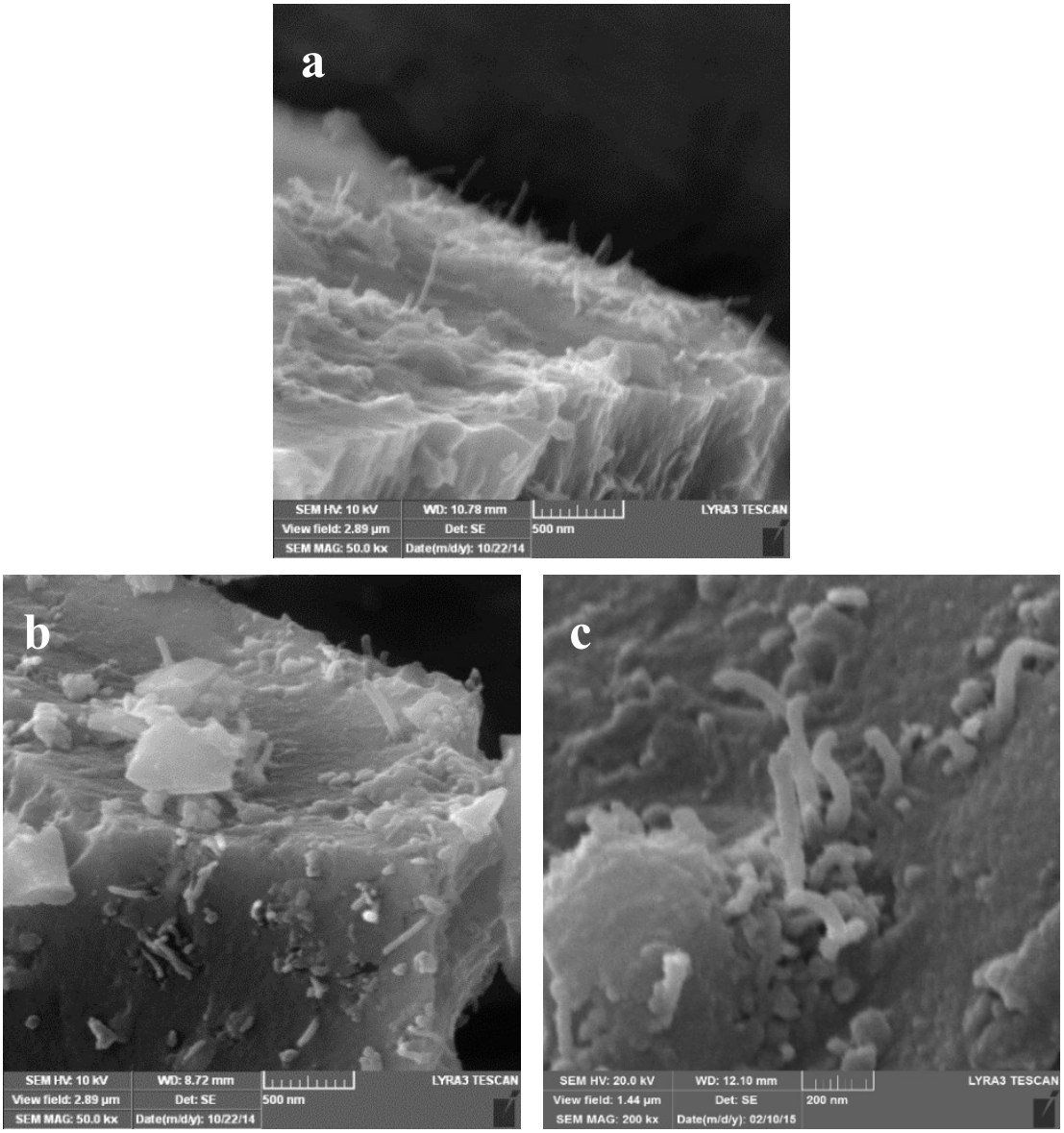

Figure 4.41 *FESEM showing distribution of reinforcement in Al_2O_3–5SiC-1CNT composite powder prepared using molecular level mixing with sonication time of* ***24hours*** *at different magnification of 50kx (a,b)and 200kx(c).*

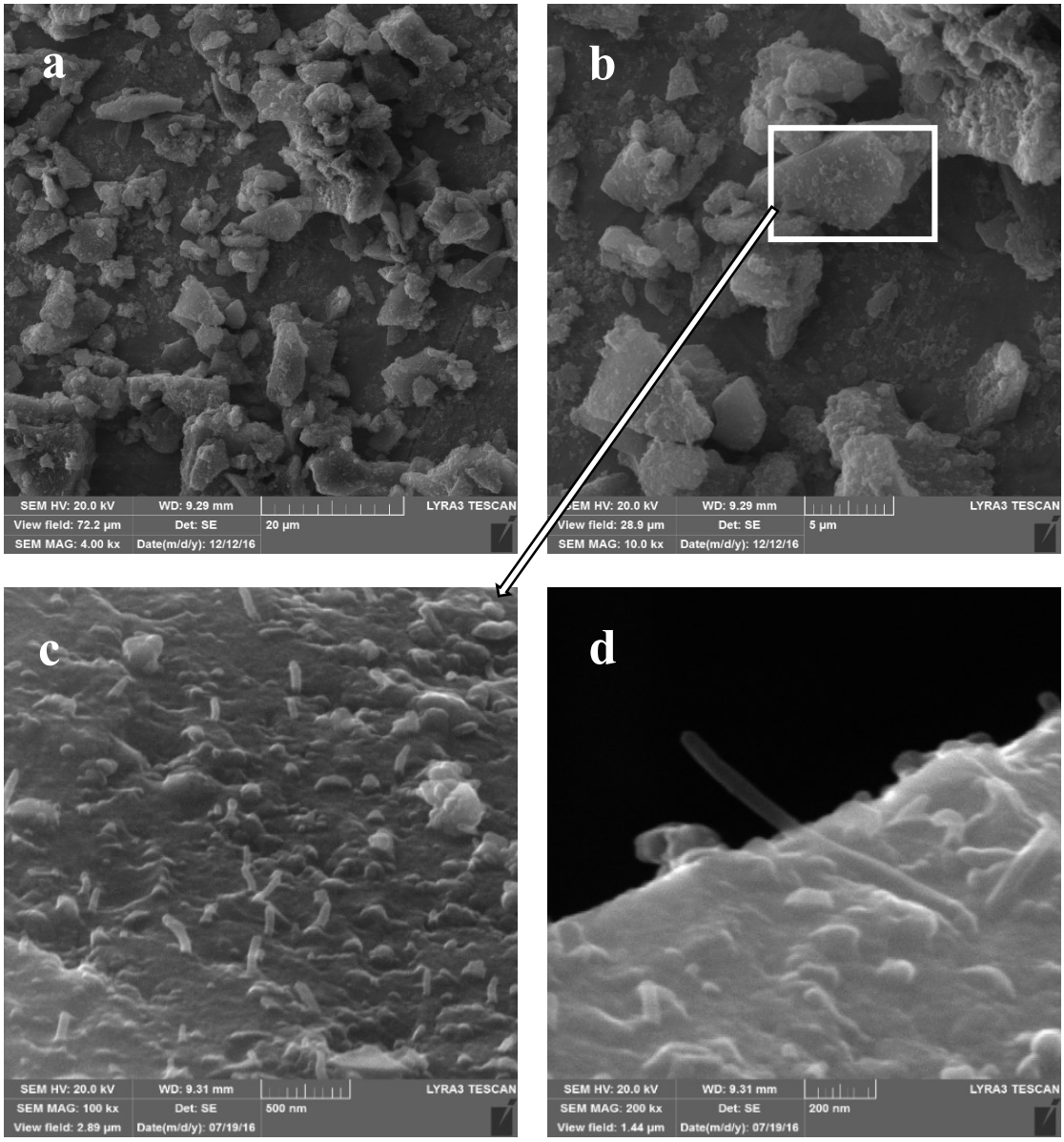

Figure 4.42 *FESEM showing Al_2O_3–5SiC-1CNT composite powder prepared using molecular level mixing with sonication time of* ***02hours****. Range of particle sizes with irregular shape is shown at 4kx(a), and 10kx(b). One of the particle at higher magnification of 100kx (c) and 200kx (d) showing improved distribution of reinforcement.*

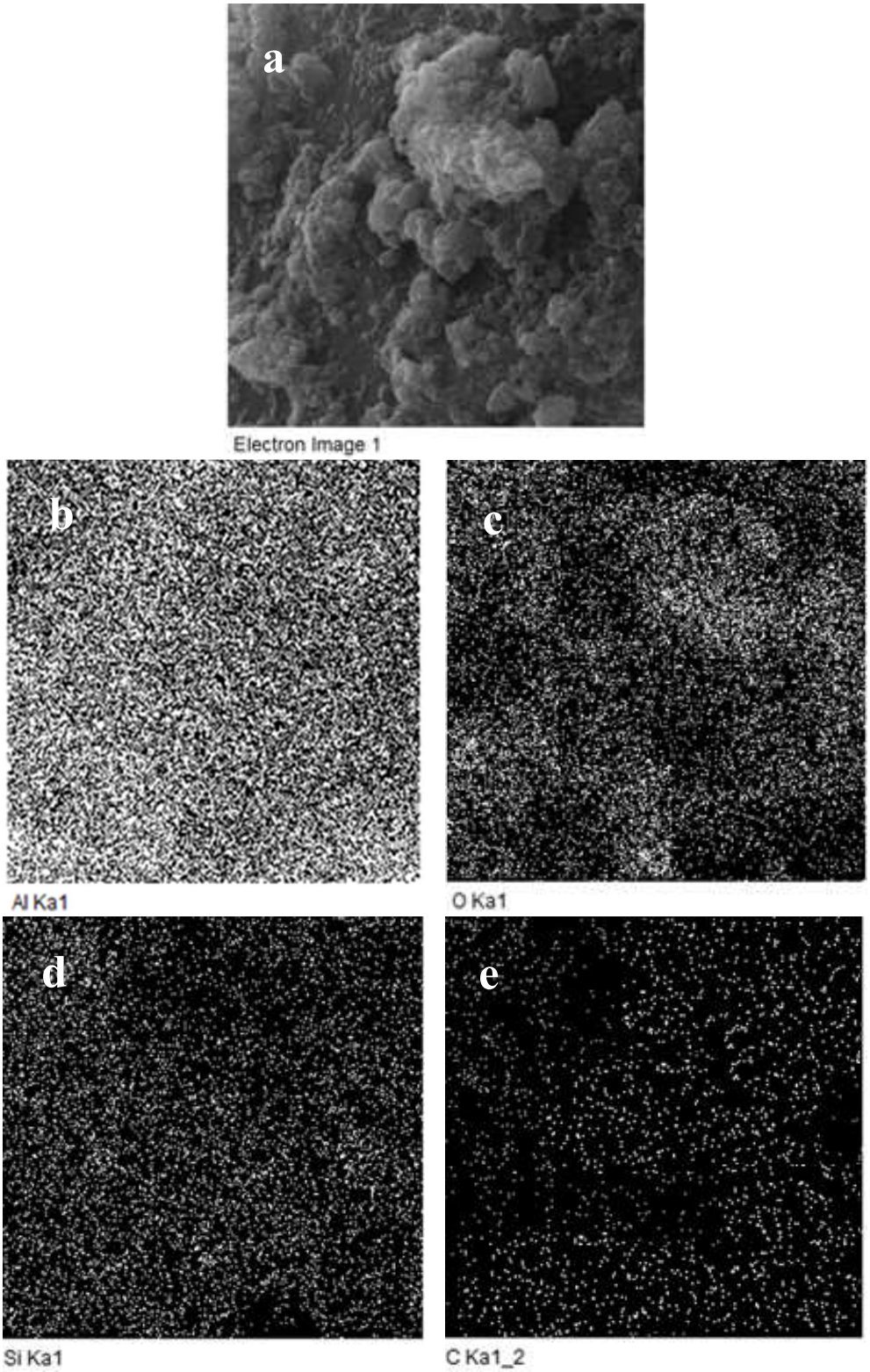

Figure 4.43 *FE-SEM micrographs of Al_2O_3-5SiC-1CNT synthesized using molecular level mixing with sonication time of 02 hours(a), and corresponding X-ray mapping of Al(b), Oxygen(), Si (d) and C (e).*

4.2.2 Densification

Al_2O_3-5SiC-1CNT powder compositions, synthesized through molecular level mixing using different sonication times, were sintered at 1500ºC for 10mins under an applied pressure of 50MPa. These sintering parameters were chosen to maintain consistency and ease in comparison with ball milled composites and monolithic alumina, which attained almost full relative densities at these sintering parameters. However, it was found that molecular level mixed powder compositions were not well sintered at these parameters and attained relatively low density values of 91.65% and 90.36% corresponding to compositions synthesized using a sonication time of 24 hours and 2 hours, respectively.

Unlike monolithic alumina, the presence of reinforcement in the composite hinders mass transportation during the densification process and is one of the basic reasons for attaining low density values in the composites. Further micro-porosity in the entangled CNTs at the grain boundaries [93] and the presence of particular hard reinforcements, such as SiC [36], reduces plastic deformation of the alumina matrix. This increases the possibility of attaining low density values in these particular nanocomposites. A large alumina particle size (almost 1μm) shown in **Figure 4.39** (a), produced during the synthesis of powder compositions through molecular level mixing, compared with the as received monolithic alumina particle size (almost 200nm) in **Figure 4.1** (b), is another important reason for low sinter-ability of the molecular level mixed nanocomposites. Smaller surface energies of large particles tend to slow down the diffusion (surface and or grain boundary) mechanism and reduce density values at particular sintering parameters. These large particles in powder compositions thus require high thermal energies by either extending the dwell time and/ or the sintering temperature to attain high relative densities.

Al_2O_3-5SiC-1CNT synthesized using a 2 hours sonication time was considered for further sintering at a high temperature, owing to the reduced risk of CNT shortening at this comparatively lower sonication time. Keeping the same heating rate of 100ºC/min, holding time of 10mins and applied pressure of 50MPa, the relative density value of Al_2O_3-5SiC-1CNT was increased to 95.16% and 98.9%, when the sintering temperature was raised to 1550ºC and 1600ºC, respectively.

Increased relative density values are due to providing high thermal energy during high temperature sintering, which passes comparatively high current amperes to the powder, based on joule heating[114]. Contact points of powder offer a high level of resistance to the increased current flow and contribute to the increased heating and thermal activation energy of material to enhance mass transport and the densification rate during spark plasma sintering [90]. This causes a reduction in porosity and a denser structure is obtained at high sintering temperatures. The dependence of diffusion on sintering temperature can also be explained by

$$D = D_0\, e^{-\frac{Q}{RT}}$$

According to this equation, a denser structure can be achieved at a higher sintering temperature. D is the diffusion coefficient, D_0 is constant, Q is the activation energy, R is Boltzman's constant and T is the sintering temperature.

Reduction in the relative density of alumina composite, due to large Al_2O_3 particles, is also documented by Rahimian *et al* [115]. The authors reported that large particles act as a barrier to rearrangement, deformation, and diffusion, and reduce the contact area between

the particles leading to higher porosity. However, the authors reported increased density with increasing sintering temperature.

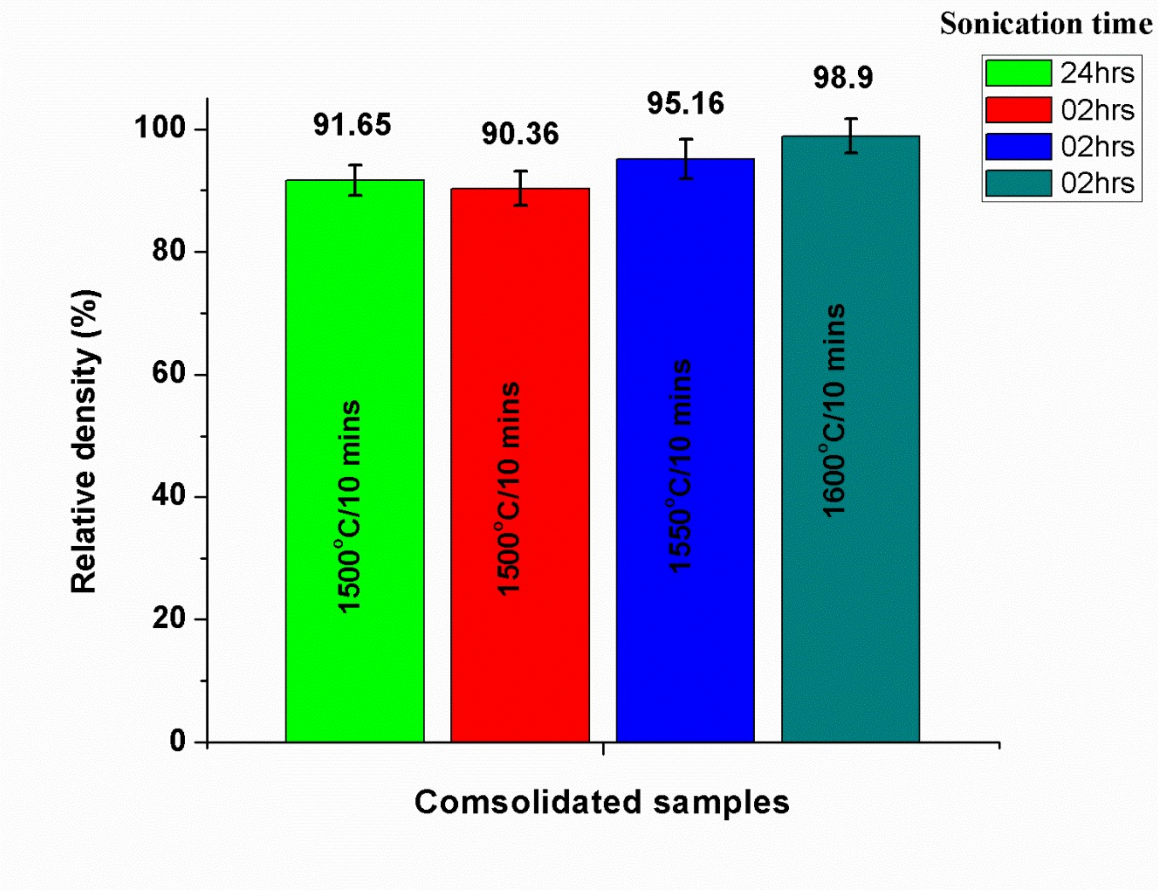

Figure 4.44 *Relative density of Al_2O_3-5SiC-1CNT nano-composites, synthesized through molecular level mixing using different sonication time of 24hours and 02hours, as a function of sintering temperatures for a dwell time of 10 minutes, under 50MPa applied pressure.*

4.2.3 Microstructure

Consolidated samples at 1500ºC, of powder compositions synthesized through molecular level mixing using a sonication time of 24 hours and 2 hours, were analyzed using x-ray mapping as shown in **Figure 4.45** and **Figure 4.46**, respectively.

Mapping of Al, O, Si and C in the consolidated sample shown in **Figure 4.46** reveals comparatively ore uniform distribution of SiC and CNT. These observations are corresponding to FESEM micrographs and x-ray mapping of powder compositions, showing improvement in the uniform distribution of reinforcement in the powder synthesized using a lower sonication time of 2 hours, as shown in section 4.2.1. The uniform distribution of reinforcement was consistent, when the same powder, synthesized using a lower sonication time, was further consolidated at a high sintering temperature of 1600^{o}C, as shown in ***Figure 4.47***. Homogeneous distribution of reinforcement in alumina matrix are crucial requirements for the improvement of mechanical properties, particularly hardness and fracture toughness.

This sample sintered at 1600^{o}C was also analyzed through FESEM for the distribution of reinforcement in the matrix. The presence of CNT at a high magnification of 200kx in FESEM micrograph as shown in **Figure 4.48** reveals its homogeneous distribution in the matrix. However, it was difficult to show distribution of SiC in the alumina matrix through the FESEM micrograph, as Al and Si yield a low contrast of only 6.7% and they are separated by one unit of atomic number.

Therefore energy dispersive X-ray spectroscopy (EDX) analysis was carried out on two different portions from the fractured surface. Specturum-4, from of a selected portion of alumina grain **Figure 4.48** (b), which has shown the peaks for both SiC and CNT as shown in **Figure 4.49** (a), confirms the presence of both SiC and CNT within alumina grains.

Correspondingly another specturum-3 from a selected portion of the same fractured surface, which shows fine particles, as shown in **Figure 4.48** (c), has shown high peaks of SiC as shown in **Figure 4.49** (c). The weight % of SiC increased from 5.22 to 14.11% when the

scanning region was changed from an alumina grain, specturum-4, to an area containing fine particles, specturum-3. The increase in intensity, as well as that in weight %, confirmed that these fine particles are those of SiC.

The presence of un-agglomerated fine SiC confirms uniform distribution within the alumina matrix. The presence of SiC particles are predominantly located along the matrix grain boundaries, while some particles are also entrapped inside the alumina grains. During consolidation, when the grain boundary reaches a particle, its free energy decreases by the product of the cross-sectional area of the particle and GB [8]. Thus, in the case of the finer particles of SiC, the reduction in grain boundary free energy is lower and can overcome the pinning effect of the particle, enabling fine particles to reside within grains contrary to comparatively large SiC. Some of the CNTs are also entrapped in alumina grains. This is most likely due to the probable orientation of alumina grains around individual CNTs during mechanical mixing and ultra-sonication. Therefore, during the sintering process, the alumina particles around the CNTs grow into one or more larger grains which result in embedded nano-tubes inside alumina grains, as shown in ***Figure*** 4.51.

Consolidated samples at different sintering temperatures of 1500ºC, 1550ºC and 1600ºC were also analyzed using x-ray diffraction as shown in ***Figure*** 4.50. All three XRD patterns clearly show strong characteristic peaks of α- alumina, which confirms its formation during the sintering process of molecular level mixed synthesized powder compositions. Characteristic peaks of SiC are also present in all three patterns, although with a low intensity, which is due to the low volume fraction of this phase. The most probable peak of MWCNT (002) is only present in composite sintered at 1600ºC, although it is shielded by an intense peak (012) of alumina, due to its low content in the composition. It is reported

that peaks of MWCNTs were visible in samples at high temperatures, as spark plasma sintering improves the crystallinity of CNTs [116]. The absence of any additional peak in any of these patterns indicates the absence of any undesirable interfacial reactions during the sintering process.

XRD patterns also indicate a slight shift of peaks towards higher 2θ. The prime characteristic peak (012) of α-alumina was observed at 25.549°, 25.708° and 25.802° corresponding to samples sintered at 1500°C, 1550°C and 1600°C as shown in **Figure 4.50**. A second (104) peak of α-alumina was detected at 35.142°, 35.289°, and 35.456° , while a third peak (110) was detected at 37.866°, 37.909°, and 37.995° with respect to each sintering temperature of 1500°C, 1550°C and 1600°C. This clearly shows that any characteristic peaks in the XRD pattern shifted towards higher 2θ, when the sintering temperature was raised. This little peak shift towards higher 2θ is due to an increase in the residual stresses imposed by the increase in thermal expansion difference between reinforcement (SiC and CNT) and alumina.

The crystallite size calculated using Scherer's equation was 41nm, 45nm and 47nm corresponding to the XRD patterns of samples consolidated at 1500°C, 1550°C, and 1600°C, respectively. Restricting crystallite size to lower than 50nm for all samples is attributed to mixing (positive metallic ions and negative organic group attached to CNTs) at the molecular level, in addition to high heating rates and low dwell times during the spark plasma sintering process.

The fractured surfaces were analyzed for the mode of fracture in the consolidated samples. The fractured surface of the consolidated monolithic alumina and nanocomposite sintered at 1500°C, for which the corresponding powder was synthesized using a sonication time of

24 hours and 2 hours, are shown in ***Figure*** 4.51 (a) and ***Figure*** 4.51 (b, c), respectively. It confirms an obvious transformation from completely intergranular (typical of alumina) to an almost completely transgranular fracture mode in the hybrid structures. The change in the fracture path from intergranular in pure alumina to transgranular in the composites suggests a strong adhesion between the reinforcement and the matrix in the nanocomposite. Clusters of fine particles of SiC, indicated by white arrows in ***Figure*** 4.51 (b), were found between the grains, which is an indication of a lower degree of homogeneity of SiC in the matrix. However, these clusters were not present in ***Figure*** 4.51 (c), where the corresponding powder was synthesized using a lower sonication time. These results correspond to the FESEM micrographs of synthesized powder where the distribution of the reinforcement was found to improve when the sonication time was reduced from 24 hours to 2 hours, as shown in **Figure 4.41** and **Figure 4.42**. Although this composite, synthesized using a sonication time of 2 hours, shows a uniform distribution in powder and consolidated samples, and also shows the transgranular fracture mode, it was not well sintered at 1500°C as depicted by the presence of voids in the respective fractured surface as shown in **Figure 4.52** (a,b). Increasing the sintering temperature to 1550°C and 1600°C, however, reduced the intensity of these voids as shown in **Figure 4.52** (c, d) and **Figure 4.52** (e, f, g, h), respectively. Besides resulting in an almost dense structure, high-temperature sintering has also revealed a twinning mechanism (twin deformation) as shown by the white arrows in these micrographs. Twin structure sintering of ceramics at high temperatures has also been reported by Sairam *et al* [114]. There is room for dislocation nucleation and dislocation pileup decreases, as the twin boundaries serve as obstacles to the dislocation motion and hence increases the strength and toughness of the material [117].

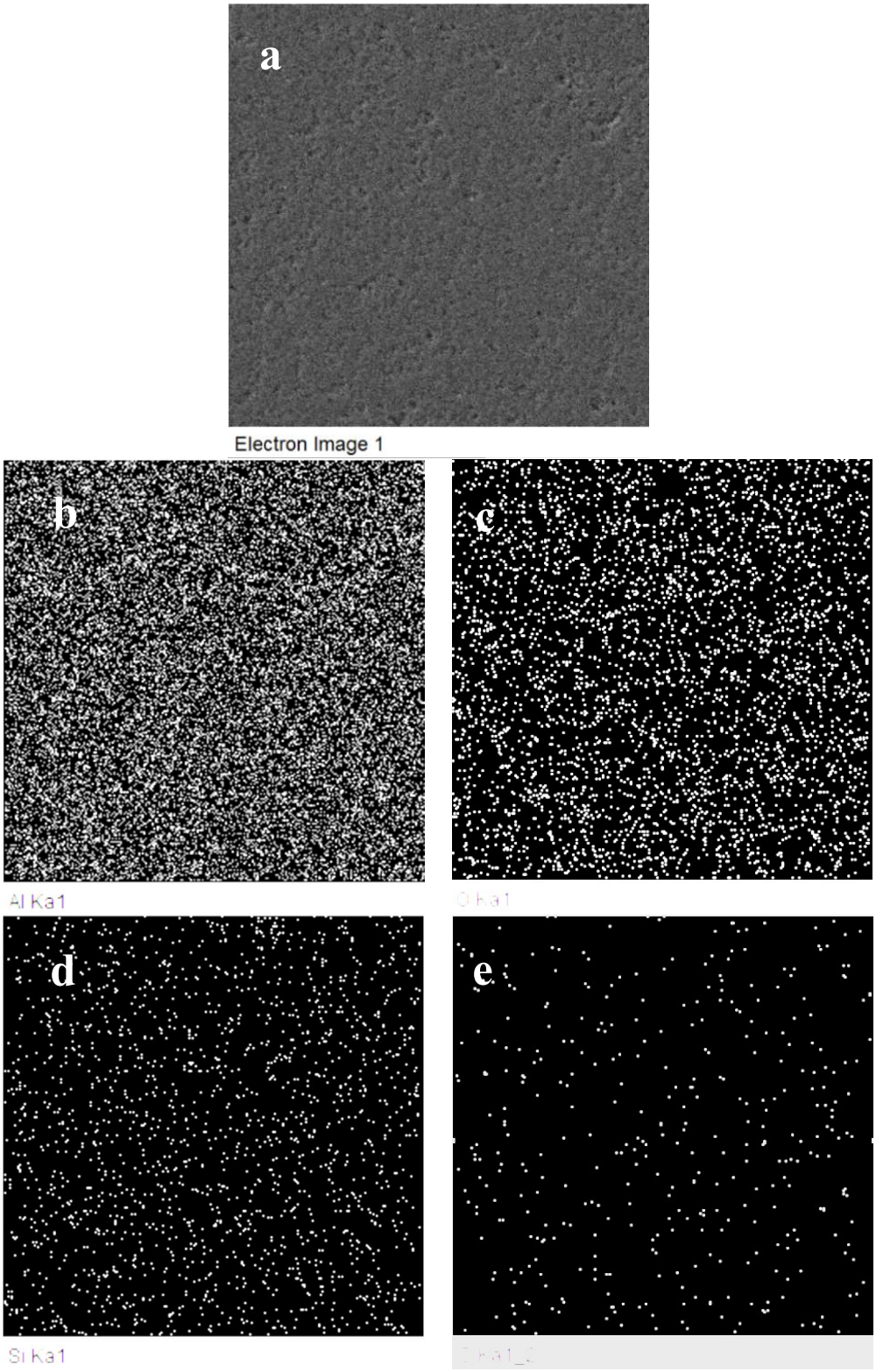

Figure 4.45 *FESEM (a) and x-ray mapping of Al(b),O_2(c), Si(d) and C(e) in consolidated sample of molecular level mixed Al_2O_3-5SiC-1CNT, synthesized using* ***24hours*** *sonication time and consolidated at 1500°C/10minutes*

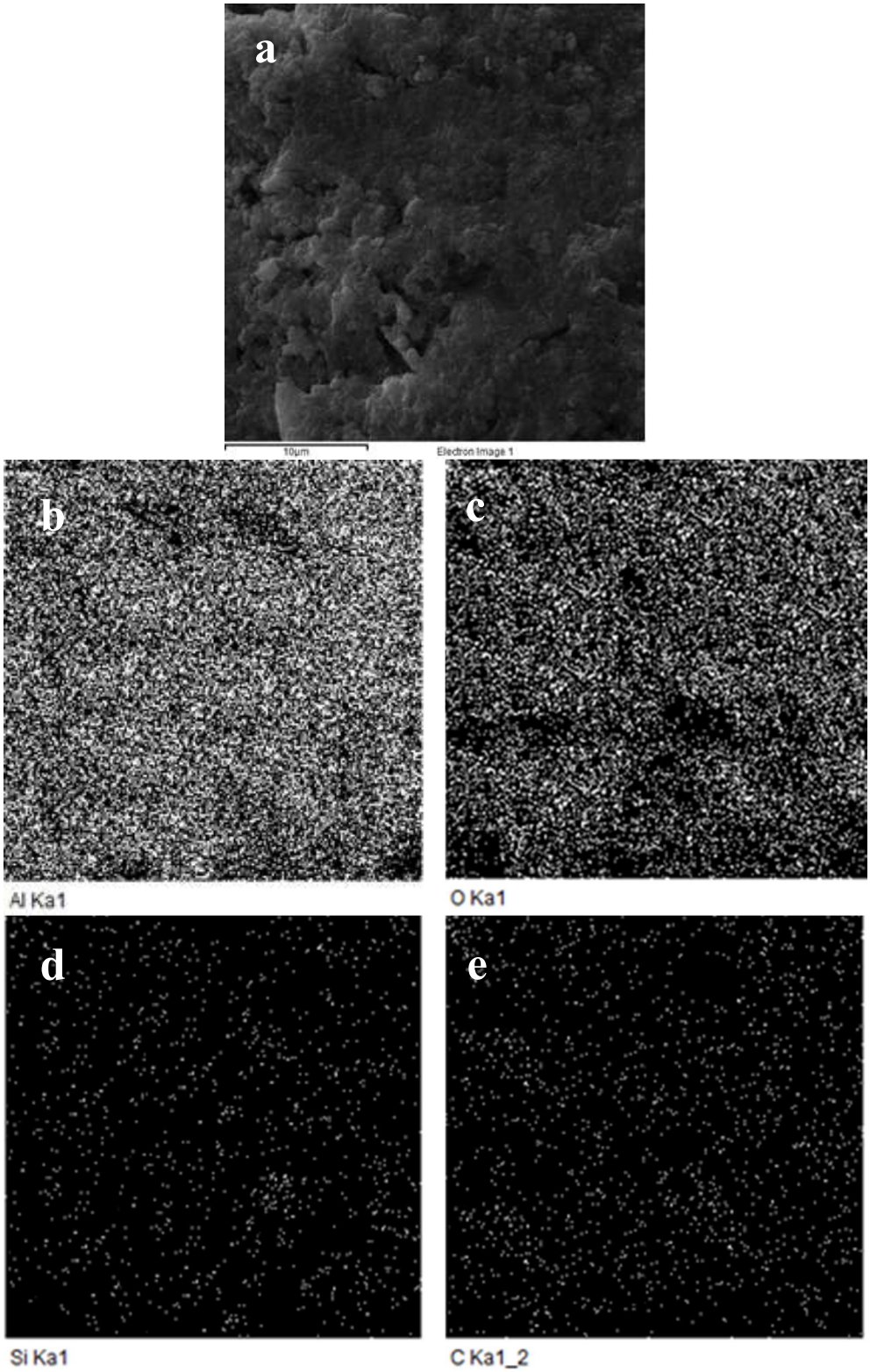

Figure 4.46 *FESEM (a) and x-ray mapping of Al(b),O_2(c), Si(d) and C(e) in consolidated sample of molecular level mixed Al_2O_3-5SiC-1CNT, synthesized using* ***02hours*** *sonication time and consolidated at 1500°C..*

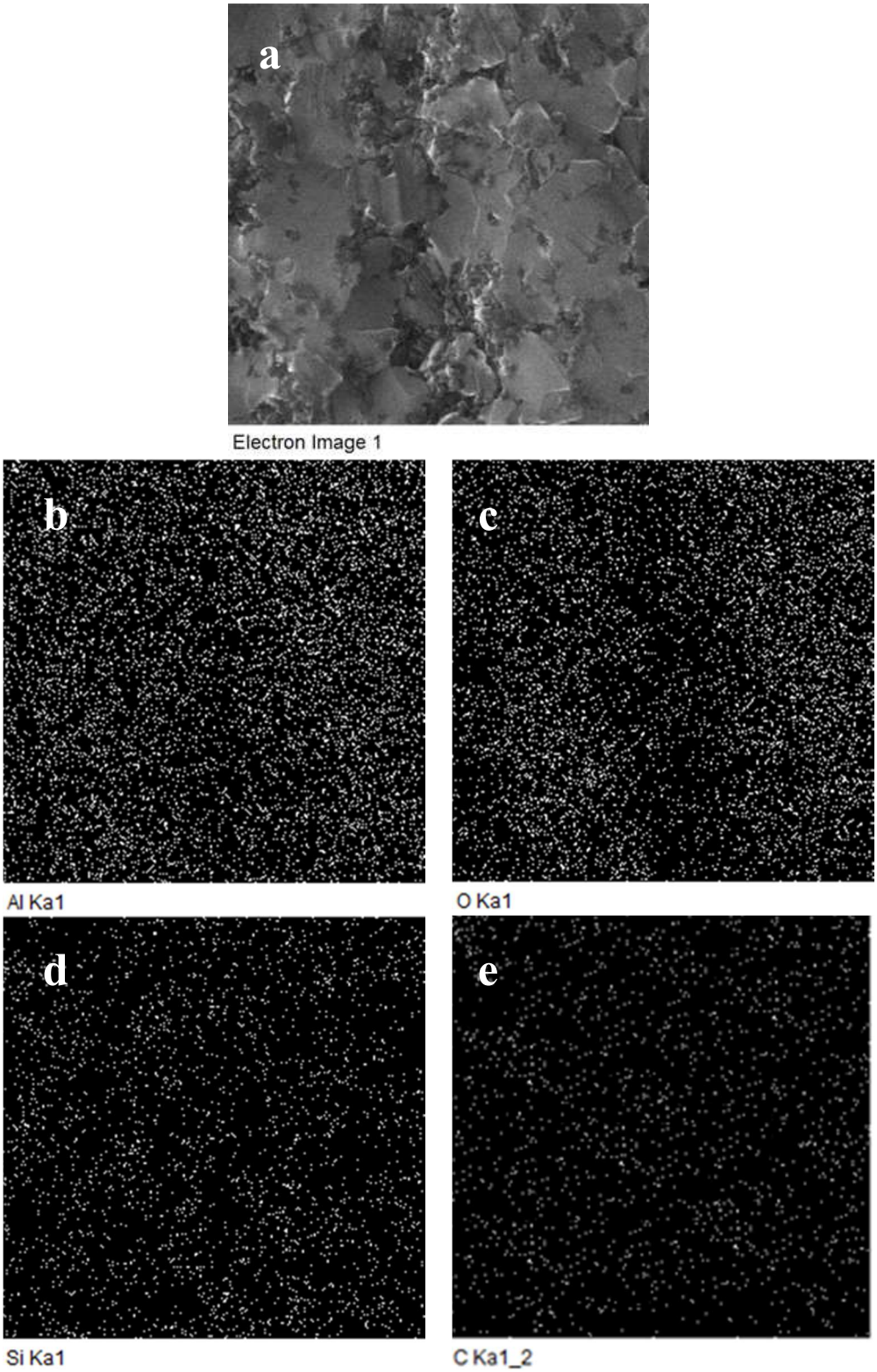

Figure 4.47 *FESEM (a) and X-Ray mapping of Al(b),O(c), Si(d) and C(e) in consolidated sample of molecular level mixed* Al_2O_3*-5SiC-1CNT, synthesized using 02hours sonication and consolidated at 1600°C.*

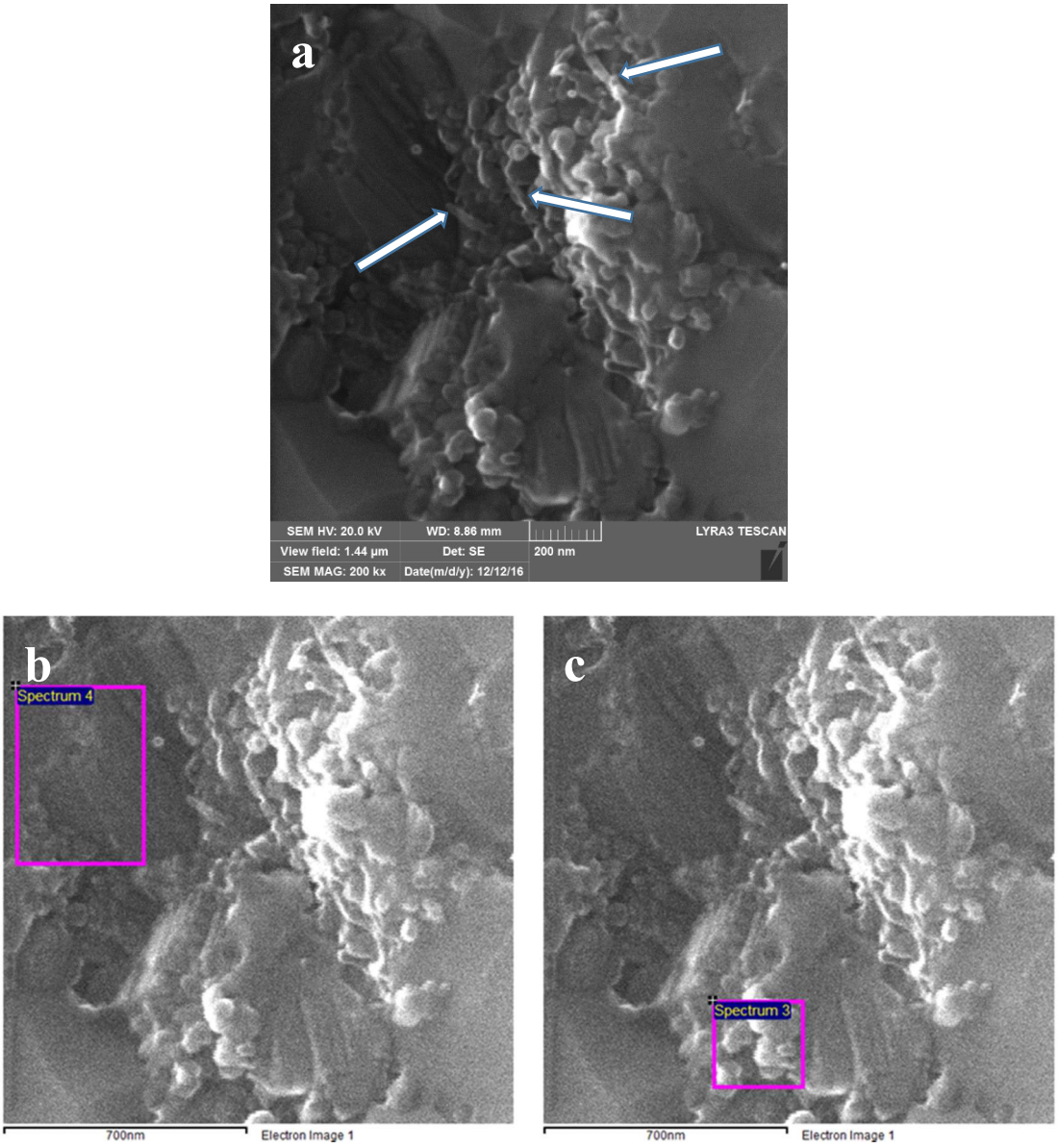

Figure 4.48 *FESEM micrograph at high magnification of 200kX showing presence of both SiC and CNT at the grain boundary.*

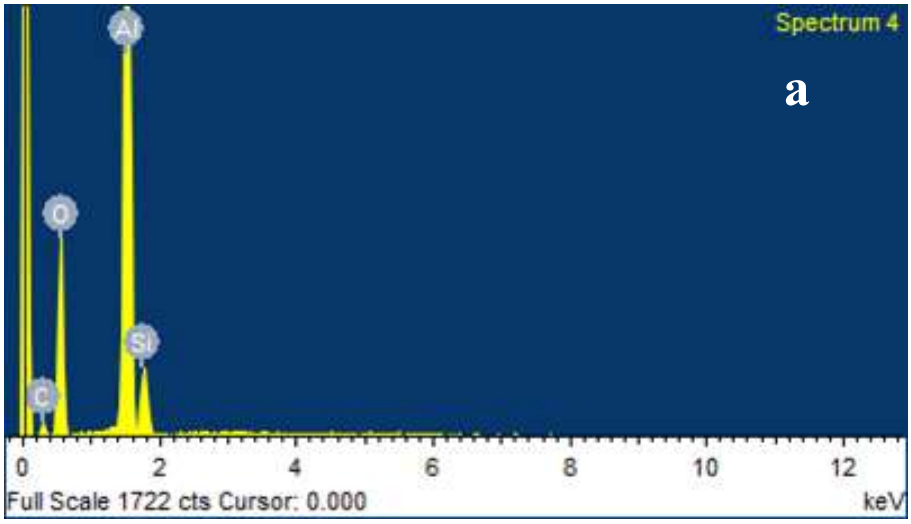

Element	Weight%	Atomic%
C K	12.29	18.95
O K	44.49	51.52
Al K	38.00	26.09
Si K	5.22	3.44
Totals	100.00	

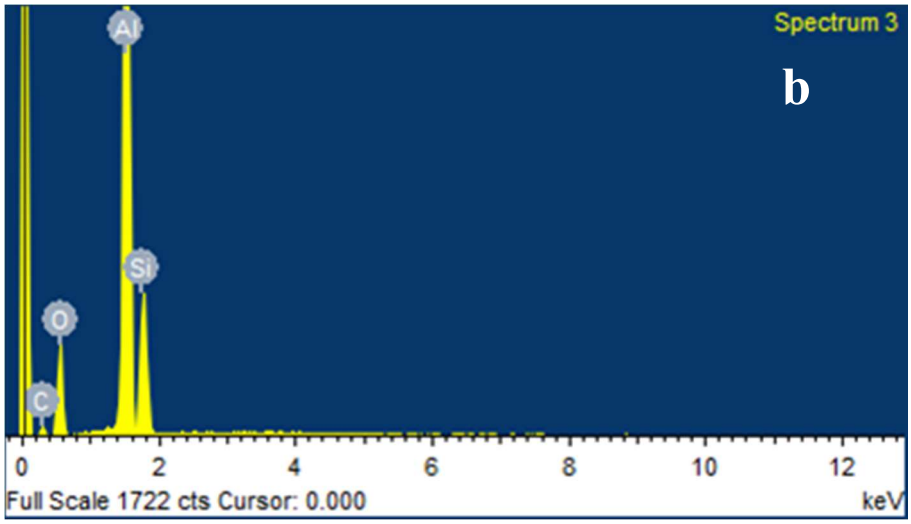

Element	Weight%	Atomic%
C K	14.00	22.65
O K	31.96	38.82
Al K	39.93	28.76
Si K	14.11	9.76
Totals	100.00	

Figure 4.49 *EDX analysis showing (a) spectrum 4 and (b) spectrum 3 of corresponding selected area as shown in* ***Figure 4.48****.*

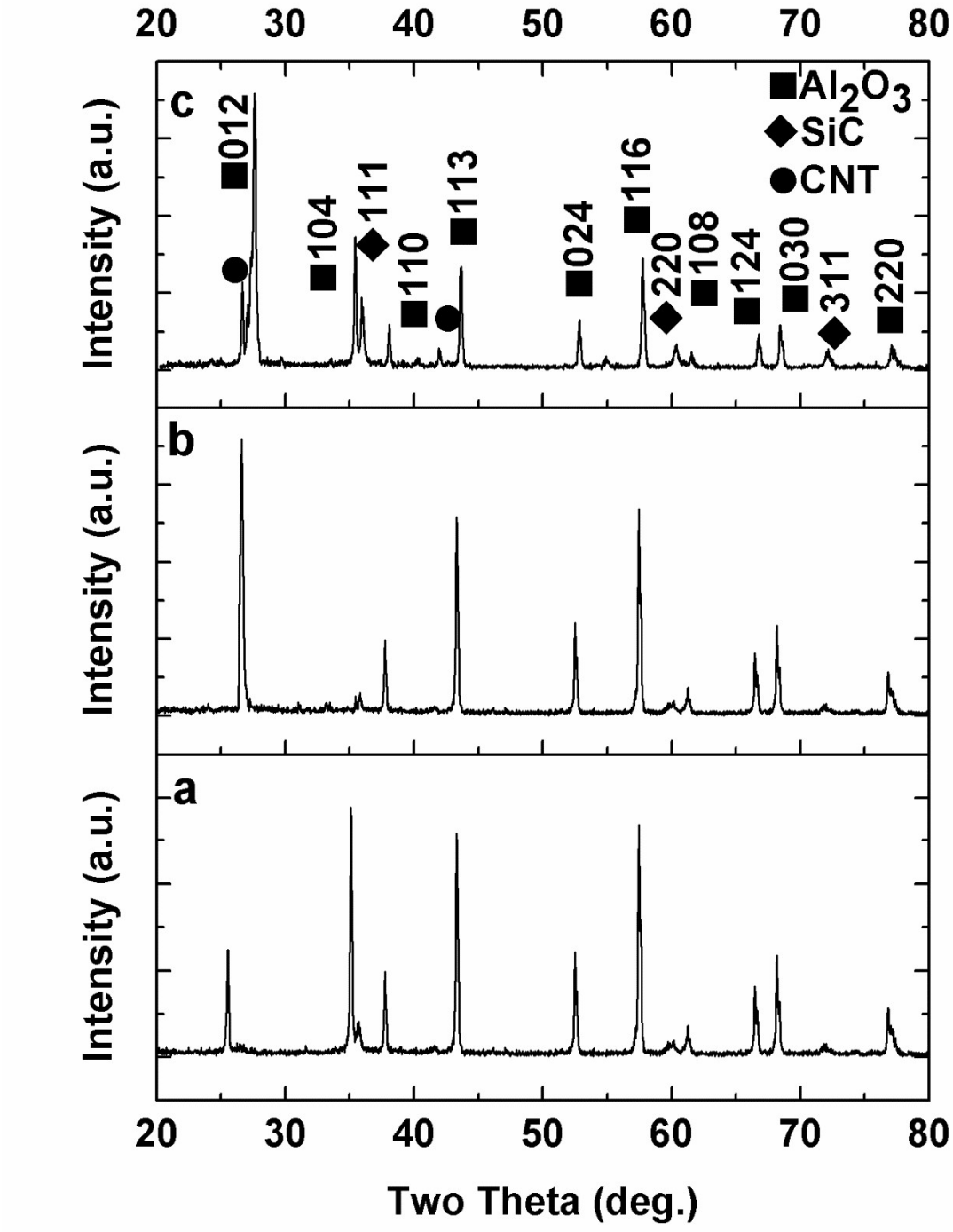

Figure 4.50 *XRD of molecular level mixed Al_2O_3-5SiC-1CNT consolidated at (a) 1500°C /10mins (b) 1550°C /10min and (c) 1600°C/10mins*

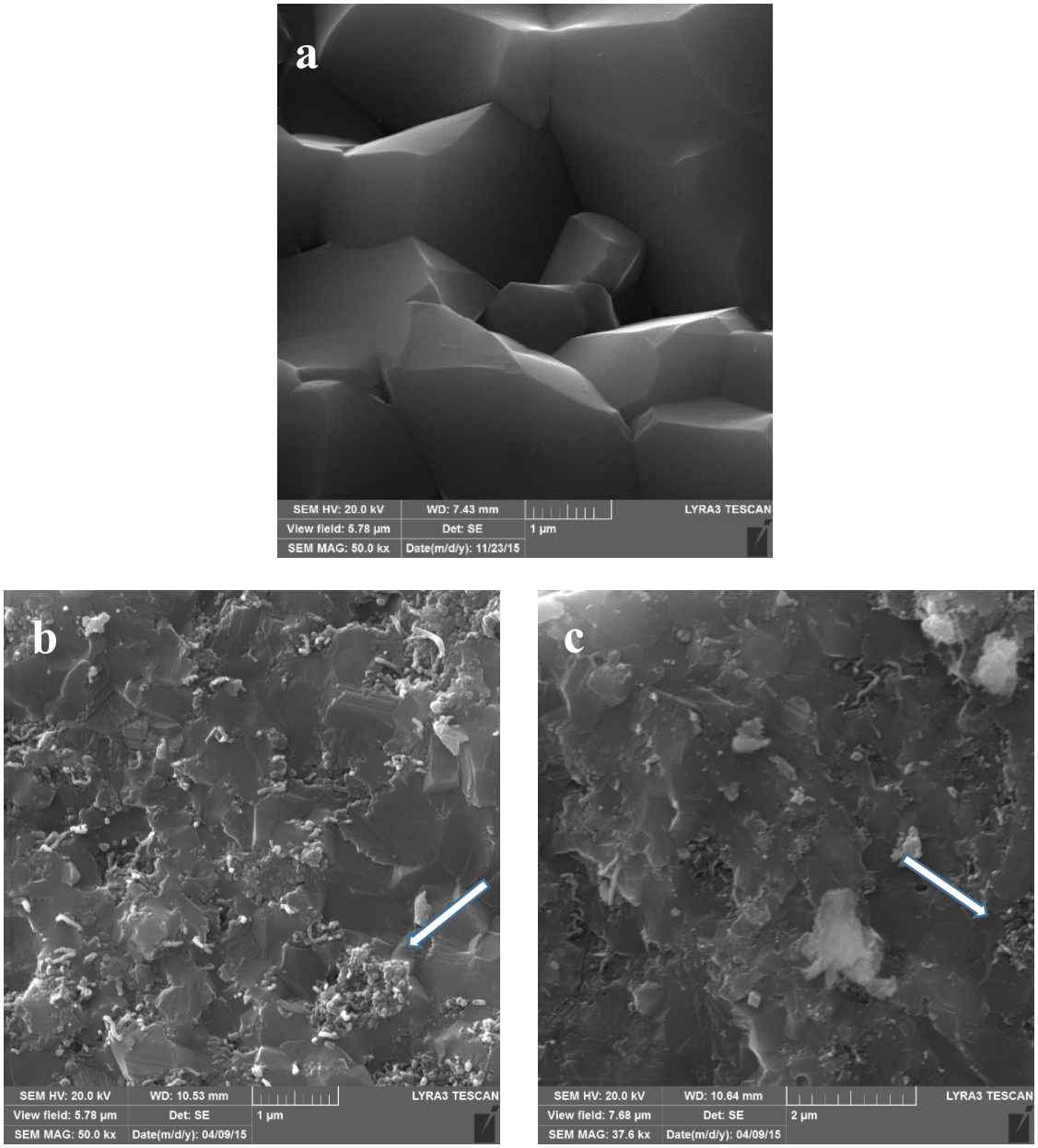

Figure 4.51 *FESEM micrographs showing completely intergranular fracture mode in the fractured surface of reference alumina (a), while almost fully transgranular fracture mode (b,c) in molecular level mixed hybrid nano composite Al_2O_3-5SiC-1CNT, synthesized using 24hours sonication time.*

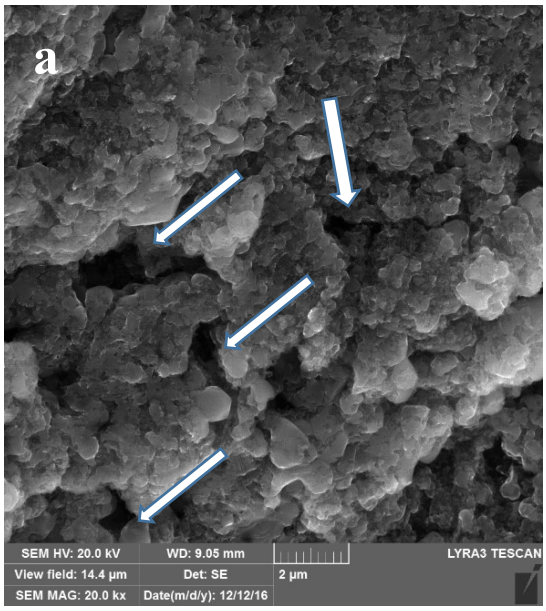
a
SEM HV: 20.0 kV
WD: 9.05 mm
LYRA3 TESCAN
View field: 14.4 µm
Det: SE
2 µm
SEM MAG: 20.0 kx
Date(m/d/y): 12/12/16

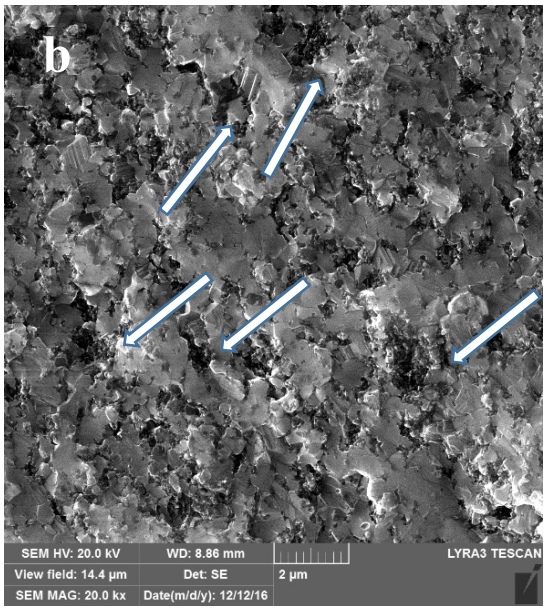
b
SEM HV: 20.0 kV
WD: 8.86 mm
LYRA3 TESCAN
View field: 14.4 µm
Det: SE
2 µm
SEM MAG: 20.0 kx
Date(m/d/y): 12/12/16

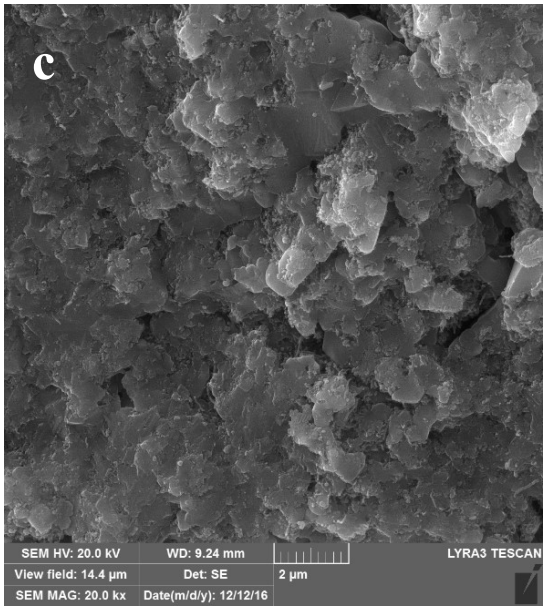
c
SEM HV: 20.0 kV
WD: 9.24 mm
LYRA3 TESCAN
View field: 14.4 µm
Det: SE
2 µm
SEM MAG: 20.0 kx
Date(m/d/y): 12/12/16

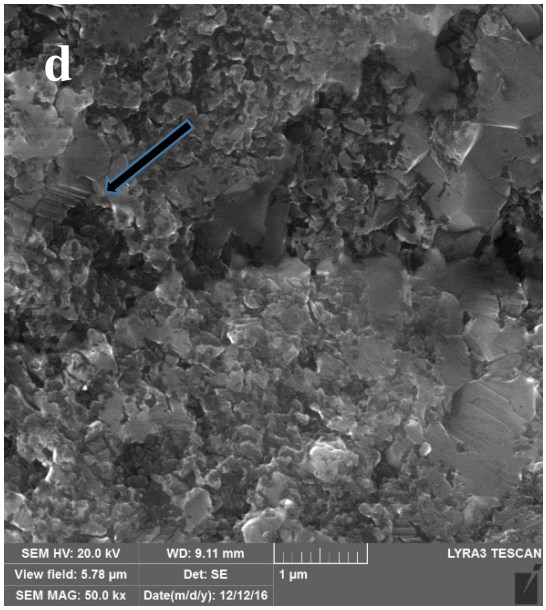
d
SEM HV: 20.0 kV
WD: 9.11 mm
LYRA3 TESCAN
View field: 5.78 µm
Det: SE
1 µm
SEM MAG: 50.0 kx
Date(m/d/y): 12/12/16

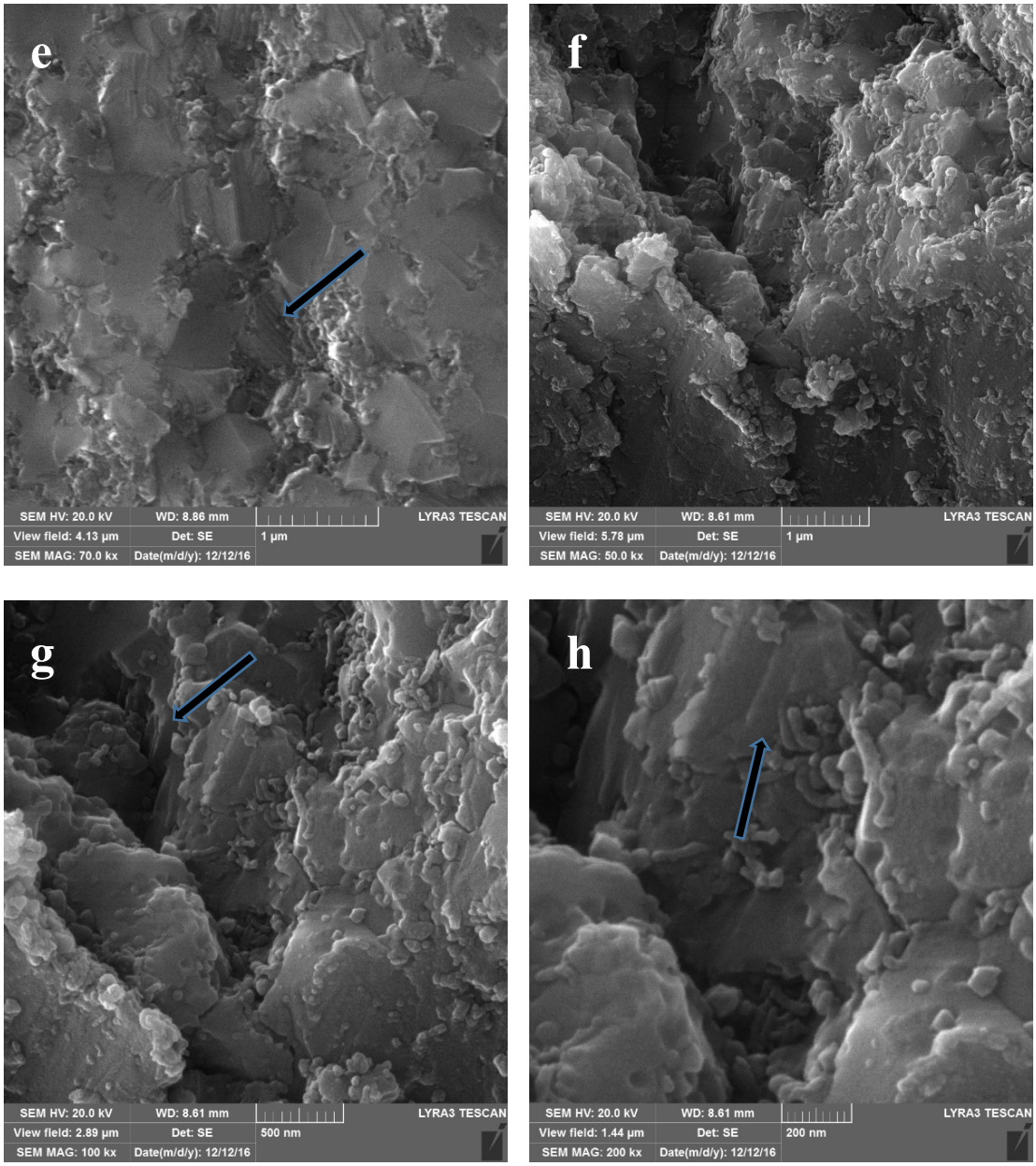

Figure 4.52 *Fractured surfaces of Al_2O_3-5SiC-1CNT synthesized using sonication time of 02 hours and sintered at 1500°C (a, b), 1550°C(c, d) and 1600°C (e, f, g, h) showing completely transgranular fracture mode. Decrease in voids content (indicated by white arrows), and increases in twin deformation (indicated by black arrows) mechanism at high sintering temperature is also shown.*

4.2.4 Mechanical Properties

Hardness

Hardness values of Al_2O_3-5SiC-1CNT synthesized at different sonication times during the molecular level mixing process, and consolidated at different sintering temperatures, are shown in **Figure 4.53**.

The nanocomposite powder synthesized using a sonication time of 24 hours and 2 hours attained hardness values of 17.81GPa and 16.9GPa respectively, when sintered at 1500ºC for 10mins. However, high hardness values of 19.75GPa and 23.32GPa were achieved, when the sintering temperature was raised to 1550ºC and 1600ºC respectively. Low hardness values of samples, consolidated at a sintering temperature of 1500ºC and increasing hardness values of samples sintered at high sintering temperatures of 1500ºC and 1600ºC correspond to their respective relative densities attained at these temperatures, as shown in **Figure 4.50**.

Almost full dense Al_2O_3-5SiC-1CNT developed with molecular level mixing attained a high hardness value of 23.32GPa which is 25.6% more than monolithic alumina and 18% more than the value attained by the same composition when synthesized using the ball milling process. This increase is primarily attributed to the enhanced homogeneous distribution of reinforcement and to the strong interfacial bonding as a result of ionic bonding during the molecular level mixing process. High density and interfacial bonding between the matrix and reinforcement contribute to high hardness values [36][114]. The interface is usually characterized by the critical shear stress needed to debond the interface. The corresponding critical pulling force is $F_{max}^{\tau} = \tau_b . \pi D L_{emb}$ [118] where D is the

diameter of the reinforcement, and L_{emb} is the embedded length in the matrix. Micro structural analysis of our developed material, shows maximum embedded CNT in the alumina matrix, as shown in **Figure 4.41**, and thus is a major cause of the higher hardness values attained.

The high hardness value of 23.32Gpa for the almost full dense hybrid material developed during this work is higher than either monolithic alumina [2][20], Al_2O_3-CNT prepared using ball milling [20],[28] and/ or using molecular level mixing [23] Al_2O_3-SiC-CNT prepared using ball milling [29]. Monolithic Al_2O_3 was sintered using spark plasma sintering at 1300ºC for 3mins by Thomson *et al* [2] and reported a hardness value of 20.9Gpa, while sintering at 1500ºC for 10mins by G Yamamoto *et al* [20] reported a value of 17.3 GPa. The authors also prepared Al_2O_3-CNT using acid-treated CNT and alumina precursor through sonication and reported a small reduction in hardness value of (16.8GPa) after sintering using the same sintering parameters. Ahmad *et al* [28] investigated CNTs reinforced alumina nanocomposites which were synthesized using ball milling and sintered using spark plasma sintering, and reported a maximum hardness value of (18.8 GPa) for Al_2O_3-1CNT. Interfacial bonding between Al_2O_3 and CNTs as reinforcement, was enhanced by synthesizing a powder mixture using molecular level mixing [23], and reported enhanced toughness due to the homogeneous distribution of CNTs in the matrix, although a lower hardness value of 17.5Gpa was also reported. A hybrid nanocomposite, where two reinforcements (SiC and CNTs) were added to Al_2O_3 matrix through ball milling [29] reported a maximum hardness value of 16Gpa for Al_2O_3-1SiC-5CNT nanocomposites.

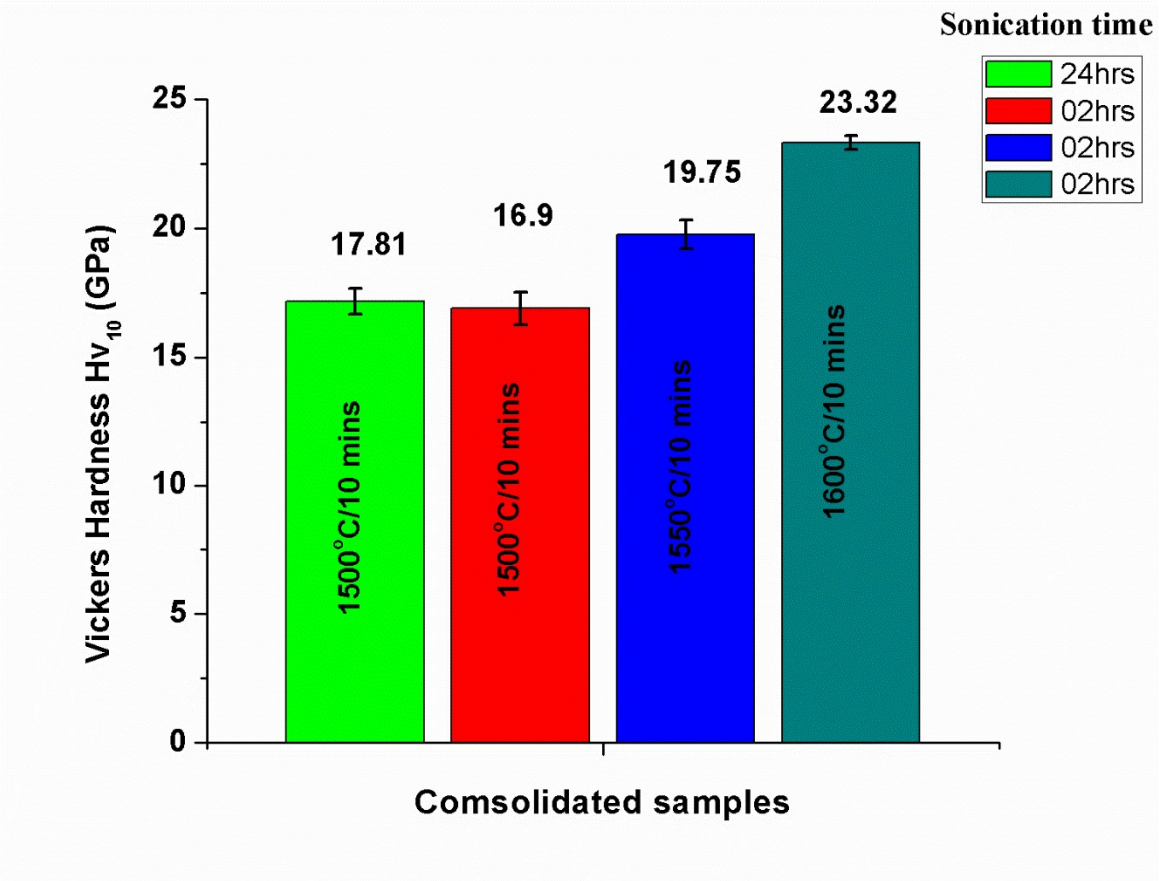

Figure 4.53 *Vickers hardness vales of composites, synthesized through molecular level mixing using sonication time of 02hours, as a function of sintering temperatures for a dwell time of 10 minutes, under 50MPa applied pressure.*

Fracture toughness

Fracture toughness values of Al_2O_3-5SiC-1CNT synthesized at different sonication times during the molecular level mixing process and consolidated at different sintering temperatures are shown in **Figure 4.54**.

Al_2O_3-5SiC-1CNT nanocomposite powder synthesized using 24 hours and 2 hours for the sonication time attained toughness values of 5.38MPam$^{1/2}$ and 5.68MPam$^{1/2}$ when consolidated at 1500^{o}C for 10mins. However, high toughness values of 6.12 MPa.m$^{1/2}$ and 7.1 MPam$^{1/2}$ were attained, when the sintering temperature of powder, synthesized using a sonication time of 2 hours, was raised to 1550^{o}C and 1600^{o}C respectively. Low toughness values for samples being consolidated at 1500^{o}C correspond to their low density, as shown in **Figure 4.44**. However, an enhanced uniform distribution of reinforcement, as shown in **Figure 4.41**, a high relative density value as shown in **Figure 4.44**, and a completely transgranular fracture mode as shown in **Figure 4.51**, have increased the toughness value to 7.10Mpam$^{1/2}$ which is a 96% increase with respect to the reference material (pure alumina).

The primary crack initiated at the diagonal of each indent, made for the hardness test, was found to be deflected as it extended, as shown in **Figure** 4.55. The deflected crack, due to its probable interaction with either CNT, fine SiC or even micro cracks, was found to travel further while respectively lowering the stress intensity at the crack tip. This deflection in propagating the crack may also be due to residual stress due to the difference in the thermal expansion coefficient of SiC, CNT, and Al_2O_3. Radial tension on reinforcement, having a higher thermal expansion coefficient than the matrix, was found to force the crack to travel

around it [119]. Further compression stresses at a distance from the particle contribute to enhancing the toughness of the material.

The crack bridging mechanism is shown in **Figure 4.56**. It is clear from this FESEM micrograph that the CNT has remained intact, as the propagating crack passes beyond it. The crack surface, as shown, is bridged by the CNT, which in turn makes further propagation difficult and thus toughens the material. The CNT bridging effect ensures high interfacial bonding between the matrix and the reinforcement, due to the ionic bonding between CNT and Al_2O_3 in this developed material. The crack branching phenomenon is also illustrated in **Figure 4.56** (c), where high interfacial bonding restricts the propagating crack, and branches into a different direction which, however, consumes energy and thus increases the toughness of the developed material.

The difference between Young's modulus of Al_2O_3 and CNT in the composites gives rise to different stresses experienced by each when they are deformed at the same level of strain. However, higher stresses are subjected to CNTs, having a higher modulus than Al_2O_3, and thus carrying more load than the matrix. This load transfer from Al_2O_3 to the CNT, works on the CNT, and will eventually either break the CNT, as shown in **Figure** 4.57 (a) or pull the CNT from the Al_2O_3 matrix, as shown in **Figure** 4.57 (b). In either case energy at the crack tip will be consumed hence increasing the toughness of the material. Fiber pull out can also occur, when a propagating crack is deflected by a high strength CNT-matrix interface. Tensile stress, generated along the CNT, when the load is being transferred to the CNT, leads to pulling the CNT from the matrix. This requires work and hence the toughening mechanism is achieved in the system.

The simultaneous increase in both the hardness and the toughness values is either limited to or lower than that attained by the molecular level mixed composite developed during this study. Previous studies of either Al_2O_3-SiC [12] [30], Al_2O_3-CNT[28], Al_2O_3-GPL[120], Al_2O_3-GPL-SiC[8], Al_2O_3-GNT-CNT[37], Al_2O_3-SiCw-CNT[38], and Al_2O_3-SiC-CNT[29] are discussed in comparison to the developed nanocomposite during this study.

N. Jiraborvornpongsa *et al* [12] used 0.2wt% SiCnw as reinforcement in alumina and prepared the composite mixture using ball milling. The mixed powder was further sintered using hot pressing. It was found that the grain size of alumina was reduced by 20%, which increased the hardness of the composite by 10% while reducing the fracture toughness by 15%.

M. Sternitzke *et al* [30] prepared Al_2O_3-SiC using ball milling and further consolidated the composite using hot pressing. The authors reported that addition of 5 vol% SiC resulted in an almost 50% increase in the strength of the nanocomposite. The hardness was also found to increase, although this was at the expense of fracture toughness. Relative densification was also reported to have been reduced in the composite.

Ahmad *et al* [28] investigated the CNTs reinforced alumina nanocomposites which were synthesized using ball milling and sintered using spark plasma sintering, and reported a maximum hardness value of (18.8 GPa) for Al_2O_3-1CNT with a fracture toughness value of 4MPam$^{1/2}$.

Liu *et al* [120] studied the effect of graphene platelets on reinforcing the alumina composite. The authors synthesized a composite using ball milling and further consolidated a different composition using spark plasma sintering. They reported maximum hardness and toughness values of 17.66GPa and 4.49MPam$^{1/2}$ for Al_2O_3-0.38 vol% GPLs.

Liu and his colleagues [8] investigated the effect of 1, 3, and 5 vol% of SiC in alumina-0.38vol% GPL (graphene platelets) which were synthesized through ball milling and spark plasma sintering and found that a 3 vol% addition of SiC resulted in the best combination of properties showing a densification of 98.85%, hardness of 24Gpa and fracture toughness of 5.0MPam$^{1/2}$.

Yazdani *et al* [37] synthesized Al_2O_3-GNT and CNT using probe sonication and consolidated them using spark plasma sintering. They attained a maximum toughness value of 5.75MPam$^{1/2}$,however, this also resulted in a lower hardness value of 15GPa.

Ahmed and Pan [29] investigated the influence of 0,5,7, and 10 vol% MWCNTs in Al_2O_3-1SiC. Sonication and ball milling were used to prepare the respective compositions which were further consolidated using spark plasma sintering. The authors reported a high fracture toughness of 7Mpam$^{1/2}$ but a lower hardness value of 16Gpa.

D. Lee and D. Yoon *et al* [38] reported a maximum value of 20.81Gpa with a lower toughness value of 4.5Mpam$^{1/2}$ for Al_2O_3–SiCw–(CNT) composites having a relative density (>99%) which was obtained by hot-pressing at 1750 °C for 1 h at 30 MPa.

However, the use of surface modified MWCNTs, with their ionic bonding with the matrix occurring during the molecular level mixing synthesis process rather than during the solid state mixing process used during previous studies, in addition to its enhanced uniform distribution and the full dense structure attained during this work, have collectively attributed to the effective and simultaneous increase in both the hardness and the fracture toughness values of 23.32GPa and 7.10MPam$^{1/2}$ respectively.

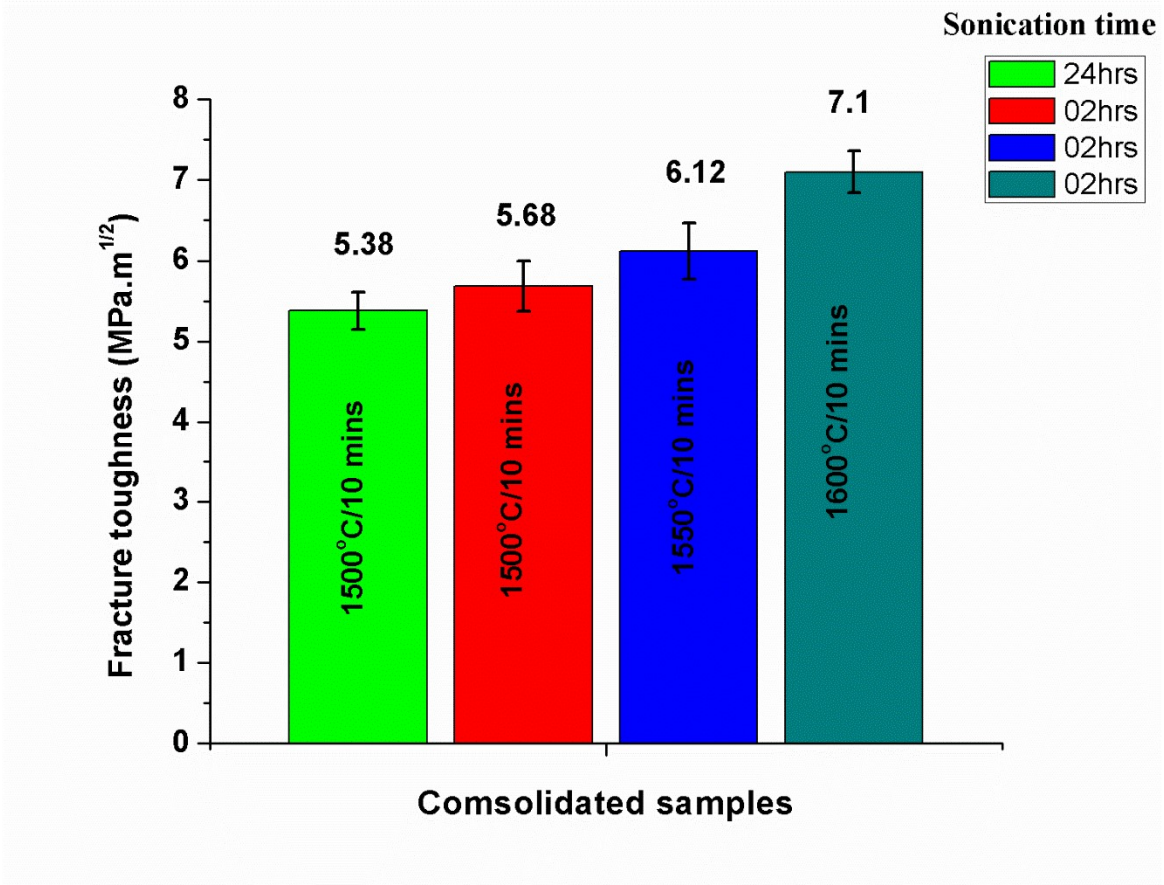

Figure 4.54 *Fracture toughness of composites, synthesized through molecular level mixing using sonication time of 02hours, as a function of sintering temperatures for a dwell time of 10 minutes, under 50MPa applied pressure.*

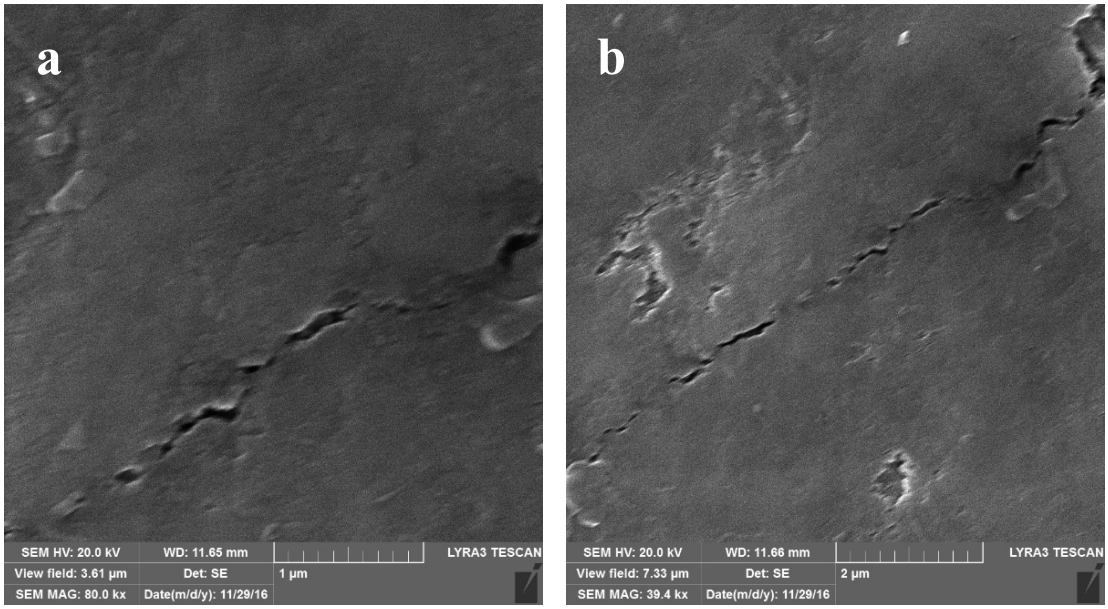

Figure 4.55 *crack deflection mechanism in molecular level mixed synthesized nanocomposite at different magnification as shown in (a), and (b).*

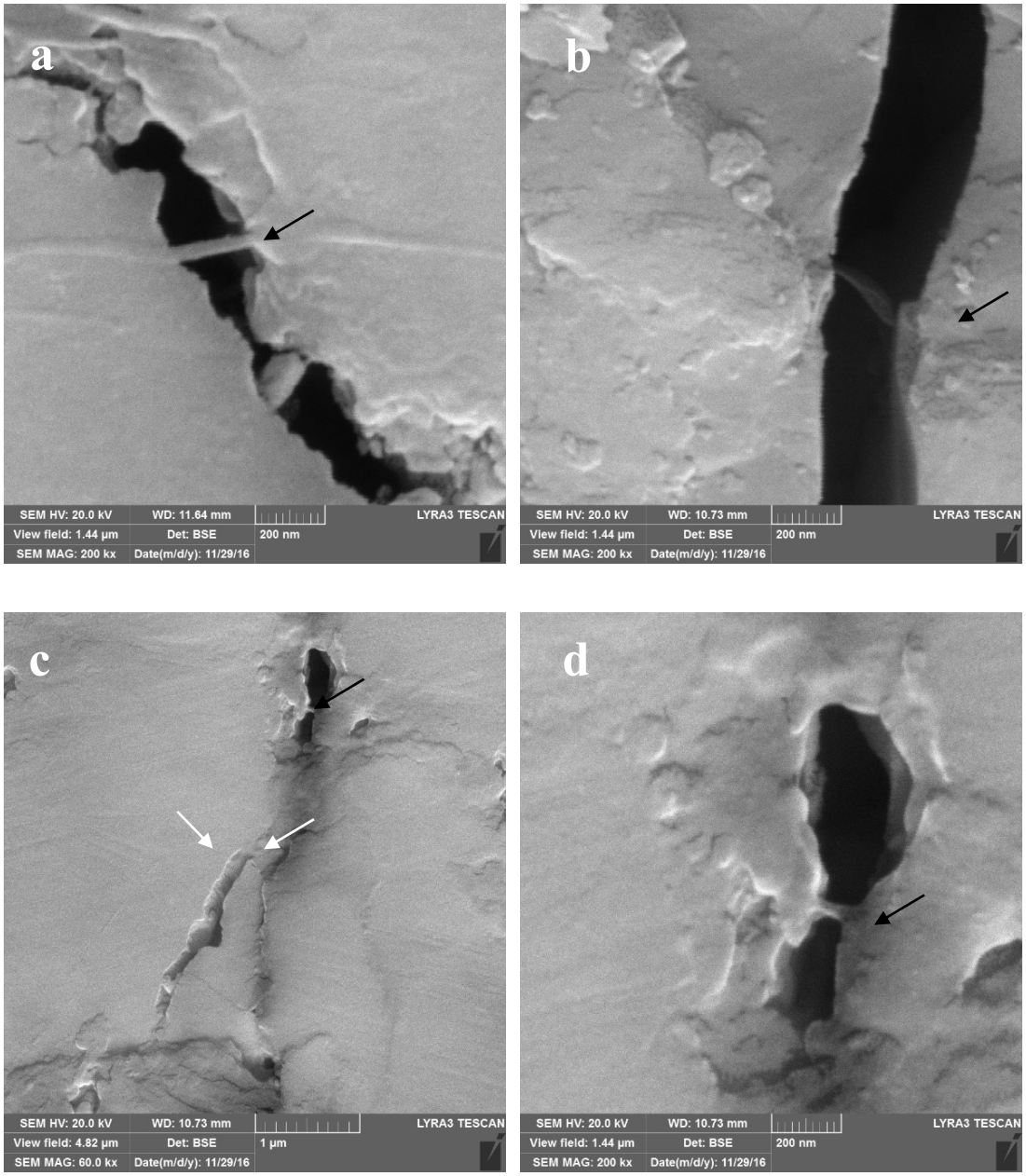

Figure 4.56 *crack bridging mechanism shown by the black arrows (a,b,c,d), while crack branching shown by the white arrows(c), in molecular level mixed synthesized nanocomposite.*

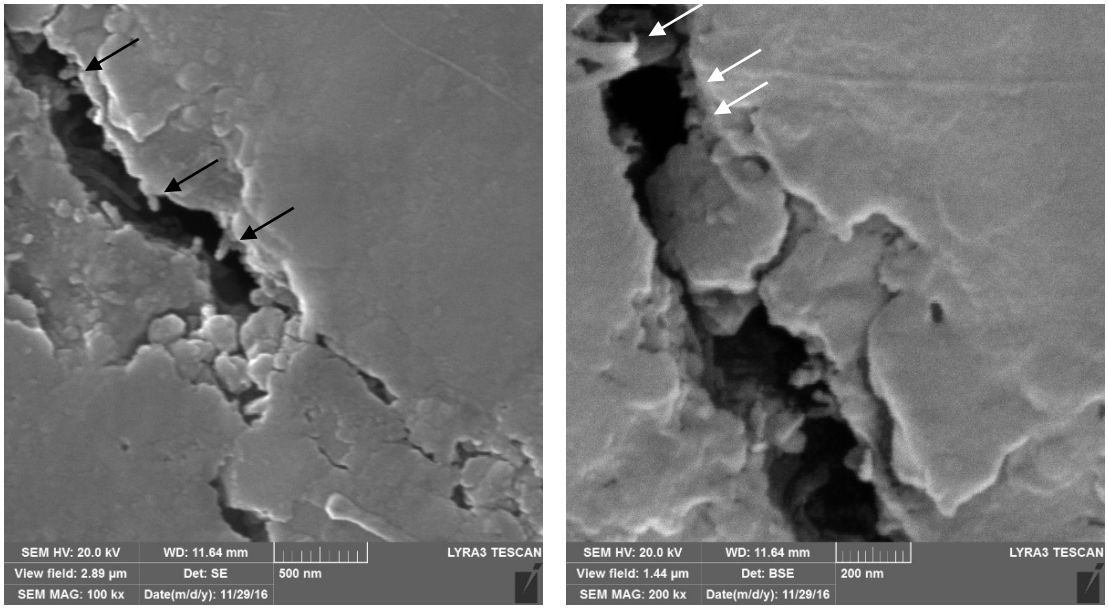

Figure 4.57 *load transfer mechanism showing either CNT breakage (black arrows) and CNT pull out (white arrows) in the synthesized molecular level mixed nanocomposite.*

Table 4.1Mechanical properties of alumina based nanocomposites as reported in recent literature.

Matrix	**Reinforcement Content**	**Synthesis**	**Sintering**	**Relative density (%)**	**Hardness (GPa)**	**Fracture toughness ($MPam^{1/2}$)**	**Reference/ year**
Al_2O_3	0 vol. %CNT	Ball milling	SPS @ 1400ºC/3mins	99.5	17	3.5	[28]/2015
	1.1 vol. % CNT			98.5	18.8	4	
	6.4 vol. %CNT			95.1	15	5.5	
	10.4 vol. %CNT			92.0	11	4.7	
Al_2O_3- 0.38 vol.% GPL	1 vol% SiC	Ball milling	SPS @1500ºC/03mins	99.03	21.34	4.77	[8]/2014
	3 vol% SiC			98.85	24.65	5.03	
	5 vol% SiC			97.35	21.58	4.94	
Al_2O_3- 0.5wt%GNT	0.5 wt% CNT	Probe sonication	SPS @ 1650ºC/10mins, 40MPa	99	15	5.75	[37]/2015
	1 wt% CNT			99	15.5	4.5	
	2 wt% CNT			97	11	4	
Al_2O_3-1SiC	0MWCNT	Ball milling	SPS @ 1550ºC/10mins, 50MPa	99.5	16	4	[29]/20008
	5MWCNT			98.2	16	6.2	
	7MWCNT			97.2	15.5	6.8	
	10MWCNT			95.1	14	5.2	
Al_2O_3- 25SiCw	0 wt.% CNT	Ball milling	Hot pressing @ 1750/1hr, 30MPa	99.85	20.6	4.6	[38]/2014
	0.1 wt.% CNT			99.7	20.8	4.5	
	0.5 wt.% CNT			99.25	20.3	4	
	1 wt.% CNT			99	20	3.5	
Al_2O_3- 0.5wt%GNP	1 wt.%CNT		Hot Pressing	99		5.7	[84]/2015
Al_2O_3-	0 vol% GPLs	Ball milling	SPS @1500ºC/3mins, 50MPa	100	18.04	3.53	[120]/2013
	0.38 vol% GPLs			99.58	17.66	4.49	
	0.76 vol% GPLs			99.92	17.46	4.11	

	1.33 vol% GPLs			99.87	16.32	3.94	
Al_2O_3-	0.035 wt. %SiC	Ball milling	Hot Pressing @1400oC/10min, 30MPa	3.96	20.8	2.7	[12]/2013
	0.1 wt. %SiC			3.95	21.2	2.6	
	0.2 wt. %SiC			3.94	21.1	2.7	
Al_2O_3			SPS @1500ºC/10mins	99.3	18.56	3.61	Self
Al_2O_3-5SiC	0wt.%CNT	Al_2O_3-SiC (ball milling) + CNT (probe sonication)	SPS @1500oC/10min, 50MPa	99.76	21.78	2.65	Self
	1wt.%CNT			99.36	19.77	3.89	
	2wt.%CNT			98.28	19.11	4.2	
Al_2O_3-10SiC	0wt.%CNT			99.03	20.89	3.64	Self
	1wt.%CNT			98.63	20.81	4.58	
	2wt.%CNT			98.02	17.50	6.98	
Al_2O_3-5SiC	1wt.%CNT	Molecular level mixing	SPS @ 1500/10min	90.36	16.9	5.68	Self
			SPS @ 1550/10min	95.16	19.75	6.12	
			SPS @ 1600/10min	98.9	23.32	7.1	

4.3 Comparative Study

In this work, Al_2O_3-SiC-CNT nanocomposite powder compositions were synthesized using two different (ball milling and molecular level mixing) processes. Synthesized powders were further consolidated to almost full dense structures using the spark plasma sintering process. Distribution of reinforcement, densification behavior, and the mechanical properties in Al_2O_3-SiC-CNT, synthesized using the two different processes, were studied for comparison.

1. Powder Synthesis

Using the ball milling process, as received Al_2O_3 (with an average particle size of 200nm) and SiC (with an average particle size of 50nm) were first wet-milled in alumina vials (250 ml in volume) together with alumina balls (10 mm in diameter) using a planetary ball mill. CNTs were further added to the slurry and sonicated under high energy probe sonication. During the molecular level mixing, functionalized CNTs having negative carboxyl groups on their surface were ionically attached to Al ions, which were acquired from the decomposition of Al-salts. SiC with an avenge particle size of 50nm were further added using high energy probe sonication.

The mass production rate is a vital consideration in selecting synthesis techniques, particularly for a commercial application, such as the cutting tool. Ball milling gives a low cost of production, with a high production rate and ease of processing compared to molecular level mixing. 20 grams of powder composition were prepared in two alumina vials using the ball milling process for 6 hours. Obtaining a powder composition prepared

using molecular level mixing was quite time-consuming, as only 2.5 grams of powder composition were produced after almost 10 hours.

2. Environment friendly

Powders produced using the molecular level process include the chemical decomposition of aluminum nitrate salt, which at later stages during the drying process, exhaust harmful gasses such as NOX, which are very toxic and dangerous for human health. Therefore these powders need to be dried and the calcination process must be carried out under proper fume hoods. Ball milling, on the other hand, doesn't exhaust any such gasses and is, therefore, more environment-friendly.

3. Distribution of reinforcement

The distribution of reinforcement has been reported as being the prime reason for obtaining lower than expected values for properties in the ceramic nanocomposite. However, both synthesis processes (ball milling and molecular level mixing) have resulted in the homogeneous distribution of reinforcement in the matrix. In particular, molecular level mixing, where Al+ ions were mixed ionically with CNTs at the molecular level. gives the best distribution of reinforcement and more specifically, each separate CNT was shown to be implanted in the alumina matrix, as shown in **Figure 4.41**. This has effectively resulted in a simultaneous increase in both hardness and toughness.

4. Densification and Sinter-ability

The initial alumina powder (as received), which was used during ball milling, had an average particle size of 200nm, as shown in **Figure 4.1**. However, the particle size

synthesized at the molecular level was comparatively large with an average size of 1μm, as shown in **Figure 4.39**. The smaller surface energies of large particles, produced during the molecular level mixing process, tend to slow down the diffusion (surface and or grain boundary) mechanism and thus require high thermal energies which can be achieved by either extending the dwell time and/ or raising the sintering temperature to attain a full dense structure. Al_2O_3-5SiC-1CNT synthesized using ball milling and molecular level mixing was sintered under the same sintering parameters at 1500°C for 10mins under an applied pressure of 50MPa. Ball milled samples attained a relative density of 99.3%, while the molecular level mixed samples could attain only 91.65%. This lower density of the molecular level mixed sample was, however, increased to 95.16% and 98.9% when the sintering temperature was raised to 1550°C and 1600°C respectively.

5. Mechanical properties

Monolithic alumina powder with an average particle size of 200nm and initial crystallite size of 39nm was consolidated to almost full dense structure when sintered under spark plasma sintering at 1500°C/10min under an applied pressure of 50MPa. The consolidated monolithic alumina was found to have a vickers hardness (Hv10) value of 18.56GPa and a toughness of 3.61Mpam$^{1/2}$. Retaining the final crystallite size to almost 93nm is attributed to the use of the spark plasma sintering process at a high heating rate (100°C/min) and a low dwell time of 10mins. The fractured surface of monolithic alumina revealed the intergranular fracture mode, with cracks propagating along the grain boundary, which is the weaker and more disordered region within the material.

Different compositions were synthesized using the ball milling process, and almost a full relative density along with enhanced mechanical properties were attained in all samples,

when consolidated at the same sintering parameters as those used for the sintering of monolithic alumina. The same sintering parameters were chosen to maintain consistency and to make it easy to compare the results of the composite and monolithic alumina. However, one common composition (Al_2O_3-5SiC-1CNT) which was prepared using both the molecular level mixing process and the ball milling process is presented in **Table 4.2** for comparison.

Al_2O_3-5SiC-1CNT, synthesized using ball milling and sintered at 1500^oC for 10mins, attained a relative density value of 99.36%, which is almost the same as that attained by monolithic alumina after consolidation using the same sintering parameters. The addition of reinforcement hinders mass transportation and in particular, hard reinforcement reduces the possibility of powders to be plastically deformed, which reduces density of the composite. However, a high dense nanocomposite structure developed under ball milling at the same sintering parameters is attributed to the use of SiC and CNT as reinforcement, which makes alumina an electrically conductive material, leading to increased flow of the current amp and diffusion rate and hence attains a high relative density. Further use of spark plasma sintering with higher local heating due to spark discharge, and the rearrangement of particles and the breakdown of agglomerates due to higher applied pressure, helped in attaining a high relative density in the nanocomposite, which was almost same as monolithic alumina.

However, Al_2O_3-5SiC-1CNT synthesized using molecular level mixing was unable to sinter at the same sintering parameters of 1500^oC for 10mins, which were used for monolithic alumina and the ball milled synthesized nanocomposite. The prime reason for the low sinter-ability was the large alumina particle size produced during molecular level mixing

(almost 1μm) **Figure 4.39** (a) as compared to the as received alumina (almost 200nm) in **Figure 4.1** (b) which was used during the ball milling process. The smaller surface energies of large particles tend to slow down the diffusion (surface and or grain boundary) mechanism and thus it was unable to sinter well. However, by maintaining the heating rate, holding time and applied pressure at constant, the relative density value of Al_2O_3-5SiC-1CNT was increased to 98.9%, when the sintering temperature was raised to 1600°C respectively.

Higher hardness values of Al_2O_3-5SiC-1CNT, synthesized through either the ball milling process or molecular level mixing, than that of monolithic alumina are attributed to the presence of fine SiC particles, which result in a finer microstructure through the pinning effect. The further presence of the hard SiC phase reduces the overall micro-plastic deformation and increases the hardness of the composite. The presence of SiC and/ or CNT at the grain boundary impedes the dislocation slips, in addition to obstructing dislocation pile-up and thus increasing the hardness of Al_2O_3-5SiC-1CNT compared to that of monolithic alumina. The high hardness value of 23.32Gpa is 25.6% more than monolithic alumina and 18% more than the value attained by the same composition, when synthesized using the ball milling process. This increase is primarily attributed to the enhanced homogeneous distribution of reinforcement and to strong interfacial bonding as a result of ionic bonding between the CNTs and alumina during the molecular level mixing process. Additionally, the high hardness values of molecular level mixed nanocomposite can also be attributed to the mixing of Al+ ions with CNT at the level of molecules, which resulted in a very fine microstructure with a crystallite size of 47nm after the consolidation process.

The crystallite size of monolithic alumina and ball milled nanocomposite was 93nm and 72nm, respectively, after the sintering process.

The fracture toughness of nanocomposite synthesized using either ball milling and or molecular level mixing was higher than that of monolithic alumina, which is mainly attributed to the change of fracture mode. The intergranular fracture mode was typical for alumina when changed to a partial or complete transgranular fracture mode. Low toughness in the intergranular fracture mode is due to the propagation of cracks along the weak regions of the grain boundaries. However, the presence of hard SiC and very strong CNT at the grain boundaries in the nanocomposite changes the crack propagation from along the grain boundary to within the grains. The change from intergranular to transgranular crack propagation is due to the tangential tensile stresses on the surface of fine SiC. These stresses are generated due to the difference in the thermal expansion co-efficient between SiC and alumina. The energy of the propagating crack is now consumed in separating the dense structure of grains, and/ or in bowing around the fine SiC (present at the grain boundary or within grains), and/ or in deflecting the crack, due to its probable interaction with either CNT, fine SiC or even micro cracks. These will now travel further and respectively lower the stress intensity at the crack tip, which increases the fracture toughness of the composite material.

The molecular level mixed nanocomposite attained high fracture toughness values of 7.10Mpam$^{1/2}$ which is 82% more than that obtained by ball milled nanocomposite and 96% more than monolithic alumina, as shown in **Table 4.2**. This increase in the toughness value of molecular level mixing is attributed primarily to the uniform distribution of CNTs, as shown in **Figure 4.42**, and SiC, as shown in **Figure 4.52** (g, h), and the completely

transgranular fracture mode, as shown in **Figure 4.51**. Further high interfacial ionic bonding consumes comparatively large amounts of energy from the propagating crack, leading to very high toughness values.

Table 4.2 *Summarized properties of monolithic alumina and synthesize Al_2O_3-5SiC-1CNT using ball milling and molecular level mixing process.*

Synthesis	**Sintering**	**Material**	**Density (%)**	**Hardness (GPa)**	**Toughness ($Mpam^{1/2}$)**	**Crystallite size (nm)**
As received	1500ºC/ 10mins	Al_2O_3	99.3	18.56	3.61	93.39
Ball milled @ 300rpm for 4hours + Sonication		Al_2O_3-5SiC-1CNT	99.36	19.77	3.89	71.58
Molecular level mixed @ sonication for 02hours	1600ºC/ 10mins	Al_2O_3-5SiC-1CNT	98.9	23.32	7.10	47

CHAPTER 5

CONCLUSIONS AND RECOMMENDATIONS 5

5.1 Conclusion and Future Recommendation

In this research work, an approach for the synthesis of homogenous Al_2O_3-SiC-CNTs hybrid nanocomposite powders via molecular level mixing was developed. In addition, homogenous Al_2O_3-SiC-CNTs nanocomposite powders that have uniform distribution of the reinforcements were prepared using ball-milling method. The synthesized powders were sintered to almost full density using spark plasma sintering technique. The influence of synthesis and sintering parameters, and reinforcements' content on the microstructure, densification, hardness, fracture toughness, and bending strength of the composites was investigated. The properties were correlated with the microstructure and possible toughening mechanisms were discussed. The following conclusions are drawn.

1. The nanocomposite powders synthesised via molecular level mixing or ball milling as well as sintered samples showed uniform distribution of SiC and CNTs.

2. The final microstructure of sintered samples comprised intergranular CNTs, along with inter- and intragranular SiC nanoparticles, which pinned the grain boundaries, and restricted grain growth.

3. Fully dense monolithic alumina and almost fully dense hybrid nanocomposites were obtained (relative density higher than 98%).

4. The mode of fracture changed from intergranular mode for the monolithic alumina to almost complete transgranular mode for the Al_2O_3-SiC-CNTs nanocomposites, which along with other toughening mechanisms improved the fracture toughness.

5. The Al_2O_3-5SiC-1CNTs composite, synthesised using molecular level mixing and sintered at 1600°C for 10 min, possessed both high hardness and toughness values of 23.32 GPa and 7.10 $MPam^{1/2}$, respectively. This constitutes an increase in hardness and toughness of 25.6 and 96%, respectively, compared with the monolithic alumina sintered under the same conditions.

6. As for the composites prepared using ball milling and sintered at 1500°C for 10 min, the composite reinforced with 10 wt.% SiC and 2 wt.% CNTs possessed a high fracture toughness value of 6.98 $MPam^{1/2}$, representing an increase of 93.95% compared to alumina. The composite reinforced with 10 wt.% SiC and 1 wt.% CNTs possessed a high hardness value of 20.81 GPa, representing an increase of 12.12 % compared to alumina. The Al_2O_3-10SiC-2CNTs composite showed marginal increase in bending strength with respect to alumina.

The SiC and CNT reinforced alumina nanocomposites had homogenous microstructure and showed simultaneous increase in hardness and fracture toughness, this make them suitable for structural applications including cutting tools. Further investigation of the developed materials is recommended. This may include:

1- Optimization of reinforcements' content, synthesis and sintering parameters to further improve the mechanical properties.

2- Sintering the composites using other non-conventional methods such as microwave sintering.

3- Characterization of thermal properties and electrical conductivity.

4- Investigation of the cutting performance of the developed materials.

References

[1] G. B. Yadhukulakrishnan, A. Rahman, S. Karumuri, M. M. Stackpoole, a. K. Kalkan, R. P. Singh, and S. P. Harimkar, "Spark plasma sintering of silicon carbide and multi-walled carbon nanotube reinforced zirconium diboride ceramic composite," *Mater. Sci. Eng. A*, vol. 552, pp. 125–133, 2012.

[2] K. Thomson, D. Jiang, W. Yao, R. Ritchie, and A. Mukherjee, "Characterization and mechanical testing of alumina-based nanocomposites reinforced with niobium and/or carbon nanotubes fabricated by spark plasma sintering.," *Acta Mater*, vol. 60, no. 2, pp. 622–632, 2012.

[3] I. Ovid'ko and A. Sheinerman, "Micromechanisms for improved fracture toughness in nanoceramics," *Rev. Adv. Mater. Sci*, vol. 29, pp. 105–125, 2011.

[4] P. Palmero, "Structural Ceramic Nanocomposites: A Review of Properties and Powders' Synthesis Methods," *Nanomaterials*, vol. 5, no. 2, pp. 656–696, 2015.

[5] A. Al-Ostaz, W. Wu, H. Alkhateb, and K. I. Alzebdeh, "The joint effect of shape and size of reinforcement on progressive damage of random composites," *Comput. Mater. Sci.*, vol. 46, no. 4, pp. 1144–1151, 2009.

[6] S. Gustafsson, L. Falk, E. Lidén, and E. Carlström, "Alumina/silicon carbide composites fabricated via in situ synthesis of nano-sized SiC particles," *Ceram. Int.*, vol. 35, no. 3, pp. 1293–1296, 2009.

[7] A. Nevarez-Rascon, A. Aguilar-Elguezabal, E. Orrantia, and M. H. Bocanegra-Bernal, "Compressive strength, hardness and fracture toughness of Al_2O_3 whiskers reinforced ZTA and ATZ nanocomposites: Weibull analysis," *Int. J. Refract. Met.*

Hard Mater., vol. 29, no. 3, pp. 333–340, 2011.

[8] J. Liu, Z. Li, H. Yan, and K. Jiang, "Spark Plasma Sintering of Alumina Composites with Graphene Platelets and Silicon Carbide Nanoparticles," *Adv. Eng. Mater.*, vol. 16, no. 9, pp. 1111–1118, 2014.

[9] H. Awaji, S. Choi, and E. Yagi, "Mechanisms of toughening and strengthening in ceramicbased nanocomposite," *Mech. Mater.*, vol. 34, pp. 411–422, 2002.

[10] M. Parchovianský, D. Galusek, J. Sedláček, P. Švančárek, M. Kašiarová, J. Dusza, and P. Šajgalík, "Microstructure and mechanical properties of hot pressed Al_2O_3/SiC nanocomposites," *J. Eur. Ceram. Soc.*, vol. 33, no. 12, pp. 2291–2298, 2013.

[11] M. Rashad, F. Pan, W. Guo, H. Lin, M. Asif, and M. Irfan, "Effect of alumina and silicon carbide hybrid reinforcements on tensile, compressive and microhardness behavior of Mg–3Al–1Zn alloy," *Mater. Charact.*, vol. 106, pp. 382–389, 2015.

[12] N. Jiraborvornpongsa, M. Imai, K. Yoshida, and T. Yano, "Effects of trace amount of nanometric SiC additives with wire or particle shapes on the mechanical and thermal properties of alumina matrix composites," *J. Mater. Sci.*, vol. 48, no. 20, pp. 7022–7027, 2013.

[13] T. Osada, W. Nakao, K. Takahashi, K. Ando, and S. Saito, "Strength recovery behavior of machined Al_2O_3/SiC nano-composite ceramics by crack-healing," *J. Eur. Ceram. Soc.*, vol. 27, no. 10, pp. 3261–3267, 2007.

[14] C. Suryanarayana and N. Al-Aqeeli, "Mechanically alloyed nanocomposites," *Prog. Mater. Sci.*, vol. 58, pp. 383–502, 2013.

[15] E. Zapata-Solvas, D. Gómez-García, and A. Domínguez-Rodríguez, "Towards

physical properties tailoring of carbon nanotubes-reinforced ceramic matrix composites," *J. Eur. Ceram. Soc.*, vol. 32, no. 12, pp. 3001–3020, 2012.

[16] A. Peigney, C. Laurent, E. Flahaut, and A. Rousset, "Carbon nanotubes in novel ceramic matrix nanocomposites," *Ceram. Int.*, vol. 26, no. 6, pp. 677–683, 2000.

[17] Z. Xia, W. a. Curtin, and B. W. Sheldon, "Fracture Toughness of Highly Ordered Carbon Nanotube/Alumina Nanocomposites," *J. Eng. Mater. Technol.*, vol. 126, no. 3, pp. 238–244, 2004.

[18] J. Sun, L. Gao, and X. Jin, "Reinforcement of alumina matrix with multi-walled carbon nanotubes," *Ceram. Int.*, vol. 31, no. 6, pp. 893–896, 2005.

[19] S. S. Samal and S. Bal, "Carbon Nanotube Reinforced Ceramic Matrix Composites-A Review," *J. Miner. Mater. Charact. Eng.*, vol. 7, no. 4, pp. 355–370, 2008.

[20] G. Yamamoto, M. Omori, T. Hashida, and H. Kimura, "A novel structure for carbon nanotube reinforced alumina composites with improved mechanical properties.," *Nanotechnology*, vol. 19, no. 31, pp. 315708–315714, 2008.

[21] J. Fan, D. Zhao, M. Wu, Z. Xu, and J. Song, "Preparation and Microstructure of Multi-Wall Carbon Nanotubes-Toughened Al_2O_3 Composite," *J. Am. Ceram. Soc.*, vol. 89, no. 2, pp. 750–753, 2006.

[22] J.-P. Fan, D.-M. Zhuang, Z. Da-Qing, Z. Gong, W. Min-Sheng, F. Wei, and Z.-J. Fan, "Toughening and reinforcing alumina matrix composite with single-wall carbon nanotubes," *Appl. Phys. Lett.*, vol. 89, no. 12, pp. 121910–121913, 2006.

[23] S. I. Cha, K. T. Kim, K. H. Lee, C. B. Mo, and S. H. Hong, "Strengthening and toughening of carbon nanotube reinforced alumina nanocomposite fabricated by

molecular level mixing process," *Scr. Mater.*, vol. 53, no. 7, pp. 793–797, 2005.

[24] J. Sun, L. Gao, W. Li, and W. Sun, J., Gao, L., & Li, "Colloidal Processing of Carbon Nanotube / Alumina Composites," *Chem. Mater*, vol. 16, no. 14, pp. 5169–5172, 2002.

[25] R. Siegel, S. Chang, B. Ash, J. Stone, P. Ajayan, R. Doremus, and L. Schadler, "Mechanical behavior of polymer and ceramic matrix nanocomposites," *Scr. Mater.*, vol. 44, no. 8–9, pp. 2061–2064, 2001.

[26] N. Saheb, N. U. Qadir, M. U. Siddiqui, A. F. M. Arif, S. S. Akhtar, and N. Al-Aqeeli, "Characterization of nanoreinforcement dispersion in inorganic nanocomposites: A review," *Materials (Basel).*, vol. 7, pp. 4148–4181, 2014.

[27] I. Ahmad, M. Unwin, H. Cao, H. Chen, H. Zhao, A. Kennedy, and Y. Q. Zhu, "Multi-walled carbon nanotubes reinforced Al_2O_3 nanocomposites: Mechanical properties," *Compos. Sci. Technol.*, vol. 70, no. 8, pp. 1199–1206, 2010.

[28] K. Ahmad and W. Pan, "Microstructure-toughening relation in alumina based multiwall carbon nanotube ceramic composites," *J. Eur. Ceram. Soc.*, vol. 35, no. 2, pp. 663–671, 2015.

[29] K. Ahmad and W. Pan, "Hybrid nanocomposites: A new route towards tougher alumina ceramics," *Compos. Sci. Technol.*, vol. 68, no. 6, pp. 1321–1327, 2008.

[30] M. Sternitzke, B. Derby, and R. J. Brook, "Alumina/Silicon Carbide Nanocomposites by Hybrid Polymer/Powder Processing: Microstructures and Mechanical Properties," *J. Am. Ceram. Soc.*, vol. 81, no. 1, pp. 41–48, 2005.

[31] K. Umino, S. Wakayama, T. Sakai, Y. Umehara, and T. Akatsu, "Mechanical

Properties of CNF Reinforced Ceramic Composites Sintered with SPS Technique," *J. Solid Mech. Mater. Eng.*, vol. 5, no. 12, pp. 866–872, 2011.

[32] M. Konishi, "Nanoparticles Technology for Industry of Ceramics Raw Materials," *Bull. Ceram. Soc. Japan*, vol. 46, no. 6, pp. 413–416, 2007.

[33] Smith CS, "Grains, phases, and interfaces: an interpretation of microstructure," *Trans Met. Soc AIME*, vol. 175, pp. 15–51, 1948.

[34] J. A. Wollmershauser, B. N. Feigelson, E. P. Gorzkowski, C. T. Ellis, R. Goswami, S. B. Qadri, J. G. Tischler, F. J. Kub, and R. K. Everett, "An extended hardness limit in bulk nanoceramics," *Acta Mater.*, vol. 69, pp. 9–16, 2014.

[35] N. Saheb and K. Mohammad, "Microstructure and mechanical properties of spark plasma sintered Al_2O_3-SiC-CNTs hybrid nanocomposites," *Ceramics International*, vol. 42, no. 10. pp. 12330–12340, 2016.

[36] K. Mohammad and N. Saheb, "Molecular level mixing: An approach for synthesis of homogenous hybrid ceramic nanocomposite powders," *Powder Technol.*, vol. 291, pp. 121–130, 2016.

[37] B. Yazdani, H. Porwal, Y. Xia, H. Yan, M. J. Reece, and Y. Zhu, "Role of synthesis method on microstructure and mechanical properties of graphene/carbon nanotube toughened Al_2O_3 nanocomposites," *Ceram. Int.*, vol. 41, no. 8, pp. 9813–9822, 2015.

[38] D.-Y. Lee and D.-H. Yoon, "Properties of alumina matrix composites reinforced with SiC whisker and carbon nanotubes," *Ceram. Int.*, vol. 40, no. 9, pp. 14375–14383, 2014.

[39] C. Suryanarayana, "Mechanical alloying and Milling," *Prog. Mater. Sci.*, vol. 46, no.

1–2, pp. 1–184, 2001.

[40] F. Inam, H. Yan, D. D. Jayaseelan, T. Peijs, and M. J. Reece, “Electrically conductive alumina–carbon nanocomposites prepared by Spark Plasma Sintering,” *J. Eur. Ceram. Soc.*, vol. 30, no. 2, pp. 153–157, 2010.

[41] Y. . Dong, F. . Xu, X. . Shi, C. Zhang, Z. . Zhang, J. . Yang, and Y. Tan, “Electrical properties of nanoceramics reinforced with ropes of single-walled carbon nanotubes,” *Mater. Sci. Eng. A*, vol. 504, no. 1–2, pp. 49–54, 2009.

[42] C. Balázsi, B. Fényi, N. Hegman, Z. Kövér, F. Wéber, Z. Vértesy, Z. Kónya, I. Kiricsi, L. P. Biró, and P. Arató, “Development of CNT/Si3N4 composites with improved mechanical and electrical properties,” *Compos. Part B Eng.*, vol. 37, no. 6, pp. 418–424, 2006.

[43] A. Kovalčíková, C. Balázsi, J. Dusza, and O. Tapasztó, “Mechanical properties and electrical conductivity in a carbon nanotube reinforced silicon nitride composite,” *Ceram. Int.*, vol. 38, no. 1, pp. 527–533, 2012.

[44] B. Baron, C. S. Kumar, G. Le Gonidec, and S. Hampshire, “Comparison of different alumina powders for the aqueous processing and pressureless sintering of Al 2 O 3–SiC nanocomposites,” *J. Eur. Ceram. Soc.*, vol. 22, pp. 1543–1552, 2002.

[45] C. Hai, T. Shirai, and M. Fuji, “Fabrication of conductive porous alumina (CPA) structurally modified with carbon nanotubes (CNT),” *Adv. Powder Technol.*, vol. 24, no. 5, pp. 824–828, 2013.

[46] C. B. Mo, S. I. Cha, K. T. Kim, K. H. Lee, and S. H. Hong, “Fabrication of carbon nanotube reinforced alumina matrix nanocomposite by sol–gel process,” *Mater. Sci.*

Eng. A, vol. 395, no. 1–2, pp. 124–128, 2005.

[47] M. A. Tarawneh and S. H. Ahmad., *Characterization and Morphology of Modified Multi-Walled Carbon Nanotubes Filled Thermoplastic Natural Rubber (TPNR) Composite, in Syntheses and Applications of Carbon Nanotubes and Their Composites*, Dr. Satoru. 2013.

[48] S. I. Cha, K. T. Kim, S. N. Arshad, C. B. Mo, and S. H. Hong, "Extraordinary Strengthening Effect of Carbon Nanotubes in Metal-Matrix Nanocomposites Processed by Molecular-Level Mixing," *Adv. Mater.*, vol. 17, no. 11, pp. 1377–1381, 2005.

[49] A. Thuault, E. Savary, J. Bazin, and S. Marinel, "Microwave sintering of large size pieces with complex shape," *J. Mater. Process. Technol.*, vol. 214, no. 2, pp. 470–476, 2014.

[50] Matthews and Rawlings, *Composite Materials: Engineering and Science*, Satoru Suz. Woodhead Publishing, 1999.

[51] RA. Andrievski, "Synthesis, structure and properties nanosized silicon carbide," *Adv. Mater. Sci.*, vol. 22, pp. 1–20, 2009.

[52] S. Iijima, "Helical microtubules of graphitic carbon," *Nature*, vol. 354, pp. 56–58, 1991.

[53] D. Galusek and D. Galusková, "Alumina Matrix Composites with Non-Oxide Nanoparticle Addition and Enhanced Functionalities," *Nanomaterials*, vol. 5, no. 1, pp. 115–143, 2015.

[54] D. SCITI, J.VICENS, and A. BELLOSI, "Microstructure and properties of alumina-

SiC nanocomposites prepared from ultrafine powders," *J. maerials Sci.*, vol. 37, pp. 3747–3758, 2002.

[55] Y. L. Dong, F. M. Xu, X. L. Shi, C. Zhang, Z. J. Zhang, J. M. Yang, and Y. Tan, "Fabrication and mechanical properties of nano-micro-sized Al_2O_3/SiC composites," *Mater. Sci. Eng. A*, vol. 504, no. 1–2, pp. 49–54, 2009.

[56] Y. M. Ko, W. T. Kwon, and Young wook kim, "Development of Al_2O_3–SiC composite tool for machining application," *Ceram. Int*, vol. 30, no. 8, pp. 2081–2086, 2004.

[57] A. Nakahira and K. Niihara, "Microstructures and fracture behaviors at high tem peratures for Al_2O_3-SiC nanocomposites," *Fract. Mec, Ceram*, vol. 9, pp. 165–178, 1992.

[58] S. Ghadami, H. Baharvandi, and F. Ghadami, "Influence of the vol% SiC on prop erties of pressureless Al_2O_3/SiC nanocomposites," *J. Compos. Mater.*, vol. 50, no. 10, pp. 1367–1375, 2016.

[59] O. T. Johnson, P. Rokebrand, and I. Sigalas, "Microstructure and Properties of Al_2O_3-SiC Nanomaterials," *Proc. World Congr. Eng.*, vol. vol II, WC, pp. 1317–1320, 2014.

[60] F. Inam, H. Yan, T. Peijs, and M. J. Reece, "The sintering and grain growth behaviour of ceramic–carbon nanotube nanocomposites," *Compos. Sci. Technol.*, vol. 70, no. 6, pp. 947–952, 2010.

[61] D.-S. Lim, D.-H. You, H.-J. Choi, S.-H. Lim, and H. Jang, "Effect of CNT distribution on tribological behavior of alumina–CNT composites," *Wear*, vol. 259,

no. 1, pp. 539–544, Jul. 2005.

[62] F. Inam, A. Heaton, P. Brown, T. Peijs, and M. J. Reece, “Effects of dispersion surfactants on the properties of ceramic–carbon nanotube (CNT) nanocomposites,” *Ceram. Int.*, vol. 40, no. 1, pp. 511–516, 2014.

[63] T. Yan and G. Wei, “Multiscale analysis of the interfacial mechanical behavior for composite of carbon nanotube and α-alumina,” *Adv. Mater. Sci. Eng.*, vol. 2014, 2014.

[64] M. Poorteman, M. Traianidis, G. Bister, and F. Cambier, “Colloidal processing, hot pressing and characterisation of electroconductive MWCNT-alumina composites with compositions near the percolation threshold,” *J. Eur. Ceram. Soc.*, vol. 29, no. 4, pp. 669–675, 2009.

[65] L. Kumari, T. Zhang, G. Du, W. Li, Q. Wang, Datye, and K. Wu, “Thermal properties of CNT-Alumina nanocomposites,” *Compos. Sci. Technol.*, vol. 68, no. 9, pp. 2178–2183, 2008.

[66] M. Estili, A. Kawasaki, H. Sakamoto, Y. Mekuchi, M. Kuno, and T. Tsukada, “The homogeneous dispersion of surfactantless, slightly disordered, crystalline, multiwalled carbon nanotubes in α-alumina ceramics for structural reinforcement,” *Acta Mater.*, vol. 56, no. 15, pp. 4070–4079, 2008.

[67] S. Maensiri, P. Laokul, J. Klinkaewnarong, and V. Amornkitbamrung, “Carbon nanofiber-reinforced alumina nanocomposites: Fabrication and mechanical properties,” *Mater. Sci. Eng. A*, vol. 447, no. 1, pp. 44–50, 2007.

[68] A. Pal, *Synthesis and characterization of CNT-Alumina nanocomposite (Master*

thesis), no. 811303004. Faculty of Engineering & Technology, Jadavpur University kolkatta, 2005.

[69] S. Chang, R. H. Doremus, P. M. Ajayan, and R. W. Siege, "Processing and Mechanical Properties of C-nanotube Reinforced Alumina Composites," in *24th Annual Conference on Composites, Advanced Ceramics, Materials, and Structures: A: Ceramic Engineering and Science Proceedings*, vol. 21, no. 3, 2000.

[70] Y. Fei, C. Z. Huang, H. L. Liu, and B. Zou, "Mechanical properties of Al_2O_3–TiC–TiN ceramic tool materials," *Ceram. Int.*, vol. 40, no. 7, pp. 10205–10209, 2014.

[71] C. H. Xu, G. Y. Wu, G. C. Xiao, and B. Fang, "Al_2O_3/(W,Ti)C/CaF_2 multi-component graded self-lubricating ceramic cutting tool material," *Int. J. Refract. Met. Hard Mater.*, vol. 45, pp. 125–129, 2014.

[72] S. K. Thakur, T. S. Srivatsan, and M. Gupta, "Synthesis and mechanical behavior of carbon nanotube–magnesium composites hybridized with nanoparticles of alumina," *Mater. Sci. Eng. A*, vol. 466, no. 1–2, pp. 32–37, 2007.

[73] P. Z. Cai, D. J. Green, and G. L. Messing, "Mechanical characterization of Al_2O_3/ZrO2 hybrid laminates," *J. Eur. Ceram. Soc.*, vol. 18, no. 14, pp. 2025–2034, 1998.

[74] N. J. Morales, S. Goyanes, C. Chiliotte, V. Bekeris, R. J. Candal, and G. H. Rubiolo, "One-step chemical vapor deposition synthesis of magnetic CNT–hercynite ($FeAl_2O_4$) hybrids with good aqueous colloidal stability," *Carbon*, vol. 61, pp. 515–524, 2013.

[75] K. A. Khalil and S. W. Kim, "Effect of Processing Parameters on the Mechanical

and Microstructural Behavior of Ultra-Fine Al 2 O 3 – By High-Frequency Induction Heat Sintering," vol. 330, pp. 322–330, 2006.

[76] F. Inam, "Development of Ceramic – Carbon Nanotube (CNT) Nanocomposites, A Thesis Submitted to University of London," UNIVERSITY OF LONDON, 2009.

[77] M. H. Aguilar-Elguézabal, A., Bocanegra-Bernal, "Fracture behaviour of α-Al_2O_3 ceramics reinforced with a mixture of single-wall and multi-wall carbon nanotubes," *Compos. Part B Eng.*, vol. 60, pp. 463–470, 2014.

[78] G. R. Anstis, P. Chantikul, B. R. Lawn, and D. B. Marshall, "A Critical Evaluation of Indentation Techniques for Measuring Fracture Toughness: I, Direct Crack Measurements," *J. Am. Ceram. Soc*, vol. 64, no. 9, pp. 539–43, 1981.

[79] O. Hanzel, J. Sedláček, and P. Šajgalík, "New approach for distribution of carbon nanotubes in alumina matrix," *J. Eur. Ceram. Soc.*, vol. 34, no. 7, pp. 1845–1851, 2014.

[80] T. A. Saleh, "The influence of treatment temperature on the acidity of MWCNT oxidized by HNO3 or a mixture of HNO_3/H_2SO_4," *Appl. Surf. Sci.*, vol. 257, pp. 7746–7751, 2011.

[81] H. L. Zhang, J.-F. Li, K. F. Yao, and L. D. Chen, "Spark plasma sintering and thermal conductivity of carbon nanotube bulk materials," *J. Appl. Phys.*, vol. 97, no. 11, p. 114310, 2005.

[82] L. Vaisman, H. D. Wagner, and G. Marom, "The role of surfactants in dispersion of carbon nanotubes.," *Adv. Colloid Interface Sci.*, vol. 128–130, no. 2006, pp. 37–46, 2006.

[83] W. Li, A. Dichiara, J. Zha, Z. Su, and J. Bai, “On improvement of mechanical and thermo-mechanical properties of glass fabric/epoxy composites by incorporating CNT-Al_2O_3 hybrids,” *Compos. Sci. Technol.*, vol. 103, pp. 36–43, 2014.

[84] Y. Z. Bahareh Yazdani, Yongde Xia, Iftikhar Ahmad, “Graphene and carbon nanotube (GNT)-reinforced alumina nanocomposites,” *J. Eur. Ceram. Soc.*, vol. 35, pp. 179–186, 2015.

[85] J. W. An and D.-S. Lim, “Effect of carbon nanotube additions on the microstructure of hot-pressed alumina,” *J Ceram Process Res*, vol. 3, no. 3, pp. 201–204, 2002.

[86] J. Tatami, Katashima, K. Komeya, and T. Meguro, “Electrically conductive CNT dispersed silicon nitride ceramics,” *J Am Ceram Soc*, vol. 88, no. 10, pp. 2889–2893, 2005.

[87] G. L. Jiang, “Densified multiwalled carbon nanotubes–titanium nitride composites with enhanced thermal properties,” *Ceram Int*, vol. 34, no. 1, pp. 231–235, 2008.

[88] A. R. Boccaccini, B. Thomas, G. Brusatin, and P. Colombo, “Mechanical and electrical properties of hot-pressed borosilicate glass matrix composites containing multi-wall carbon nanotubes,” *J Mater Sci*, vol. 42, no. 6, pp. 2030–2036, 2007.

[89] J. Ning, J. Zhang, Y. Pan, and J. Guo, “Fabrication and mechanical properties of SiO2 matrix composites reinforced by carbon nanotube,” *Mater Sci Eng A*, vol. 357, no. 1–2, pp. 392–396, 2003.

[90] U. Anselmi-Tamburini, J. E. Garay, and Z. A. Munir, “Fundamental investigations on the spark plasma sintering/synthesis process,” *Mater. Sci. Eng. A*, vol. 407, no. 1–2, pp. 24–30, 2005.

[91] N. Bakhsh, F. A. Khalid, and A. S. Hakeem, “Synthesis and characterization of pressureless sintered carbon nanotube reinforced alumina nanocomposites,” *Mater. Sci. Eng. A*, vol. 578, pp. 422–429, 2013.

[92] S. C. Zhang, W. G. Fahrenholtz, G. E. Hilmas, and E. J. Yadlowsky, “Pressureless sintering of carbon nanotube-Al_2O_3 composites,” *J. Eur. Ceram. Soc.*, vol. 30, no. 6, pp. 1373–1380, 2010.

[93] S. Tjong, “Mechanical Properties of Carbon Nanotube–Ceramic Nanocomposites,” in *Carbon Nanotube Reinforced Composites: Metal and Ceramic Matrices*, Wiley-VCH Verlag GmbH & Co. KGaA, Weinheim, Germany. doi: 10.1002/9783527626991.ch7, 2009.

[94] M. Jaafar, G. Bonnefont, G. Fantozzi, and H. Reveron, “Intergranular alumina-SiC micro-nanocomposites sintered by spark plasma sintering,” *Mater. Chem. Phys.*, vol. 124, no. 1, pp. 377–379, 2010.

[95] Z.-Y. Deng, Y. Zhou, M. E. Brito, J.-F. Yang, and T. Ohji, “Fracture-Mode Change in Alumina-Silicon Carbide Composites Doped with Rare-Earth Impurities,” *J. Am. Ceram. Soc.*, vol. 86, no. 10, pp. 1789–1792, 2003.

[96] J. D. Erika Csehova, Jana Andrejovsk“, Apichart Limpichaipanit and R. Todd, “Indentation load-size effect in Al_2O_3-SiC nanocomposites,” *J. Electr. Eng*, vol. 61, pp. 305–307, 2010.

[97] A. Krell and P. Blank, “Grain size dependence of hardness in dense submicrometer alumina,” *J. Am. Ceram, Soc*, vol. 78, pp. 1118–1120, 1993.

[98] M. A. Meyers, A. Mishra, and D. J. Benson, “Mechanical properties of

nanocrystalline materials," *Prog. Mater. Sci.*, vol. 51, pp. 427–556, 2006.

[99] C. S. Pande and K. P. Cooper, "Nanomechanics of Hall–Petch relationship in nanocrystalline materials," *Prog. Mater. Sci.*, vol. 54, no. 6, pp. 689–706, 2008.

[100] A. Peigney, F. L. Garcia, C. Estournès, A. Weibel, and C. Laurent, "Toughening and hardening in double-walled carbon nanotube/nanostructured magnesia composites," *Carbon*, vol. 48, no. 7, pp. 1952–1960, 2010.

[101] K. Ahmad, W. Pan, and Z. Qu, "Multifunctional Properties of Alumina Composites Reinforced by a Hybrid Filler," *Int. J. Appl. Ceram. Technol.*, vol. 6, no. 1, pp. 80–88, 2008.

[102] K. Ahmad and W. Pan, "Microstructure-toughening relation in alumina based multiwall carbon nanotube ceramic composites," *J. Eur. Ceram. Soc.*, vol. 35, no. 2, pp. 663–671, 2015.

[103] Guo-Dong Zhan and Amiya K. Mukherjee, "Carbon nanotube reinforced alumina-based ceramics with novel mechanical, electrical, and thermal properties," *Int. J. Appl. Ceram. Technol.*, vol. 1, no. 2, pp. 161–171, 2004.

[104] L. Changxia, Z. Jianhua, Z. Xihua, and S. Junlong, "Fabrication of Al_2O_3/TiB_2/AlN/TiN and Al_2O_3/TiC/AlN composites," *Mater. Sci. Eng. A*, vol. 465, no. 1–2, pp. 72–77, 2007.

[105] B. Nam Kim, S. Wakayama, and M. Kawahara, "Characterization of 2-dimensional crack propagation behaviour simulation and analysis," *Int J Fract*, vol. 75, no. 3, pp. 247–259, 1996.

[106] B. Lee, M. Koo, S. Jin, K. Kim, and S. Hong, "Simultaneous strengthening and

toughening of reduced graphene oxide/alumina composites fabricated by molecular-level mixing process," *Carbon*, vol. 78, pp. 212–219, 2014.

[107] F. A. Abuilaiwi, T. Laoui, M. Al-harthi, and M. A. Atieh, "Modification and Functionalization of Multiwalled Carbon Nanotube," *Arab. J. Sci. Eng.*, vol. 35, no. 1C, p. 37–48., 2010.

[108] C. Boissiere, D. Grosso, A. Chaumonnot, L. Nicole, and C. Sanchez, "Aerosol route to functional nanostructured inorganic and hybrid porous materials," *Adv. Mater.*, vol. 23, no. 5, pp. 599–623, 2011.

[109] P. Nayar, A. Khanna, D. Kabiraj, S. Abhilash, B. Beakec, Y. Lossetc, and B. Chen, "Structural, optical and mechanical properties of amorphous and crystalline alumina thin films," *Thin Solid Films*, vol. 568, pp. 19–24, 2014.

[110] K. T. Kim, S. Cha, T. Gemming, J. Eckert, and S. Hong, "The role of interfacial oxygen atoms in the enhanced mechanical properties of carbon-nanotube-reinforced metal matrix Nanocomposites," *Small*, vol. 4, pp. 1936–1940, 2008.

[111] L. Wang, Y. Cui, B. Li, S. Yang, R. Li, Z. Liu, R. Vajtai, and W. Fei, "High apparent strengthening efficiency for reduced graphene oxide in copper matrix composites produced by molecule-lever mixing and high-shear mixing," *RSC Adv.*, vol. 5, pp. 51193–51200, 2015.

[112] C. A. Hewitt, M. Craps, R. Czerwb, and D. L. Carroll, "The effects of high energy probe sonication on the thermoelectric power of large diameter multiwalled carbon nanotubes synthesized by chemical vapor deposition," *Synth. Met.*, vol. 184, pp. 68–72, 2013.

[113] Hema Vijwani and S. M. Mukhopadhyay, “Palladium nanoparticles on hierarchical carbon surfaces: A new architecture for robust nano-catalysts,” *Appl. Surf. Sci.*, vol. 263, pp. 712–721, 2012.

[114] K. Sairam, J. Sonber, C. Murthy, C. Subramanian, R. Fotedar, P. Nanekar, and R. Hubli, “Influence of spark plasma sintering parameters on densification and mechanical properties of boron carbide,” *Int. J. Refract. Met. Hard Mater.*, vol. 42, pp. 185–192, 2014.

[115] M. Rahimian, N. Ehsani, N. Parvin, and H. reza Baharvandi, “The effect of particle size, sintering temperature and sintering time on the properties of Al-Al_2O_3 composites, made by powder metallurgy,” *J. Mater. Process. Technol.*, vol. 209, no. 14, pp. 5387–5393, 2009.

[116] K. Yang, J. He, Z. Su, and A. M. Rao, “Intertube bonding, graphene formation and anisotropic transport properties in spark plasma sintered multi-wall carbon nanotube arrays,” *Carbon*, vol. 48, no. 3, pp. 756–762, 2010.

[117] D. Kochmann and K. C. Le, “A continuum model for initiation and evolution of deformation twinning,” *J. Mech. Phys. Solids*, vol. 57, pp. 987–1002, 2009.

[118] G. Yamamoto, K. Shirasu, T. Hashida, T. Takagi, J. W. Suk, J. An, R. D. Piner, and R. S. Ruoff, “Nanotube fracture during the failure of carbon nanotube/alumina composites,” *Carbon*, vol. 49, no. 12, pp. 3709–3716, 2011.

[119] G. C. WEI and P. F. BECHER, “Improvements in Mechanical Properties in SiC by the Addition of TiC Particles,” *J. Am. Ceram. Soc.*, no. 8, pp. 571–574, 1984.

[120] J. Liu, H. Yan, and K. Jiang, “Mechanical properties of graphene platelet-reinforced

alumina ceramic composites," *Ceram. Int.*, vol. 39, no. 6, pp. 6215–6221, 2013.

Curriculum Vitae

Khwaja Mohammad

https://www.researchgate.net/profile/Khwaja_Mohammad

Contact:

King Fahd University of Petroleum
and Minerals
Department of Mechanical Engineering,
Materials and Manufacturing
Saudi Arabia

wawakhan@kfupm.edu.sa
Mobile: 00966-53-6419760

Education:

Jan 2013 – Dec' 2016	*King Fahd University of Petroleum and Minerals* *Doctor of Philosophy, Mechanical engineering (Materials and Manufacturing)* *Dhahran, Saudi Arabia*
Feb 2011 – Dec 2012	*King Fahd University of Petroleum and Minerals* *Master of Science, Mechanical engineering (Materials and Manufacturing)* *Dhahran, Saudi Arabia*
Sep 1995 – May 1999	*Ghulam Ishaq Khan Institute of Engineering Sciences and Technology* *Bachelor of Engineering, Metallurgy and Materials engineering* *Topi, Pakistan*

ISI Journal Publications and US Patent.

1. N. Saheb, **K. Mohammad**: Microstructure and mechanical properties of spark plasma sintered Al_2O_3-SiC-CNTs hybrid nanocomposites. Ceramic International 5/2016; 42(10):12330-12340.
2. **K. Mohammad**, N. Saheb: Molecular level mixing: An approach for synthesis of homogenous hybrid ceramic nanocomposite powders. Powder Technology 12/2016; 291:121-130.
3. N.Saheb and **K.Mohammad**, "Hard and Tough Al_2O_3-SiC-CNT Hybrid Nanocomposite Produced by Molecular Level Mixing and Spark Plasma Sintering," Powder Technol.(submitted).